Optimisation of ultrasound-mediated delivery of mRNA to mammalian cells

Alexander Martin

Wadham College

University of Oxford

Supervisors: Prof. Robin O. Cleveland & Prof. Robert Carlisle

Thesis submitted for the degree of

Doctor of Philosophy

Hilary term 2022

“What’s your best discovery?” – asked the mole.

“That I am enough as I am” – said the boy.

The Boy, the Mole, the Fox and the Horse.

Abstract

Gene delivery will cure all. That was the hope of many since the discovery and therapeutic implementation of genetic research. Although some of that hope has been realised, the delivery of nucleotides to cells in the body remains a major barrier in wider application. Ultrasound mediated delivery of drugs has been investigated in various forms for decades and continues to be an area of engineering and science that is much explored. The body of work presented in this thesis strides to bring the two areas of research endeavour together.

Ultrasound mediated delivery of drugs and antibody particles, normally in conjunction with cavitation nucleation agents, has been shown to be effective both *in vitro* and *in vivo*. In this work we focus on nucleotide delivery, in particular mRNA, which has yet to be fully explored, especially in the context of achieving delivery of non-encapsulated, 'free' mRNA. Data presented here explores the relationship between cavitation and the transfer of, and protein expression from, free mRNA. The protein expression exhibited in various cell lines *in vitro* was further tested *in vivo*, using either sub-micron or micron-sized cavitation nuclei and the effects on transfection efficiency and expression time were examined. A luciferase reporter gene assay was used to characterise events *in vitro* across different cell lines including cancer and non-cancerous types. The impact and varying acoustic exposure parameters and cavitation on expression was assessed and differences in expression time and transfection rate were observed. These data were used to determine appropriate acoustic parameters for in vivo delivery. Cavitation-mediated delivery was examined *in vivo* in two types of cancer tumours and mRNA expression was quantified using in vivo fluorescence imaging and using excised homogenised tumour tissue. The results presented here lay the foundations for cavitation-mediated delivery and transfection of free mRNA both *in vitro* and *in vivo* by identifying appropriate acoustic parameters and cavitation nucleation agents which result in enhanced

delivery and by identifying the appropriate time-windows for measurements to quantify expression.

Statement of Originality

I hereby declare that this submission is my own work, and, to the best of my knowledge, it contains no materials previously published or written by another person, or substantial proportions of material which have been accepted for the award of any other degree of diploma at the University of Oxford or any other educational institution, except where due acknowledgement is made in the thesis.

Alexander Martin
February 2022

Acknowledgements

I'd like to also thank my supervisors, Professor Robin Cleveland and Professor Robert Carlisle. Robin, thank you so much for the chats, catch-ups, and long and difficult conversations. Not only has your academic advice been invaluable, but your personal input and consideration has been priceless to me. And to Bob, for all the help and listening to my "out there" experiment ideas, I really appreciate the time and effort you made for me. Thank you.

I would like to thank all my family and friends who have supported me on this and every journey. To the special people in my life who have supported me even when they had every reason not to. I would also like to especially mention "aunty" Rose and "uncle" Joe, who have always believed in me and while having no idea what I actually do, have been by my side each step of the way. To my mother, brothers and sisters thank you for always caring and for always being there.

To Cameron, Catherine, Jamie, Luca, Tammy, as well as all the others in the BUBBL group, thank you so much for listening to me complain for years even after some of you have left. I promise I am not that crazy in general, but your friendships have been pivotal to surviving this experience.

To Charnete, thank you so much for the friendship spanning two degrees for both of us. Thank you for always being there when I needed to chat and for reminding me that I am good enough. And to Professor James Davis, who supervised me at Ulster University and guided me in more than my research, I will be eternally grateful for your input, chats, and belief in me.

Contents

Chapter 1 – Introduction, literature review and motivations

1.1 Introduction

Gene therapy has been believed to hold the key to unlocking potential treatment for an array of diseases and genetic conditions. Many studies have focused primarily on cancer treatment and vaccine development regarding delivering genes to cells. The work in gene therapy and gene-based vaccines has been ongoing since the early 1990s. Gene therapy is hypothesized to be the solution to reversing or treating genetic disorders such as cystic fibrosis and immune-related diseases and even repairing unhealthy and damaged cells like those in heart disease (1–4). However, much more recently, the tremendous effort that has been put into vaccine development using mRNA as a protagonist to induce immune responses has led to greater understanding and development of RNA-based technologies and delivery vehicles to carry the genes to where they are required.

Gene therapy's potential to treat disease is ever growing with the rapid development of new techniques and technologies. Modifying cells within the host and allowing cells to behave or express proteins differently could significantly affect the population's health. When compared with current treatments for a disease like cancer, the benefits of successful gene therapy could revolutionise treatments.

Currently, the three primary therapies for cancer treatment in the United Kingdom are 1) Surgery to remove the tumour and affected area, 2) Chemotherapy, and 3) Radiotherapy (5). These treatments require significant time to be spent in the hospital and lead to an associated higher cost for treatment (6). The systemic effects of chemotherapy are well documented and known to include hair loss, nausea, weight loss, and an overall feeling of tiredness (7,8). So, if a targeted, cell-specific treatment could be developed, this could lead to a monumental change in people's treatments and their quality of life while undergoing treatments. The important caveat to this is the use of a delivery system. Ultrasound-mediated delivery is one system

currently being investigated and will be discussed in this thesis. This is where ultrasound and cavitation can target a specific area, an organ, or tissue region to push and move drugs within that system. Many vehicles and techniques have been tested to insert the gene or encapsulate the delivered genes, including viral vectors, lipoplexes, and lipid nanoparticles. This will be discussed in more detail later in this chapter.

This thesis examines the use of ultrasound and cavitation for additional and improved delivery of mRNA. The study of ultrasound-enhanced drug delivery has an extensive history. Briefly, as discussed later in this chapter, ultrasound has the advantage of being non-invasive, using regulatory-approved equipment, and a range of users already able to administer and monitor. It can be targeted to a minimal area depending on the equipment used. The biological effects of ultrasound and cavitation on human and non-human mammalian cells have been long studied and have improved uptake of model drugs and drugs *in vitro* and *in vivo,* depending on the application. Current applications and ultrasound-mediated delivery testing also use already "off the shelf" medically-approved contrast agents such as SonoVue Microbubbles (SV MBs). Thus, treatment times, costs, and outcomes are ready to be used when shown to benefit.

There are, however, many barriers to overcome with gene delivery *in vivo*. Traditional barriers still exist when using ultrasound-mediated delivery, including the dense extracellular matrix (ECM) of the tumour microenvironment (9,10), when discussing cancer, or the targeting of specific organs like the heart, with the difficulties the rib cage and bones present to the ultrasound waves (11). As well as biological barriers, there are regulatory and implementation barriers to overcome; for example, the cavitation agents used in this thesis are SonoTran Particles (STPs) which are currently awaiting regulatory approval for use in humans. Traditional barriers and how ultrasound-mediated delivery can be a step in overcoming them are discussed later in the chapter.

1.2 Nucleic Acids

Nucleic acids can be delivered in one of two forms; either deoxyribonucleic acid (DNA) or ribonucleic acid (RNA). Both RNA and DNA have long been believed to be the key to treating a vast array of diseases and genetic disorders, for example, targeting and silencing a pathological gene (2,12), changing gene expression, and causing the expression of a beneficial protein (1). Both DNA and RNA have key characteristics and differences in how they produce the gene, the location they need to be within the cell, and the long-term effects, to mention a few. Below RNA and DNA will be comprehensively reviewed to explain the key reasons behind choosing each for different applications.

1.2.1 RNA

Structurally, ribonucleic acid is a heteropolymer made up of nucleotides consisting of a sugar, phosphate group, and a nitrogenous base (13,14). Many forms of RNA exist, each with specific roles, such as small-interfering RNA (siRNA), transfer RNA (tRNA), ribosomal RNA (rRNA) and messenger RNA (mRNA) (15). In work discussed in this thesis, messenger RNA was used. Messenger RNAs, when occurring naturally in the cell, the function is to carry the genetic information required to produce proteins (16). The genetic information originates from the DNA of the cell, which requires relaying to the ribosomes in the cytoplasm (13). Messenger RNA bridges this gap and allows the cell to begin producing the required proteins. Messenger RNA that is introduced to a cell can encode for a range of different proteins, and by introducing mRNA, the need for interaction with the DNA or to deliver to the cell's nucleus is removed.

Native mRNA is a single-stranded molecule responsible for carrying genetic information from the DNA in the cell nucleus to the ribosomes in the cytoplasm (17). mRNA formation occurs when RNA polymerase travels along sections of the DNA double helix for a given gene, reads the code, and synthesises pre-mRNA transcript (18). This results in the produced pre-mRNA transcript having a complementary sequence to that of the DNA sequence, with a small change,

where the base thymine (T) is replaced with uracil (U) (19). The pre-mRNA transcript is then spliced in the nucleus, with sequence sections called introns excised. The remaining exons are joined together to form a single strand of mature mRNA, which codes for a specific protein. Cap and tail terminals are made up of adenine (A) residues, allowing the mRNA to be transported from the nucleus to ribosomes, where it can be translated (20,21). The single-strand nature of mRNA makes it particularly susceptible to degradation by extracellular enzymes found systemically (22), either in the blood or native to tissue (23), for example, RNases.

A range of human RNA-based therapies exists for genetic disorders, cancer therapies, and vaccines, some of which are currently undergoing clinical trials. One of the more recent developments in mRNA use in vaccines is the recent development by Pfizer and others for the SARS-CoV-2 vaccine (24). There are many different forms of RNA being used, and therapy can be classified into three categories: 1) therapeutic RNA such as mRNA; 2) RNA originating from double-stranded RNA that targets mRNA; 3) naturally occurring catalytic RNA. For the purposes of this thesis, category 1, therapeutic RNA, will be the focus. The premise is as follows - mRNA can be used to create any protein, meaning that if mRNA can be delivered to a cell, it will result in the associated protein being produced by the cell.

A range of RNA forms can be used for gene delivery, including but not limited to mRNA, double-stranded RNA (ds RNA), small interfering RNA (siRNA), and naturally occurring catalytic RNA. These forms work differently; however, they have some key advantages to their use and many other forms of RNA.

The development of RNA therapeutics required that several major hurdles be overcome, specifically the (1) rapid degradation of exogenous RNA by RNases (25); (2) delivery of negatively charged RNA across the negatively charged cell membrane (26); and (3) strong immunogenicity of exogenous RNA that impaired translation into therapeutic proteins (27).

Many of these hurdles have started to be overcome with new techniques and rapidly improving technologies. Furthermore, the drive for advancing further with RNA is heavily rooted in the ability of RNA to act on difficult or impossible targets for other small molecules or proteins to reach. In other words, RNA allows for the “undruggable” cells to be affected.

Advantages of using RNA over DNA fall into the following main areas – 1) Location of where the RNA needs to be to become therapeutic, 2) they do not present the risk of unintentional genetic effects, 3) their cost-effective development in comparison to recombinant proteins, and 4) the ability to “personalise” mRNA constructs.

Location is key to any gene delivery; can the correct area be reached? Can it be targeted? How long until the protein is expressed, and where? These are all questions that must be asked and considered when choosing the form of gene delivery used. RNA, like DNA, needs to get into the cell. However, unlike DNA, when RNA reaches the cytoplasm, it can begin to be translated when taken to the ribosomes by transfer RNA (tRNA)(28). At this point in the delivery process, delivery can be deemed successful. Once in contact with ribosomes, the translation from RNA to protein can begin, and the cell will start to produce the protein product for the cell. This means that access to the nucleus and thus another barrier to protein production can be bypassed.

Still, considering a short-term therapeutic reduces the risk of accidental long-term adverse genetic effects. It allows RNA to be considered safer in this regard. While RNA can be used to produce proteins, it can also be used to prevent expression (29). Small interfering RNA can inhibit the translation of mRNA to proteins (29), which can be beneficial in a therapeutic sense for overexpressing cancer cells. However, once again, the transient nature of RNA means that redelivery will be required for a long-term effect. The lack of a long-term impact is certainly a disadvantage in some circumstances for treatments, and this is one area where DNA holds an advantage. Unlike DNA, which stores and encodes for all the cell's genetic information, RNA

exhibits transient expression (30), meaning that the effects of the gene's presence and protein production are short-lived and will not be passed on to subsequent daughter cells. This could certainly be considered a disadvantage for long-term genetic illnesses.

Many RNA therapies are now in the clinical trial phase of development, and the Coronavirus pandemic has led to many RNA-based vaccines being translated. Table 1.2.1 shows there are also several RNA agents approved and in clinical trials for genetic diseases such as muscular atrophy, muscular dystrophy, cancer, and heart disease.

Drug	Type of RNA	Company	Route of delivery	Condition/Disease	Status
Nusinersen (Spinraza)	ASO	Ionis	Intrathecal	Spinal muscular atrophy	FDA approval in 2016
Eteplirsen (Exondys 51)	ASO	Sarepta	Intravenous	Duchenne muscular dystrophy	FDA approval in 2016
Inotersen (Tegsedi)	ASO	Ionis	Subcutaneous	Familial amyloid polyneuropathy	FDA approval in 2018
Volanesorsen (Waylivra)	ASO	Ionis	Subcutaneous	Familial chylomicronemia syndrome	EU approval in 2019
Patisiran (Onpattro)	siRNA	Alnylam	Intravenous	Polyneuropathy	FDA approval in 2018
Givosiran (Givlaari)	siRNA	Alnylam	Subcutaneous	Acute hepatic porphyria	FDA approval in 2019
Cobomarsen (MRG-106)	miRNA	miRagen (Viridian)	Intravenous/subcutaneous	Blood cancers	Phase II
Remlarsen (MRG-201)	miRNA	miRagen (Viridian)	Intradermal	Keloids	Phase II
MRG-110	miRNA	miRagen (Viridian)	Intradermal	Tissue Repair	Phase I
Pegaptanib (Macugen)	Aptamer(RNA)	Bausch + Lomb	Intravitreal	Macular Degeneration	FDA approval in 2014
Empticap pegol (NOX-E36)	Aptamer(RNA)	NOXXON	Intravenous/Subcutaneous	Diabetic nephropathy, lung and pancreatic cancer	Phase II
Olaptesed pegol (NOX-A12)	Aptamer(RNA)	NOXXON	Intravenous	Brain cancer	Phase I/II
BNT162b2	mRNA	BioNTech and Pfizer	Intramuscular	COVID-19	FDA authorization for emergency use in 2020
mRNA-1273	mRNA	Moderna	Intramuscular	COVID-19	FDA authorization for emergency use in 2020
CVnCoV	mRNA	CureVac	Intramuscular	COVID-19	Phase III
AZD8601	mRNA	Moderna/Astrazeneca	Epicardial	Ischemic heart disease	Phase II
mRNA-1647	mRNA	Moderna	Intramuscular	Cytomegalovirus infection	Phase II
P-BCMA-101	mRNA	Poseida	Intravenous	Multiple myeloma	Phase II
mRNA-4157	mRNA	Moderna	Intramuscular	Cancer	Phase II
mRNA-3704	mRNA	Moderna	Intravenous	Methylmalonic aciduria	Phase I/II
MRT5005	mRNA	Translate Bio	Inhalation	Cystic Fibrosis	Phase I/II
mRNA-2416	mRNA	Moderna	Intratumoral	Solid tumors/ lymphoma/advanced ovarian carcinoma	Phase I/II
BNT131 (SAR441000)	mRNA	BioNTech/ Sanofi/Genmab	Intratumoral	Advanced melanoma	Phase I/II
Descartes-08	mRNA	Cartesian	Intravenous	Generalized myasthenia gravis	Phase I/II
BNT122	mRNA	BioNTech	Intravenous	Solid tumors	Phase I/II
mRNA-2752	mRNA	Moderna	Intratumoral	Solid tumors	Phase I
MEDI1191	mRNA	Moderna	Intratumoral	Solid tumors	Phase I
mRNA-1944	mRNA	Moderna	Intravenous	Chikungunya infection	Phase I
CV8102	mRNA	CureVac	Intratumoral	Solid tumors	Phase I
ARCT-810	mRNA	Arcturus	Intravenously	Urea disorder	Phase I
CV7202	mRNA	CureVac	Intramuscular	Rabies	Phase I
mRNA-1893	mRNA	Moderna	Intramuscular	Zika	Phase I
CV9202	mRNA	CureVac	Intradermal	Non-small cell lung cancer	Phase I
mRNA-5671	mRNA	Moderna	Intravenous	Cancer	Phase I
BNT111	mRNA	BioNTech	Intravenous	Advanced Melanoma	Phase I

The table summarizes information available at ClinicalTrials.gov (https://clinicaltrials.gov/) as of January 26, 2021. ASO, antisense oligonucleotide; siRNA, small interfering RNA; miRNA, microRNA; RNA, ribonucleic acid; mRNA, messenger RNA.

Table 1.2.1: The table is taken from "The Limitless Future of RNA Therapeutics", showing the number of ongoing clinical trials using RNA as of January 2021. Table reproduced with permission from authors.

1.2.2 DNA

DNA comprises three parts, a 5-carbon sugar-deoxyribose, a nitrogenous base, and a phosphate group (20). The structure is made up of 4 bases, which consist of two complementary pairs that bind to form the well-known double-stranded structure of DNA: adenine (A) and thymine (T),

and guanine (G) and cytosine (C). DNA can be seen as a double helix in an antiparallel structure where the helix, made up of two strands of sugar-phosphate backbone, run in opposite directions. Each strand has a 5' end and a 3' end (21).

For therapeutic DNA delivery to be successful, the DNA molecules must first bypass the cell membrane and then be transported to the nucleus, thereby passing the nuclear envelope (31). This process allows the DNA to begin replication, whereby the desired protein can be produced or switched off. This process is a semi-conservative process whereby each DNA strand acts as a template to produce two new strands (32). Replication requires complementary base pairing, where adenine always pairs with thymine and cytosine with guanine. Replication is achieved by breaking hydrogen bonds that hold the base pairs together(33). The helix then separates and opens, allowing each strand to act as a template for synthesising a new complementary strand (32). The process occurs in the nucleus of cells. It requires several enzymes but relies primarily on DNA polymerase to synthesize the new strands together, acting both as a facilitator and a proofreader for the process (34).

The cell nucleus is the only place where transgene expression can occur. Any delivered DNA must be transported through the cytoplasm and past the nuclear envelope while remaining functional to be transcribed in the nucleus (34). This remains one of the most challenging obstacles to gene delivery using DNA. This is an essential consideration of the work in this thesis, as DNA was not used because of the associated difficulties with transfecting the nucleus.

Various methods for improving DNA therapy have been employed to improve delivery efficiency and therapeutic outcomes. These include the use of plasmid DNA (pDNA) and DNAzymes. Plasmid DNA is effectively circular DNA molecules, typically derived from bacteria's extra chromosomal space (35,36). Plasmid DNA contains promoter and enhancer sequences for gene expression regulation and sites for processing the resulting pre-mRNA

transcript (36). Plasmids comprise an origin of replication, reproducing the behaviour of endogenous DNA before mitosis. DNAzymes are single antisense DNA strands that can target sequence-specific RNA/DNA, cleaving fragments to cause a degree of gene inhibition or gene sequence mending (21,36).

Since DNA that transfects the nucleus can affect the subsequent daughter cells of the original target cell, the effects and long-term repercussions must be known and thoroughly investigated. Some considerations for using DNA as a therapeutic are 1) the long-term effects, 2) the high associated costs, 3) accidental genetic effects, 4) Immune response, and if using viral vectors, 5) cell targeting specificity (37–39).

This is important for many reasons, including the risk of an accidental mutation (40) and the long-term consequences, an essential link in the targeting and delivery to specific cell types. For example, if targeting cancer cells to overexpress a particular marker for destruction by the immune system, the effect would be disastrous if this DNA ends up in healthy cells. The research on using DNA as a therapeutic is ongoing and encouraging, even with all these considerations.

1.3 Delivery Vehicles

Whether RNA or DNA is chosen as the macromolecule to be introduced to the cell, many barriers are still overcome. These barriers include both regulatory and biological. There have been many concerns regarding the effectiveness and usefulness of gene therapy, including regulatory ones. These include worries over gene therapy using somatic cells, which is banned in the UK (41), the fears over “designer” babies, and the ill-informed ideas regarding changing genetic DNA. The regulations surrounding gene therapy are determined by each region or country, like medicines and medical devices.

Biological barriers are much more extensive and require additional help to overcome. This help comes in the form of delivery vehicles and systems. One such barrier is the environment they are delivered into. It is inhospitable, with an abundance of ribonucleases, blood components, and the immune system ready to break down and destroy the delivered gene (42). Moreover, the delivery system, method, and vehicle/carrier are crucial to the successful therapy outcome.

1.3.1 Transport Vectors

A key component of ultrasound-mediated drug or gene delivery systems is transport vectors. Vectors can be classified into two types, viral vectors and non-viral vectors. The role of the vector in drug or gene delivery is a multistep one: 1) protect the payload from degradation, 2) ensure that target cells are reached, and 3) release the load. To further understand the role of each vector classification, it is important to consider various types of viral and non-viral vectors and their current position in the field.

1.3.2 Viral Vectors

In gene delivery, the biological nature of a virus, i.e., the way it replicates and can be readily taken up by cells, is exploited. When delivering genes, the gene must pass the cell membrane and even the nuclear envelope for DNA. To make this easier and fully utilise viral vectors, the pathogenic gene sequences are removed and replaced by therapeutic sequences (43) while leaving the structures in place that allow for viruses to infect cells, such as the fusogenic proteins (44), which enables the fusion to the membrane and protein expression.

Viral vectors are the most utilised method for gene delivery as their transfection efficiency in vivo is very high (1). However, some drawbacks remain that may halt their clinical applications, including the cost of a large-scale, good manufacturing process (GMP) production of viral vectors is difficult and expensive (45); a viral vector has instigated an immune response within a subject/patient, which while rare, can result in fatal consequences (46,47). Finally,

because the therapeutic gene is placed where once the pathogenic region existed, it is limited in size (48), limiting the amount of gene that can be delivered to the cell. Some leading viral vectors studied and used include the adenovirus, herpes simplex, and retrovirus (49). Each with advantages and disadvantages, usually concerning transduction rates and insert size for therapeutic genes (50), but much of which is beyond the scope of the work contained within this thesis.

1.3.3 Non-Viral Vectors

The development of non-viral vectors arose from the drawbacks of viral vectors, namely the small number of genes that can be inserted and the potential for severe immune responses (51). Non-viral vectors have been developed that have advantages over viral vectors. The delivery method can vary based on the vector used, discussed below. A range of non-viral vectors has been developed for drug and gene delivery, including lipoplexes, calcium phosphate precipitates (CPP), and lipid nanoparticles.

1.3.4 Lipoplexes

Lipoplexes are non-viral lipid carriers made up of three basic components; a neutral lipid, cationic lipid, and either plasmid DNA, or more recent studies have incorporated RNAs (52). The positive surface charge of lipoplexes allows for an innate interaction between cell membranes and the lipoplexes (53). The lipoplex aims to protect from the DNA/RNA's enzymatic degradation and prevent immune system activation (54). An example of a lipoplex is liposomes. Liposomes are often used as the delivery vehicle for therapeutic DNA or RNA delivery and have the ability to self-assemble (55). Liposomes can form many shapes and sizes, and their surface charge can be controlled (56). They are formed by self-assembling dissolved lipid molecules with a hydrophobic head group and hydrophilic tails. Bimolecular lipid leaflets can also be formed (57). These leaflets are formed with hydrophobic tails facing each other, with the hydrophilic head groups facing outwards. This shape formation results from the

hydrophobic tails initially still in contact with water, which forces the lipid into a bilayer formation, resulting in the hydrophilic heads being in contact with water (58).

Cationic liposomes have been shown to positively impact transfection levels (53), with the likelihood that positively charged lipids more readily interact with cellular membranes due to the electrostatic attraction and the native negative charge of the cellular membrane (59). Lipoplexes have been shown to fuse with the cell membrane or utilise the clathrin-mediated pathway (52) to deliver directly into the cell.

One downside of lipoplexes is their low-efficiency rate (60). This can be due to similar barriers when delivering naked genes. Upon entering the cell, lipoplexes remain at risk of being encapsulated by endosomes or lysosomes and their drug or gene not being delivered.

1.3.5 Calcium Phosphate Precipitates (CPP)

Calcium phosphate precipitates (CPP) are a novel non-viral method for gene delivery. Calcium phosphate precipitates are achieved by mixing nucleic acids with calcium chloride in a saline or phosphate solution (61). The resulting precipitates can be used to transfect cells as the calcium phosphate allows enhanced binding to the cell membrane surface and the nucleic acid to enter the cell through endocytosis (62,63).

The advantages of CPP over viral vectors include being biocompatible, bioactive, relatively inexpensive, easily degradable within lysosomes, and potentially high loading capacity (64,65). The preparation of CPP nanoparticles is co-precipitation of calcium phosphate with DNA, where the DNA is adsorbed onto the precipitates (65). Calcium phosphate is found in all hard tissues within the body. It will degrade to ions already present in the body, resulting in straightforward clearance of the particles and an established biological process (61). *In vitro*, CPPs have been shown to use clathrin and caveolae endocytosis pathways (66) and exhibit stability early through late endosomal encapsulation (67).

While their properties seem advantageous over viral vectors, a few disadvantages mean a CPP-based clinical therapy remains unlikely. CPPs have only been used *in vitro* to date, and transfection must be performed rapidly after precipitation (68). There is also limited control over precipitates' size, structure, and distribution during production, meaning reproducibility issues. A key consideration for production and clinical application is highly dependent on consistent batch-to-batch methodology, and while true for all production processes, the high variability seen with CPP production on small scales means large scale production is unlikely. Crucially there is no means of providing target cells selectively, and blood stability is very poor, meaning the method is restricted to *ex vivo* applications

1.3.6 Lipid Nanoparticles

Lipid nanoparticles (LNPs) are similar to lipoplexes. LNPs are made up of lipid layers and can be categorised into the following categories; solid lipid nanoparticles, nonlamellar lipid nanoparticles, cationic lipid nanoparticles and many more (69). LNPs became prevalent in the early 1990s as an alternative to traditional carriers, such as the polymeric nanoparticles and liposomes discussed above. Lipid nanoparticles used as a carrier have many benefits: 1) they shield the payload from systemic degradation, allowing for a longer circulation time, and 2) they can be specifically targeted to relevant tissues and cells through modification of the design of the LNP (12,70).

Lipid nanoparticle design is crucial in how the DNA or RNA macromolecule will be delivered to the cell and is an essential factor impacting the transfection rate. Some of the considerations for the design of LNPs include whether the LNP will have a cationic, neutral, or anionic charge, which impacts its delivery, as discussed above. The charge of the LNP plays a pivotal role in how the LNP interacts during circulation, in its extravasation to tissue, and in how it interacts with target cells (12,71). The charge can be essential in improving or preventing the uptake of the carrier's contents, and as such, the LNPs can be controlled through their formulation (72).

1.3.7 Non-Viral Vector Design

The design of nanocarriers can play a pivotal role on their ability to be delivered and thus whether they are deemed successful. Some of the key properties that lead to success include 1) the ability of the carrier to protect the DNA/RNA from extracellular nuclease digestions, 2) allowing for cell-specific targetting and uptake, 3) providing a route for endosomal escape, 4) producing limited immunological interactions, 5) biocompatibility and low levels of toxicity, and 6) clearance route of the delivery vehicle must be safe and efficient.

Lipid nanoparticles have been designed to carry oligonucleotides, ensuring that the DNA/RNA remains protected and unexposed to extracellular biological fluids through having the DNA or RNA encapsulated within a lipid shell, which can be designed to camouflage from the immune system (73). For example, messenger RNA (mRNA) is highly unstable in extracellular fluid due to the prevalence of nucleases such as RNase and serum in the blood (74).

Many designs of LNPs have relied on the passive uptake into cellular targets. However, there is growing interest in and further study those designed with active targeting ligands. The most common formulations include four components: an amine-containing lipid, phospholipid, cholesterol, and lipid anchored polyethylene glycol (75). The formulation of the LNP plays a key role in encasing the therapeutic agent.

Nanoparticles coated with polyethylene glycol (PEG) have many benefits, including preventing interactions with blood components (76,77). PEG coating of nanoparticles has been shown to reduce uptake and clearance by immune cells by cloaking the delivery vehicle (78) and increase the systemic circulation time and bio-distribution by preventing nonspecific interactions within the biological environment controlling the charge of the particle (79). PEGylation can also be used to increase the density of nanoparticles. This increases the

extravasation of the nanoparticle when stimulated via mechanical stimuli such as ultrasound, thus allowing for further penetration into the tissue and greater exposure to target cells (80).

The mechanism of uptake of LNPs into cells is still being explored. Many mechanisms have been suggested, but this thesis focuses on LNP uptake using ultrasound-mediated delivery and the delivery of naked mRNA to various cell types. The cellular delivery of RNA-loaded LNPs is both dynamic and complex. It is a multistep process that requires highly interconnected cellular uptake, intracellular processing, and gene silencing activities (81,82).

However, the same problems with endosomal and lysosomal encapsulation remain, where the delivered load is encapsulated and sometimes removed by the cell (83). This also leads to the risk of the gene's degradation or inactivation. Despite the challenges described above for the successful delivery of genes, much work has been carried out to improve DNA and RNA based delivery therapies, some of which will be elaborated upon below.

1.4 Barriers to drug delivery

A key consideration to understanding the limitation of drug delivery to tumours, is the tumour type and the resulting microenvironment. The tumour microenvironment (TME) is unlike any other environment within a healthy body. Many properties of the TME make it very difficult to deliver adequate volumes of therapeutic agents. The TME develops to support the tumour, promote its growth, and manipulate the intrinsic properties of the tissue. Cancer cells undergo rapid mitosis (84), causing rapid growth in cell numbers. Increasing the initial genetic mutations leads to an ever-increasing chaotic environment where rapid angiogenesis occurs, which allows the tumour to develop into an adversary to traditional drug delivery methods. Rapid angiogenesis leads to poorly formed and leaky blood vessels in and around the tumour (85,86). The poor condition of the blood vessels means that the TME is highly heterogenous,

with some areas perfused and oxygenated, whereas others are not perfused and are hypoxic (87,88). The barriers to drug delivery can vary between tumour types, but many core characteristics are shared between different tumour types and locations.

1.4.1 Biological barriers to drug delivery

Tumours can be broken into several different regions, referred to as 1) the necrotic core, 2) the quiescent region, and 3) the proliferative/periphery region. An example of these regions in a tumour can be seen in Figure 1.4.1(89) .

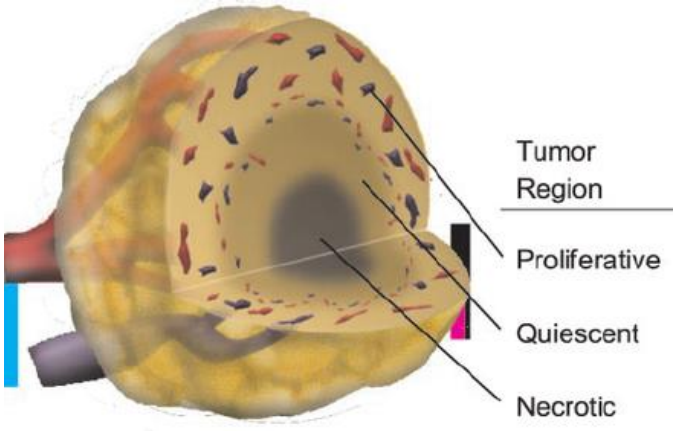

Figure 1.4.1: Schematic of tumour regions, demonstrating examples of the formation of a tumour's proliferative, quiescent and necrotic regions. The Schematic has been modified and reproduced with the original author's permission.

The necrotic core lies at the centre of the tumour and is fundamentally a hypoxic central region consisting of a collection of dead and dying cancer cells (90). The cells die due to a combination of factors, including the hypoxic nature of the core due to poor vascularisation, nutrient starvation, and metabolite toxicity (91). This region contains no blood vessel structures and has a damaged lymphatic system resulting in elevated interstitial fluid pressure (IFP) (84,92). This lack of perfusion and elevated IFP limits transvascular transport.

The quiescent region is home to various living and dead cancer cells. There is some perfusion with some blood vessels found on the outskirts of this region, but this is still less than found in healthy tissue or that of the periphery region of the tumour itself (84). The interstitial fluid

pressure (IFP) is still high in this area due to the damage to the lymphatic system, but with fluid still able to flow in, it results in a place where pressure builds (93–95). Some proliferating cells can be found in this region, usually towards the boundary in the periphery of the tumour with interstitial and transvascular transport compromised (96) and remain lower than healthy tissue.

Finally, in the outermost region of the tumour exists the periphery. There are many blood vessels, along with the area where the vast majority of proliferating cells exist (84). This is the region where drugs are most efficiently delivered due to leaky vasculature, as discussed earlier. Interstitial and transvascular transport can be seen to be higher in this region of the tumour than in normal tissue, partly due to the leaky nature of the blood vessels caused by the rapid angiogenesis period of tumour development. This may play a key role in explaining how delivered therapeutics can accumulate in this tumour's outer region. Each of these regions has unique properties, all playing a role in the barrier to drug delivery while simultaneously helping create a nurturing microenvironment for the tumour.

The main features of the TME that are barriers to drug delivery and have an effect on therapeutic outcomes are 1) the dense interstitium and the extracellular matrix, 2) the elevated interstitial fluid pressure within the tumour, 3) the resulting hypoxic regions that develop within the tumour, and 4) the changes in pH that occur within a tumour.

Each of these properties alone can play a role in preventing drug delivery, but together they become a formidable barrier. The dense interstitium, containing the extracellular matrix (ECM), comprises macromolecules with distinctive biochemical, biomechanical, and physical properties. The ECM forms a pivotal part of multicellular structures and allows for cell adhesion, cell-to-cell communication, and differentiation as some of its primary functions (97,98). As a result, there are many regulatory mechanisms at play. The ECM plays a role in cellular behaviour and any major developmental processes. Changes to the mechanisms of the

ECM can lead to abnormal cellular behaviour and diminish the function of the tissue or organ. Healthy ECM comprises many components, including proteins, proteoglycans, glycoproteins, and polysaccharides (99). Each of these components plays a significant role in the properties and function of the ECM. For example, it has been shown that removing proteoglycans and glycoproteins can impact the number of particles allowed to move through the ECM freely(100).

As well as biochemical interactions with drugs and other particles, the ECM acts as a scaffold to support tissue. Some of the fundamental physical characteristics of the ECM that allow for this function also play a role as a barrier to drug delivery (101). These properties include the porosity and topography of the ECM, which impact the movement of particles. For example, an increase in the number of fibrous structural proteins such as collagen, elastin, fibronectin, and laminins which provide much of the structural integrity of ECM, as observed in cancer tumours (97,102), will impede larger particles and result in a more tortuous path.

Size exclusion and abnormal ECM characteristics play a role in hindering drug delivery. It has been shown that when particles are too small, they can be cleared naturally, e.g. renal system or via the mononuclear phagocytic system (103,104), whereas particles that are too large are prevented by ECM pore size. Even when drugs of appropriate size ranges are delivered, they can still fail to penetrate substantially into the tumour. This can be due to various reasons discussed here, including the irregular vascular network within the tumour and the high interstitial fluid pressure limiting the movement of particles into the tumour environment (105,106).

Size is not the only consideration. The ECM contains high levels of glycosaminoglycan (GAG) side chains (10,107), and this gives the ECM a high net negative charge (108,109) and a greater ability to trap water. These GAG side chains form part of the proteoglycans proteins that form

an essential biochemical element of the ECM. While the GAG side chains are negatively charged, they are attached to positively charged core proteins (110), attracting and showing a binding affinity for differently charged particles. One of the effects charge has on drug delivery can be seen with the use of neutral nanoparticles, which display faster interstitial transport (111). This is likely due to their minimal interactions between the positively charged core proteins and the negatively charged GAG side chains. On the other hand, charged particles are limited in their transport due to binding or volume-excluding interactions with the GAGs and various proteins, such as positively charged collagens (112).

Some mechanisms allow for the surface charge of a particle to be hidden from the components of the ECM, such as PEGylation (113–115). PEGylation, the process of coating a particle with polyethylene glycol (PEG), is a standard method used to try and increase the efficiency of encapsulated drug, gene, and vaccine delivery. The PEG coatings applied to particles or carriers allow shielding from the electrostatic attractions that would otherwise occur. It also has the additional benefit of improving the systemic circulation time of nanoparticles by covering the surface from aggregation and phagocytosis (78). By changing the particle's surface chemistry, one can change the interactions between the particle and components of the ECM and produce an immunologically camouflaged particle (78). Using the enhanced permeability and retention effect (EPR) can actively target tumours. PEG can also be used to increase the density of the particle (116). It has been shown that an increased density results in an increase in ultrasound-mediated transport (117), which indicates that this is an important consideration in the design of nanoparticle therapeutics.

Even with changes and modifications to the particles, drug delivery still has barriers, with the elevated interstitial fluid pressure (eIFP) being a major consideration (118–120).

During the initial formation of tumour development, vascular endothelial growth factor (VEGF) production is increased by tumour cells, leading to the rapid formation of blood vessels (84). However, the rapid production of blood vessels leads to leaky endothelial cell junctions in the blood vessel walls (84,121,122), which, in turn, leads to hyperpermeability (86,123). While easily imagined as a positive development in particle delivery, this hyperpermeability comes with its problems. During the rapid formation of the tumour and blood vessels, the density increases rapidly, which puts pressure on the lymphatic system; lymphatic vessels are often damaged in cancerous tissue (92). This damage to the lymphatic systems has the undesired result of impairing drainage at the tumour site. This results in an inward fluid flow and, with minimum drainage, leads to fluid build-up, resulting in elevated IFP in the tumour region (124). This leads to particles that reach the tumour site being faced with a wall of pressure. This resistance leads to 90% (125) of the tumour receiving little to no drug, making regrowth likely, and particles remaining in the periphery of the tumour, where blood vessels are more regularly organised.

Typically, in healthy tissue, the distance between blood vessels and the cells they supply with oxygen and nutrients is around 90 μm (126). In contrast, this distance to the nearest blood supply in cancer tumours is typically about 150 μm (127). This is a problem for the oxygenation of the cells. Oxygen can readily diffuse in sufficient concentration to nourish cells over distances of ~ 100 μm, an ability that rapidly decreases at distances over 100 μm. The distance from the blood supply between healthy and cancerous cells means oxygen struggles to diffuse in great enough concentrations, causing hypoxic areas and necrotic cores in tumours. These hypoxic regions are accompanied by a change in the pH of the surrounding tissue. The greater the distances that oxygen must diffuse to reach the cancer cells, the more likely this effect will occur. An increased distance for oxygen to diffuse also represents an increase that particles and drugs must diffuse.

Tumour extracellular pH is often low (128) due to acidic metabolites. An example, lactic acid, is formed due to anaerobic glycolysis in hypoxia regions. This is commonly accepted as the "Warburg effect." For this reason, higher lactate levels typically indicate metastases and tumour reoccurrence (129,130). These increased lactate levels also facilitate inflammatory mediators, which, in turn, increase interleukin production by T-cells and macrophages. These increased levels of interleukins lead to chronic inflammation within tumour microenvironments (131). Lactate also inhibits monocyte migration and cytokine release while promoting tumour cell mobility. The acidic microenvironment contributes to tumour radioresistance due to the antioxidant properties (132).

While the acidic properties of the tumour microenvironment form a formidable barrier to traditional drug-based therapies, it opens the door to new drugs and new delivery methods that utilise the properties of the TME. Nanomaterials have been widely explored as drug carriers and use the acidic nature of the TME as a signal for the packages to release their payloads. Nano-therapies have shown great potential in many areas, including multiple targeting functionalisation, combined drug delivery, extended circulation time, and systemic control release(133). Nanosystems have been designed to incorporate stimulus-responsive materials, allowing them to use tumours' biological and biochemical properties (134). Several pH-sensitive nanosystems have been designed and approved by the Food and Drug Administration (FDA) for cancer treatment (133).

A better understanding of the TME, both in composition and functionality, has allowed these innovations in drug delivery. Still, one thing has been made clear, to better target and increase the efficiency of the drugs delivered, a multidisciplinary approach must be taken. Understanding how particles move through the TME, interact with different components, and how the structure, perfusion, and delivery method can significantly impact how the drug reaches, interacts, and ultimately impacts the tumour.

1.5 Delivery Methods

The use of mRNA as a therapeutic agent in various areas, such as vaccines and direct therapeutic agents, has a significant advantage in how it facilitates protein production through translation. This is a process that never requires entry into the cell nucleus. Hence, in contrast to DNA delivery, which requires transcription in the nucleus and subsequent translation (31), transcription is circumvented in mRNA delivery. If mRNA is successfully delivered to the cell and can avoid degradation during this journey, the cell can produce the associated protein in the cytosol. This means no direct gene editing but rather a temporary change to the proteins produced by the cells. One way to improve delivery and efficiency is choosing an appropriate delivery method, RNA or DNA. Some of these systems will now be discussed.

1.5.1 Electroporation

Electroporation (EP) was first used in 1982 to insert DNA into viable mouse lyoma cells (135). Electroporation works by suspending cells and selected molecules in a conductive solution, where an electrical pulse is applied on the order of a millisecond (135). This disrupts the phospholipid bilayer and changes the electrical potential across the membrane(136). Doing so allows charged molecules like DNA or RNA to be driven across the membrane (137). While EP has had consistently good results *in vitro* with various tissues and tumour types (136), it is limited by several factors for *in vivo* applications. Biological and physical factors play a role in how successful EP is in vitro, such as cell size, shape and density, pulse duration, and electronic field intensity (136). Even though EP has an impressive transfection rate, the likelihood of use *in vivo* is low due to the difficulty of transferring DNA into a large tissue area with the limited effective range of the electrodes, which require surgical placement (138). Due to the power employed for this technique, there is a risk of harm and damage to the tissue and the patient. Overall, as a method for *in vitro* transfection, EP has advantages over other methods

in terms of transfection efficiency. However, as a clinical application, its invasiveness and safety concerns make its use an unrealistic prospect.

1.5.2 Gene Gun

In the early nineties, a new transgene delivery method called gene gun therapy was employed (88, 89). Gene gun therapy uses DNA-coated bioinert particles, for example, gold or silver, propelled through the skin and tissue to target sites, either by vaporisation water under high voltage electric spark or through helium discharge(140). When using this method, key considerations are the carrier particle's size, the gas pressure used to accelerate the particle to the target, and the transgene dosage (140). Gene gun therapy is limited to DNA coating only, as RNA degrades too quickly when using this method (141). Despite the invasiveness and the limited applications, the expression levels are relatively quickly and can be long-lasting (140). However, the limitation may prove too much for therapy in its present form, as many research groups have moved away from this delivery method.

1.5.3 Sonoporation

Sonoporation is the formation of pores on the cellular membrane, modulated by ultrasound and the associated cavitation. Sonoporation leads to increased membrane permeability, leading to higher transfection rates and higher quantities of drugs being delivered. Sonoporation has been used to deliver nucleic acids into various tissue types, including muscle, liver, kidney, tumours, and cardiac cells (142–146). The advantage of sonoporation over many other delivery methods is that it is relatively safe, non-invasive, and can be targeted to specific body locations (147). Sonoporation efficiency depends on several factors, including ultrasound intensity, frequency, cavitation regime, the concentration of delivered gene or therapy, the exposure period, and contrast agents or cavitation nuclei to improve extravasation (148,149).

1.5.4 Hydrodynamic Injection

Hydrodynamic injection was first used in the mid-1990s and works by inserting a high volume of plasmid DNA via high-speed intravenous (IV) injection within a few seconds (150,151). The method works by utilising the hydrodynamic force of the large volume of nucleic acid solution and permeabilising capillary endothelium and then generating pores in the membranes of surrounding cells (151,152).

The simplicity of this method makes it popular. However, there are drawbacks to using a hydrodynamic injection that make it irrelevant for human gene delivery. Predominantly, the DNA solution injected must be 8-9% of the subject's body weight (150,151). In rodents, this works well. However, this would need a volume of 7.5 L to be injected in seconds for a male weighing 83 kg (average weight for a male, England, 2020. (153). This would ultimately lead to heart failure or cardiac arrest due to increased blood volume. Its use for transferring genes in rodents continues with success.

1.6 Ultrasound as a delivery system

Ultrasound-mediated delivery of particles is a growing area of scientific research. Over the last 20 years, research in the area has become extensive. Researchers have explored the biological and mechanical effects of using ultrasound on cells in vitro with varying levels of success. This section will discuss how ultrasound works as a modality, is currently used as a treatment, and could be used clinically for drug delivery. Also, the methods used to monitor and assess the process, in the form of cavitation, will be discussed, along with the biological effects and what that means for potential therapies.

Traditionally when people think of ultrasound, they imagine classic b-mode images carried out during pregnancy. However, the ultrasound discussed in this thesis differs significantly in both

its objectives and how it functions. Several different ultrasound forms exist, including A-line imagining, b-mode imaging and high intensity focused ultrasound (HIFU) (154,155). Each utilises various forms of equipment and works in very different ways. For the work in this thesis, most of the equipment more closely relates to HIFU, which will be discussed further.

Ultrasound is soundwaves with frequencies above that of the upper audible limit of human hearing, around 20 kHz (156), and ultrasound waves behave the same way as waves that humans can hear. To achieve these waves, an ultrasound transducer is used to produce a beam. Several transducers are available, including concave, phased array and flat transducers (157).

In this work, ultrasound waves were generated using a piezoelectric transducer which is excited by an alternating voltage and responds by vibrating, which produces an ultrasound wave (158–161). By shaping the materials as a spherical cup, the pressure wave can be focused at a distance nominally. The beams focus depends on the radius of the curvature and geometry of the transducer, the frequency of the ultrasound and the properties of the medium through which the soundwave is travelling (161).

As the ultrasound wave passes through the tissue, the tissue can be compressed and stretched at different parts of the wave, and heating effects from the ultrasound can be introduced (162). Another effect that is seen with HIFU that is utilised in this thesis is cavitation effects. Cavitation effects in HIFU can be seen in even perfectly degassed medium due to the energy being deposited overcoming the medium's tensile strength, and when used on native tissue *in vivo*, this can occur at even lower thresholds due to the presence of trapped gas (163). Any gas bubbles will also experience the same contraction and tensile phases as the tissue in the sound wave path. One of the reasons cavitation nuclei are used is to lower the threshold where cavitation will occur, so that native tissue does not need to be heated to the point of damage to

see these cavitation effects and allows for greater control about how and when this occurs (164). This will be discussed in greater detail below.

The principles of HIFU are utilised in the body of work in the form of focused ultrasound (FUS) while trying to mitigate the heating effects. This can be achieved in several ways, 1) by moving the focus area of the beam, through the movement of the target, in this case, tumours, and 2) by altering the ultrasound parameters such as duty cycle, number of cycles, pulse repetition frequency (PRF), the frequency of the transducer used, and the pressure amplitude applied (155). There is greater control over the effects of using ultrasound and, therefore, a greater likelihood of success by controlling for the parameters.

1.6.1 Cavitation

Cavitation can occur when a volume of gas in the form of a bubble is trapped in the ultrasound field (165). The bubble absorbs the energy from the ultrasound, and it will experience a growth and compression phase where it will oscillate. When the bubble absorbs so much energy that the kinetic energy overwhelms the restoring pressure forces, then the bubble grows (166). The effects of cavitation vary on the tissue depending on the amount, period, and sustained levels. However, cavitation can be used to the benefit of drug delivery if it is controlled. The process of native cavitation in the tissue occurs at high pressures, to the required pressure, and therefore the threshold for cavitation, cavitation nuclei can be introduced (167).

Introducing different cavitation nuclei can lead to two types of cavitation being achieved, 1) non-inertial cavitation and 2) inertial cavitation.

For non-inertial cavitation, as bubbles interact with pressure waves, they expand under low and contract under high pressures. Gas bubbles can oscillate over many cycles, resulting in non-inertial cavitation and microstreaming effects (168). This is where fluid begins to circulate around the expanding and shrinking bubbles in the form of microstreaming. The resulting

microstreaming results in shear forces that are proportional to the amplitudes of oscillations (169), which can result in significant enough shear force to open erythrocytes(170) and, more importantly, can be used to open liposomes or other nanocarriers.

Inertial cavitation occurs when the ultrasound intensity and oscillations increase to a point where the inward moving fluid has enough inertia that it cannot reverse direction when the acoustic pressure reverses (171). Instead, the gas in the bubble is continuously compressed to a smaller and smaller volume leading to high pressure and temperature. Inertial cavitation can damage or break cells and vesicles due to the high pressures involved and high temperatures experienced, and the effects, such as the formation of free radicals and the shock wave produced by bubble collapse (172). Microjetting happens when a bubble is near a solid boundary upon collapse; the fluid surrounding the bubble collapses into the bubble towards the solid boundary (173). Both these effects can be used to aid in drug delivery and distribution. However, the biological effects of cavitation itself can be quite extensive using these cavitation nuclei.

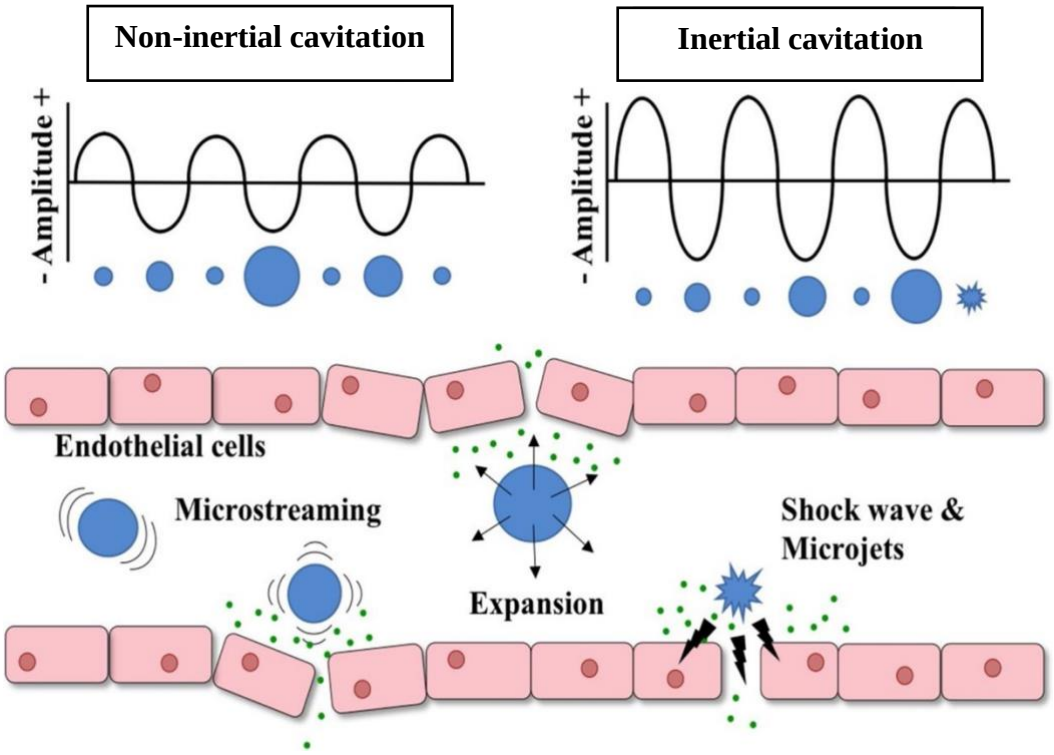

Figure 1.6.1.1: Modified figure from "Perspectives on cavitation enhanced endothelial layer permeability". The figure shows the difference between non-inertial and inertial cavitation in terms of ultrasound amplitude and the effects of the compression and rarefractional phase on the cavitation nuclei. As well as showing the effects most often associated with each type of cavitation – microstreaming and subsequent "pushing" of particles, and shockwaves and microjets creating paths for particles to move. Reproduced with permission

1.6.2 Cavitation nuclei

There are many forms of cavitation nuclei, microbubbles (MBs), nanobubbles, nanodroplets and solid particles. Cavitation nuclei can range in size, and the size of the cavitation nuclei will affect their behaviour and effects in the ultrasound field (174,175), such as the pressure needs to be increased for nanodroplets in comparison with microbubbles due to the need for nanodroplets to vaporise before forming the gas that can be cavitated(176). Microbubbles are used clinically as contrast agents for imaging due to their echogenicity and propensity to disrupt under acoustic pressures. Due to the high compressibility of MBs, under the right ultrasound conditions, their radius can vary by as much as a factor of two, leading to mechanical effects on the surrounding environment (177).

There have been various designs of MBs to better target and release payloads, including an FDA-approved Doxil MB combination (178). These MBs have Doxil attached to the surface

of the MB via molecular linkers, and oscillations occur, which allow for the shedding of the Doxil (179). There are also applications for other drugs, DNA and RNA, to which extent these molecules can be absorbed onto the surface of the MBs (180). Some downsides to utilising MBs as drug carriers include the size increase that the MB experiences under oscillation, which can mean the bubble is between 2 and 10 um in diameter (181), preventing accumulation in some tumours.

The barriers MBs face are like those experienced by drug-loaded liposomes and oncolytic viruses. Accumulation due to the enhanced permeability and retention effect (EPR) is not significant enough to impact tumours (182). The limitations of MBs are highlighted when the pressures needed for drug delivery are applied to the agents. It has been shown that the MBs can be destroyed in the HIFU ultrasound field relatively quickly (around 30 s), which means that they cannot sustain cavitation long enough to ensure substantial drug delivery without re-administration of the agents (183,184). This would mean multiple injections of MBs would be required to ensure cavitation continued for a long enough duration to enable deep tissue penetration of therapeutics. While MBs have been approved as contrast agents for ultrasound contrast imaging, they are limited in dosage to a maximum of 4 mL per treatment (185).

SonoTran Particles (STPs) were developed to circumvent the limitations with MBs to allow for longer and sustained cavitation and increased circulation time (186). These STPs are approximately 480 nm (186), have a negative zeta potential of greater than -20mV, and can be seen to remain cavitating for up to 10 minutes *in vivo* in mice (186). They are produced using a seeded polymerization technique and made using bioinert polystyrene (Figure 1.6.2.1) (186,187). The STPs are coated with divinyl benzene (DVB) which induces swelling and deformation of the polystyrene and methyl methacrylate (MMA). This leads to a cup-shaped polystyrene structure, which is then dried, set, and re-suspended in water, where it traps air (186,187).

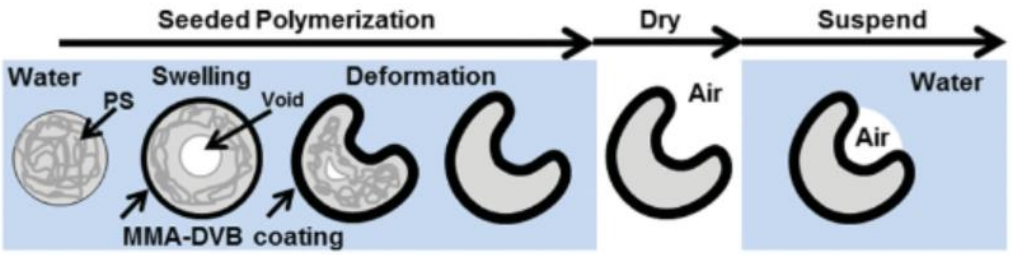

Figure 1.6.2.1: Adapted schematic from "Ultrasound-Propelled Nanocups for Drug Delivery" shows the seeding technique used to produce STPs. Polystyrene is coated with MMA and DVB. The DVB cross-linked MMA induces swelling and deformation of the polystyrene particles. Once deformation has occurred, the suspension is dried. When resuspended, the particles will trap gas within the newly formed cavity.

When these STPs are placed in an ultrasound field, the gas bubble trapped in the cup begins to expand and eventually detaches from the cup, Figure 1.6.2.2. The bubble experiences inertial cavitation under the ultrasound conditions set out and finally collapses (186). The STPs can be 'tuned,' meaning the acoustic response can be tailored over a range of pressure amplitudes. There is a direct correlation between the cavity size of the cup and the amplitude at which cavitation occurs: the smaller the cavity, the larger the pressure amplitude required to achieve cavitation (166).

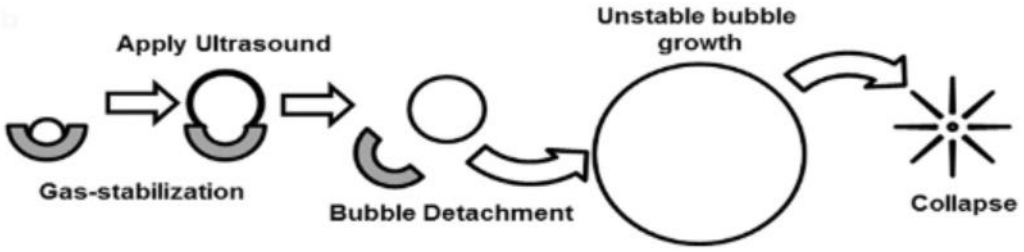

Figure 1.6.2.2: Adapted schematic from "Ultrasound-Propelled Nanocups for Drug Delivery" showing the behaviour of STPs in the presence of an ultrasound field. As the gas bubble experiences the rarefractional pressure phase of the ultrasound wave, the bubble grows and will detach from the STP. Once the bubble has detached, it will continue to grow in the rarefractional phase until the compression phase of the wave, where it will undergo a rapid collapse.

When treating tissue or using therapeutics sensitive to higher pressure amplitudes and localised temperature increases, this is important to consider. The size of the STPs allows for using the intratumoural (IT) injection method. When STPs are injected intravenously (IV), they accumulate within the liver (186), with 15-20% remaining in circulation up to 20 minutes post-

injection in mice, which is up to 10 times longer than MBs circulate (188). Enhanced and sustained cavitation can allow a greater ability to penetrate deeper into tissue and tumours with loaded nanocarriers, allowing for a higher dose of therapeutic or oligonucleotide. Using cavitation agents and ultrasound to drive drugs and carriers further and deeper into tissue is one of the mechanisms that can be utilised from a range of already clinically approved methods.

Three main characteristics can categorise Ultrasound-induced mechanisms of drug delivery, 1) enhanced transport of particles, 2) perturbation of nanocarriers and 3) cell permeabilisation and epithelial disruption. Looking in more detail at each, it is a distinct and significant advantage of ultrasound to be able to enhance the transport of particles. This transport of particles occurs in several ways. First, starting with the presence of the drug/agent if present in the blood via intravenous injection, but aiming the ultrasound at a target area, using cavitation nuclei and the correct parameters, these drugs and agents have been shown to move from the blood vessels (189,190), across the capillary wall and into the dense ECM awaiting. Furthermore, to enhance the amount and allow for targeting, further extravasation through the ECM has been demonstrated (89,191,192). This allows for further investigation into drugs and agents that may treat tumours directly or change the make-up of the ECM to make other forms of treatment more successful, such as changing the levels of hypoxia so radiotherapy can be more effective (193). Much in the same way as this can be used for drugs and agents, and it can transport nanocarriers housing more advanced forms of disease treatment further and to specific targets.

Moreover, finally, another defining characteristic of ultrasound-mediated drug delivery is the ability to permeabilise cells and cause epithelial disruption to allow delivery *in vivo* (194). *In vitro,* the wide-ranging effects of ultrasound-mediated delivery have been widely shown, whether through sonoporation, sonopermeabilisation or inducing different endocytotic uptake pathways (195,196). This has been much more difficult to show *in vivo.*

Enhanced transport of particles can occur in the presence of ultrasound without cavitation agents. Fluid can begin to oscillate in the presence of cavitation nuclei that are in an ultrasound field (197). This oscillation is increased in the presence of cavitation agents and can be controlled by controlling the concentration of the cavitation nuclei for the reasons mentioned above, including lowering the cavitation threshold for the medium containing the agents. *In vitro,* diffusivity and convection have been shown to increase the driving of particles (198,199). However, *in vivo*, this effect is likely lessened due to the fluid convection that occurs rapidly within a vessel.

The oscillations of a bubble produce greater effects, and cavitation can result in microstreaming (200). Convection can be created due to the stable oscillation of a bubble. Microstreaming can result in circular currents, which can drive particles at high velocities up to 10 m/s (201), and extremely high viscous shear forces near the bubble's surface (202). The acoustic pressure due to oscillating bubbles also play a role in enhancing the transport of particles. Particles denser than the suspension are pushed towards the bubble compared to less dense particles, which are made away from the bubble, increasing the dispersive transport of carriers (203). When cavitation agents are within the same ultrasound field, they spread and attract more dense carriers such as liposomes.

This leads onto the role ultrasound plays in the distribution of nanocarriers. The shear stresses caused by oscillating bubbles can be used to break open vesicles (204). collapsing bubble produces a shock wave, resulting in a wave moving through the fluid that can be used to break open carriers such as vesicles (205,206). A collapsing bubble produces a shock wave that results in a wave moving through the fluid. Again, this wave of pressure in the fluid can be used to break open carriers, such as vesicles, if the critical stress is exceeded (205,206). As the shock wave passes through the fluid, it loses energy, meaning it can no longer rupture carriers.

However, it can still create a carrier's movement, pushing towards and into the microenvironment.

The stresses from oscillating bubbles affect the nanocarriers and the cells that experience the stress (207). Cells are subjected to microstreaming, microjetting, and temperature increases over rapid timescales caused by oscillating and collapsing bubbles. If this is experienced by a cell at a rigid boundary such as a capillary, this can result in a liquid jet hitting that cell, causing rupture of the affected cell (206). Rupture of the epithelial cell lining may play a role in the greater than normal extravasation seen with ultrasound/cavitation-based drug delivery systems. The stresses may also play a more mechanical role in permeabilization. The cellular response to physical stresses has been well documented in tissue engineering (208), and physical stresses can be enough to change the normal function or permeability (143).

Cavitation nuclei can also be loaded with proteins, ligands, and other targeting agents to improve specificity. An example is microbubbles produced and labelled with transferrin to target specific cancer cells (209,210).

1.6.3 Biological effects of ultrasound

For the past three decades, ultrasound and cavitation have been explored as ways of "opening" up cells and delivering drugs and macromolecules. Extensive research has gone into the process and looked at the effects. There are multiple different biological effects attributed to the use of ultrasound and cavitation, and they include sonopermeabilisation, sonoporation, sonoprinting, destruction of cells, heating of tissue, and immune responses, to name a few. Below these will be discussed in more detail.

As briefly mentioned, sonoporation is the formation of pores on the cellular membrane, modulated by ultrasound and the associated cavitation. Sonoporation leads to increased membrane permeability, leading to higher transfection rates and higher quantities of drugs

being delivered. The advantage of sonoporation over many other delivery methods is that it is a non-invasive and specific procedure, allowing specific areas of the body to be targeted. The efficiency of sonoporation is under constant scrutiny. It is dependent on several factors, including ultrasound parameters such as intensity, frequency, cavitation energy delivered, the concentration of delivered gene or therapy, the exposure period, duty cycle, and the use of contrast agents or cavitation nuclei to improve extravasation.

Tissue destruction and thermal ablation are considerations when using focused ultrasound. Thermal ablation and tissue damage can be mitigated by using specific ultrasound parameters to control the amount of energy deposited over a time period (211). One way to do this is to manage the number of cycles and the duty cycle of the ultrasound. Reducing the "on" time of the ultrasound allows the thermal effects to be controlled. Another way to control the energy deposited is by tightly controlling the pressure amplitudes used (212). This biological effect of the thermal ablation can be used positively in terms of controlled destruction of cancer cells in the case of tumours (213). However, depending on the goal of the treatment using ultrasound, for example, gene delivery, thermal ablation must be avoided.

The damaging effects of ultrasound and cavitation are not limited to thermal ablation. Non-thermal effects of focused ultrasound can also destroy or damage cells (214). Due to the effects discussed here, there is increased likelihood of an immune response to the damage or destruction of cells and tissue (215)

Whether to control delivery or damage, it is important to be aware of and monitor cavitation levels during exposure. One way this is done is through Passive Acoustic Mapping (PAM). Passive acoustic mapping allows for real-time, three-dimensional monitoring and will enable users to adjust treatments as they occur. It works by "listening" to the cavitation events within the target tissue (216). This is achieved by using an ultrasound array, often in the form of a b-

mode receiver, which can detect and relay the events to the computer and overlay the events as an image on the tumour or tissue of the target. PAM analysis was used to monitor the real-time signal of acoustic emissions from tumours and in vitro samples for the work discussed in this thesis.

Chapter 2 – Examination of *in vivo* ultrasound and SonoTran particle exposure

2.1 Introduction

The conventional definition of gene therapy is a therapy in which a dysfunctional copy of an aberrant gene is replaced. However, this definition has broadened as the range of different types of nucleotide-based therapies at our disposal has increased, and our understanding of how these therapies can achieve a therapeutic effect has improved. Indeed, 'gene therapy' may now be more accurately described as an approach that uses nucleotides as a drug. This includes the use of double- or single-stranded DNA and RNA for effector functions as different as gene replacement (CRISPR/Cas9), production of a wild-type copy of the desired protein (mRNA), or destruction of the mRNA transcript of a mutant protein (siRNA). This project is particularly interested in the delivery of messenger ribonucleic acid (mRNA) encoding wild-type proteins, which has garnered much recent research interest (41,217,218). This is because mRNA could offer a relatively simple means of producing proteins to restore normal cellular function, stimulate the immune response in vaccination strategies, or inhibit the survival of cancer cells. This project is mainly concerned with the latter of these applications and, to that end, how mRNA can be optimally delivered to tumours to instigate a therapeutic response.

Unfortunately, many factors still limit gene therapy despite the great potential and some notable recent successes (219–222). These include the inability of free therapeutic nucleotide to avoid detection and destruction within the human body, the rapid clearance of gene therapy vectors from the bloodstream and the low transfection efficiency of any injected gene therapy dose that does reach its tissue target (25,223,224). Indeed, achieving efficient gene delivery is one of the biggest challenges facing the field of gene therapy today. In response, a wealth of research has been performed to investigate the use of viral and non-viral nanoparticles as delivery vehicles for gene delivery (225). Nanoparticles are designed to protect nucleotide cargo from rapid degradation within the bloodstream/tissue and immune-mediated clearance (226). Unfortunately, this remains very much 'work-in-progress' as pre-existing immunity often

neutralises viral vectors, whilst non-viral vectors are destabilised by blood components and/or subject to reticuloendothelial cell-mediated clearance in the liver and spleen. However, even if improved systemic circulation times can be achieved, significant barriers to drug delivery remain (10,227,228). Indeed, to date, only one non-viral gene delivery vector (229) has gained FDA approval for intravenous administration and analysis of its pharmacokinetics suggests it is subject to very rapid clearance by the liver, a process that probably involves destructive removal of the majority of dose by the kupffer cells, but allows a just sufficient amount to reach target hepatocytes as well.

With specific regard to cancer treatment, passive accumulation within the tumour environment remains limited (230,231), and the efficiency with which nanocarrier systems release their cargo upon arrival within the target can vary greatly. These inefficiencies have led to the design of a raft of technologies that provide mechanisms for tumour-targeting mechanism and triggered release of therapeutic cargo (232–235).

Both cavitation forms, inertial and non-inertial, have distinct acoustic emission profiles, with inertial cavitation exhibiting broadband frequency acoustic emissions and non-inertial cavitation giving rise to acoustic emissions that are harmonics and ultra-harmonics of the exposure frequency. The bubble oscillations produce a sound wave that travels back to a receiver, either in the form of a single element transducer or the elements of an array which enables beam forming. This allows for the cavitation to be detected, monitored, and compared between experiments.

Passive acoustic mapping is a technique used to monitor cavitation events, being able to not only detect, but localise and quantify cavitation during a therapeutic treatment. By utilising B-mode ultrasound arrays (materials and methods section), a way of mapping cavitation events on top of B-mode images of tumours was used to detect where cavitation events were occurring.

The ability to quantify the amount of cavitation is crucial considering the potential for tissue damage from high levels of cavitation. There are of course limitations to the set-up and comparing the quantitative nature of the PAM analysis across different systems and set-ups, however when using the same system throughout experiments, comparisons can be made with the work presented in this and all chapters of this thesis.

At the time of writing, there are 46 active clinical trials utilising RNA as a treatment or specific marker for a range of cancers (236). Many companies are dedicated to using RNA as a treatment for various diseases, including Moderna, BioNtech and Astra Zeneca. This means mRNA therapies are being developed to treat multiple diseases and conditions, including cancer, cardiovascular and infectious diseases. To achieve this, mRNA has been encapsulated in lipid nanoparticles (237). The use of encapsulated mRNA reiterates how the human body has adapted and evolved different defence mechanisms to protect against the invasion of RNA and DNA. These defences lead to free 'naked' RNA degradation in the blood and tissue through nuclease activity and immune-mediated responses (238,239). One mechanism to overcome this degradation is to encapsulate the nucleotide in a nanocarrier. Such a lipid-based nanocarrier was developed by AstraZeneca and was tested here; this LNP has a near-neutral zeta potential and an average size of 88.5 nm. Encapsulating the nucleotide allows a Trojan horse approach, whereby the package to be delivered is hidden from the immune system. This work aimed to assess how this process could be used in conjunction with ultrasound and cavitation nuclei to deliver the encapsulated mRNA. A comparison study with different cavitation nuclei and naked mRNA was also conducted. Previous work (240) had been completed *in vitro*, using CT26 cells in agar phantom models. It indicated that the combination of ultrasound and cavitation nuclei could improve the uptake and expression of the encapsulated mRNA.

This Chapter describes the processes and optimisations involved in evaluating the uptake of mRNA constructs into mammalian cells and profiling the resulting protein expression. The

studies examine the effects of ultrasound and cavitation on the expression of a reporter protein encoded by the delivered mRNA and the effects these cavitation events can have on the tumour environment. Comparisons are made between free, i.e., 'naked' mRNA and encapsulated mRNA, examining the impact of cavitation on both. A range of cavitation regimes are explored and examined as a potential mechanism for delivery.

2.2 Materials and methods

2.2.1 Cell line and cell culture

Murine colorectal carcinoma CT26.WT cells (ATCC, CRL-2638; American Type Culture Collection, Rockville, MD, USA) were grown to approximately 90% confluence with a minimum of 95% viability using Roswell Park Memorial Institute 1640 medium (RPMI 1640; R8758, Sigma-Aldrich Company Ltd, Dorset, UK) supplemented with 10% fetal bovine serum (FBS; F7524, Sigma-Aldrich, Dorset, UK). Cells were grown to the confluence at 37 °C in a humidified atmosphere of 5% carbon dioxide. Once at the desired confluence, cells were harvested and prepared for implantation. Cells were washed using Dulbecco's Phosphate Buffer Saline solution (PBS; D8537, Sigma-Aldrich, Dorset, UK) and harvested using 1X trypsin-EDTA (T3924, Thermo Fisher Scientific, UK). Once the cells had detached from tissue culture flasks, the trypsin was neutralised using three times the volume of RPMI. Subsequently, the cell mixture was taken off the flask, placed in a centrifuge tube, and centrifuged at 1000 relative centrifugal force (RCF) for 5 minutes at room temperature to form a cell pellet. The excess RPMI 1640 and trypsin were removed after the pellet formation. The cells were once more resuspended in fresh RMPI 1640, and the centrifuge step was repeated to ensure all trypsin had been removed. The cells were then suspended in either FBS-free RPMI 1640 or PBS as per the animal project licence. A cell count and viability assessment were then obtained using the trypan blue dye exclusion method and a haemocytometer. Cells were then prepared to the desired concentration for *in vitro* testing or implantation into murine models by adding FBS-free RPMI 1640 or PBS as required to form a stock solution for implantation.

2.2.2 Tumour inoculation and animal welfare

Balb/c mice aged 5-6 weeks (BALB/cAnNCrl; Charles River Research Animal Models and Products, UK) were purchased and allowed to acclimatise for one week before tumour inoculation. Cells were prepared as described above and transported to the animal unit on ice.

Each mouse had its weight recorded and was uniquely marked. The mice were then placed under anaesthetic using 2-5% isoflurane. The mice were placed on a face mask to maintain anaesthesia, and a heating pad was placed under each mouse to help maintain body temperature. Each mouse was then inoculated with 50 µL containing 5 x 10^5 CT26 cells by subcutaneous injection with 27-gauge needle. When using bilateral models, a subcutaneous injection took place in each flank. The mice were then monitored to assess their recovery from both the anaesthesia and the procedure, with additional monitoring carried out twenty-four hours post-procedure and every three days after that. Weights and tumour growth were monitored for each mouse. Tumour size was calculated using callipers and half the product of the tumour's length, width, and depth. When tumours reached >85 mm^3, they were deemed treatable. Animals were housed and cared for according to UK Home Office guidelines, and experiments were performed under a Home Office approved and regulated and local ethics committee approved project licence.

2.2.3 Lipid nanoparticles and mRNA

The lipid nanoparticles (LNPs) were formulated by AstraZeneca (UK) and were complexed with firefly luciferase (FLuc) mRNA (Trilink biotechnologies, L-7202). The LNPs had a mean diameter of 88.5 nm as assessed by dynamic light scattering (Malvern Zetasizer Nano, figure 2.2.3.1) and a net surface charge of +9 mV as assessed by zeta potential measurements (Malvern Zetasizer Nano, table 2.2.3.1). A total of 3 repeat LNP samples were run for each analysis method. Dynamic light scattering was used as the size of the LNPs fit within the dynamic measuring range given by the manufacturer. The free, naked mRNA also encoded for FLuc and was purchased from Trilink biotechnologies.

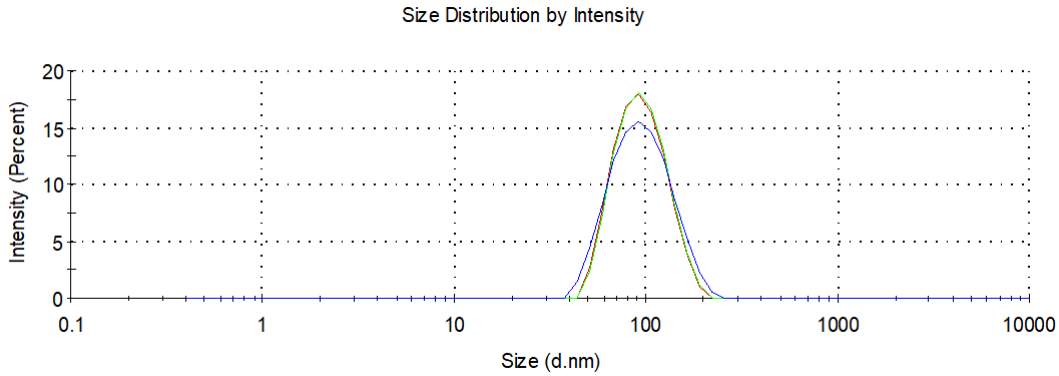

Figure 2.2.3.1: Dynamic light scattering measurement of lipid nanoparticle samples, conducted at room temperature in PBS at pH 7 as per DLS manufacturer's recommendations. 3 samples were measured with a mean diameter of 88.57 nm and a standard deviation of 0.59.

Charge measurements

Measurement values	8.42 mV
	8.43 mV
	8.16 mV
Mean	8.34 mV
Standard deviation	0.15 mV

Table 2.2.3.1: Dynamic light scattering measurements of the zeta potential of lipid nanoparticle samples, conducted at room temperature in Hepes buffer solution at pH 7.2, per DLS manufacturer's recommendations. 3 samples were repeated.

2.2.4 Ultrasound

The ultrasound set-up was comprised of two high-intensity focused ultrasound (HIFU) transducers (Figure 4.2.4.1), which were perpendicularly aligned, with a focal length of 63 mm from the centre of each transducer. The transducers had a fundamental frequency of 0.5 MHz. Each transducer had a rectangular cut-out to allow for the placement of an L11-5v 128-element linear array (Verasonics Inc.), allowing the detection and mapping of cavitation events. B-mode imaging was utilised during the treatment to ensure that the tumour was in the correct position, and cavitation maps were applied using a custom PAM algorithm (OxSonics Ltd, UK) to allow temporal and spatial mapping of cavitation events occurring in the tumour. The transducers

and mouse were submerged in the water tank filled with degassed water and heated and maintained at 37°C.

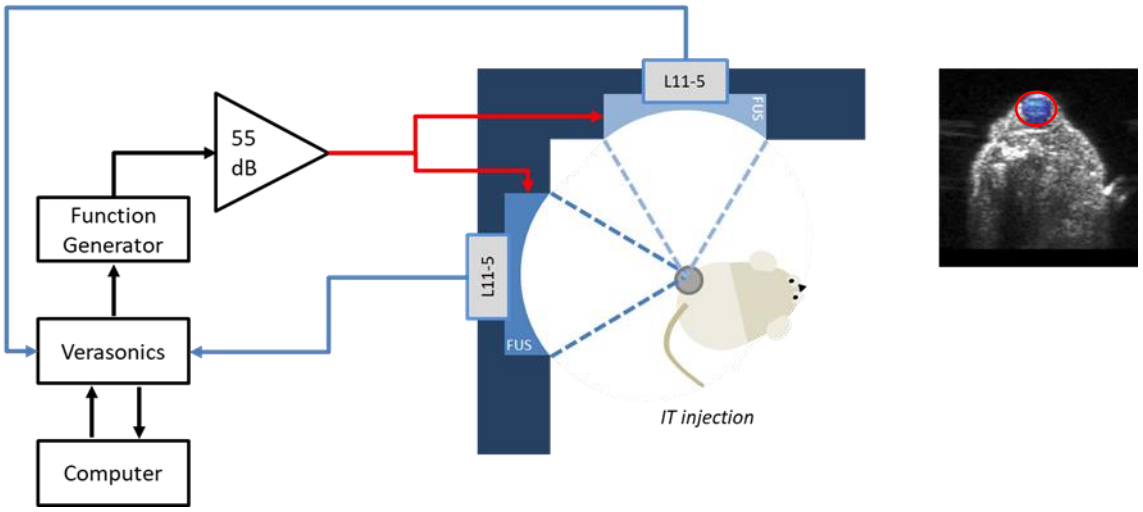

Figure 2.2.4.1 Schematic of the ultrasound set-up used to treat mice, showing the focused ultrasound transducers and b mode imaging transducers (L11-5) arrays. Inset is an image of the b-mode of a treated tumour (red circle) depicting the overlay of cavitation regions

The ultrasound parameters are as follows: a driving frequency of 0.5 MHz, a pulse repetition frequency of 0.5 Hz, and a duty cycle of 5% was used for STP-treated mice. Number of cycles was changed for microbubble treated mice, from 50,000 to 100 per burst, with a total treatment time of 300 seconds for both STP and microbubble-treated mice. The pressure amplitudes for ultrasound treatments using STPs varied, but the cycles remained fixed at 50,000 cycles. Number of cycles chosen based on previous successful *in vivo* delivery of viral vectors and antibodies (241–244). The pressure was reduced for the microbubble cavitation nuclei, and the cycles were decreased. The peak rarefactional focal pressure (PRFP) varied from 0.3 – 2.1 MPa was used, with an exposure time of 300 seconds for each mouse, resulting in differing amounts of energy delivered.

To calculate the quantities of energy experienced, the passive acoustic mapping magnitude (PAM) plot generated by the OxSonics Matlab script was used, an example of which can be seen in Figure 2.2.4.2. PAM units are calculated by measuring the first 200 ms of the signal received by the array. This information is taken and stored for each event and used to determine

the amount of cavitation delivered to the mouse over time. The area under the curve was calculated and used as a comparative metric between experiments.

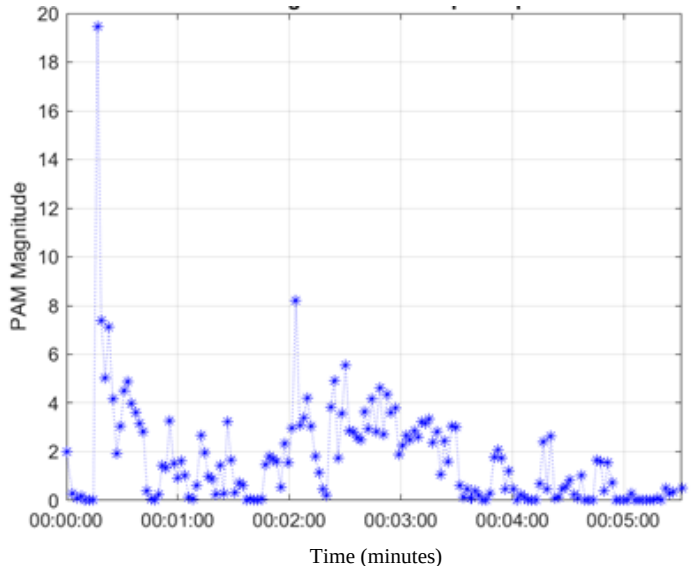

Figure 2.2.4.2: An example of a PAM magnitude plot generated by the Matlab script used to compare cavitation received by different animals. The area under the curve is calculated and denoted as cumulative cavitation.

Before treatment, tumours were measured, and a welfare assessment was performed, ensuring the mice were healthy regarding weight and for the absence of signs of any pain or distress. Using isoflurane, the mice were then placed under anaesthetic at 3 – 5 % and maintained under anaesthetic using 2 – 3%. Subsequently, they were placed on a bespoke holder with a face mask to maintain anaesthesia. The mice were depilated to prevent air from being trapped on the surface of the fur and secured to the holder before any treatment. The mice were then lowered into a water tank, ensuring the head and face mask remained above the water line and then treated.

Before treatment, a cannula was preloaded with LNPs or naked mRNA and inserted intratumourally. 5 µL of PBS was then used for flushing the LNP or naked mRNA through the cannula. Subsequently, 5 µL of cavitation nuclei at varying concentrations (0.1 µg/µL or 1 µg/µL for STPs and 2 x 10^5 /µL for microbubbles) were flushed through to be followed finally by 10 µL of PBS to ensure cavitation nuclei were in the tumour.

2.2.5 Cavitation nuclei

Two types of cavitation nuclei were employed in the study; SonoTran particles (STPs, OxSonics Ltd, UK) were prepared from a stock concentration of 25 mg/mL and diluted to 21.4 mg/mL using 40% glucose to create a new standard stock solution of 21.4 µg/µL in 5% glucose before injection. This standard stock solution and a 1:10 further dilution were used for treatments, resulting in a 0.1 µg delivered dose in total blood volume. SonoVue® microbubbles (Bracco, Milan, Italy) were prepared as per the manufacturer's guidelines to a concentration of 1-4 $x10^8$ bubbles per mL.

2.2.6 *In vivo* imaging

Each mouse was imaged at three-time points post-treatment - 12, 24, and 48 hours - to monitor the luciferase transgene expression from within the tumours. These time points were chosen based on expression levels in previous pilot studies and project licence restrictions. At each time-point, the mice were anaesthetised, as discussed in section 2.2.2, and given an intraperitoneal (IP) injection of Pierce™ D-luciferin Monopotassium Salt (88294, Thermo Fisher Scientific) made up to a concentration of 15.8 mg/mL in PBS and delivered at a volume of 100 µL. The mice were then imaged using a Perkin Elmer Lumina LT series III 10 minutes post the IP injection to allow for adequate uptake of d-luciferin. The IVIS was set to have an open emission filter and bioluminescence measurements selected from the imaging wizard, with a set exposure time of 10 seconds. The mice were recovered within fifteen minutes of the start of the procedure and monitored for recovery for 30 minutes after the 12- and 24-hours imaging sessions. At 48 hours, the mice were culled at the end of the IVIS imaging session and tumours excised. The excised tumours were photographed and frozen in a -80 ˚C freezer for additional analysis. The IVIS images were later analysed using Perkin Elmer Living images® software, where regions of interest and radiance were analysed for expression.

2.2.7 Tumour cell viability assay

Cell viability was tested to ensure the chosen parameters of the US exposure would not cause cell death before the mRNA had the opportunity to be delivered and translated. Tumours which were exposed to the same treatment conditions, including delivered volume, but without either LNPs or free mRNA, were also collected. The tumours were immediately removed post-treatment and placed in PBS supplemented with 5% FBS to maintain viability while being transferred on ice from the animal facility to the laboratory. The tumours were then placed in C-max tubes with 10 mL of digestion media. The digestion media consisted of RPMI 1640, 1.25 mg/mL collagenase (C5138, Sigma-Aldrich, Dorset, UK), and 0.3 mg/mL DNase (10104159001, Sigma-Aldrich, Dorset, UK). The tumours were then blended using a gentleMACS™ Octo Dissociator (Miltenyi Biotec, Surrey, UK), set to a pre-programmed tumour tissue protocol. The homogenate was then filtered through a 70 µm cell strainer. The samples were spun at 500 x g for 5 minutes at 4 °C, and the supernatant was removed. Zombie violet (cat. no. 423113, BioLegend) is an immunofluorescent stain used for flow cytometry assessment of live/dead staining and was prepared to various concentrations in PBS 1:100, 1:500, and 1:1000 dilutions, as per the product recommendation. This was to ensure the correct flow cytometry gating to see the cell samples could be achieved. The samples were then incubated with 100µL of zombie violet dye for 20 minutes before being tested using the flow cytometer, a BD FACS Canto II.

2.2.8 Quantification - Luciferase Assay

Tumour samples were stored at -80 °C for 24 hours post removal. Following a freeze-thaw cycle, the tumours were analysed for luciferase expression using the Luciferase Assay System (E1500; Promega, Southampton, UK) and a microplate reader (FLUOstar Omega; BMG Labtech, Aylesbury, UK) for luminescence measurements. Tumour samples were prepared using 10 µL of 1x cell lysis buffer per 1 mg of tissue. Each tumour was then homogenised and

freeze-thawed for a second time to ensure the maximum destruction of the cells to allow the protein to be free and interact with the luciferase assay. The luciferase assay kit was then prepared as per manufacturers' guidelines. Costar white 96 well plates (CLS3912, Sigma-Aldrich, Dorset, UK) were used to hold 20 µL of sample and 100 µL of the luciferin assay solution. Each sample was plated in triplicate, the luminescence emission measured, and the mean value was calculated.

2.3 Results

2.3.1 Optimisation of ultrasound for in vivo delivery of lipid nanoparticles (LNP)

Several *in vivo* delivery studies were conducted using the set-up described in the methods (Section 2.2.4). Due to the poor reported pharmacokinetic (PK) profile of the LNP formulation tested here following intravenous delivery, an intratumoural injection route was used. Data on the impact of ultrasound on the viability of CT26 cells post IT injection was scarce, so this first had to be profiled.

2.3.2 Tumour cell viability post cavitation events

An *in vivo* experiment was designed and performed to assess the impact of change in pressure and concentration of STPs on tumour cell viability. Four groups were employed (Table 2.3.2.1), using high pressure (2.1 MPa) or low pressure (1.6 MPa). Each group was treated with either the standard concentration of STPs or a 1:10 dilution, with all groups using delivery via intratumoural (IT) injection. Control tumours were also included, which were not exposed to ultrasound or cavitation, but otherwise followed the same experimental and tissue processing protocol. Treatment parameters are defined in table 2.3.2.1.

Group	STP Concentration (mg/mL)	Pressure (MPa)	Number of cycles	Duty cycle	Duration
Control	0	0	N/A	N/A	300 s
1	1	2.1	50,000	5%	300 s
2	1	1.6	50,000	5%	300 s
3	0.1	2.1	50,000	5%	300 s
4	0.1	1.6	50,000	5%	300 s

Table 2.3.2.1: Mice were divided into 1 control group and 4 treatment groups, as seen in the table. Number of cycles, duty cycle and duration of treatment remain fixed. STP concentration was between 1 and 0.1 mg/mL with pressure between 2.1 and 1.6 MPa. Control group with no STPs and no ultrasound as control. N=3

The tumours were removed and processed for flow cytometry (section 2.2.8), and zombie violet was used to assess viability. Example flow cytometry gating of zombie violet-stained samples of is shown in Figure 2.3.2.1. Table 2.3.2.2. shows the flow cytometry results, where zombie violet was used per the manufacturer's guidelines to determine live and dying cells. Notably, even the control tumours (no ultrasound) had an average death of 12.8%. This may relate to the underlying number of dead cells within a CT26 tumour or losses in viability during the rescue and processing of the sample. Regardless, it demonstrates the importance of this control, and this average was subtracted from the cell death percentages of each of the treated samples and before plotting of values in Figure 2.3.2.2.

	Sample Number	Percentage Dead	Average	Standard deviation
Control (No US)	1	11.1		
	2	14.6		
	3	12.7	12.8	1.8
Group 1	1	79.4		
	2	74.0		
	3	69.9	74.4	4.6
Group 2	1	53.4		
	2	50.6		
	3	47.7	50.1	2.2
Group 3	1	72.3		
	2	70.0		
	3	70.7	71.0	1.2
Group 4	1	13.8		
	2	37.9		
	3	33.7	29.5	10.8

Table 2.3.2.2: Flowcytometry results for each group, showing the individual percentage death, the average, and the standard deviation for each group of treated mice. N = 3

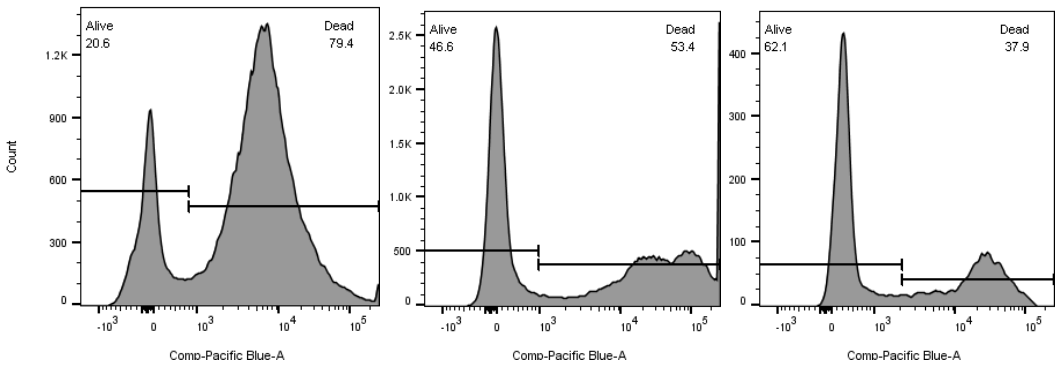

Figure 2.3.2.1**:** Example of forward and side scatter and flow cytometry histograms for a single sample from each of groups 2, 3 and 4. Staining with Zombie Violet®. Cells were collected, prepared and assayed as described in methods section**.** 10,000 events were counted with original gating in fsc and ssc maintained for all samples.

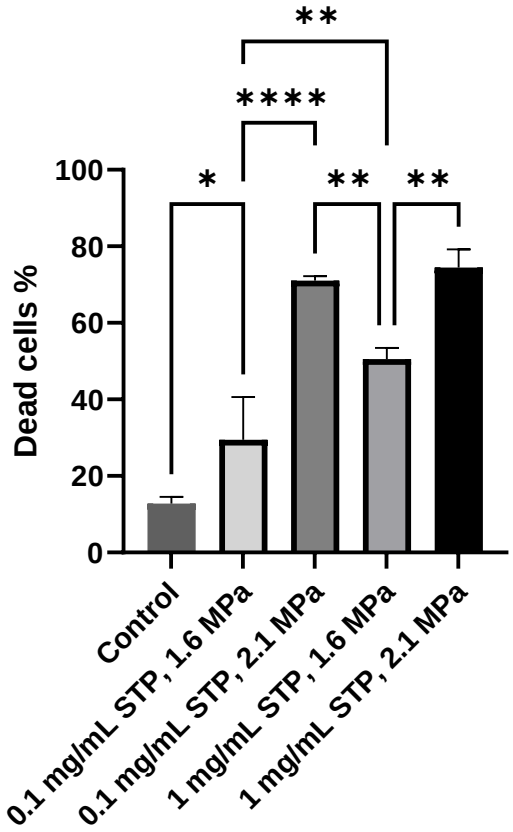

Figure 2.3.2.2: Percentage cell death upon exposure to ultrasound and STP as measured by flow cytometry. Average for each group is plotted. N=3,; error bars represent standard deviation, '*' $p<0.05$, '***' $p<0.001$ using one-way ANOVA, all groups compared with Tukey HSD.

Figure 2.3.2.2 suggests a relationship between the control corrected cell death, and the pressure applied, and the dose of STP, as mice exposed at 2.1 MPa with 1 mg/mL displayed ~ 2.5-fold

greater cell death than those exposed to 1.6 MPa with 0.1 mg/mL (74.4% vs 29.5%, $p<0.01$). For the pressure of 1.6 MPa, there was also greater cell death with the higher STP concentration.

To probe the relationship between the amount of cavitation and the level of cell death, the two are plotted against each other in Figure 2.3.2.3. The data is 'control corrected', i.e., the level of death within the tumour in the absence of exposure (~12%) has been removed. Cell death correlates strongly ($R^2 = 0.987$) with the cumulative cavitation suggesting that cavitation likely contributes to cell death.

As expected, when the cavitation levels were calculated (Section 2.2.4) and related to exposure parameters, higher pressure and higher STP concentration led to higher cavitation. However, it is notable that the differential in cell death level between 1.6MPa with 1mg/mL and 1.6MPa with 0.1 mg/mL is greater than the differential between these two doses at 2.1MPa. For example, 1.6MPa with 0.1 mg/mL exhibited the lowest cell death percentage, averaging 16.3% above the control group. The cavitation levels were also much lower for this group, four times lower than the highest cavitation in the 2.1 MPa and the 1mg/mL STP group, and three times lower than the 0.1mg/mL STPs but at 2.1MPa, as can be seen from Figure 2.3.2.3

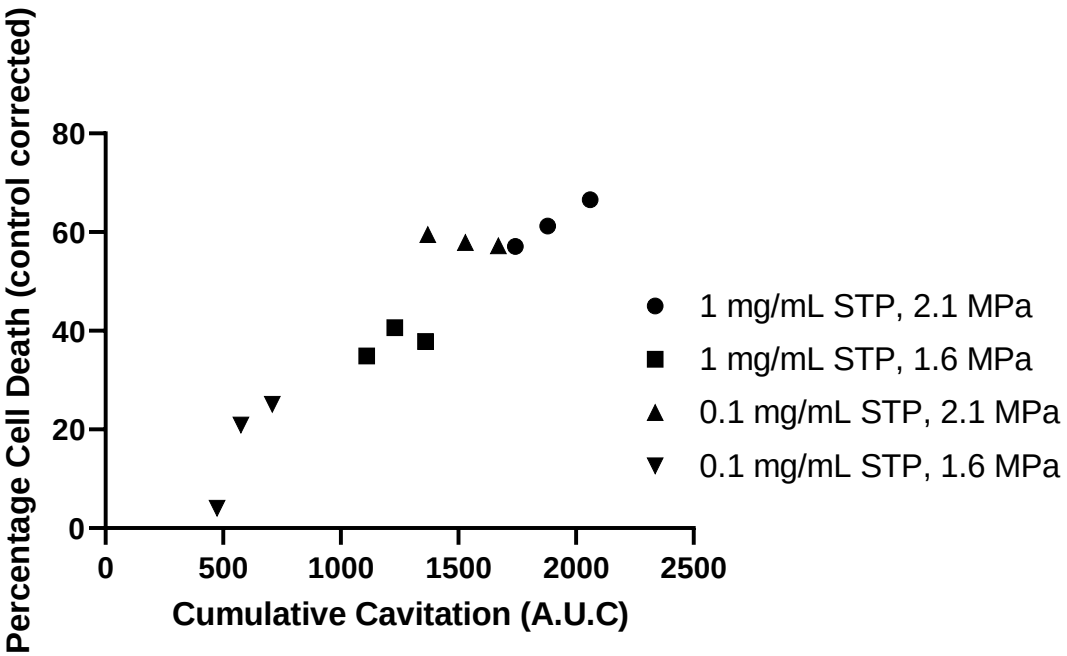

Figure 2.3.2.3: Relationship between cavitation measured and cell death for each treated tumour. Percentage cell death as measured by flow cytometry; control corrected for groups 1-4. Group 1 (Circle) –1 µg/µL STP at 2.1 MPa, Group 2 (Square) – 1 µg/µL STP at 1.6 MPa, Group 3 (triangle) – 0.1 µg/µL STP at 2.1 MPa and Group 4 (inverted triangle) – 0.1 µg/µL STP at 1.6 MPa. Cumulative cavitation was calculated using the area under the PAM magnitude plot for each mouse.

This may indicate that the cell death at higher pressure is a consequence of both STP nucleated cavitation and cavitation nucleated by gas bubbles in the solution, making it less likely to be dependent on the STP concentration alone. As part of the experiment, pictures of the tumours were taken following excision to examine for any visible damage, these images can be seen in Figures 2.3.2.4.

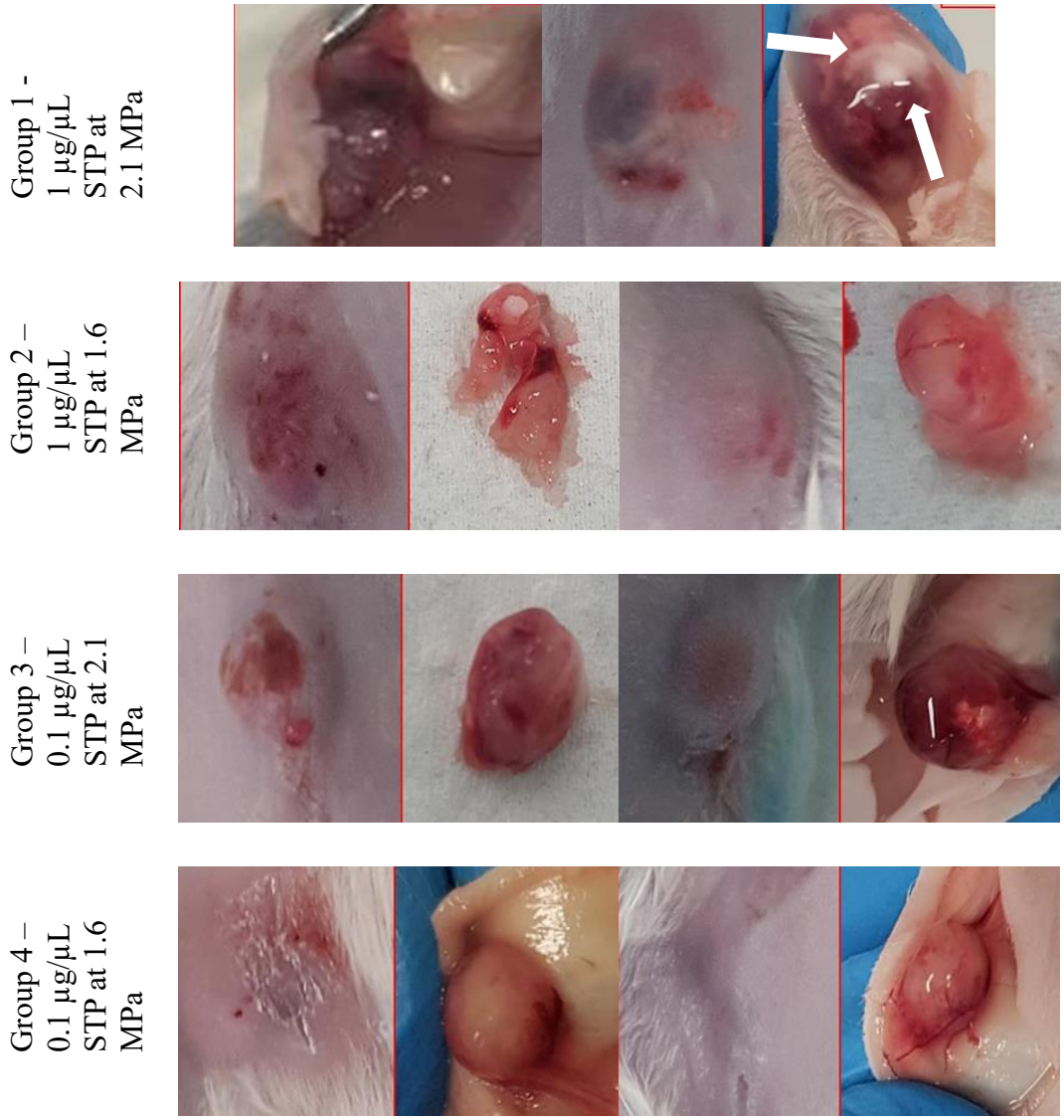

Figure 2.3.2.4: Examples of treated tumours pre and post excision. As can be seen from the images, tumours varied in appearance post-treatment. Initial damage that can be seen with the eye can be seen translated in flow cytometry measurements. Group 1 – (1 mg/ mL STP at 2.1 MPa), Group 2 – (1 mg/ mL STP at 1.6 MPa), Group 3 – (0.1 mg/ mL STP at 2.1 MPa) and Group 4 – (0.1 mg/ mL STP at 1.6 MPa). The 1st and 3rd columns show the external view of the tumours the 2nd and 4th show the same tumours after removal of the skin. These are 2 examples of the total of n=4.

The group which received the standard 1 mg/ mL concentration of STPs and was treated at 2.1 MPa exhibited the highest cell death percentage, with an average of 62%. From Figure 2.3.2.4 the extent of the damage was visible on the tumour samples, with some exhibiting signs of haemorrhage within the tumour capsule. In addition, there are areas of tissue with white hard

tissue, suggesting the possibility that ablation has occurred within the tumour (white arrow, Figure 2.3.2.4).

When a standard 1 mg/mL concentration of STPs was used in combination with a constant pressure of 1.6 MPa the average cell death was 38.2%. Visual inspection showed the level of superficial damage in the tumours reflected the change in cell death seen at 1.6MPa compared to 2.1MPa.

At 0.1 mg/ mL STP concentration and 2.1 MPa a greater mean level of cell death was observed (58.7%) by flow cytometry. The photographs of the tumours from this group show blood in the tumour capsule, visible immediately to the naked eye. Notably, whilst the tumours from the 0.1 mg/ mL STP at 1.6MPa group showed little to no external signs of damage, bruising, or bleeding post-treatment compared to controls (see Fig 2.3.2.4), the mean cell death for this group was still 29.5%.

These data demonstrate that the sensitivity of CT26 cells within a syngeneic tumour to cavitation events can be roughly gauged by visual assessment of the tumours, but below a certain level of cavitation, the obvious ablation events and haemorrhagic pools of blood do not appear, but raised CT26 cell death is still evident by flow cytometric analysis.

This tumour cell viability study gave more information regarding the effect of direct intratumoural dosing and which ultrasound parameters should be used. It was decided that the least cytotoxic parameters from group 4 (0.1 mg/ mL STPs and 1.6 MPa) would be used for further studies to assess reporter protein expression from a luciferase-expressing mRNA construct.

2.3.3 *In vivo* delivery of naked mRNA

It is clear from Figure 2.3.2.4 that high cavitation levels can have a detrimental impact on cell viability, an impact that diminishes the ability of the cells to translate mRNA into protein. To

examine the effects of the level of cavitation on reporter mRNA translation into protein, a study was conducted with either LNP-condensed mRNA ('LNPs') or naked mRNA, both encoding for luciferase. The experiment examined how the change in pressure, from 2.1 MPa to a consistent 1.6 MPa, and a lower concentration of STPs (from 1 mg/ mL to 0.1 mg/ mL) would impact on uptake and expression. In addition to these changes, an additional time point at 12 hours after US treatment was added to define the expression levels over time more completely. The shift in expression over time for naked mRNA can be seen in Figure 2.3.3.1, where mRNA only was compared to mRNA plus ultrasound only, mRNA with ultrasound and STPs.

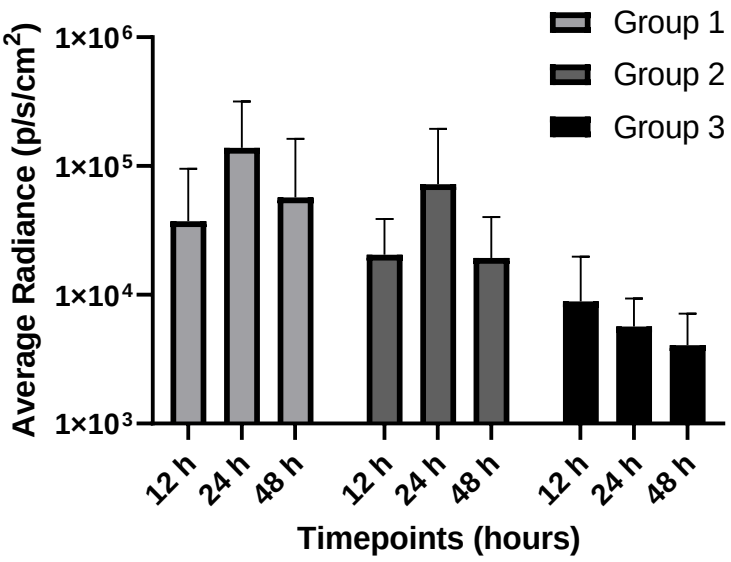

Figure 2.3.3.1: Average radiance measured using the Lumina LT series III for each group at 12, 24, and 48 hours. Dosing and imaging was performed as described in section 2.2.4-6, and groups comprised of mRNA only (Group 1, light grey colour bars), mRNA and ultrasound at 1.6 MPa (Group 2, dark grey colour bars) or mRNA with 0.1 mg/ mL STPs ultrasound at 1.6 MPa (Group 3, black colour bars) were compared. N=4, bars represent mean values, error bars represent standard deviation.

The results from IVIS imaging indicated that naked mRNA had peak expression at 24 hours, with more than a two-fold decrease by 48 hours. For tumours treated with mRNA with ultrasound alone, i.e., no STPs (and therefore minimal cavitation), a peak of expression at 24 hours was seen, but by 48 hours, the expression level was three times lower than with mRNA alone. The mRNA plus STP plus US group demonstrated minimal expression at all time points,

with a ten-fold decrease compared to the control group of mRNA without ultrasound and a six-fold reduction compared with mRNA and ultrasound without STPs. Notably, the time profile of expression was also altered for the mRNA plus STP plus US group, which demonstrated a peak at 12 hours and more than halved by 24 hours. Figure 2.3.3.2 shows an example of a mouse from each group, where a region of interest (ROI) has been centred around the treated tumour of each mouse. After the final imaging session, tumours were excised and stored for further testing, where an *in vitro* luciferase assay was used to validate mRNA expression levels measured by IVIS.

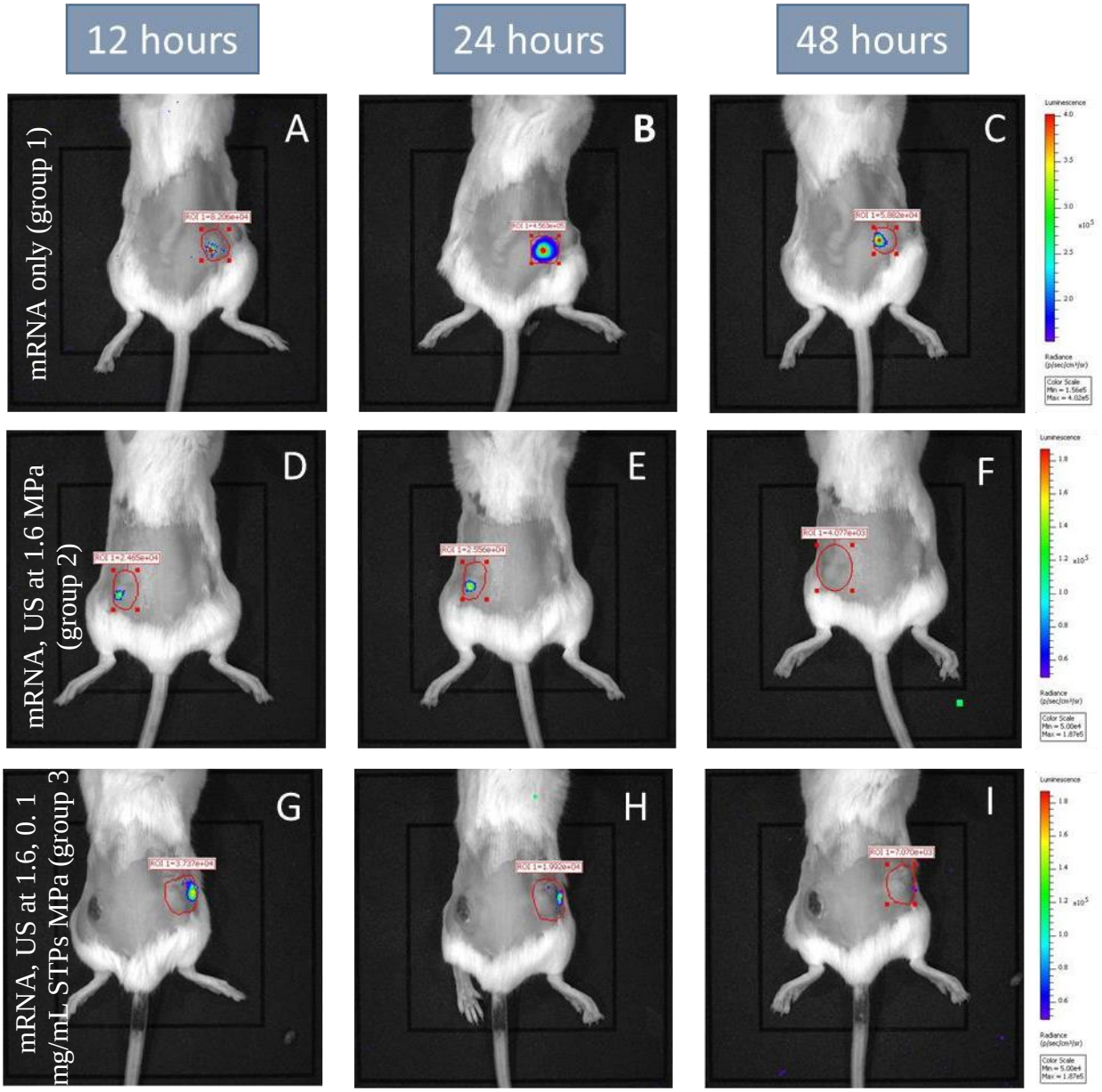

Figure 2.3.3.2: Example IVIS images for each treatment group at 12-, 24-, and 48-hour time points. Images A-C are an example of mRNA-only treatment group, D-F mRNA and ultrasound at 1.6 MPa group, and G-I mRNA with ultrasound at 1.6 MPa and 0.1 mg/mL STPs group

The luciferase signal as measured i*n vitro* post cull, excision and processing of tumours (see methods section 2.2.8) can be seen in Figure 2.3.3.3. The assay's outcome shows that the mRNA control, i.e., no ultrasound or STPs, exhibits greater expression than the ultrasound plus mRNA group as well as the ultrasound plus STPs plus mRNA group. This is consistent with the *in vivo* data in Figure 2.3.3.2. Luciferin reacts with the luciferase produced in cells that have taken up the mRNA and translated it to allow the luminescence process to be measured.

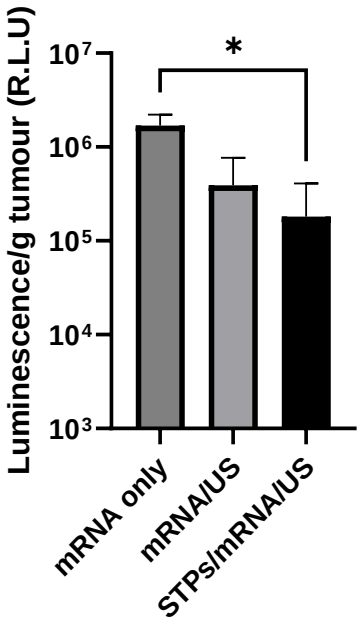

Figure 2.3.3.3: Luminescence measured by luciferase assay *in vitro* on tumour samples recovered at 48 hours. Control group of mRNA only, mRNA with ultrasound at 1.6 MPa, and mRNA with ultrasound and 0.1 mg/mL of STPs. Pressure used was 1.6 MPa, with a treatment time of 300 seconds, 5 % duty cycle and 50,000 cycles, injection volumes and process as described in methods (section 2.2.4). Bars represent mean of N=3 values, error bars are the standard deviation, * = $p < 0.05$.

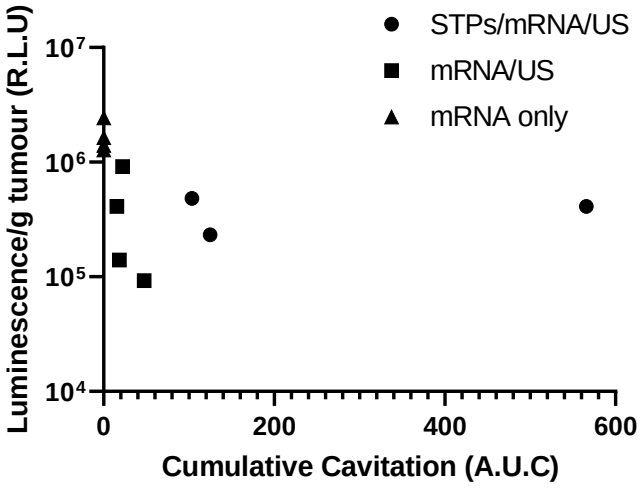

Figure 2.3.3.4: Luminescence measurements from *in vitro* luciferase assay of excised tumour plotted against the cumulative cavitation unit as calculated as described in section 2.2.4), generated using the area under the curve for each PAM magnitude plot for each mouse. mRNA only, mRNA plus ultrasound only and mRNA with ultrasound and 0.1 mg/mL STPs. Pressures for ultrasound treated groups were 1.6 MPa, with a treatment time of 300 seconds, 5 % duty cycle and 50,000 cycles. Outlier at 580 AU likely due to an injection error with mouse.

2.3.4 *In vivo* delivery of lipid nanoparticles

Delivery of 'naked' RNA has been shown to be ineffective, especially following intravenous delivery, due to rapid degradation and an absence of a cell entry mechanism. However, success with lipid nanoparticle formulation suggests such technology offers a route to overcoming such limitations and turning RNA into a viable therapeutic. Experiments were performed to study the impact of encapsulating the mRNA using lipid nanoparticles (LNPs) and its response to ultrasound. LNPs were injected IT at a concentration of 1 mg/mL to a volume of 10 µL (see section 2.2.5). The 3 LNP treatment groups were, LNPs only, LNPs and ultrasound alone, and LNPs plus ultrasound plus STPs. For ultrasound groups, a pressure of 1.6 MPa was used.

The results of IVIS imaging at 12, 24, and 48-hour time-points can be seen in Figure 2.3.4.1. the LNP only group, showed an increase of luminescence at 24 hours and then a decay. LNPs with ultrasound alone, exhibited no change in luminescence compared to LNPs plus ultrasound plus STPs, showed an increase at 24 hours and then a decay, but this increase was not as pronounced as the LNPs only group. This suggests that the ultrasound negatively affects the uptake of, or expression from, LNPs.

The difference in expression between the ultrasound and non-ultrasound groups in both studies, i.e., regardless of whether naked mRNA or LNPs was being delivered, indicated that while the levels of damage were visually reduced by using 1.6 MPa, there still may be an effect to understand, which is discussed in Chapter 3. Such damage to cell viability may mask any improvements made to delivery. There appears to be an increase in signal at 24 hours for the LNP and STPs and US group, in Figure 2.3.4.1, 12 hours after the initial increase seen in the mRNA treatment group, Figure 2.3.4.1.

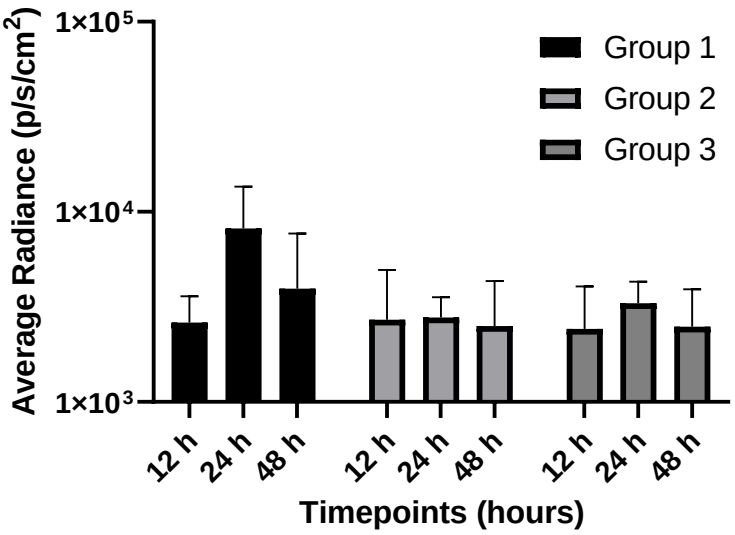

Figure 2.3.4.1: Average radiance (photons/sec/cm^2) measured using the Lumina LT series III for each group at 12, 24, and 48 hours. Group 1 - LNPs only, Group 2 - LNPs and ultrasound only at 1.6 MPa, Group 3 - LNPs 0.1 mg/mL STPs at 1.6 MPa. Bars represent mean of N=4, error bars show standard deviation.

The luciferase assay results on excised and homogenised tumours can be seen in Figure 2.3.4.2. The group with LNPs only exhibited the greatest expression levels with an average expression of 8.9E4 p/s/cm^2. Whilst the addition of ultrasound caused a small non-significant decrease in the luciferase expression, there was an order of magnitude difference in luciferase expression between the LNP group and the LNPs plus US plus STPs group. Analysis of the levels of cavitation showed that the LNP plus US plus STPs gave a 10-fold greater level than the level with LNP plus US, as observed in Figure 2.3.4.5.

Notably, the peak of expression for the LNP plus US plus STP group was at 12 hours, while the peak for mRNA plus US plus STP was at 24 hours. These differences may result from the LNPs being delivered via cavitation-generated pores directly to the cytoplasm, whereupon there is a delay in the release of the mRNA from the LNP, compared to when mRNA is delivered via cavitation into the cytoplasm and may be immediately available. This process will delay the overall expression time for the protein. There were no changes in the time profile for expression for the mRNA-only group compared to the LNP-only group.

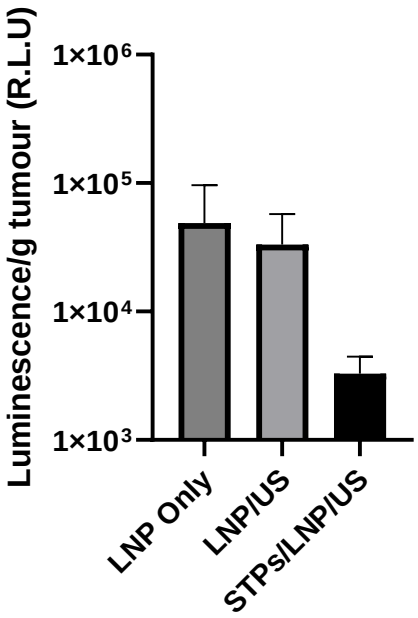

Figure 2.3.4.2: Luminescence measured by *in vitro* luciferase assay of tumours recovered at 48 hours. control group of LNPs only, LNPs with ultrasound only, LNPs with ultrasound and 0.1 mg/mL of STPs. Pressures used was 1.6 MPa, with a treatment time of 300 seconds, 5% duty cycle, and 50,000 cycles. Bars show the mean value of n = 4, error bars show the standard deviation

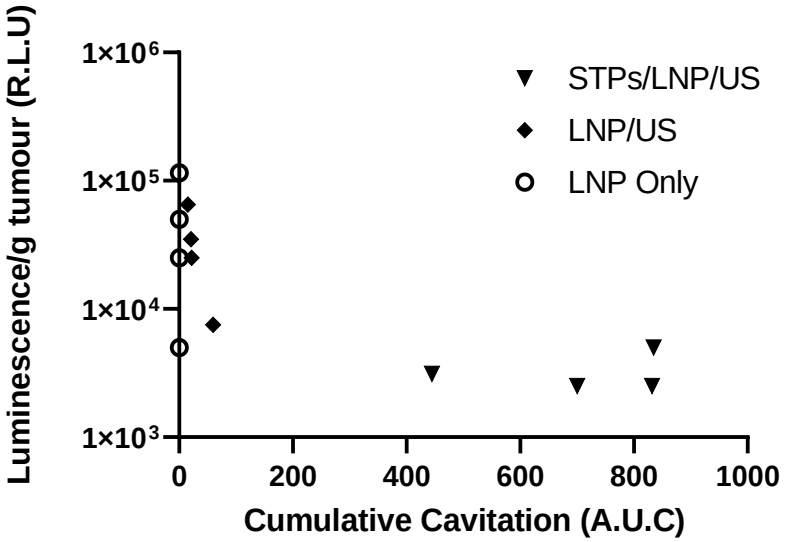

Figure 2.3.4.3: *In vitro* luminescence measurements from luciferase assays of excised tumours at 48 hours, plotted against the cumulative cavitation generated during treatment using the area under the curve for each PAM magnitude plot for each mouse. LNPs only, LNPs with ultrasound, LNPs plus ultrasound and 0.1 µg/µL STPs. Pressures for ultrasound-treated groups were 1.6 MPa for 300 s, 5% duty cycle, and 50,000 cycles.

2.3.5 Delivery of naked mRNA with microbubbles

Solutions of STPs produce a distinctive balance of inertial and non-inertial cavitation over unusually long durations. As cell damage appeared to be a restricting factor despite efforts to reduce pressure and decrease STP concentration, it was deemed worthwhile to test alternative cavitation nuclei with different features. Hence, naked mRNA was tested in conjunction with SonoVue® microbubbles (SV MBs). SonoVue® was made up to a count of 2 x10^8 bubbles/mL as described in Section 2.2.5, with 10 µL injected (2 x10^6 microbubbles). For this study, the ultrasound parameters were changed to 100 cycles rather than 50,000, with the pressure decreased to 0.3 MPa, in line with favourable nucleation conditions for SonoVue. Mice were divided into two groups, mRNA only and mRNA plus ultrasound plus SV MBs. The trend of greater expression at 12 or 24 hours continued, which can be seen in Figure 2.3.5.1, which shows example IVIS images, where the regions of interest (red circles) show the tumour and the overlay of expression seen in rainbow colour. At 12 and 24 hours, there are definitive regions of expression, however, by 48 hours in the same mice, these regions of expression have decreased to the extent that the signal cannot be viewed on the same scale as previously

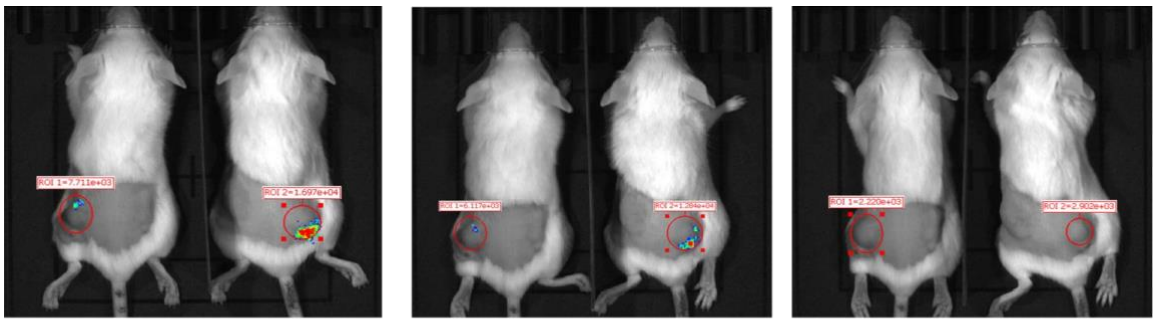

.

Figure 2.3.5.1: Imaging of 2 representative mice treated with mRNA and ultrasound at 0.3 MPa and SV MBs using IVIS. The tumour areas are highlighted in red as the region of interest for luminescent measurement. The signal can be seen to be higher at the earlier time points, with the signal decreasing over time. IVIS imaging, as described in section 2.2.5

In Figure 2.3.5.2, the results show that the mRNA plus US plus SV group had a 2-fold increase in the level of luciferase expression in excised and homogenised tumours compared to the

mRNA only group at 48 hours. The cavitation levels, as shown in Figure 2.3.5.3, show an expected lower level of cavitation when compared with the STPs, but comparing the two directly is difficult due to the likely difference in cavitation regimes employed. This was expected with the use of SV MBs with fewer cycles and markedly lower pressure in comparison to the STPs and a pressure of 1.6 MPa because the change in parameters is more likely to result in non-inertial cavitation and much less violent collapse of the bubbles, resulting in a change in the acoustic emissions. The SV MBs are also known to cavitate for a much shorter period in vivo, which was also seen with these in vivo experiments.

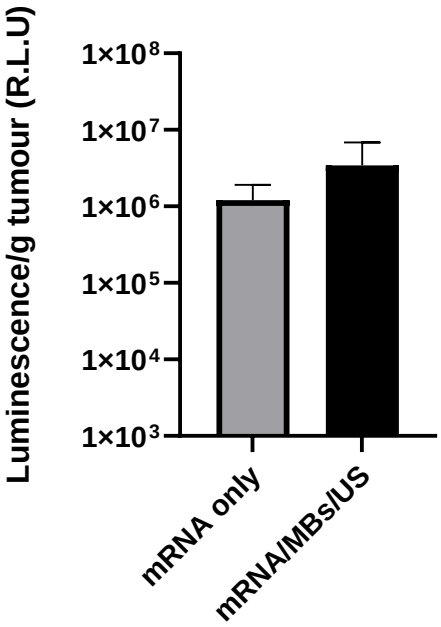

Figure 2.3.5.2: Luminescence measurements from luciferase assays. mRNA only, or mRNA with ultrasound, and 2E8/mL SonoVue® microbubbles. N =3, Error bars represent the standard deviation.

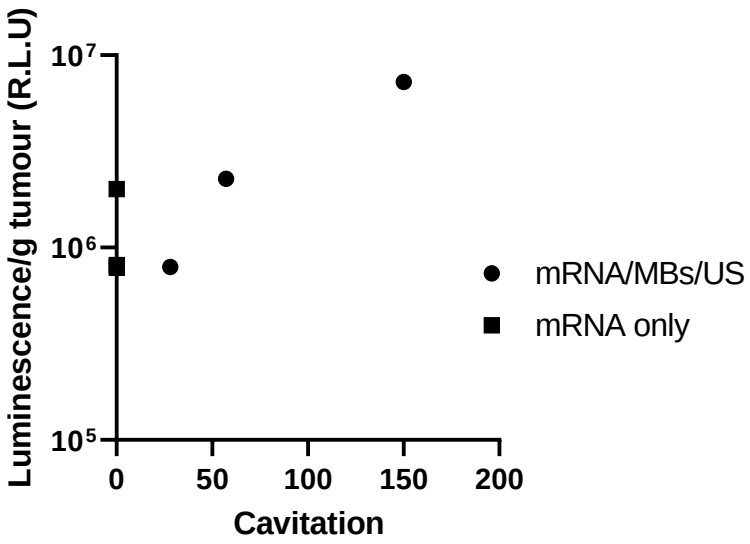

Figure 2.3.5.3: *In vitro* luminescence measurements from luciferase assays plotted against the cumulative cavitation, generated using the area under the curve for each PAM magnitude plot for each mouse. Mice treated with mRNA only are compared to mRNA with ultrasound at 0.3 MPa and 2E8/mL SonoVue® microbubbles. Luminescence measured as described in section 2.3.8 cavitation quantified as described in section 2.2.4

2.4 Discussion

To identify a level of cavitation which could provide successful mRNA delivery without excessive cell death, an *in vivo* experiment was performed to examine the role of the ultrasound parameters used and how these could affect the uptake and expression of mRNA. Previous studies have successfully used STPs as a cavitation nuclei in an intravenous delivery context with the aim of improving the movement of drugs from the bloodstream into the tumour environment (243,245). For the work completed in this Chapter, intratumoural injections were employed to more rigorously control the concentration of STPs delivered and to ensure the delivery of naked mRNA could be compared to that of encapsulated mRNA on a more equivalent basis (naked mRNA cannot be injected IV). Furthermore, two different cavitation nuclei were employed to evaluate the effect of cavitation on delivery: STPs and SV MBs, and means of detecting and quantifying cavitation were deployed.

The first step in establishing the correct ultrasound parameters for IT delivery of mRNA was to examine previously used parameters (243–245) for *in vivo* studies. Previous studies using

IV injection have used pressure ranges starting at 1.6 MPa and ranging up to 2.3 MPa, with treatment times of 5 to 10 minutes, and 20 mg/mL of STPs, with the same number of cycles, duty cycle, PRF and frequency of transducer as used in this Chapter (243–245). Due to the direct nature of IT injection and the associated losses of STP concentration with IV delivery, a STP concentration of 1.0 or 0.1 mg/mL was used.

However, at the reduced pressure of 1.6MPa, the concentration of STPs had a greater impact on the damage that resulted. The effects of the STPs can be seen with the increased cavitation between each of the 1.6 MPa groups in Figure 2.3.2.2. This means that to control the damaging effects, and ensure more transfected cells can survive to produce the transgenic protein, both pressure and cavitation nuclei concentration need to be carefully controlled.

Notably, IT injection does offer greater control of the dose of cavitation nuclei delivered compared to IV delivery which is at the mercy of the highly heterogeneous tumour vasculature and perfusion. In theory, by directly injecting into the tumour environment, the researcher can know both the concentration of the cavitation nuclei and the drug being delivered, as well as delivering otherwise vulnerable genetic material, i.e., naked mRNA. For the tumour cell viability study in this Chapter, a typical intravenous dose of STPs, 1 mg/mL, was delivered but at a reduced volume. The concentration of STPs used was then reduced to a 1:10th dilution calculated to be in the bloodstream following IV delivery because the delivery from vessels to the tumour of agent is poor due to high interstitial fluid pressure, endothelial cells lining vessels and the chaotic nature of angiogenesis in the tumour environment (246). The starting dose was calculated using a typical delivery concentration of 20 mg/mL, at a delivered volume of 50 - 100 µL (75 µL was used) in a total blood volume of between 1.4-1.6 mL as per total blood volume of a 20 g balb-c mouse (247).

IT injection of naked mRNA is unlikely to be used clinically to treat the diseases discussed in Chapter 1 due to rapid degradation and absent/uncertain delivery mechanisms. One way to overcome these limitations is to encapsulate it in polymers that protect it from degradation and provide a mechanism for cell entry. For a comparison of how mRNA directly injected into the tumour performs versus a method of encapsulation, lipid nanoparticles (LNP) were employed as an encapsulation device. LNPs are at the cutting edge of gene delivery, as described in Chapter 1. LNPs offer high nucleic acid encapsulation and efficiency due to using positively charged lipids and being able to form stable nanoscale complexes (248,249). While LNPs offer a leap forward in protection and delivery of nucleic acids and large-scale manufacturing and reproducibility, their IT use is limited. The difference between naked mRNA and encapsulated mRNA is apparent from Figures 2.3.3.1, 2.3.3.3 and 2.3.4.1 and 2.4.3.2. Naked mRNA has an earlier expression profile than mRNA/LNP once introduced to the cell, which fits with previous studies in literature, and may be a consequence of the reduced level of processing/'un-coating' needed with 'naked' RNA. Another important note is that levels of expression were over 100 times lower for encapsulated mRNA when compared with naked mRNA. Indeed, the actual mechanism of entry of naked mRNA into the cells is still not defined, but it may be the consequence of damage to cell membranes caused by the needle tip.

One aspect that was looked at closely was the timing of the measurements of reporter gene expression. mRNA can take as little as four hours to be translated into a functional protein once within the cytoplasm (28), but the nature of lipid encapsulated mRNA requires additional time to escape the lipid nanoparticle and the endosome. These factors can be protein- and cell type-dependent (250).

The importance of pressure and cumulative cavitation and the effects this has on the uptake and expression of mRNA was further explored using a different cavitation nuclei in the form of SonoVue microbubbles or STPs. SonoVue microbubbles have been used *in vitro* and *in vivo*

to examine sonoporation and sonopermeability (171,235,251). The effects of STPs on the tumours was well established by tumour cell viability study at the start of this Chapter (section 2.3.1), but to compare whether SV MBs would benefit the uptake and expression of naked mRNA, a small pilot study was conducted. The results of this study show that the levels of cumulative cavitation nucleated by SV were much lower for each tumour than when using STPs, Figures 2.3.3.4 and 2.3.5.2, although much reduced pressures was used for SV compared to STPs. However, the SV MBs have some considerable drawbacks as the MBs only exhibit a cavitation time on the order of 30-60 seconds (252). Indeed, at the pressure and cycles used in these experiments, the SV nucleated cavitation time was on the order of 20-25 seconds for each mouse. In comparison, the STPs can cavitate for minutes following a systemic administration and in the order of tens of minutes *in vitro* (186), which, if applied clinically, could provide a substantial advantage.

The role of cavitation in these experiments cannot be overlooked. Cavitation effects have long been recognised and continue to be explored in more detail. The effects of cavitation can range from what has been demonstrated here in terms of destruction of cells but have also been shown to induce uptake through various mechanisms, whether that be sonoporation (253–255) sonopermeabilisation effects or inducing endocytotic pathways (81). The cumulative cavitation delivered in this chapter's work can be seen to have a detrimental effect in terms of cell death, Figure 2.3.3.3. This cell death could be caused by the destructive nature of the cavitation events, which leads to increased apoptosis of the cells(256), but also the destructive nature of the cavitation events cannot be ignored, where cells can be ripped apart by the forces involved leading to cellular debris. Contrary to expectations, although parameters could be refined to reduce such cell death, parameters which would give enhanced delivery could not be found in Figures 2.3.3.4, 2.3.4.3 and 2.3.5.2. Further experiments with STPs and refinement of parameters may help identify a region in this cumulative cavitation where the damaging effects

are further limited so that delivery without death can be achieved. Within these regions, further experimentation is required and will be explored in the Chapters to come.

2.5 Conclusion

Initial studies identified a combination of ultrasound pressure and concentration of cavitation nuclei that would provide a substantial stimulus while maintaining high cell viability, these parameters still proved to be of no benefit in enhancing delivery. Alteration of the cavitation nuclei used, i.e., a change from STPs to MBs, provided an improvement. Still, more development of the ultrasound parameters is required for a more robust enhancement of the delivery of mRNA and LNPs via IT injection. There was evidence to warrant additional *in vitro* and *in vivo* testing regarding peak expression time points and how this will translate into more coherent and accurate *in vivo* data collection, addressed in the following Chapter.

The work in this Chapter provides vital information for moving forward with *in vivo* experiments and establishment of IT protocols. Whilst no advantage was provided by STP-mediated cavitation in terms of total expression, there was a change to the time profile of expression. A shift in the peak expression to the 12-hour time point suggests an altered, potentially more direct, route to the cytoplasm via sonoporation. Such a shift may be of value in application where early expression is favoured, for example in tissue engineering, provided parameters can be adjusted to raise the levels achieved. These important questions about when is best to measure luciferase expression, the uptake profile of the mRNA, and whether a further reduction in pressure to further control cavitation levels is of benefit will be addressed.

Chapter 3 – *In vivo* investigation in expression time course and *in vitro* assessment and protocol development for ultrasound-mediated delivery of mRNA to cancer cells

3.1 Introduction

The data presented in Chapter 2 of this thesis showed that much was to be learned and, in turn, applied to optimise ultrasound-mediated delivery of nucleotide to cells. In particular, understanding; the time profile of the expression of the encoded protein, the cavitation dose, and the experimental protocol needed additional refinement. In response, this chapter's work explores the impact of changing ultrasound parameters, both *in vitro* and *in vivo*, and how this influences target cells and tumours. This chapter further explores the time to best observe and measure the expression *in vivo*. The *in vitro* work in this chapter provides a fundamental and new understanding of the time course of cavitation-mediated mRNA entry into cells and the resulting transgene expression profile. This gives valuable insight into how the parameters and time entry points can be tailored for better overall expression. This chapter also explores the effects of cavitation on cell viability and determines the relationship between cavitation dose and expected cell death and damage. Such a relationship has been explored before (257–260) but not in the same detail or across a wide range of cells. Elucidating these key relationships allowed for a tailored approach to the *in vivo* experiments, as elaborated in Chapter 5.

The main themes of this chapter are the effects of fetal bovine serum (FBS) on mRNA uptake *in vitro* and the ability to measure and establish when the mRNA achieves cavitation-mediated cell entry. Changes in ultrasound parameters have on both *in vitro* and *in vivo* results, the time points for maximum expression *in vivo* and, overall, the foundation for the working protocol for the remaining chapters are also examined.

Understanding the ideal conditions for delivering mRNA into cells allows for the optimal time and maximal protein expression to be established. This is important for both *in vitro* and *in vivo* applications. It is crucial for potential *in vitro* applications, such as modifying the cell for commercial applications or achieving new protein production. Two important clinical

applications where exquisite understanding of the control and timing of nucleotide delivery to cells *in vitro* are the generation of modified T-cells in cancer treatment (261–263) and stem cell manipulation in tissue engineering (35,264). It is also critically important when considering the potential *in vivo* uses, for example, in combination cancer therapy. Previous studies have probed the timeline from mRNA entering the cells to maximum biological output (265–267) with mixed results, dependent on the cell line, RNA type and delivery method (196). One crucial element of the work in these chapters is that, in contrast to many transfection studies (268,269), the transfection of all the cells in this thesis, RNA types and *in vitro*/*vivo* delivery methods, is done without any additional transfection reagents or chemical modifications of the cells (except where they were required as a control).

All the work in this thesis utilises cavitation as the methodology for transfecting cells. Although this has been studied many times (270–274), a comprehensive study of the optimal conditions and time course of RNA delivery is lacking. Earlier bodies of work have looked at the effect of using ultrasound and cavitation nuclei such as microbubbles, with varying degrees of success. By utilising microbubbles as cavitation nuclei, the cavitation regimes used can exhibit non-inertial and inertial cavitation regimes depending on the concentration of cavitation nuclei and ultrasound parameters such as pressure, number of cycles and duty cycle (3,89,275,276). Many studies have used a high bubble-to-cell ratio or single bubble-to-cell contact to examine the effects of cavitating bubbles on the cellular membrane (277,278). The impact of cavitating bubbles on the cell membrane has been studied extensively and continues to be elaborated on with studies in pore formation, sonopermeabilisation and the short and long-term effects of such events (148,279–284). Due to the range of different parameters that can be used, it is unsurprising that there has been variability in the reported impact of cavitation on the cells.

The sonoporation effect on cells varies depending on several factors:

1 – Ratio of cavitation nuclei to cells,

2 – ultrasound parameters (such as duty cycle, pressure, duration),

3 – Cell type.

It has been documented that the effects of sonoporation can last from microseconds to tens of minutes after the cavitation events subside (279,284–286). Studies have shown that the cells can be sonoporated for tens of minutes, recover, and grow healthily. These results have been achieved using non-inertial cavitation in an *in vitro* setup, where microbubbles were targeted to the cell at a ratio of 100(s) bubbles per cell. These results and the parameters used would seem to be highly pertinent to the work presented here, but some important factors must be considered.

Notably, many *in vitro* studies discussed in Chapters 1 and above do not translate to *in vivo* well. The *in vitro* systems are an idealised delivery setup. The commonly used cavitation nuclei, microbubbles, have shortcomings *in vivo* that are difficult to overcome. The limiting factors of microbubbles for *in vivo* use include circulation time (287), size (288,289) and ability to penetrate tissue (290), all of which impact the ability to achieve the effective *in vitro* bubble-to-cell ratios when performing *in vivo* experiments.

For this reason, the work in this chapter exclusively uses SonoTran particles (STPs). STPs, as discussed in detail in Chapter 1, have both limitations and advantages compared to microbubbles when used as cavitation nuclei for drug delivery. STPs are made using bio-inert polystyrene, and because of their shape and ability to cavitate for long periods - 20 minutes (187) - they are ideal for the longer exposure times required *in vivo*. One drawback, however, is the relatively high-pressure threshold required for cavitation and the subsequent dominating inertial cavitation regime, as inertial cavitation has been reported to be inherently more destructive to the cells (190).

The inertial cavitation that occurs with the STPs also can be destructive in tissue. This is often due to the mechanical stress caused by inertial cavitation, the temperature changes and the pressure associated with achieving it, though all these factors are cavitation nuclei dependent (291,292). Overall, the STPs have previously been studied *in vivo* and offer the possibility of sustained cavitation without the need to readminister (186). In vivo studies using these STPs have reported no adverse events.

The biological effects of the different cavitation regimes, including sonoporation and microstreaming, have been discussed in Chapter 1. However, it is essential to consider that the destructive effects of the STP nucleated inertial cavitation may dominate the enhanced delivery impact achieved, and it is vital to understand the duration of these effects.

The final part of this chapter investigates the expression of the encoded reporter protein *in vivo*, i.e. the time it takes to peak and the rate at which it drops off. It also examines different pressures to confirm the conclusion from Chapter 2 regarding pressure being the dominating factor in cell death and consequently lower levels of reporter protein expression. The work in this chapter lays the groundwork for the *in vivo* experiments discussed in Chapter 5. Many techniques have been used for this aspect of the chapter, including IVIS imaging and luciferase assay analysis.

3.2 Materials and methods

3.2.1 Cell lines and cell culture

Murine colorectal carcinoma CT26.WT cells (ATCC, CRL-2638; American Type Culture Collection, Rockville, MD, USA) were prepared for implantation in the same way described in section 2.2.1 of Chapter 2 and were implanted in the same manner as described there. CT26 cells were prepared for *in vitro* using the same steps but were then suspended in either FBS-free RPMI 1640 or RPMI 1640 containing 10% FBS. A cell count and viability assessment were obtained using the trypan blue dye exclusion method with a haemocytometer. Cells were then prepared to the correct concentration for *in vitro* testing, adding additional FBS-free RPMI 1640 or RPMI 1640 with 10% FBS, as required, to form a stock solution for *in vitro* experimentation.

3.2.2 *In vitro* sample preparation

The total cell count and viability were taken and recorded before ultrasound treatment, with each sample prepared at a concentration of 1E6 cells per mL, at a total volume of 0.5 mL. The cells in suspension were placed in a 2 mL Eppendorf (022431102, Eppendorf AG, Germany) and put on ice to prevent enzymatic degradation before treatment. After ultrasound exposure, 20 µL of cells were taken to record cell count and viability. An additional 200 µL was taken to run samples at different time points post-treatment using flow cytometry. The remainder of the cells was used to plate in a 96-well plate (CLS3610, Sigma, UK) for incubation for later use in the luciferase assay. In the 96-well plate, each sample was plated in a total volume of 200 µL in either FBS-free RPMI 1640 or RPMI 1640 with 10% FBS at a concentration of 10E3 per well. Each plate was incubated at 37°C in a humidified atmosphere of 5% carbon dioxide. The plates were then removed at 6, 8, 10, 12, 14 and 24 hours to measure the luciferase expression using the luciferase assay kit described below.

3.2.3 mRNA

Naked mRNA purchased from Trilink biotechnologies (Product code: L-7202), encoded for firefly luciferase protein production. And for each sample, 5 μg of mRNA was added to a total volume of 0.5 mL with a cell concentration of 1E6/mL. The expression was measured using a luciferase assay (E1500; Promega, Southampton, UK) and following the standard protocol for luminescent measurement using a plate reader, FLUOstar Omega multidetection microplate reader, (BMG LABTECH Ltd., UK).

3.2.4 *In vitro* Ultrasound

In vitro, each sample tube was placed in a heated (37°C) and degassed water tank. The transducer setup (see schematic 3.2.5.1) utilised one of the two high-intensity focused Ultrasound (HIFU) transducers, which were perpendicularly aligned, with a focal length of 63 mm from the centre of each transducer. The transducer has a fundamental frequency of 0.5 MHz. Each transducer has a rectangular cut-out to allow for the placement of an L11-5v 128-element linear array (Verasonics Inc.) to detect and map cavitation events. B-mode imaging was utilised during the treatment to ensure that the sample was in the correct position, and cavitation maps were applied using a custom PAM algorithm (OxSonics Ltd, UK) to allow for temporal and spatial mapping cavitation events occurring in reference to the sample. The total PAM energy was later quantified using a custom MATLAB script.

The ultrasound exposure parameters comprised of a driving frequency of 0.5 MHz with a pulse repetition frequency of 0.5 Hz, a duty cycle of 5%, and 50,000 cycles per burst. A range of peak rarefactional focal pressures (PRFP) of between 0.7 and 2.1 MPa was used, with a total exposure time of 300 seconds for each sample. Before ultrasound exposure, 5 μg of mRNA was added along with 10 μL of 0.1 μg/μL STPs. For control samples with no cavitation nuclei, 10 μL of 5% glucose was added instead to match the final concentration of the glucose content in the same volume of STPs.

3.2.5 *In vivo* Ultrasound

In vivo ultrasound was performed using the same setup described in Chapter 2, section 2.2.4. Before commencing treatment and delivering mRNA, a cannula was preloaded with naked mRNA and inserted intratumourally. 5 µL of PBS was then used for flushing naked mRNA through the cannula. Subsequently, 10 µL of cavitation nuclei at 0.1 mg/mL were flushed with 10 µL of PBS to ensure cavitation nuclei were in the tumour. This process ensured that delivery of sample into the tumour could be initiated after the tumour had been aligned with the focal region of the US transducers, whilst also ensuring there was no dead volume wasted in the tubing and the total injection volume still did not exceed 25 µL.

3.2.6 Cavitation analysis

As with the *in vitro* data, cavitation analysis was performed using a customised MATLAB script, which integrated the area under the curve from PAM magnitude plots, an example of which can be seen in Figure 3.2.6.1, produced by the custom OxSonics code. This analysis was used for all *in vivo* and *in vitro* comparisons of the cavitation dose delivered.

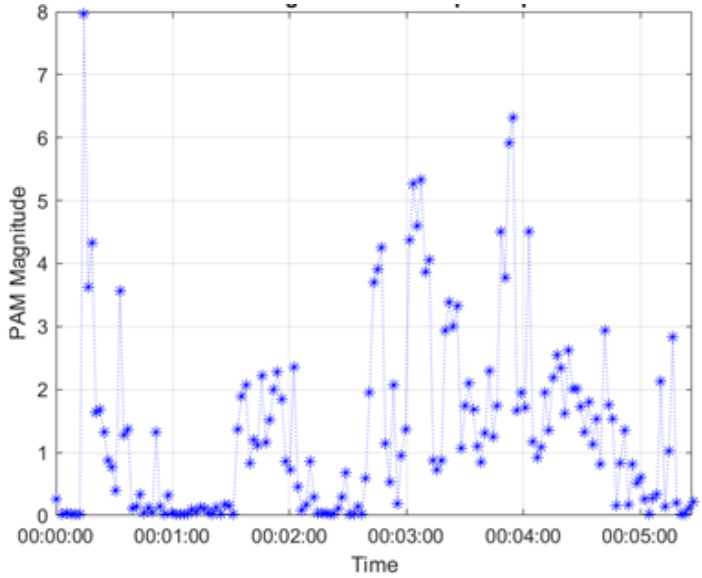

Figure 3.2.6.1: An example of a generated PAM magnitude plot. The X-axis is time in minutes, and Y-axis is an arbitrary value attributed to the signal returning to the B -mode transducers.

3.2.7 SonoTran Particles

SonoTran particles (STPs, OxSonics Ltd, UK) were prepared from a stock concentration of 25 mg/mL and diluted to 21.4 mg/mL using 40% glucose to create a new standard stock solution of 21.4 µg/µL in 5% glucose before addition to sample. This stock solution was further diluted by 1:10.

3.2.8 Quantification - Luciferase Assay

For *in vitro* analysis, at predefined time points of 6, 8, 10, 12, 14 and 24 hours, 96 well plates were removed from incubation. Media was removed from each well, and samples were prepared following the Luciferase Assay System kit (E1500; Promega, Southampton, UK). A microplate reader (FLUOstar Omega; BMG Labtech, Aylesbury, UK) was used for luminescence measurements. The luciferase assay kit was prepared per manufacturers' guidelines, and samples were read.

For analysis of *in vivo* samples, tumours were removed, freeze-thawed for one cycle and then homogenised using cell lysis buffer and a handheld T 10 basic ULTRA-TURRAX Homogeniser (Product number: 0003737002, IKA® England LTD). After homogenising each sample, the blades were inspected for tumour tissue, and if present, using sterile tweezers, the tissue was added back to the sample and homogenised again. Before beginning a new sample, the homogeniser was cleaned using ethanol to remove any trace amounts of mRNA between samples and subsequently washed with deionised water and dried 3 times before use on the next tumour sample.

Tumour samples were prepared with 10 µL of cell lysis buffer per mg of the tumour sample. Analysis was then conducted on 20 µL of the sample with 100 µL of luciferase assay solution, as per the manufacturer's protocol.

3.2.9 Flow cytometry

Flow cytometry was employed to confirm viability measurements taken by the trypan blue method and examine any permeabilisation effects. Propidium iodide (PI) (ab139418, Abcam, UK) was used as both a marker for cell permeabilisation and death, depending on the time point of measurement. Samples were split and measured at different time points to confirm findings. The flowcytometry PI kit was purchased from Abcam and used as per the manufacturer's guidelines.

As discussed above, cells were prepared for treatment, and 5 µL of 50 µg/mL PI was added to groups at different time points. Groups were separated in four groups: cells that received PI either 1) immediately before treatment, 2) immediately post-treatment, 3) 15 minutes post-treatment, or 4) 30 minutes post-treatment. This allowed for analysis of when, if any, effects of the treatment were occurring and, if so, for how long.

3.2.10 Tumour inoculation and animal welfare

Balb/c mice aged 5-6 weeks (BALB/cAnNCrl; Charles River Research Animal Models and Products, UK) were purchased and allowed to acclimatise for one week before tumour inoculation. Cells were prepared as described above and transported to the animal unit on the ice. Each mouse had its weight recorded and was uniquely marked. The mice were then placed under anaesthetic using 2-5% isoflurane. The mice were placed on a face mask to maintain anaesthesia, and a heating pad was placed under each mouse to help maintain their body temperature. Each mouse was then inoculated with 5×10^5 CT26 cells by subcutaneous injection. When using bilateral models, a subcutaneous injection took place in each flank. The mice were then monitored to assess their recovery from both the anaesthesia and the procedure, with additional monitoring, carried out twenty-four hours post-procedure and every three days after that. Weights and tumour growth were monitored for each mouse. Animals were housed and cared for according to UK Home Office guidelines. Tumour size was calculated using

callipers and half the product of the tumour's length, width, and depth. When tumours reached >85 mm^3, they were deemed treatable.

3.2.11 *In vivo* Imaging

Mice were imaged at time points 6, 8, 10, 12, 14 and 24 to monitor the luciferase transgene expression from within the tumours. These time points were chosen based on previous experiments showing varying levels of expression, as seen in Chapter 2, and project licence restrictions. Mice were allocated groups, as licence restrictions limit the number of times one mouse can be imaged within 24 hours. For example, one mouse can only be imaged 2 times within 24 hours, so therefore mice were split to cover the various time points described above. Mice were also culled at each time point to use the more sensitive *in vitro* luciferase assay kit to determine expression levels. The mice were anaesthetised and given an intraperitoneal (IP) injection of Pierce™ D-luciferin Monopotassium Salt (88294, Thermo Fisher Scientific) made up to a concentration of 15.8 mg/mL in PBS and delivered at a volume of 100 µL. The mice were then imaged using a Perkin Elmer Lumina LT series III 10 minutes post the IP injection to allow for adequate uptake of d-luciferin. The mice were recovered within fifteen minutes of the start of the procedure and monitored for recovery after each imaging session. At the end time points, the mice were culled at the end of the imaging session and tumours excised, photographed using a camera and then frozen in a minus 80˚C freezer for additional analysis. The IVIS images were later analysed using Perkin Elmer Living images® software, where regions of interest and radiance were analysed for reporter gene expression levels.

3.3 Results

The bloodstream and extracellular environment within a tissue bed are harsh environments for naked nucleotide as serum, and extracellular fluid contains nucleases. Indeed, fetal bovine serum (FBS) has well-recognised nuclease activity. Therefore, the presence of FBS will impact

any 'naked' delivery of nucleotide, and the time course over which this happens gives insight into the time course of cellular entry.

3.3.1 FBS-free media vs Media with 10% FBS

Hence, to examine the effect of FBS on the STP-nucleated cavitation-mediated uptake and expression in CT26s, cells were tested in either FBS-free media or media with FBS at pressures of 2.1 or 1.6 MPa. A no ultrasound control was also performed. The results of which can be seen in Figure 3.3.1.1

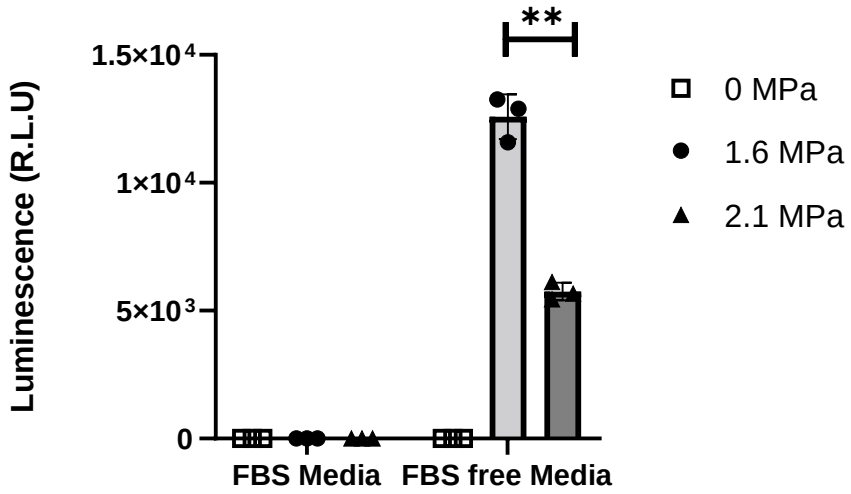

Figure 3.3.1.1 – Assessing the impact of STP nucleated cavitation on the delivery of mRNA-Luc into CT26 cells. Cells (1e6) in media with FBS or without FBS and 5 µg mRNA-Luc and 5 µg STP were exposed in the ultrasound setup as in schematic 3.2.5.1 to 0, 1.6 or 2.1 MPa for 5 min. Cells were then plated, and 6 hours later, luciferase expression was assayed as described in section 1.2.8. Bars represent means of 3 data points, error bars represent standard deviations. ** = $p<0.01$ by ANOVA analysis.

The results in Figure 3.3.1.1 suggested that ultrasound pressure and, therefore, cavitation was required for delivery and expression of the mRNA-Luc, with no signal detected when no ultrasound was applied/cavitation was detected. Notably, the higher pressure (i.e. 2.1 MPa) tested here gave significantly lower expression (~5 $x10^3$ vs 1.2 $x10^4$, $p<0.01$) than 1.6 MPa.

FBS had a dramatic and detrimental effect on the delivery of mRNA-Luc and, therefore, the level of luciferase expression decreased approximately 10,000-fold in the presence of FBS. This finding presented an opportunity to utilise the powerful inhibitory activity of FBS to

define the time and cavitation dependency of mRNA entry into cells. This allowed a better fundamental understanding of the process as well as helping optimise conditions for subsequent studies. Table 3.3.1.1 and Figure 3.3.1.2 confirm that delivery is only achieved when ultrasound exposure is performed in the absence of FBS.

Pre US/cav exposure			**Post** US/cav exposure			
mRNA-luc added prior to US treatment	US and cavitation	FBS free media for treatment	mRNA added post treatment	FBS free media for plating (over 24 hrs)	FBS media for plating (over 24 hrs)	Luciferase Expression?
☑	☑	☑	-	☑	-	Yes
☑	☑	☑	-	-	☑	Yes
-	☑	☑	☑	☑	-	No
☑	☑	-	-	☑	-	No

Table 3.3.1.1: Examples of parameters tested and whether there was an effect on luciferase expression. Each sample (N=3) was treated at the same ultrasound parameters of 1.6 or 2.1 MPa, 50,000 cycles, 5% duty cycle, 0.5 PRF, for 300 seconds. Each sample was plated and measured 8 hours post exposure.

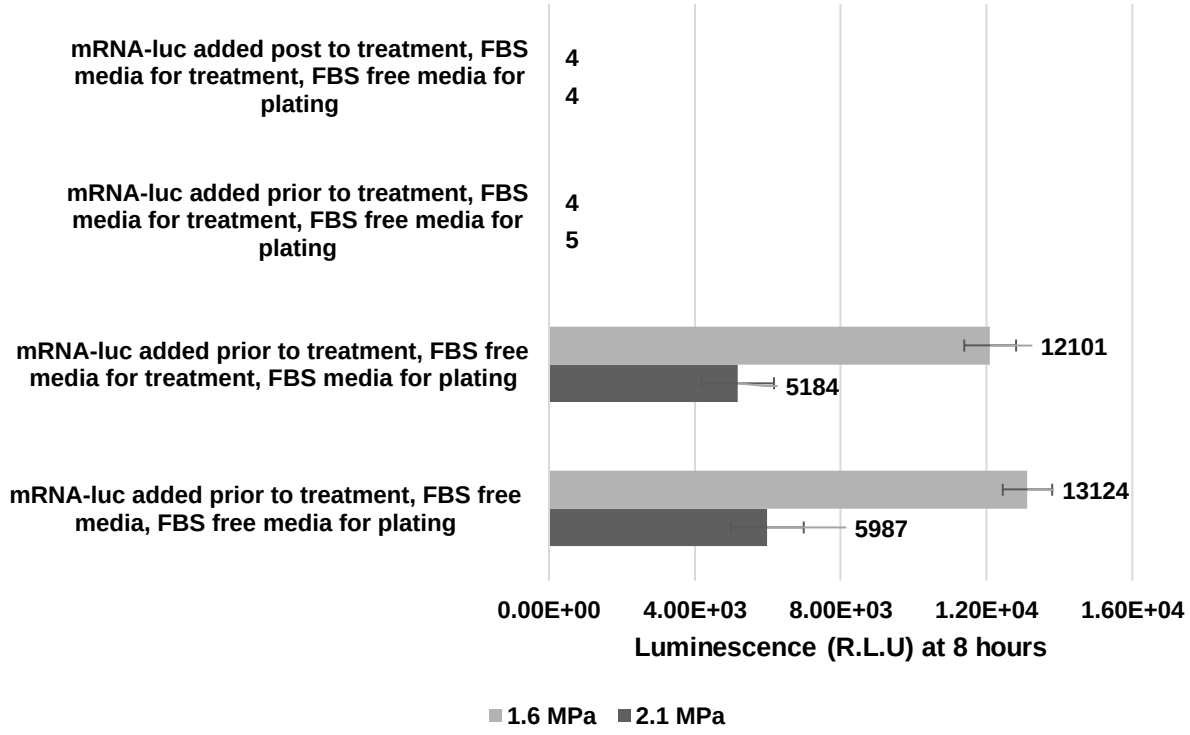

Figure 3.3.1.2: Expression profiles of the groups in table 3.3.1.1. Each sample was treated at either 1.6 or 2.1 MPa with the ultrasound parameters described in table 3.3.1.1. Error bars are the standard deviation for each group. N of 3 for samples.

Furthermore, as nucleases in the FBS completely inhibit mRNA, those samples that show expression when FBS was absent during exposure but present during subsequent plating must already have the mRNA present in the cell at the point of plating. In addition, even in the absence of serum throughout, when RNA was added after the ultrasound exposure was concluded, no expression resulted. These two findings demonstrate that cell entry is only

achieved during cavitation. This most probably reflects a rapid membrane 're-sealing' rate after cavitation ends, as also reported by Zhou et al., (293). However, it cannot be discounted that membrane holes may remain beyond the cavitation exposure window, but the stimulus of enhanced convection which also results from cavitation is also needed to propel the RNA and allow it to take advantage of such holes.

3.3.2 Cell death measurements

To further examine the window-of-opportunity for cell entry that the cavitation generates, whilst also considering the *in vivo* in Chapter 2 results, the viability of the samples for each group was examined both through the trypan blue method and using flow cytometry using PI as an indicator of the membrane permeabilisation effect. The results can be seen in table 3.3.2.1 and figure 3.3.2.1

Groups	PI present during treatment and measured directly after	Trypan blue measurement directly after treatment	PI added directly after treatment	PI added 15 mins post-treatment	PI added 30 mins post-treatment
2.1 MPa	48	29	32	30	30
1.85 MPa	44	23	24	22	24
1.6 MPa	38	20	19	18	17
1.35 MPa	33	16	18	15	14
1 MPa	27	13	13	14	12
0.7 MPa	24	6	7	8	8
Ctrl (no US + STPs)	2	1	1	2	2
Ctrl (no US/no STPs)	2	2	2	2	3

Table 3.3.2.1: Details of PI and trypan blue staining and the subsequent percentage of cells that stained positively at each parameter at different time points. PI present during treatment is when PI was added immediately prior to ultrasound exposure, trypan blue was added immediately

This data set demonstrates that higher pressure (i.e., greater levels of cavitation) leads to more cell death, but that by 0.7 MPa, just 6-8% of cells are killed. This data set is also notable for demonstrating that confirmation of cell death by trypan blue staining correlates very closely with positive staining when PI is added at 15- or 30-minutes post treatment. It also raises the

intriguing possibility that the differential between the dead population evident at 15 and 30 min and the higher level of staining evident when PI is present at the time of ultrasound exposure represents cells that are permeabilised but not to the extent where they die. Notably, for the highest pressure (2.1 MPa), this 'live permeabilised' population represents only a third of the total permeabilised population, whilst for 0.7 MPa, over two-thirds of cells permeabilised during ultrasound appear to be viable 15 and 30 min later still.

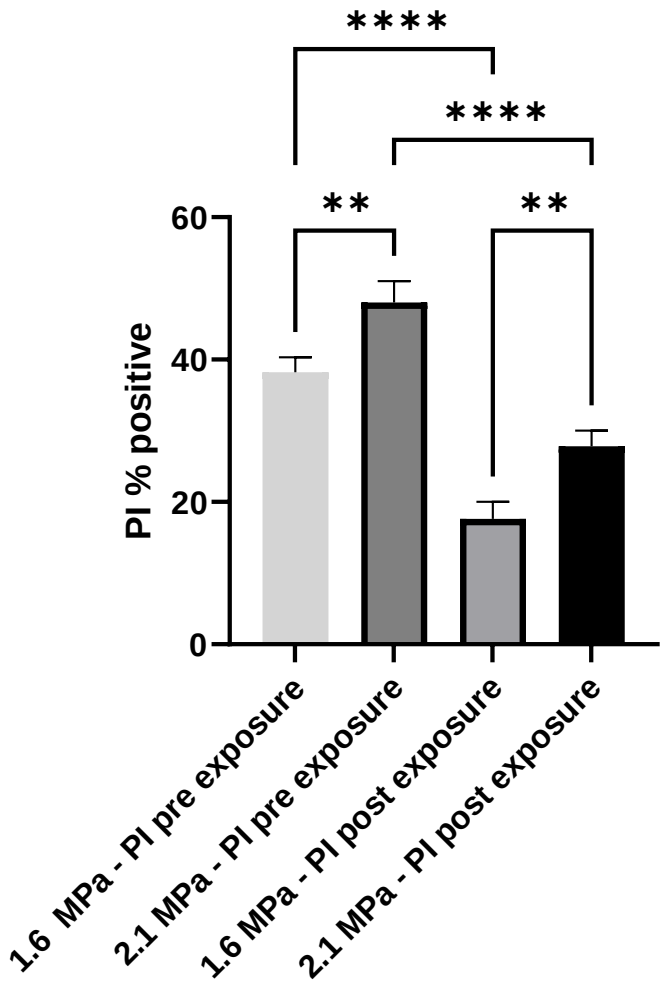

Figure 3.3.2.1: Percentage of PI-positive cells under different ultrasound conditions. PI pre-exposure is when PI is added immediately before ultrasound treating cells, i.e., as a measure of sonopermeabilisation. PI post-exposure samples had PI added to cells samples immediately post US treatment. N of 3 for each group, with error bars as standard deviation.

3.3.3 *In vivo* analysis of luciferase expression over time

Having established important timing and pressure parameters *in vitro,* experiments could now be performed to probe delivery *in vivo*. To establish a link between pressure, cavitation and

time of expression, an *in vivo* experiment was designed as described in section 3.2.5. In accordance with these *in vitro* and previous in vivo studies (Chapter 2), which indicated cells *in vivo* to be more sensitive to cavitation events, 1.6 MPa was the maximum pressure tested and 2.1MPa was omitted from hereon. The mice were divided into treatment groups based on pressure, table 3.3.3.1. Luciferase expression was measured via IVIS, with tumours then excised and luciferase expression measured using luciferase assay at time points of 8, 10, 12, 14 and 24 hours.

Group number	Parameters
1	1.6 MPa, 0.5 ug STPs, 5 μg mRNA, 300 s treatment time
2	1.3 MPa, 0.5 ug STPs, 5 μg μg mRNA, 300 s treatment time
3	1.0 MPa, 0.5 ug STPs, 5 ug mRNA, 300 s treatment time
4	0 MPa, 0.5 ug STPs, 5 μg mRNA, 300 s treatment time

Table 3.3.2.2: *In vivo* treatment groups indicating ultrasound pressure and treatment time parameters, concentration of STPs and concentration of RNA used. All other ultrasound parameters were kept the same, i.e., 50,000 cycles, 5% duty cycle, 0.5 PRF.

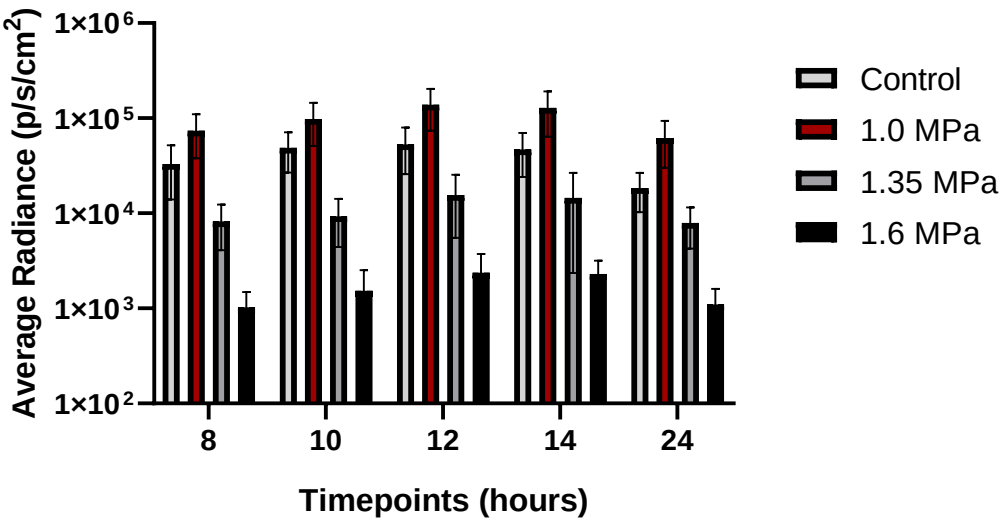

Figure 3.3.3.1: The luminescence levels measured per group at 5 time points over a 24-hour period. Luminescence is measured in average radiance per tumour. N of 4 for each measurement. Error bars represent the standard deviation of each group and time point.

Mice with CT26 tumours were injected with RNA-Luc and STP and exposed to ultrasound as described in section 3.2.5. Figure 3.3.3.1 shows the IVIS measurements taken (see methods) at different time points post-treatment for each pressure group. This data set provides several interesting points for discussion. Firstly, it is notable that the 'control' where no US was applied produced levels of expression that were about 5 and 10-fold greater than groups treated at 1.3 and 1.6 MPa, respectively. It is most probable that this decrease in expression, as a result of the application of ultrasound during delivery, is a consequence of raised cavitation-mediated cell death. This indicates that the cells within the tumour may be more fragile to cavitation events than cells *in vitro*, where 1.6 MPa represented the optimum pressure. This theory supports the fact that a 1MPa exposure gave optimal delivery in vivo, with levels 2-3-fold higher than the no ultrasound control group. Intriguingly, it is unclear what the mechanism of entry into the cells is for the control group as the instability of mRNA in the extracellular environment and its net negative charge should render it as ineffective *in vivo* as it proved to be *in vitro*. As the time profile of the expression in the control group is very similar to the ultrasound-treated groups, with levels rising between 6 and 10 hours and plateauing then decreasing thereafter, this may indicate that in common with the ultrasound-treated tumours membrane perturbation is the mechanism of entry. Such perturbation may result from mechanical disruption caused by the needle tip or by osmotic or pressure changes as a result of the injection of a volume of 25µL into the tumour (with a typical size of 100 – 150 mm^3).

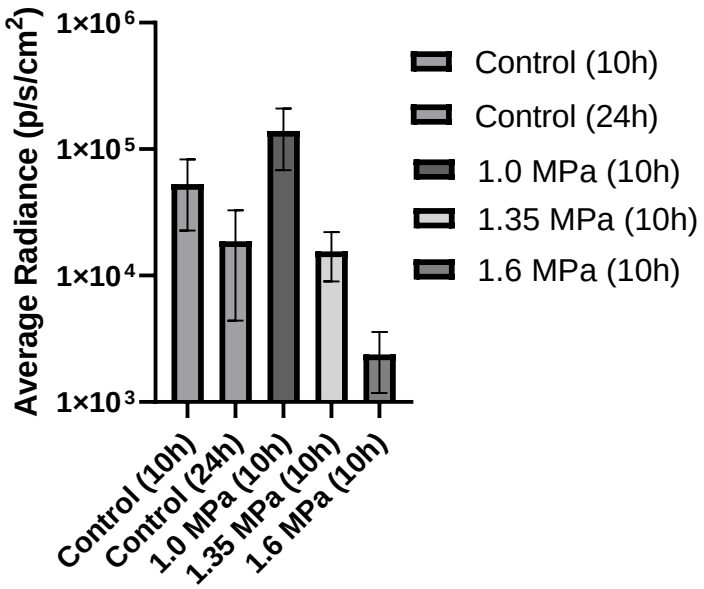

Figure 3.3.2. Average radiance was measured using the Lumina LT series III for each group at the time of maximum expression. N=4, error bars standard deviation

Whilst IVIS imaging benefits from being real-time, can give an indication of the spatial distribution of signal and allows more than one data time-point to be captured from each animal, it can be limited by attenuation of signal through layers of tissue. Information on gross expression levels can be gathered by excising tumours, homogenising them, adding luciferase reagent to the homogenate and measuring in a plate reader (see methods 3.2.8). Data from this analysis can be seen in Figure 3.3.3.3.

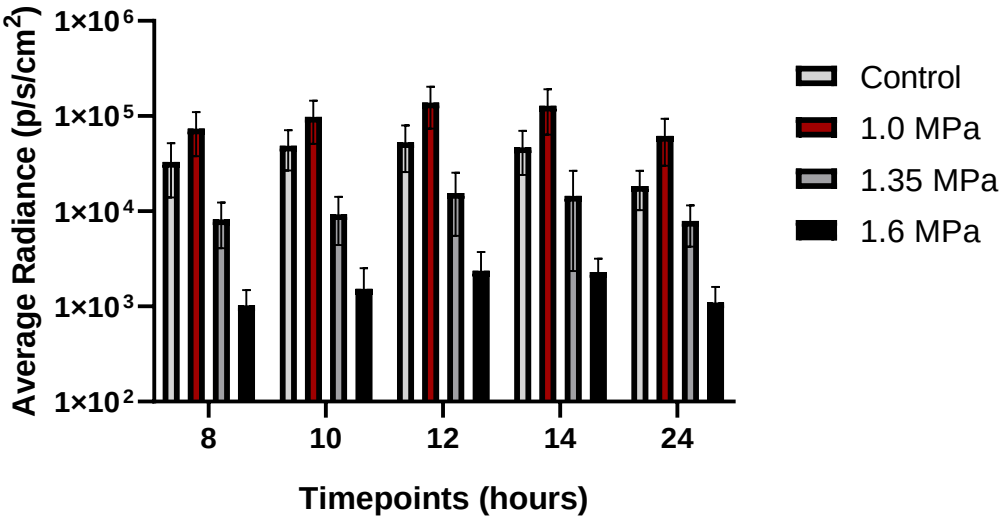

Figure 3.3.3.3: Luminescence per gram of tumour as measured my FLUOstar microplate reader using luciferase assay. N of 4, error bars are the standard deviation.

The IVIS data and post cull in vitro analysis for ultrasound exposed groups aligned well with the same pressure and time profiles evident. A maximum level of expression was observed between 10 and 12 hours for the treatment groups with a decrease, resulting in a 5- to 10-fold decrease between maximum expression at 10 hours and the 24-hour time-point as seen in figure 3.3.3.4. The IVIS analysis and *in vitro* luciferin assay results suggest that the highest expression levels coincide with a reduction in pressure, with 1 MPa exposure proving optimal. Notably, the profile of post-cull *in vitro* analysis of luciferase for the control group differed markedly from the IVIS analysis. The level was 10-fold lower than in the 1MPa group at 8 hours but increased at every subsequent time point so that by 24 hours, the level matched that in the 1 MPa group. This raises questions about the discrepancy between the IVIS and post-cull analysis for the control group and also whether the mechanism of delivery in the control and ultrasound treated groups is different. Figure 3.3.3.4 shows the maximum expression levels for each treatment group. The maximum levels were observed at 10 hours, and the difference between 1.6 MPa and the controls at 10 and 24 hours can be clearly seen and gives great insight into the results observed in Chapter 2, leads to the question regarding end time points for the experiments conducted in the next chapters.

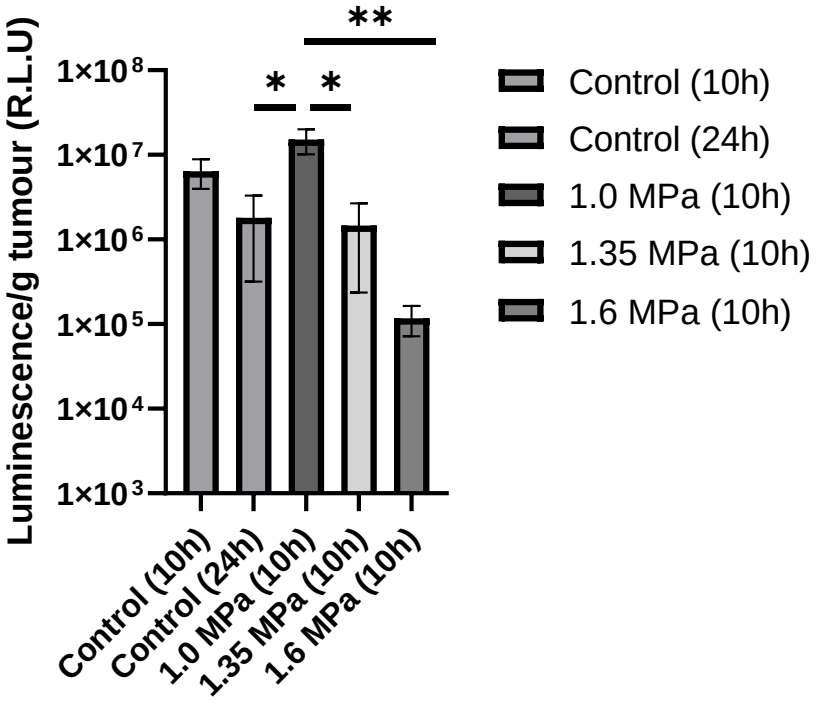

Figure 3.3.3.4: Luminescence per gram of tumour as measured my FLUOstar microplate reader using luciferase assay. For each group, the maximum expression at time = 10 hours was used for each group, and compared with 10- and 24-hour control groups. N of 4, error bars are the standard deviation.

Figure 3.3.3.5 examines the relationship between cavitation and expression of luciferase. As the pressure is increased, the cavitation also increases. However, a negative correlation with pressure and expression was observed after 1.0 MPa and a window of ~ 50 cumulative cavitation arbitrary units.

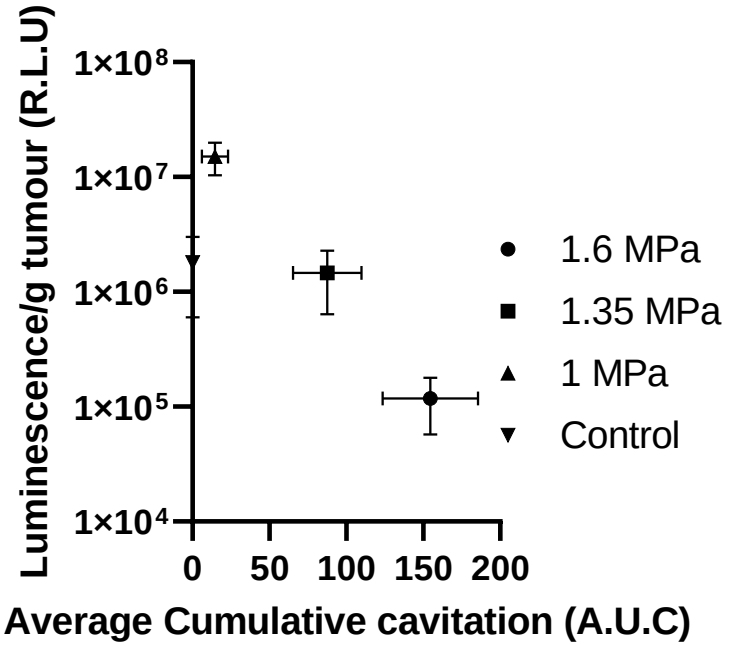

Figure 3.3.3.5: Luminescence per gram of tumour as measured my FLUOstar microplate reader using luciferase assay versus the average cumulative cavitation for each group. N of 4, X error bars are the standard deviation of the cumulative cavitation measured and Y error bars the standard deviation for samples measured for luminescence.

3.4 Discussion

This chapter provides data which contributes to our understanding of four important aspects; the impact of serum on RNA delivery, the timing and mechanism of RNA entry, the predictive value of *in vitro* studies for *in vivo* application and finally, the mechanisms of cavitation-assisted and non-assisted uptake. These aspects will be discussed in turn.

3.4.1. The impact of serum on RNA delivery

Figure 3.3.1 reports the relationship between FBS-free media and media containing 10% FBS and the level of expression from the mRNA within cells. Cells were tested in both FBS-free media and media containing FBS. The cells that were treated in a suspension containing FBS showed no expression. This is unsurprising when the high level of nucleases present within the FBS is considered (294,295). The modification of the uracil base in the mRNA used here is intended to ameliorate the impact of such degradation once the RNA enters the cell (296,297), but even with this modification the effect on degradation in the presence of FBS is limited. Such modifications are a common feature of the DNA-based nucleotide therapeutics that have

been tested pre-clinically (297), in particular, the use of oligonucleotides in the treatment of muscular dystrophy has relied on modifications to achieve successful delivery. Where RNA is concerned, aptamers have been developed for targeting, which have carried modifications to prevent degradation (298,299). Such modifications can lower nuclease degradation rates but often add complexity and expense to production and scale-up.

Uptake of functional mRNA could be assessed by monitoring the expression of the encoded protein and using this as a proxy for the level of sonoporation achieved. When assessing the results from Figure 3.3.1.1, it is evident that there are much higher expression levels for samples US treated in FBS-free media compared to media with FBS, this indicates that the speed of nuclease degradation of the RNA exceeds the rate of US mediated uptake. The work was progressed by testing post-US exposure 'plating media', which was FBS-free and comparing results to those obtained with plating media containing FBS.

One important consideration when examining these results is the long-term effect of the absence of FBS on plated cells. Cells were plated at a concentration of 1E4 per well and grown for 24 hours. Over this time, multiple samples of the cells were taken and analysed for luciferase expression. This was achieved by having a large number of wells treated with the same sample and sacrificing n=6 wells at set time-points over the course of 24 hours. Cells plated with media containing FBS exhibited a morphology similar to untreated cells, indicating exposure to US did not have lasting effects for the cells that survived and were plated. Cells were also plated in FBS-free media. While such cells still exhibited relatively healthy behaviour, they did not show the same growth rate. This is an important consideration when analysing the results. Over time, the expression of both groups – FBS-free and FBS plated cells - were examined and measured.

The results in Figure 3.3.1.2 show that the overall expression was different when plating was in FBS positive or negative media, however, not significantly ($p>0.05$), even if visually obvious differences in morphology were evident. These findings have repercussions for the use of nucleotide in the *in vitro* transfection of cells, for example in the modification of T-cells for cancer therapy or of stem cells for tissue engineering applications, suggesting that if techniques such as electroporation or ultrasound are to be used consideration of the duration that the cells need to be, and can be, grown without serum is needed.

In summary, cells exposed to RNA and ultrasound in the absence of FBS then go on to give the same expression level regardless of whether subsequent plating is in the absence or presence of FBS. Furthermore, adding RNA to cells in FBS free media after they have been exposed to ultrasound, gave no expression. These 2 findings combine to reveal that transfer of the RNA only happens during the period of ultrasound exposure. This suggests that the permeabilisation events are only fleetingly evident during ultrasound exposure. After the ultrasound mediated cavitation ceases, there is no further delivery. This may be due to rapid 're-sealing' of membrane pores or pore may remain open, but diffusion alone may not be sufficient for uptake, and a mechanism of cavitation mediated propulsion/movement of the RNA through such pores may still be required.

These data, therefore, add valuable evidence to current discussions about the nature and time-course of sonoporation, because although it is widely accepted that ultrasound exposure can create pores in the membranes of cells (300,301), a definitive understanding of the process is still needed. Indeed, the time-course of pore opening and re-sealing is hotly debated (300), with some researchers reporting creation of pores in the membrane that last in the order of minutes (302) whilst others report re-sealing within seconds (279). The question of whether such pore creation is sufficient a phenomenon to ensure delivery of co-located freely diffusing nucleotide

or whether the continued stimulus of microstreaming and shockwaves created by cavitation are important for entry through such pores also needs addressing.

The debate and the confused picture created around these questions results from the huge variability in the way different research groups have performed their experiments. For example, a huge variety of cell lines has been used, cells have been tested in an adherent state or in suspension, the type and concentration cavitation nuclei has varied, and crucially the duration, pressure, frequency, duty cycle, pulse repetition frequency and focal volume of ultrasound exposure have differed, see table 3.4.1.1. An example of the impact of these changes can be seen across studies where frequencies of 0.5 MHz – 2 MHz have been used to varying success (81,285,286,303–306) . The choice in PRF, frequency and pressure varied to see different cavitation regimes, and the effect of this change can be seen in re-seal times in general. However, there are many other variables that need to be considered before drawing firm conclusions. In the same studies, cell lines varied, use of cells adhered or in suspension, novel and commercial bubbles used, and varying bubble to cell concentrations. These variables play a critical role in the cellular response and overall 'success' of delivery and need to be considered with the same scrutiny as the ultrasound parameters.

Furthermore, in many instances, little consideration has been given in the literature to monitoring the cavitation events driving the membrane permeabilisation.

There are several advantages of the experiments performed compared to previous studies. Firstly, cavitation has been monitored and a relationship between the level of cavitation measured during exposure and the level of expression achieved has been established (Figure 3.3.3.5). Such feedback has great potential clinical utility in providing real-time verification of successful delivery. Secondly, cells were treated in suspension. This reduces the amount of preparation time and means cells can immediately be plated or seeded to scaffold without the

need for a step where transfected cells have to be rescued from their monolayer support. Thirdly, the exposure time used in the experiments reported here was just 5 minutes, this compares on a par with other sonoporation protocols, which have used 1-9 min (81,285,286,303–306) and very favourably with chemical transfection reagents which can require up to 48 hours from start to end of protocol (307,308).

However, it is important to note there is no 'ideal' system, and the setup used here could be criticised for the use of a cavitation nuclei awaiting regulatory approval and the bespoke nature of the cavitation setup, parameters, and monitoring, which all still require further optimisation for *in vitro* transfection.

Cavitation agent	***vol/conc agent***	***Cell type***	***Cell conc/tumour vol***	***Reseal***	***Ref***
SV microbubbles (MBs)	150,000 bubbles/mL 1:1 (MBs to cell)	MRC-5 fetal fibroblasts	150,000 cells/mL (0.6mL used - 90,000 cells)	within 30 s after the onset of perforation	(277)
MBs	1:1	human umbilical vein endothelial cell (HUVEC)	Single cell (1 cell to 1 bubble)	Both apical and basal cell membranes are breached and completely re-seal in-plane (~12 min).	(302)
BR14 bubbles	1:1	Human U-87 MG glioblastoma cells	plated cells	duration of membrane recovery was shown to range from a few seconds to a maximum of a few hours.	(285)

Table 3.4.1.1: Examples of microbubbles and cell lines used where sonoporation was achieved and measured. Various conditions are used, and a wide sonoporation window reported.

It is clear, therefore, that although these studies add a unique and valuable contribution to a growing body of literature around the subject of ultrasound-mediated uptake, there is still much to learn about the micro-second scale of timing and mechanism or pore formation. However,

assessing the measurements taken from the propidium iodide/trypan blue (Chapter 4) and the mRNA delivery experiments (Chapter 5) in this thesis would suggest that the sonopermeabilisation effect that occurs using STPs is a temporary one that only occurs during the 'ultrasound on' time of treatment. This conclusion seems appropriate given that for the same ultrasound conditions where mRNA is added pre ultrasound treatment, Figure 3.3.1.2 shows no expression if the mRNA is added post-treatment, regardless of the media conditions.

These studies advance our understanding of the level of cavitation required for delivery of RNA into cells, but do not specifically address the mechanism of entry and whether cavitation is needed only to generate pores or as a stimulus to propel the RNA through those pores. However, in an attempt to address this, an experiment was performed whereby the level of interaction between the RNA and the potentially US permeabilised cells was increased vortexing the mixture after it had been ultrasound exposed. Such vortexing gave no enhancement of luciferase expression (data not shown). Although this vortexing study was a rather simplistic way to try and address this question, it is notable that those who have tried to use ultrasonic waterbaths as a simple *in vitro* technique for gene delivery have reported little progress. With these findings in mind, it is fair to conclude that more work is needed to fully define the extent to which cavitation contributes to entry of nucleotide cargo and pore formation. High resolution microscopy using ultra-high-speed cameras may allow the time course of pore formation and closure to be more closely defined.

To probe the timing and mechanism of entry in more detail, a study was devised where PI was used as a 'dummy delivery' drug and added at specific time points. PI, membrane impermeable fluorescent dye, which intercalates with DNA with little to no sequence preference (309). Since PI is impermeable to cell membranes, it is typically used as a marker for dead or dying cells (310,311), but it can also be used as a "dummy" drug to test whether a membrane has been made permeable by a treatment, i.e., sonoporation (312–315).

In these studies (see section 3.3), when used 'before US treatment', PI was added, and cells were then exposed to ultrasound for five minutes, in the same way as samples to which mRNA was added. PI was also added immediately, 15 minutes or 30 minutes post-treatment. By doing this, the time point when the PI entering into the cell could be monitored, whilst cell death could be further observed and verified by the trypan measurements.

The results from table 3.3.2.1 show that when PI was added to the samples which were subsequently exposed to ultrasound, an increase in the amount of PI entering into the cells was measured compared with the conditions where PI was added immediately after ultrasound or at the later time points of 15- or 30- minutes post treatment. Notably, the level of PI staining at 15 and 30 min correlated with the level of dead cells as detected by trypan blue. Hence, the level of PI staining at 15 or 30 min represents the population of cells which suffered terminal, non-reversable permeabilisation. The differential between the PI staining in samples co-exposed to PI and US vs sample where PI was added 15 or 30 min post-US represents the population of cells that was successfully temporarily permeabilised and then recovered, a permeabilisation process which only happened during the US exposure. It can be seen from the table that as the pressure is increased, the amount of PI entering the cell increased as well. However, there is a trade-off: for the 2.1 MPa pressure group, there was an average of 48% of the cells stained with PI during treatment, but subsequent cell death measurements at 15- and 30-minutes using PI show an average of 30% of the cells stained, likely indicating cell death (as confirmed by trypan blue staining). This probably means that the differential of about 18% of cells (i.e., those that were permeabilised and PI stained but recovered) were amenable to transfection with mRNA.

In contrast, while fewer cells were initially stained with PI during exposure to lower pressures amplitudes, a higher proportion of the cells were both stained and survived. For example, at 1.85 MPa, 44% were stained during US treatment. However, only 22% were stained at 15 or

30 min and are therefore likely dead at these time points. This would indicate that around 22% of the cell were sonoporated and remained alive, an improvement compared to 2.1 MPa. At 1.6 MPa, these numbers become 38% stained with PI during US exposure and 18% stainable at 15 minutes, and, therefore, 20% likely to survive and be amenable to transfection with mRNA. For 1.35, these numbers decrease a little to 33% and 16%, resulting in 17% of cells alive and amenable to transfection with mRNA. For the 0.7 MPa group, 15% of cells are alive and transfectable with mRNA. This study again displays the balancing act needed to optimise permeabilisation % and cell survival and emphasises the need for tight control and monitoring of cavitation events.

The results would suggest that, while there is an initial increase in PI at the higher pressures, this comes with additional levels of irreparable damage to the cells. Moving forward, it is important to monitor how this PI relationship correlates with the expression shown by cells over time. If the cells can only internalise mRNA during the 'on' time of treatment, differences of expression will be reflected over a period of time. This information from *in vitro* studies was then used to guide the planning and performance of *in vivo* studies.

A significant lesson learned from Chapter 2 related to the strong correlations between exposure to high amplitude pressure and high concentration of cavitation nuclei and the level of tissue damage that resulted. To explore these findings further, both variables were changed from the original study in Chapter 2 for the experiments in Chapter 3. Firstly, the initial concentration of STPs was decreased to a 1:10 concentration to give 0.1 mg/mL for IT injection. The pressures examined were 1.0, 1.3 and 1.6 MPa, because of the lower damage levels seen in Chapter 2 when these pressure were used. Time points ranging from 8 to 24 hours were studied. These conditions were thought to give the mRNA the best chance of not being degraded whilst achieving uptake into viable tumour cells.

There were substantial and significant differences in the delivery and expression achieved at the different pressures (Figure 3.3.3.4). Whilst there was expression in the higher-pressure 2.1 MPa group was seen, higher levels were evident in the 1.6 MPa group. This appears to concur with the data from the PI and trypan blue studies (Figure 3.3.2) and gives further evidence for a reduction in pressure and overall energy delivered to achieve acceptable levels of expression and cell viability, where the cell count remains consistently above 60% post exposure. Indeed, further refinement by reducing the pressure amplitude further demonstrated a benefit.

It can be seen in Figure 3.3.3.3 that the 1.0 MPa group exhibited greater levels of expression when compared with the other treatment groups of 1.6 and 1.3 MPa. The luciferase expression level for the 1.0 MPa group at 10 and 12 hours was over two orders of magnitude higher than for the 1.6 MPa group. The study shows that lowering the pressure but maintaining some level of cavitation is beneficial to the uptake and expression of genes. However, a significant challenge remains, the control group with no US still outperformed the 1.6 and 1.3 MPa groups, by 60-fold and 4-fold, respectively, that may require additional changes to the ultrasound parameters used. However, the important increase observed using 1.0 MPa group versus the control remains a robust and potentially useful finding.

Another important element to this study is the identification of the time points at which the greatest expression occurs *in vivo*. A build-up in luciferase protein production over time was evident for all the groups, from the first point at 6 hours to the maximum expression for the groups between 10 and 12 hours. This was followed by a rapid decline over the next 12 hours to the at the final time point at 24 hours. This much lower expression level at 24 hours indicates that the *in vivo* parameters discussed in Chapter 2 could have been further refined by adjusting the time points for measuring expression levels. Moving forward from this study, all end-time points have been adjusted to 12 hours. The maximum expression levels were further confirmed

to be between 10 and 12 hours using a luciferase assay on the excised and homogenised tumours

As discussed in Chapter 2, addressing why or how the control delivery of mRNA shows any expression is an important further question to answer. One crucial factor is the change in intratumoral pressure upon injecting the volume of mRNA, STPs and PBS into the mouse. This volumetric change can cause mechanical effects which could change the behaviour of the uptake. Indeed, hydrodynamic delivery had at one point been proposed as being a clinically viable option for gene therapy delivery, until the surgical complexity and toxicity of the injection volumes involved became apparent.

This findings in Chapter 3 build on those in Chapter 2 and provide a useful advance in the understanding of cavitation mediated transfection. In this chapter, an optimal delivery methodology was formulated, allowing for maximum mRNA transfection with maximum viability. Building on this work, Chapters 4 and 5 take a comprehensive look at the impact of different cell lines and types and the translatability of *in vitro* methodology to *in vivo* protocols.

3.5 Conclusion

Several studies were devised and executed to understand the critical timing and mechanisms involved in delivering mRNA into CT26s. These studies provided the basis on which the decision to change timings for measurements was made and a comprehensive overview of the delivery-expression-time profile of the CT26 cell line. A better understanding of the required permeabilisation level and the timing of transfer of nucleotide into the cell has been obtained. However, the mechanism of how the mRNA enters cells *in vitro* remains to be fully elucidated, a situation which is even more unclear *in vivo,* where naked RNA with no cavitation appears to provide reasonable levels of expression.

However, the results correlate with the results gained from the *in vivo* pilot study in Chapter 2. In the following chapters, the parameters established in this chapter were used to optimise the work further, to examine whether there was an additional parameter set that may increase the overall delivery and expression levels.

Chapter 4 – *In vitro* exposure to cancerous and non-cancerous cell lines for ultrasound-mediated delivery of mRNA

4.1 Introduction

Information from studies performed in Chapter 3 was used as a platform for more detailed examination of optimal transfection conditions and to address the crucial question of cell-line dependence of the effects observed. To do this, in addition to the CT26 cell line, a further 5 cell lines were included in the studies reported in this Chapter 4. The aim of this work was, therefore, twofold – to test the capabilities of the setup and parameters for *in vitro* transfection of different cell lines and to build a basis for further *in vivo* work by establishing time of expression profile and how that may change depending on ultrasound exposure parameters.

In vitro transfection of cells has long been investigated for gene delivery and tissue engineering applications, and as such, the exploration of a methodology which uses no additional chemical transfection reagents offers a potentially valuable alternative to current methodologies and practices.

Successful *in vitro* transfection of cells requires a few key conditions to be met. Cells must remain viable and maintain health, behaviour, and morphology post-transfection (unless otherwise desired), and there should also be high gene delivery efficiency. Current common practices for cell transfection include the use of viral vectors (2,225), electroporation (316–318) and/or the use of cationic chemicals such as Lipofectamine, Cellfectin II, DMRIE-C transfection reagent (319,320).

For transfection reagents, some common limiting factors apply. For example, Lipofectamine and DMRIE-C transfection reagents require between 24-72 hours before cells should be tested for transgene expression, even if RNA rather than DNA is delivered (307,308,321). In addition to the time, it takes before delivery leads to substantial transgene expression, preparation time for use of such reagents can range from 45 mins to 2 hours (307,308,321). Cells are also

recommended to either be plated in 96 or 6 well plate format for the transfection process. This limits cell numbers and the ease of the manipulation of the cells post transfection. While higher volumes can be used, the ratio and volumes of reagent required mean cell suspensions of the volume and high cellular counts needed for clinical translation will require much more of the reagent at a higher cost. The increased duration before transgene expression is achieved when using these chemical methods means there is often another period of cell division and even another cycle of plating and rescue before cells can be used. This delay before expression may be easy to explain for DNA, i.e. it is caused by the need for cell division and breakdown of the nuclear membrane to allow transfer of DNA cargo from the cytoplasm into nucleus (a mechanism for such transfer is not provided by chemicals), but it is less clear why RNA also shows a delay. Regardless of the reason, these approaches add time and complexity to the protocol. Using a methodology where cells in suspension are immediately transfected and achieve peak expression in a matter of hours means they can potentially be used directly from their exposure chamber to seed a scaffold or used for implantation in the knowledge that transgene expression will commence as the cells incorporate into their new environment, this can save research time and money.

Another consideration when using transfection reagents is the toxicity to cell lines. The toxicity can be dependent on the cell line and reagent employed. The various reagents in the lipofectamine family (RNAiMAX, lipofectamine 2000, lipofectamine 3000) have been shown to have a wide-ranging cell-line-dependent effects on viability, giving a range of viabilities from 50% to 90% post transfection (322). This is just one example of how the use of such reagents can provide successful delivery but also requires considerations for long term use of the cells post transfection.

As with many of the transfection methods mentioned above, use *in vivo* is extremely rare (viral vectors excluded). Hence, a method that could be used both *in vitro* and *in vivo*, with only small

changes to the protocol, i.e., ultrasound parameter changes, may prove to be useful for gene delivery.

The work in this Chapter explores the relationship between using a mechanical stimulus in the form of cavitation and the uptake and expression of mRNA in a range of different cell types. The cells chosen for this Chapter include 2 murine models, one of which (CT26) has been used in Chapters 2 and 3, and the EMT6 cell line, which can be used in the same mice for future *in vivo* work. In addition, 2 human cancer cell lines, a primary human stem cell line and a rat cardiomyocyte cell line, were also tested. The cell lines were chosen based on potential applications and therapeutic benefit. For example, the transfection of cardiomyocytes has long been a goal for gene delivery, with many studies examining the potential therapeutic benefit if successful. Transfecting human stem cell lines rapidly, with high efficacy and low toxicity in an easy to manipulate and scalable setup, may have an industrial application and lead to advances in tissue engineering. The time profile of expression for all these cell lines, CT26 cells, murine mammary carcinoma (EMT6) cells, human lung carcinoma (A549) cells, human cervix adenocarcinoma (HeLa) cells, mesenchymal stem cells (MSCs), and rat cardiomyocytes, and the consistent effect that cavitation has in mediating delivery of RNA, will be discussed below.

4.2 Materials and Methods

4.2.1 Cell lines and cell culture

For the body of work contained in this Chapter, six different cell lines were used, culturing and growth methods were as follows. These 6 cell types covered a range of species origin (human, mouse, rat), organ origin (colorectal, mammary, cardiac, lung) and developmental or transformed status. This selection, therefore, forms the basis for assessing if 'universal' ultrasound transfection parameters can be identified or whether a more cell-specific set of parameters needs to be identified for each.

4.2.2 CT26 cells

Murine colorectal carcinoma CT26.WT cells (ATCC, CRL-2638; American Type Culture Collection, Rockville, MD, USA) were grown to approximately 90% confluence with a minimum of 95% viability using Roswell Park Memorial Institute 1640 medium (RPMI 1640; R8758, Sigma-Aldrich Company Ltd, Dorset, UK) supplemented with 10% fetal bovine serum (FBS; F7524, Sigma-Aldrich, Dorset, UK). Cells were grown to a maximum of 13 passages.

4.2.3 EMT6 cells

Murine mammary carcinoma, EMT6 cells (ATCC, CRL-2755; American Type Culture Collection, Rockville, MD, USA) were grown to approximately 90% confluence with a minimum of 95% viability, using Waymouth MB 752/1 media (W1625, Sigma-Aldrich Company Ltd, Dorset, UK) supplemented with 10% fetal bovine serum (FBS; F7524, Sigma-Aldrich, Dorset, UK). Cells were grown to a maximum of 6 passages.

4.2.4 A549 cells

Human lung carcinoma, A549 cells (ATCC, CCL-185; American Type Culture Collection, Rockville, MD, USA) were grown to approximately 85% confluence with a minimum of 95% viability using Dulbecco′s Modified Eagle′s Medium (DMEM; D777, Sigma-Aldrich Company Ltd, Dorset, UK) supplemented with 10% fetal bovine serum (FBS; F7524, Sigma-Aldrich, Dorset, UK). Cells were grown to a maximum of 12 passages.

4.2.5 HeLa cells

Human cervix adenocarcinoma, HeLa cells (ATCC, CRM-CCL-2; American Type Culture Collection, Rockville, MD, USA) were grown to approximately 90% confluence with a minimum of 95% viability using Dulbecco′s Modified Eagle′s Medium (DMEM; D777, Sigma-Aldrich Company Ltd, Dorset, UK) supplemented with 10% fetal bovine serum (FBS; F7524, Sigma-Aldrich, Dorset, UK). Cells were grown to a maximum of 10 passages.

4.2.6 Mesenchymal Stem Cells

Human-induced pluripotent stem cell-derived mesenchymal stem cells, MSC cells (ATCC, ACS-7010; American Type Culture Collection, Rockville, MD, USA), were grown to approximately 90% confluence with a minimum of 95% viability using Dulbecco′s Modified Eagle′s Medium (DMEM; D777, Sigma-Aldrich Company Ltd, Dorset, UK) supplemented with 10% fetal bovine serum (FBS; F7524, Sigma-Aldrich, Dorset, UK). Cells were grown to a maximum of 6 passages.

4.2.7 Cardiomyocyte cells

Rat myocardium cells (ATCC, CRL-1446; American Type Culture Collection, Rockville, MD, USA) were grown to approximately 80% confluence with a minimum of 90% viability using Dulbecco′s Modified Eagle′s Medium (DMEM; D777, Sigma-Aldrich Company Ltd, Dorset, UK) supplemented with 10% fetal bovine serum (FBS; F7524, Sigma-Aldrich, Dorset, UK). These cells were a subclone of the original clonal cell line derived from embryonic BD1X rat heart tissue. Cells were grown to a maximum of 3 passages.

4.2.8 Cell Culture

All cells were grown to the stated desired confluence at 37 °C in a humidified atmosphere of 5% carbon dioxide. Once at confluence, cells were harvested and prepared for *in vitro* testing or implantation. Cells were washed using Dulbecco's Phosphate Buffer Saline solution (DPBS; D8537, Sigma-Aldrich, Dorset, UK) and harvested using 1X trypsin-EDTA (T3924, Thermo Fisher Scientific, UK). Once the cells had detached from tissue culture flasks, the trypsin was neutralised using three times the volume of their culture media, e.g., RPMI for CT26 cells, DMEM for HeLa cells.

Subsequently, the cell were taken off the flasks, placed in a centrifuge tube, and centrifuged at the appropriate RCF and time, taken from their corresponding ATCC cell culture protocol, at

room temperature to form a cell pellet. Upon the formation of the pellet, excess media and trypsin were removed. The cells were resuspended in fresh culture media, and the centrifuge step was repeated to ensure all trypsin had been removed. The cells were then suspended in either FBS-free media or media containing FBS. A cell count and viability assessment were then obtained using the trypan blue dye exclusion method and a haemocytometer. Cells were prepared to the correct concentration for *in vitro* testing to a concentration of 1E6/mL in 0.5 mL total media volume or 1E5/0.1mL in FBS free media for implantation.

4.2.9 *In vitro* setup

The ultrasound setup employed two high-intensity focused ultrasound (HIFU) transducers, as described in Chapter 3, which were perpendicularly aligned with a common focus where the sample was placed. The setup, parameters and data processing was as described in Chapter 3, section 3.2.

Table 4.2.9.1 shows how each cell line was allocated into groups. The experiment aimed to examine how pressure amplitude and resulting cavitation may affect the level, duration and timing of transgene expression *in vitro.*

	Cell Line: ***Generic* example**	
Group	**Conditions**	**Fixed conditions**
1	2.1 MPa (with STPs)	50,000 cycles 5% duty cycle, 0.5 Hz PRF, using 0.5 MHz transducer
2	1.85 MPa (with STPs)	
3	1.6 MPa (with STPs)	
4	1.35 MPa (with STPs)	
5	1.0 MPa (with STPs)	
6	0.7 MPa (with STPs)	
7	2.1 MPa without STPs	
8	0.7 MPa without STPs	
9	mRNA only, without STPs, no US	N/A
10	mRNA only with STPs, no US	

Table 4.2.9.1: Treatment conditions for each group (repeated for each cell line).

Before ultrasound exposure, 5 µL of mRNA and 10 µL STPs were added and mixed into each sample, leaving a total volume of 515 µL in a 2 mL eppendorf tube. For control samples that had no STPs added, 10 µL of 5 % glucose was added in place of the STPs. Each sample was manually inverted three times to ensure adequate mixing before being placed in the tank, aligned, and treated.

4.2.10 Cell death measurements

After each sample was exposed, 15 minutes post exposure (a time point chosen based on work in Chapter 3), two cell death measurements were taken for each and averaged. This was done by taking 20 µL total (2 x 10 µL) from the cell suspension sample and adding to 2 x 10 µL of trypan blue. Cells were then counted, and comparisons made to the total number of cells pre and post exposure and the number of trypan blue positive cells. Cells were counted on an automated cell counter, Invitrogen Countess ii (ThermoFisher Scientific, AMQAF1000). For cells counted as "remaining whole", this means the number of cells able to be counted, still intact enough to stain and see when counting cells, the exclusion of cellular debris.

4.2.11 SonoTran Particles

SonoTran particles (STPs, OxSonics Ltd, UK) were prepared from a stock concentration of 25 mg/mL and diluted to 21.4 mg/mL using 40% glucose to create a new standard stock solution of 21.4 µg/µL in 5% glucose, before injection. A 1:10 dilution of this stock was used as the experiments in Chapters 2, and 3 demonstrated this dilution was likely to give the greatest chance of success.

4.2.12 mRNA

CleanCap® FLuc mRNA (5moU), which encodes for firefly luciferase protein production, was ordered from Trilink biotechnologies (L-7202) and was 1929 nucleotides long, and is fully substituted with 5-Methoxy-U. The modified uracil base is designed to allow greater time

before degradation of the mRNA takes place. The sequence also includes a poly-A tail residues for enhanced stability.

4.2.13 Quantification - Luciferase Assay

Post exposure, cell samples were plated into a 96 well plate using the appropriate cell media. Each sample was plated to achieve triplicate measurement at each of the following time points; 6, 8, 10, 12, 14, and 24 hours. Cells were plated to a density of 1E4 and placed in the incubator immediately after being plated in 200 µL of the appropriate media and only removed for the luciferase assay.

To perform the luciferase assay, media was removed from each sample, and samples were gently washed using 100 µL of PBS. Once washed, the PBS was removed, and 100 µL of 1x Cell lysis buffer supplied in the luciferase assay kit was added to the sample. After 2 minutes, 20 µL of the luciferase assay reagent (Luciferase Assay System (E1500; Promega, Southampton, UK) was added to each sample.

After adding the luciferase assay reagent, each sample well was analysed for luciferase expression using a microplate reader (FLUOstar Omega; BMG Labtech, Aylesbury, UK) using pre-set luminescence measurements.

4.3 Results

4.3.1 CT26 *in vitro* exposure results

CT26 cells were exposed in suspension as described in the Methods section 4.2.9; the cell counts taken immediately before and after exposure at different parameters can be seen in table 4.3.1.1. Before exposure, the cell count was 1E6/mL, while after exposure, the number of remaining cells varied greatly, with as much as a 3-fold difference between 2.1 MPa with STPs and US (31%) versus 0.7 MPa with STPs and US (93%).

Group	Conditions	% Cells remaining whole
1	2.1 MPa	31 +/-6.5
2	1.85 MPa	36 +/- 3.9
3	1.6 MPa	56 +/- 3.1
4	1.35 MPa	69 +/- 2.9
5	1.0 MPa	88 +/- 2.1
6	0.7 MPa	93 +/- 1.2
7	2.1 MPa without STPs	41 +/- 3.2
8	0.7 MPa without STPs	94 +/- 1.1
9	mRNA only, without STPs, no US	98 +/- 0.9
10	mRNA only with STPs, no US	98 +/- 0.8

Table 4.3.1.1: Impact of different ultrasound parameters, as denoted in table, on CT26 cell viability as determined using the Countess machine. 500,000 live cells were exposed, and then the number of 'event' classified as a live cell calculated. Cells were assessed using trypan blue post treatment and the Countess Cell counting machine. N of 3 for each group, with the '+/-'representing the standard deviation for each group

It is evident that decreasing the pressure 0.5 MPa, i.e. between 2.1 and 1.6MPa, resulted in a reduction in cell death from 69% destroyed to only 44%. Table 4.3.1.1, therefore, further strengthens the conclusion outcomes from Chapter 2 in showing that the use of 2.1 MPa, with STPs and US is too damaging for the CT26 cell line and emphasises the importance of testing a range of parameters. Another noteworthy finding is the observation that, even in the absence of STPs, 2.1 MPa induced substantial immediate cell death, indicating that in this setup at this pressure, cavitation can be instigated without the need for addition of cavitation nuclei. Furthermore, at 0.7MPa, there was negligible difference in cell death (6% v 7%) in the presence and absence of STPs, but this level of death was higher than that seen in the complete absence of US (2%). This suggests that even at this reduced pressure, a low level of damaging cavitation is possible in the absence of STPs, this cavitation level was barely detectable by the currently available PAM method (see Figure 4.3.1.2) but clearly substantial enough to have a biological impact.

Ultrasound and, specifically cavitation, can result in the total loss of cell structure to the extent that the cell is no longer recognised, and the total cell count drops. It is also apparent that a

level of damage can be incurred, which may lead the cell to become permeabilised but not immediately destroyed and therefore not excluded by cell counting. Over the subsequent 24 hours, the cell may then recover from such damage or not. Defining this population of cells which are permeabilised but recover provides insight into the population which may be available for uptake and expression of the RNA. To probe this phenomenon, membrane impermeable dyes such as trypan blue and propidium iodide were used.

Of the cells that remained post-treatment, table 4.3.1.2 quantifies those that also stained positive for trypan blue. These measurements were performed as described in the Methods section 4.2.10, and counts were performed 15 minutes post-treatment and before plating. For CT26s, table 4.3.1.2 shows that the highest pressure of 2.1MPa with STPs leads to higher immediate cell death, with just 310,000 of the initial 1,000,000 surviving long enough to be detected, and of these remaining 310,000 cells, 93,000 (i.e., 30%) subsequently stained positive for trypan blue. Notably, this pressure in the absence of STPs resulted in 24% trypan blue positivity, suggesting that cavitation could be instigated without and exogenously added nuclei, figure 4.3.1.2. As the pressure was reduced, the percentage of immediate cell death and subsequent trypan blue staining decreased so that by 0.7MPa with STPs, 93% of exposed cells could be counted immediately after exposure and only 5% of these subsequently stained with trypan blue. Intriguingly, whilst use of 0.7MPa without STPs gave equivalent immediate counts, the level of trypan blue staining was 3-fold lower than when 0.7MPa was used with STPs. When the information in table 4.3.1.1 and 4.3.1.2 are taken together, at high pressures for CT26 cells, the cells are destroyed, and of those that survive the initial process and remain intact, up to 30% of those are alive but permeabilised and may go on to die or are already dead. Unpicking the particular ratios of these populations by cell counting and staining at 24 hours may provide insight, but such studies would be complicated by the recovery and division of the cells that have survived.

		CT26 (/mL)		
Group	**Conditions**	**Post treatment cell count average (thousands)**	**Average Trypan positive cells (thousands)**	**% stained**
1	2.1 MPa	310	93, +/- 7.2	30
2	1.85 MPa	360	101, +/- 6.8	28
3	1.6 MPa	560	112, +/- 6.4	20
4	1.35 MPa	690	82.8, +/- 3.6	12
5	1.0 MPa	880	88.0, +/- 3.9	10
6	0.7 MPa	930	46.5, +/- 3.6	5
7	2.1 MPa without STPs	410	98.4, +/- 5.3	24
8	0.7 MPa without STPs	940	18.8, +/- 1.1	2
9	mRNA only, without STPs, no US	980	9.8, +/- 0.9	1
10	mRNA only with STPs, no US	980	19.6, +/- 1.2	2

Table 4.3.1.2: Shows the number of CT26 cells remaining intact post treatment and the number of those cells that stained positively with trypan blue indicting dead cells. N of 3, with '+/-'representing standard deviation.

The results for the expression of luciferase over time can be seen in Figure 4.3.1.1. This Figure shows that the group with the highest number of trypan blue positive cells (1.6MPa with STPs, 112,000 cells) had the highest expression ~1.6e4 RLU. Figure 4.3.1.1 also indicates that, regardless of the US pressure applied, the time point of peak expression time is 10 hours, with a pattern of signal growth over the first 10 hours post-exposure, followed by a drop off at 12 hours which continues until the final time point of 24 hours. By 24 hours, the expression has decreased at least 2-fold for each group which confirms how critical the choice of time points and endpoints for the *in vivo* work presented in Chapter 2 may be. Consideration of the cell death and trypan blue staining in the context of the RNA delivery and expression may provide interesting insights into the mechanism of transfer. When 2.1 MPa was applied without STPs, the levels of immediate cell death, trypan blue staining at 15 min and luciferase expression at 24 hours were all very similar to the levels achieved with 2.1MPa with STPs. At 0.7MPa in the absence of STPs, out of the 5E5 cells exposed, only 10,000 fewer cells were immediately killed,

and only 28,000 fewer cells were positive for trypan blue staining, compared to 0.7MPa with STPs, and yet the luciferase expression was 10-fold lower in the absence of STPs. It is clear that a balance needs to be struck between high transfection, with high cell death achieved at higher pressures, and low cell death and low transfection at lower pressure or no US. These data suggest that in this cell line in this setup, the optimum pressure for the greatest number of transfectable cells is 1.6MPa.

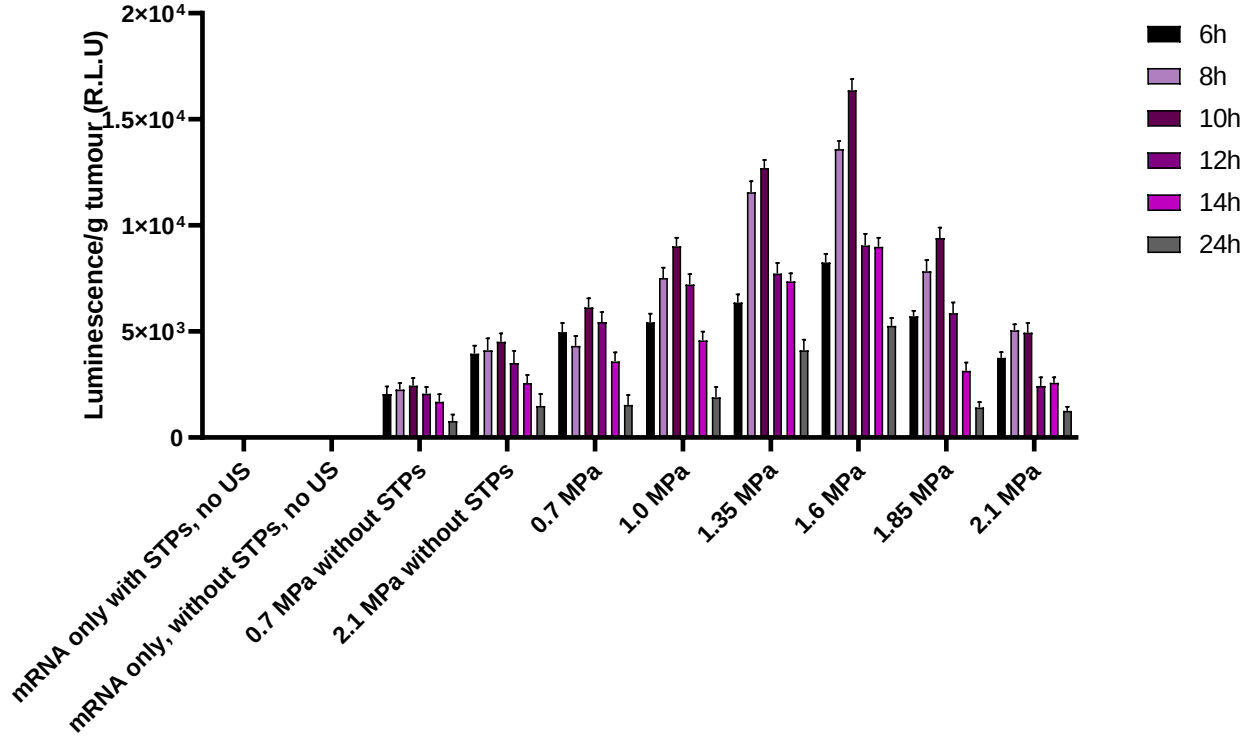

Figure 4.3.1.1: Expression of luminescence in relative light units (R.L.U) in CT26 cells over 24 hours following US exposure, as measured using a microplate reader. 2.1-0.7 MPa groups include STPs with Ultrasound. 9 samples per group at each time point, 3 group measurements, with triplicates for each, averaged. N of 3, error bars are the standard deviation.

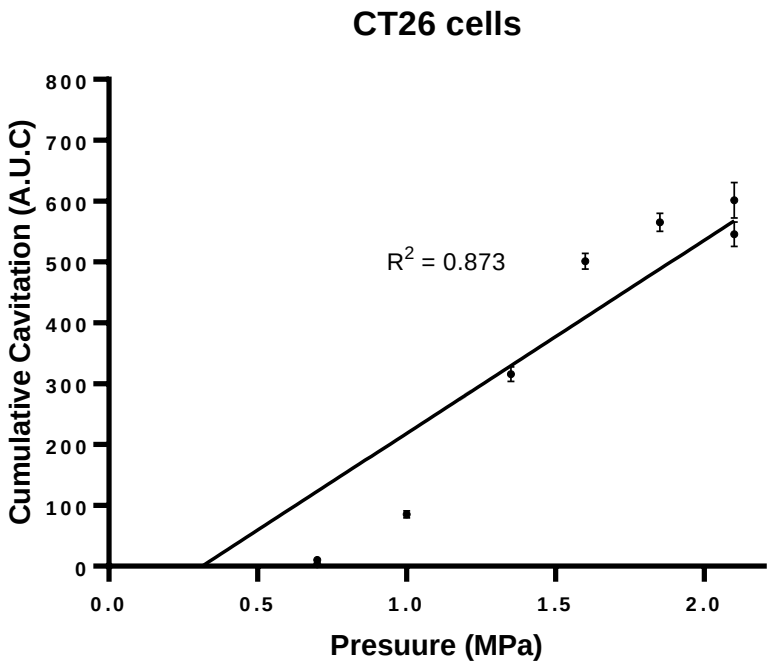

Figure 4.3.1.2: The average cumulative cavitation for each CT26 group plotted against the pressure of exposure. As pressure is increased, the cumulative cavitation increased for each group. Each data point represents the mean of N of 3, error bars are the standard deviation for cumulative cavitation. Data points represent the mean of three. Cavitation PAM AUC values at specified pressure (0, 1, 1.35, 1.6, 1.85, 2.1 MPa)

Figure 4.3.1.2 examines the relationship between pressure applied and the cavitation detected. At pressure above 0.7 MPa, the relationship can be seen as linear with an R^2 value of 0.875, with increases in pressure leading to predictable increases in levels of cavitation. Linearity may diminish at pressure levels over 2 MPa as, at these pressures, bubble cloud formation may produce a shielding effect and therefore limit the amount of cavitation.

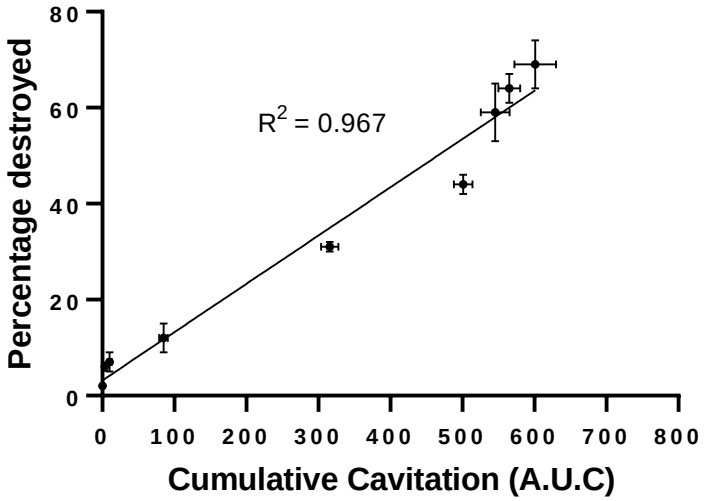

Figure 4.3.1.3: Average cumulative cavitation for each CT26 group and the corresponding percentage of cells destroyed. Cells in the setup described in section 4.2.9 were exposed to defined pressure for 5 minutes and cavitation energy acquired during exposure and cell death assayed after exposure by trypan blue measurement. N of 3 for pressure point (and hence cavitation range), X error bars are the standard deviation for each group, y error bars are the standard deviations but are hard to view due to the low variability in viability measurements.

Figure 4.3.1.3 shows the relationship between cumulative cavitation and the percentage of the cells destroyed during the treatment. As can be seen, as the cavitation increases, so does the number of cells destroyed in a predictable linear fashion ($R^2 = 0.9747$). The fact that higher pressure results in more significant cell death is confirmed in Chapter 2 and is detrimental to the uptake and expression of mRNA. That such reliable relationships can be drawn raises hopes that 'universally' useful effective parameters can be identified and demonstrates how cavitation measurement may provide an early, reliable, and non-invasive metric of success.

4.3.2 EMT6 *in vitro* exposure results

EMT6 cells were treated and exposed in the same manner as CT26s, and the initial number of cells that remained intact post-treatment can be seen in table 4.3.2.1. As can be seen from the table, there are similarities in the number of cells that remain after treatment across the EMT6 cell line compared with the CT26 response above. There is a decrease in the number of cells

intact at the higher pressures of 2.1 MPa, 1.85MPa and 1.6MPa, with on average 3 % more cells destroyed across these three groups for the EMT6s compared to CT26.

Group	Conditions	% Cells remaining whole
1	2.1 MPa	28 +/- 4.9
2	1.85 MPa	34 +/- 4.2
3	1.6 MPa	55 +/- 3.9
4	1.35 MPa	71 +/- 3.4
5	1.0 MPa	86 +/- 2.5
6	0.7 MPa	92 +/- 1.8
7	2.1 MPa without STPs	38 +/- 3.6
8	0.7 MPa without STPs	93 +/- 1.3
9	mRNA only, without STPs, no US	97.5 +/- 0.4
10	mRNA only with STPs, no US	97.5 +/- 0.6

Table 4.3.2.1 Impact of different ultrasound parameters, as denoted in table, on cell viability. Cells were assessed using trypan blue post treatment (see methods). N of 3 for each group, with the '+/-' representing the standard deviation for each group

Table 4.3.1.1 would indicate that when compared to the CT26 results, the EMT6 cells appear to be more sensitive to the damaging effects of ultrasound and cavitation. Across all the groups, there are more cells destroyed (table 4.3.1.1) and more cells being stained positively 15 minutes post-exposure.

		EMT6 (/mL)		
Group	**Conditions**	**Post treatment (thousands)**	**Trypan positive cells (thousands)**	**% Stained**
1	2.1 MPa	280	95.2	34
2	1.85 MPa	340	105	31
3	1.6 MPa	550	143	26
4	1.35 MPa	710	156	22
5	1.0 MPa	860	120	14
6	0.7 MPa	920	73.8	8
7	2.1 MPa without STPs	380	95	25
8	0.7 MPa without STPs	930	37.2	4
9	mRNA only, without STPs, no US	975	19.5	2
10	mRNA only with STPs, no US	975	19.5	2

Table 4.3.2.2: Shows the number of EMT6 cells remaining intact post treatment and the number of those cells that stained positively with trypan blue indicting dead cells. N of 3 for each group

Table 4.3.2.2 confirms the findings of 4.3.2.1 in showing that the EMT6 cells seem to exhibit more sensitivity to the effects of the ultrasound.

Notably, the impact of this increased sensitivity can be seen in the expression levels of the EMT6 cells that remain. As shown from Figure 4.3.2.1, there are some critical differences between the results in Figure 4.3.1.1 for CT26s and the results below for EMT6s. Most striking are the levels of expression across all groups being higher for that of the EMT6 cells apart from at 2.1 MPa with STPs. The expression levels for the EMT6 are approximately 10% higher than with CT26 cells for pressures of 1.6, 1.35 and 1.0 MPa. Despite differences in absolute expression levels, the optimal pressure and time profile of expression is similar to that observed for the CT26 cells, with the maximum expression found at 1.6MPa and the maximum time point for expression being 10 hours, with the signal decreasing over the subsequent 14 hours.

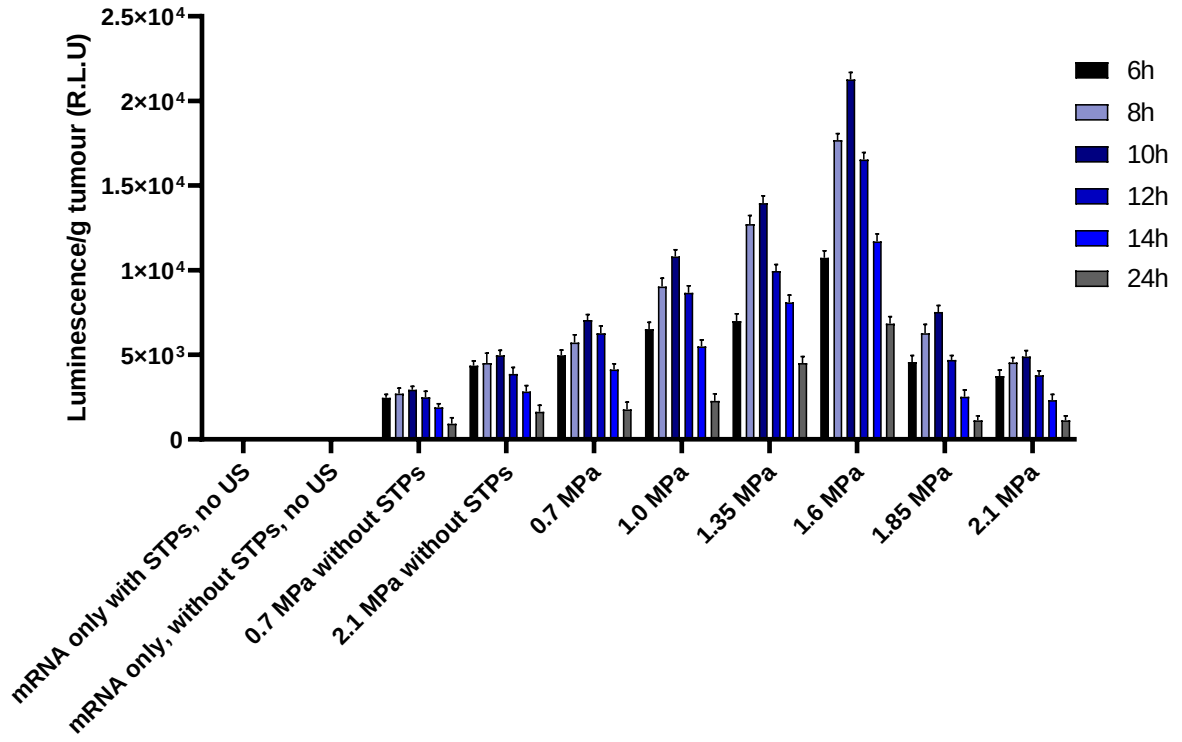

Figure 4.3.2.1: Expression of luciferase in EMT6 cells in relative light units (R.L.U) over 24 hours after treatment, as measured by microplate reader. 2.1-0.7 MPa groups include STPs with ultrasound. 9 samples per group at each time point, 3 group measurements, with triplicates for each, averaged. N of 3, error bars are the standard deviation.

Figure 4.3.2.2 shows the relationship between detected cavitation and pressure applied. As expected, as the pressure is increased, so too follows the cavitation detected.

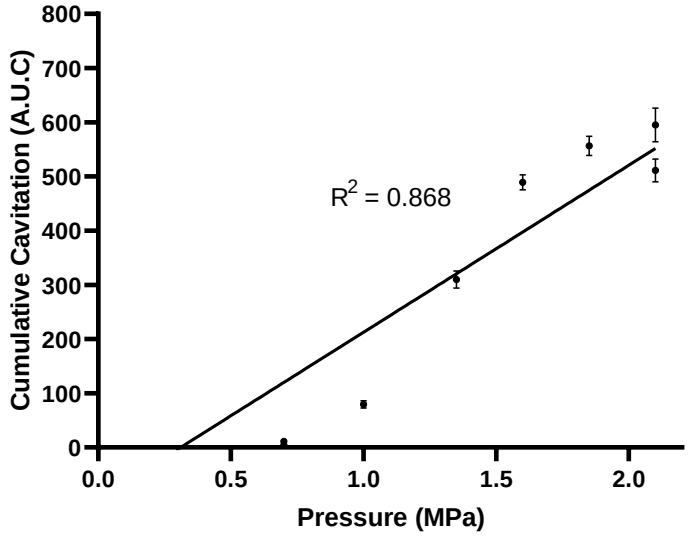

Figure 4.3.2.2: The relationship between pressure of exposure and the average cumulative cavitation for each EMT6 group. As pressure is increased, the cumulative cavitation increases for each group. N of 3, error bars are the standard deviation for cumulative cavitation.

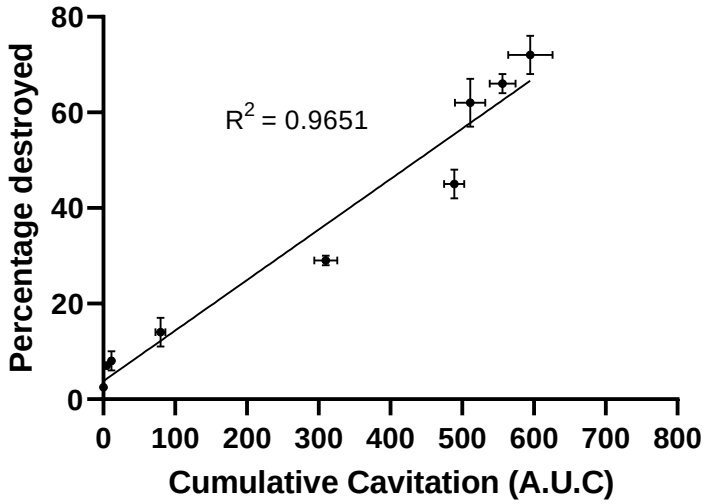

Figure 4.3.2.3: Average cumulative cavitation for each EMT6 group and the corresponding percentage of cells destroyed. N of 3 for pressure point (and hence cavitation range), X error bars are the standard deviation for each group, y error bars are the standard deviations but are hard to view due to the low variability in viability measurements.

Experiments with EMT6 cells exhibited the same behaviour as those with CT26 cells, whereby an increase in cavitation led to an increase in cellular destruction. However, as shown in tables 4.3.2.1 and 4.3.2.3, this had a lesser effect on the overall luciferase expression in the EMT6 cells. The close accordance between the pressure applied and cavitation detected in testing in the two cell lines argues for the differences in luciferase expression levels being related to differences in the sensitivity of the cells to the cavitation events rather than there being different levels of cavitation.

4.3.3 A549s *in vitro* exposure results

To investigate if different effects would be evident in different cell line types, the human lung cell carcinoma, A549 cell line, was investigated. The results of the impact of ultrasound exposure can be seen in table 4.3.3.1. It can be seen that immediately post-treatment with ultrasound mediated cavitation, there was less of a destructive effect evident in A549 cells compared to both the CT26 and EMT6 cell lines (see 4.3.1. and 4.3.2), suggesting this cell line

may be more robust. For example, even at 2.1 MPa, 45% viability was evident, a marked improvement on the ~30% seen with CT26 and EMT6 cells.

Group	Conditions	% Cells remaining whole
1	2.1 MPa	45
2	1.85 MPa	60
3	1.6 MPa	70
4	1.35 MPa	83
5	1.0 MPa	88
6	0.7 MPa	93
7	2.1 MPa without STPs	49.5
8	0.7 MPa without STPs	97.5
9	mRNA only, without STPs, no US	99.5
10	mRNA only with STPs, no US	99.5

Table 4.3.3.1: Impact of different ultrasound parameters on A549 cell viability. Cells were assessed using trypan blue post treatment. N of 3 for each group, with the '+/-'being the standard deviation for each group

Table 4.3.3.2 shows the outcome for how many cells stained for trypan blue, and thus were permeabilised and post-treatment. There is a decrease in the number of cells stained after exposure at each pressure used when compared to results with both CT26 and EMT6s. This may be indicative of the A549s having less of a response to the ultrasound-mediated cavitation, and therefore this might limit the ability of ultrasound to impact on transfection, Figure 4.3.3.1. Alternatively, the difference may be due to the levels of cavitation being lower, which can be seen in Figure 4.3.3.3.

		A549s (/mL)		
Group	Conditions	Post treatment (thousands)	Trypan positive cells	% stained
1	2.1 MPa	450	180	28
2	1.85 MPa	600	144	24
3	1.6 MPa	700	133	19
4	1.35 MPa	830	125	15
5	1.0 MPa	880	88.0	10
6	0.7 MPa	930	74.4	8
7	2.1 MPa without STPs	495	114.5	23
8	0.7 MPa without STPs	975	48.8	5
9	mRNA only, without STPs, no US	995	995	< 1
10	mRNA only with STPs, no US	995	995	< 1

Table 4.3.3.2: Analysis of A549 cell viability post treatment as assessed by cell counting and trypan blue staining. N of 3 for each group

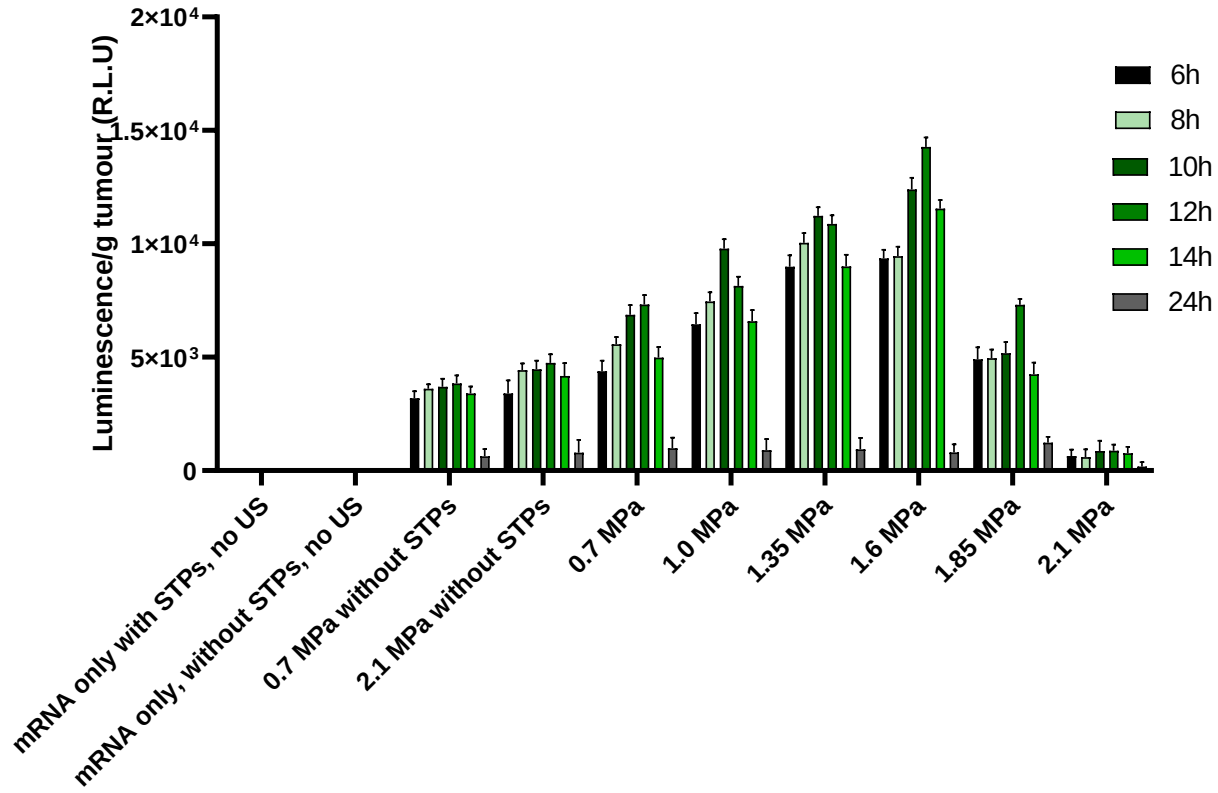

Figure 4.3.3.1: Level of A549s luciferase expression over the 24 hour period following treatment, in relative light units (R.L.U) as measured using a microplate reader. 2.1-0.7 MPa groups include STPs with Ultrasound. 9 samples per group at each time point, 3 group measurements, with triplicates for each, averaged. N of 3, error bars are the standard deviation.

Figure 4.3.3.1 shows that the levels of transfection and thus expression of luciferase was lower for the A549s in comparison to that of CT26 and EMT6 cells. A pressure of 2.1 MPa plus STPs showed a decrease between 8-10 fold compared to CT26 and EMT6 cells. At all pressures, the expression for A549s was lower than that of the equivalent groups for CT26 and EMT6 cells. The general pattern within the results for A549s follows that of the CT26 and EMT6, whereby the 1.6 MPa exposure plus STPs group had the highest expression. However, there was a change to the time-profile of luciferase expression. For CT26 and EMT6 cell lines, this maximal time point was seen at 10 hours, but for the A549s, this time point has clearly shifted to 12 hours post exposure, with a decrease thereafter to the endpoint of 24 hours. Such a shift may relate to cell-specific endogenous rates of mRNA processing and translation.

Figure 4.3.3.2 shows the relationship between detected and measured cavitation and the pressure applied for each group. The same relationship as can be seen for the CT26 and EMT6 groups is exhibited.

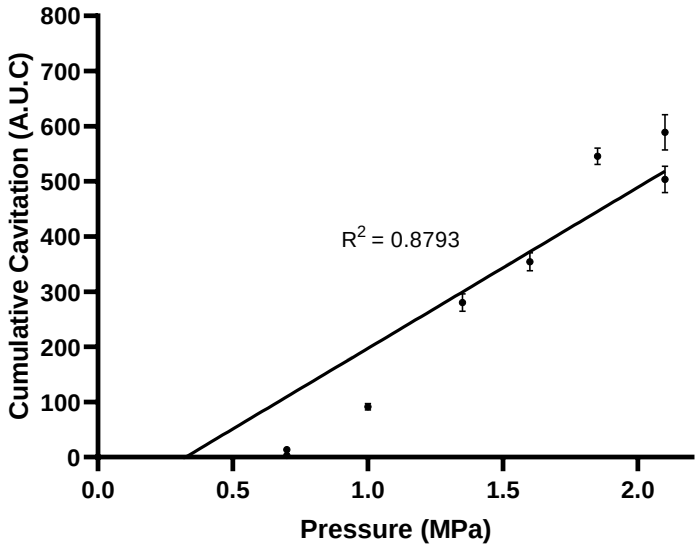

Figure 4.3.3.2: Relationship between exposure pressure and the average cumulative cavitation for each A549 group. As pressure is increased, the cumulative cavitation increases. N of 3, error bars are the standard deviation for cumulative cavitation.

Another noteworthy result is the 2.1 MPa with no cavitation nuclei group, which shows an interesting response. The levels of expression are where one would expect 2.1MPa plus STPs to be. By looking at the cavitation data, Figure 4.3.3.3, some insight can be gained.

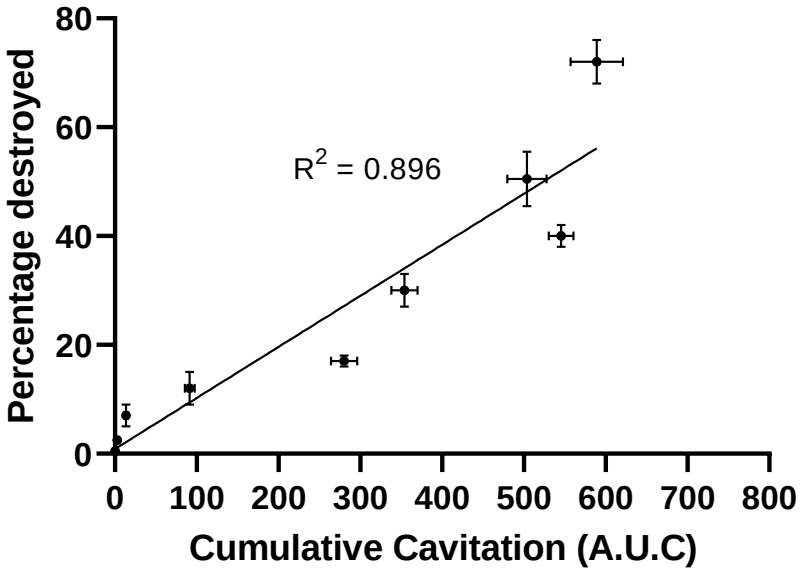

Figure 4.3.3.3: Average cumulative cavitation for each A549 group and the corresponding percentage of cells destroyed. N of 3 for pressure point (and hence cavitation range), X error bars are the standard deviation for each group, y error bars are the standard deviations but are hard to view due to the low variability in viability measurements.

The cavitation levels experienced by the A549s were lower than that of the CT26 and EMT6s in general, but the difference is not significant ($p>0.05$), and therefore the effect is likely limited. However, when looking at the expression in Figure 4.3.3.1, lower expression levels are evident

4.3.4 HeLa *in vitro* exposure results

As well as looking at human lung carcinoma, the HeLa cell line (originally derived from a cervical cancer) was also investigated. The cells were treated under the same conditions as CT26, EMT6 and A549s and tested post-treatment in the same way. The results from the immediate cell count are shown below in table 4.3.4.1, which shows that the cells had a different response to that of the A549s but a much more similar response to that of the CT26s and EMT6 cell lines.

Group	Conditions	% Cells remaining whole
1	2.1 MPa	27
2	1.85 MPa	39
3	1.6 MPa	73
4	1.35 MPa	81
5	1.0 MPa	88
6	0.7 MPa	91
7	2.1 MPa without STPs	42
8	0.7 MPa without STPs	92
9	mRNA only, without STPs, no US	94
10	mRNA only with STPs, no US	94

Table 4.3.4.1: HeLa cell viability at different ultrasound exposure parameters as denoted. Cells were assessed using trypan blue post treatment. N of 3 for each group, with the '+/-'being the standard deviation for each group

Immediately post-treatment, the cells were counted as above. Once again, the HeLa's had a similar response to the ultrasound and cavitation regimes to that of the CT26s and EMT6 cell lines. At 2.1 MPa plus STPs, 30% of cells stained positively with trypan blue and by 0.7 MPa plus STPs, 9% stained positively. Notably, this did not translate to higher luciferase expression levels, as seen in Figure 4.3.4.1.

		HeLa (/mL)		
Group	Conditions	Post treatment (thousand)	Trypan positive cells (thousand)	% Stained
1	2.1 MPa	270	81.0	30
2	1.85 MPa	390	101.0	26
3	1.6 MPa	730	168.0	23
4	1.35 MPa	810	162.0	20
5	1.0 MPa	880	132.0	15
6	0.7 MPa	910	81.9	9
7	2.1 MPa without STPs	420	105.0	25
8	0.7 MPa without STPs	920	64.4	7
9	mRNA only, without STPs, no US	940	18.8	2
10	mRNA only with STPs, no US	940	9.3	1

Table 4.3.4.2: Shows the number of HeLa cells remaining intact post treatment, and the number of those cells that stained positively with trypan blue indicting dead cells. N of 3 for each group

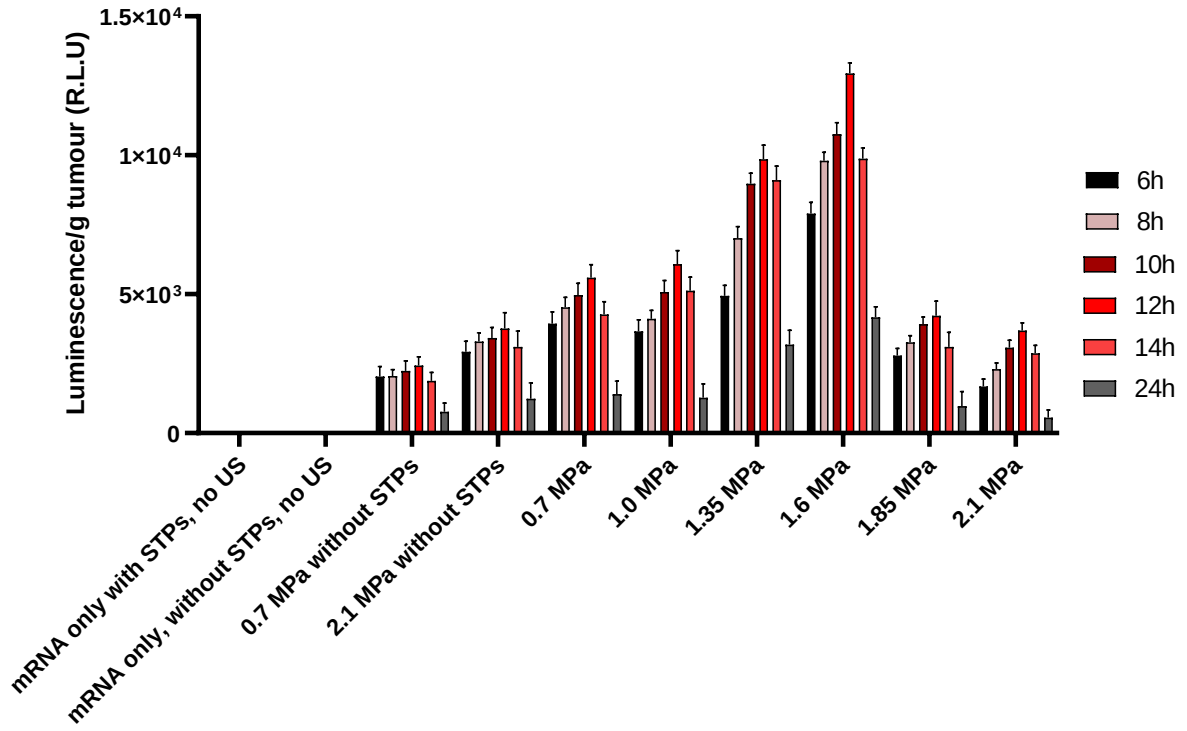

Figure 4.3.4.1: Level of luciferase expression in HeLa cells over the 24 hours following treatment in relative light units (R.L.U) as measured by microplate reader. 2.1-0.7 MPa groups include STPs with Ultrasound. 9 samples per group at each time point, 3 group measurements, with triplicates for each, averaged. N of 3, error bars are the standard deviation

The HeLa data demonstrates a pattern similar to that for the CT26 and EMT6 in that pressures of 2.1 and 1.85 exhibit much lower expression than that of pressures of 1.6 MPa plus STPs and 1.35 and 0.7 plus STPs. The 1.6 MPa plus STPs again demonstrates the highest overall expression, but unlike the CT26 and EMT6 cells and in common with A549 cells, this peak is at 12 hours, not 10 hours.

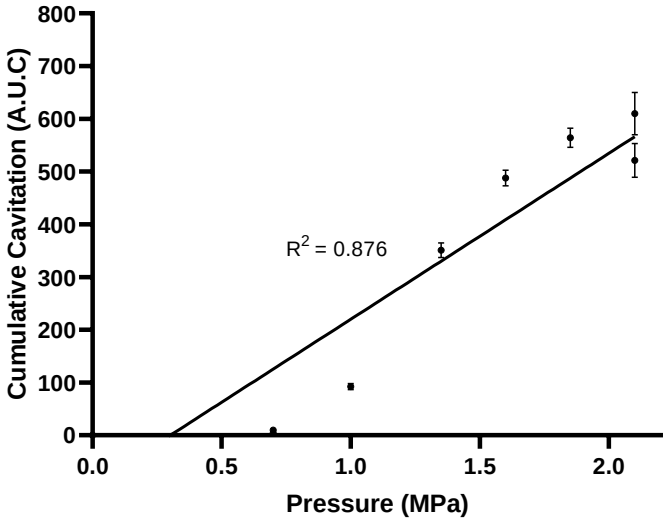

Figure 4.3.3.2: Relationship between exposure pressure and the average cumulative cavitation for each HeLa group. As pressure is increased, the cumulative cavitation increases. N of 3, error bars are the standard deviation for cumulative cavitation.

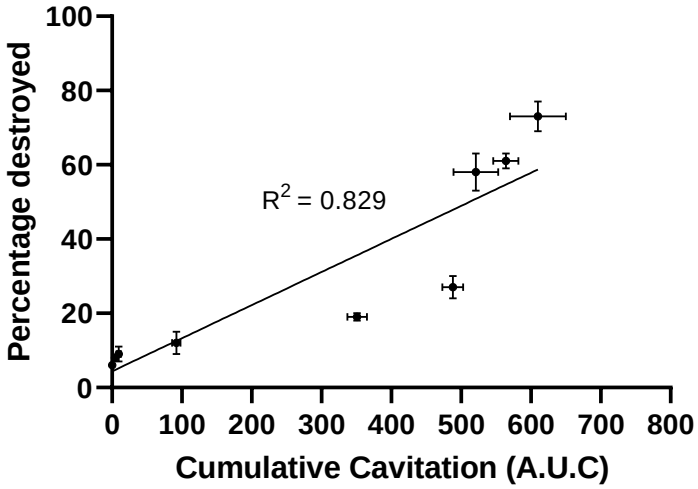

Figure 4.3.4.3: Average cumulative cavitation for each HeLa group and the corresponding percentage of cell death. N of 3 for pressure point (and hence cavitation range), X error bars are the standard deviation for each group, y error bars are the standard deviations but are hard to view due to the low variability in viability measurements.

It is evident from the cavitation data that the relationship between cavitation and cell death was less reliable (R^2 = 0.82) for the HeLa cell line compared to the CT26, EMT6 and A549 cells (R^2 = 0.87, 0.86, and 0.87 respectively). This will be discussed further in the discussion section.

4.3.5 MSCs *in vitro* exposure results

As well as looking a murine and human cancer cell lines, non-cancerous human and rat cell lines were examined. MSCs were investigated with the same setup and parameters as used for the cancer cell lines. The initial results of the ultrasound effects can be seen in table 4.3.5.1, where once again, 2.1 MPa plus STPs exhibited a detrimental but more marked impact on the cells. An interesting note is that the effect is reduced once the pressure threshold is lowered sufficiently, so that although just 21% of cells remained after exposure to 2.1MPa plus STPs (the lowest % in all tested cells), by 1.35 MPa plus STPs, almost 90% of cells were intact.

Group	Conditions	% Cells remaining whole
1	2.1 MPa	21
2	1.85 MPa	45
3	1.6 MPa	78
4	1.35 MPa	88
5	1.0 MPa	92
6	0.7 MPa	95.5
7	2.1 MPa without STPs	41
8	0.7 MPa without STPs	98
9	mRNA only, without STPs, no US	98.5
10	mRNA only with STPs, no US	98.5

Table 4.3.5.1: The impact of different ultrasound parameters, as denoted in table, on cell viability. Cells were assessed using trypan blue post treatment. N of 3 for each group, with the '+/-'being the standard deviation for each group

The MSCs appeared more sensitive to ultrasound effects, which was confirmed by the trypan blue staining results, where it can be seen in table 4.3.5.1 that a higher proportion of the cells were stained positively for trypan blue than for CT26 and EMT6 cell lines.

		MSCs (/mL)		
Group	Conditions	Post treatment (thousands)	Trypan positive cells (thousands)	% stained
1	2.1 MPa	210	79.8	38
2	1.85 MPa	450	158.0	35
3	1.6 MPa	780	257.0	33
4	1.35 MPa	880	264.0	30
5	1.0 MPa	920	184.0	20
6	0.7 MPa	955	115.0	12
7	2.1 MPa without STPs	410	139.0	34
8	0.7 MPa without STPs	980	49.0	5
9	mRNA only, without STPs, no US	985	19.7	2
10	mRNA only with STPs, no US	985	19.7	2

Table 4.3.5.2: Shows the number of MSCs cells remaining intact post treatment and the number of those cells that stained positively with trypan blue indicting dead cells. N of 3 for each group

The increased response to the ultrasound parameters for the MSCs can be seen further in Figure 4.3.5.1, where the expression levels are shown.

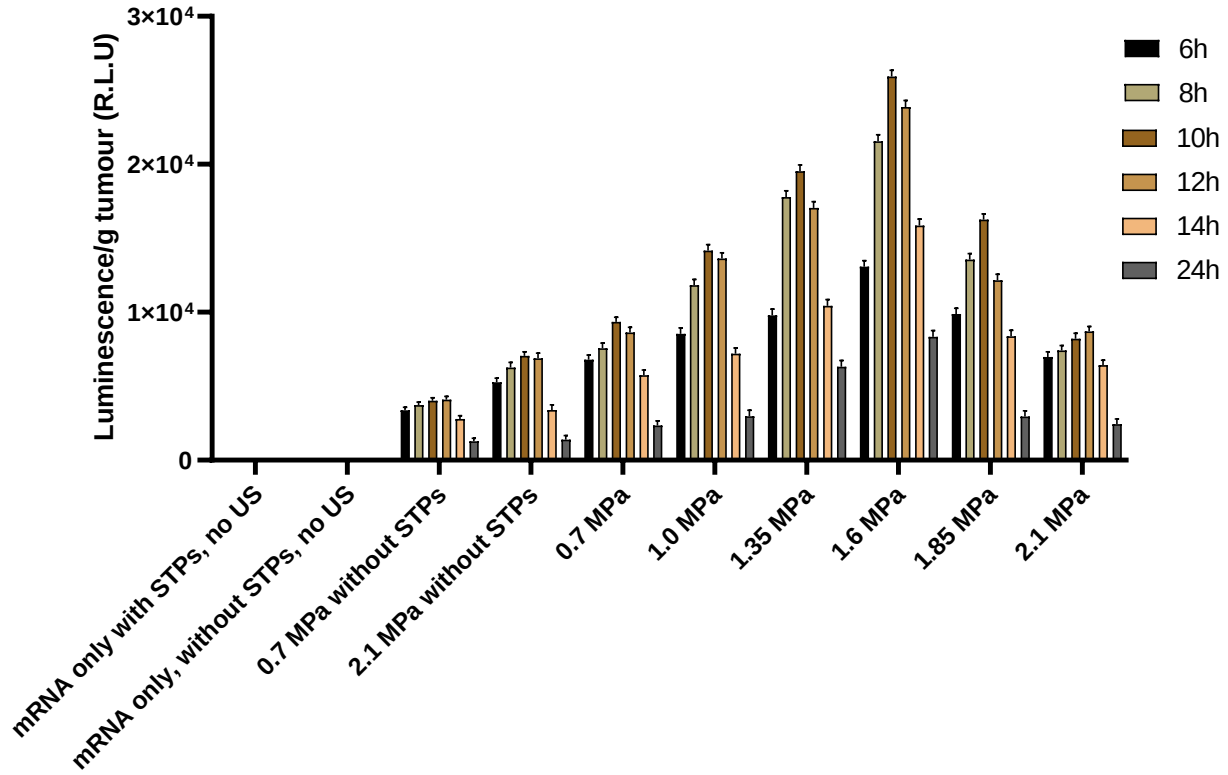

Figure 4.3.5.1: Level of luciferase expression in MSCs over the 24hours following treatment, in relative light units (R.L.U) as measured using a microplate reader. 2.1-0.7 MPa groups include STPs with Ultrasound. 9 samples per group at each time point, 3 group measurements, with triplicates for each, averaged. N of 3, error bars are the standard deviation.

Figure 4.3.5.1 shows higher levels of expression in comparison to that of the cancerous cell lines shown above, even though there are fewer viable cells left post-treatment. This may indicate that more mRNA is getting into the viable cells that remain. Figure 4.3.5.2 shows the relationship between exposure pressure and detected cavitation with non-significant difference ($p>0.05$) between the relationship for the other cell lines. Figure 4.3.5.3 shows the average cavitation and number of cells remaining post-treatment. And here, the effect of the cavitation on the MSCs can be seen. The relationship between cavitation level and cell death seems least robust ($R^2 = 0.839$) for these cells, which may reflect their greater sensitivity.

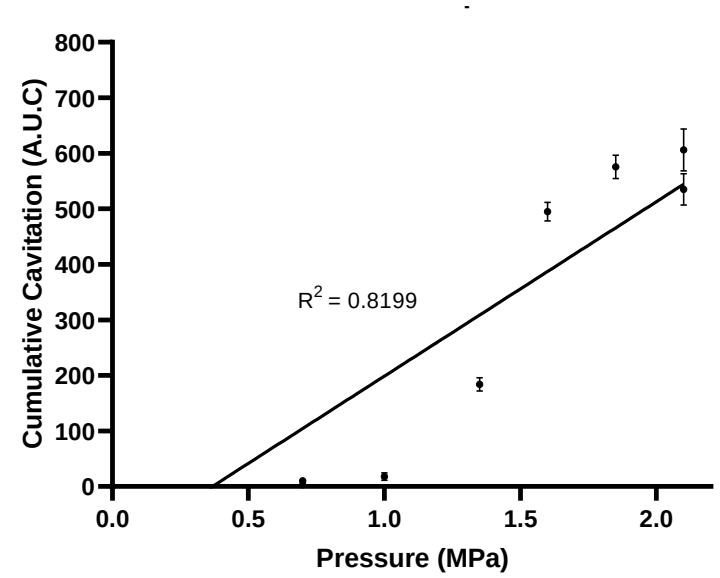

Figure 4.3.5.2: Pressure compared with the average cumulative cavitation for each MSCs group. As pressure is increased, the cumulative cavitation increases for each group. N of 3, error bars are the standard deviation for cumulative cavitation.

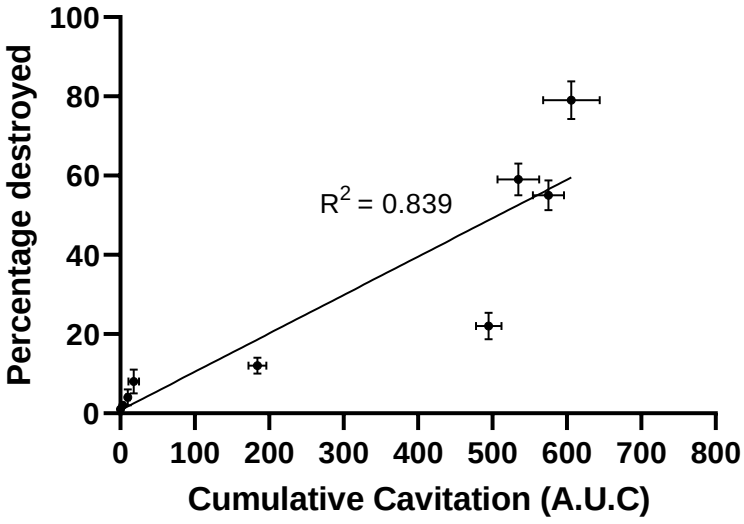

Figure 4.3.5.3: Average cumulative cavitation for each MSC group and the corresponding percentage of cells destroyed. N of 3 for pressure point (and hence cavitation range), X error bars are the standard deviation for each group, y error bars are the standard deviations but are hard to view due to the low variability in viability measurements

4.3.6 Cardiomyocytes *in vitro* exposure results

Cardiomyocytes were the final cell line examined. As may be expected from a non-cancerous cell line, the results differed extensively from the human and murine cancer cell line results. Immediately it can be seen from table 4.3.6.1 that the ultrasound and cavitation groups have a

more considerable effect on these cells. Approximately 85% of the cells at 2.1 MPa plus STPs were destroyed by the treatment process, which is much higher than the 60-70% for previously tested cell lines. Even in the 1.6MPa plus STPs group, the levels of cells remaining was only 64%, which is closer to the average for the other cell lines at 2.1MPa plus STPs.

Group	Conditions	% Cells remaining whole
1	2.1 MPa	15
2	1.85 MPa	28
3	1.6 MPa	36
4	1.35 MPa	55
5	1.0 MPa	81
6	0.7 MPa	89
7	2.1 MPa without STPs	31
8	0.7 MPa without STPs	90
9	mRNA only, without STPs, no US	95
10	mRNA only with STPs, no US	95

Table 4.3.6.1- The impact of different ultrasound parameters, as denoted in table, on cell viability. Cells were assessed using trypan blue post treatment. N of 3 for each group, with the '+/-'being the standard deviation for each group

The effects of the ultrasound and cavitation can be evidenced further by the results in table 4.3.6.2, using trypan blue. The results show that a high proportion of the cells that remain intact post-exposure stain positively for trypan blue, this would indicate that additional changes in parameters are required.

Group	Conditions	Cardiomyocytes (/mL)		
		Post treatment (thousands)	Trypan positive cells (thousands)	% Stained
1	2.1 MPa	150	82.5	55
2	1.85 MPa	280	134.0	48
3	1.6 MPa	360	151.0	42
4	1.35 MPa	550	204.0	37
5	1.0 MPa	810	146.0	18
6	0.7 MPa	890	89.0	10
7	2.1 MPa without STPs	310	124.0	40
8	0.7 MPa without STPs	900	63.0	7
9	mRNA only, without STPs, no US	950	9.5	1
10	mRNA only with STPs, no US	950	19.0	2

Table 4.3.6.2: Shows the number of Cardiomyocytes cells remaining intact post treatment, and the number of those cells that stained positively with trypan blue indicting dead cells. N of 3 for each group

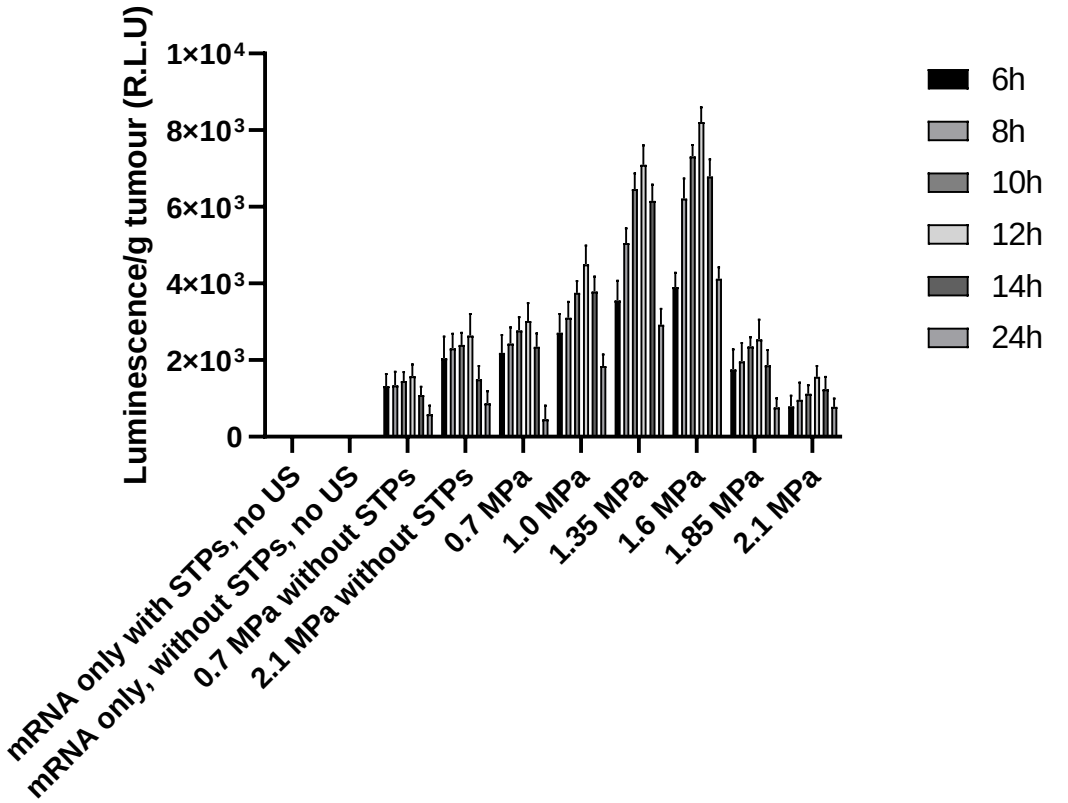

Figure 4.3.6.1: Levels of luciferase expression in cardiomyocyte over the 24-hour period following treatment, as shown by luminescence in relative light units (R.L.U) as measured using a microplate reader. 2.1-0.7 MPa groups include STPs with Ultrasound. 9 samples per group at each time point, 3 group measurements, with triplicates for each, averaged. N of 3, error bars are the standard deviation.

As can be seen from figure 4.3.6.1, the expression levels are more than 2-fold less than for the MSC cell line (figure 4.3.5.1).

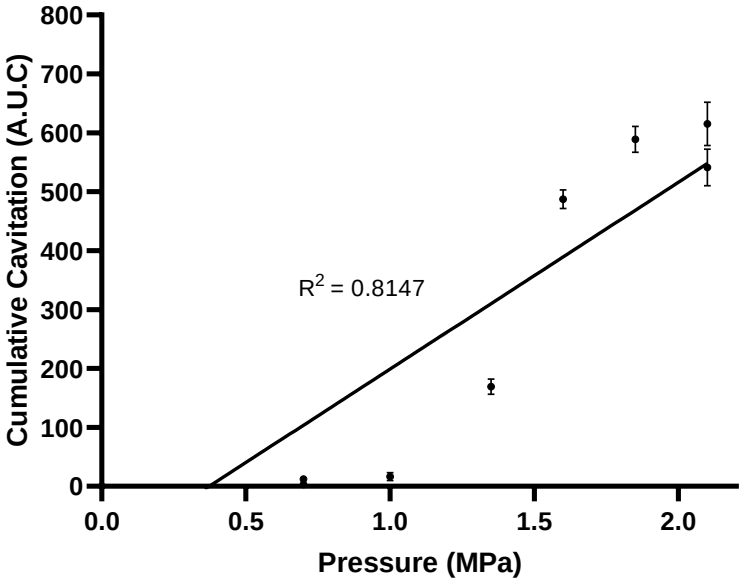

Figure 4.3.6.2: Pressure compared with the average cumulative cavitation for each cardiomyocyte group. As pressure is increased, the cumulative cavitation increases for each group. N of 3, error bars are the standard deviation for cumulative cavitation.

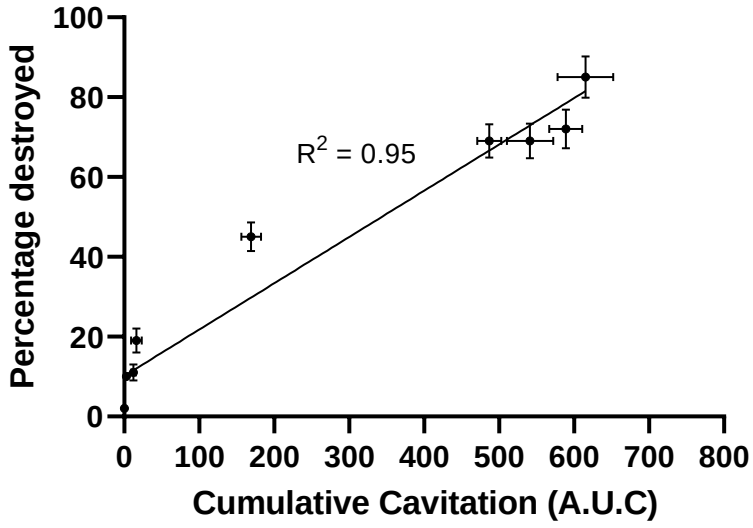

Figure 4.3.6.3: Average cumulative cavitation for each Cardiomyocyte group and the corresponding percentage of cells destroyed.. N of 3 for pressure point (and hence cavitation range), X error bars are the standard deviation for each group, y error bars are the standard deviations but are hard to view due to the low variability in viability measurements.

Overall, the expression for the cardiomyocytes was lower than all the other groups used in the Chapter. This may relate to the greater sensitivity to cavitation or may be a result of lower global translation levels due to a lower rate of growth and division.

4.3.7 Overall Viability and Expression at optimal time points

Figure 4.3.7.1 shows the relationship between the amplitude of ultrasound exposure experienced by the samples and the average cell viability after exposure. It shows that the relationship is more destructive for the cardiomyocytes than for any of the other cell lines. It also shows that the cancer cell lines respond in a similar way to the ultrasound. Differences between cell lines are less apparent at lower pressures (0.7MPa), where all viability values are between 88 and 95% than at higher pressure (2.1 MPa), where the range spans from 45% for cardiomyocytes to 72% for A549 cells. The pressure of 1.35 MPa, which typically corresponds to 170 cavitation units, is the 'tipping' point where differential sensitivity becomes apparent.

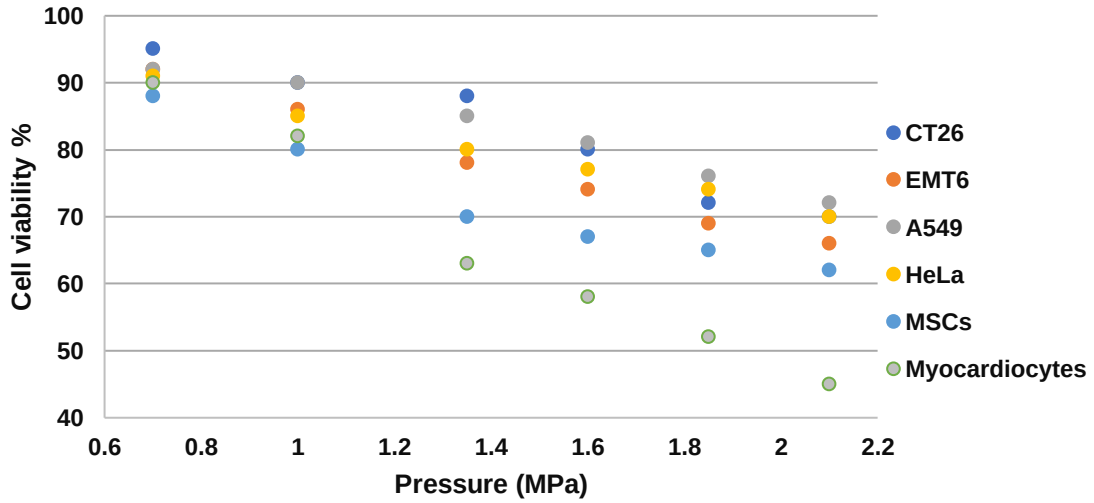

Figure 4.3.7.1: The relationship between viability and ultrasound exposure pressure for each cell line. Viability was calculated by cell counting using the countess device pre and post exposure. N of 3 for each sample, error bars are the standard deviation.

Figure 4.3.7.2 examines the maximum expression achieved for each cell type. Each cell type showed optimal expression at 1.6MPa plus STPs, but the time point at which the maximum

expression occurred varied. The CT26, EMT6 and MSCs showed maximal expression at 10 hours, whereas for HeLa cells and cardiomyocytes maximum was at 12 hours.

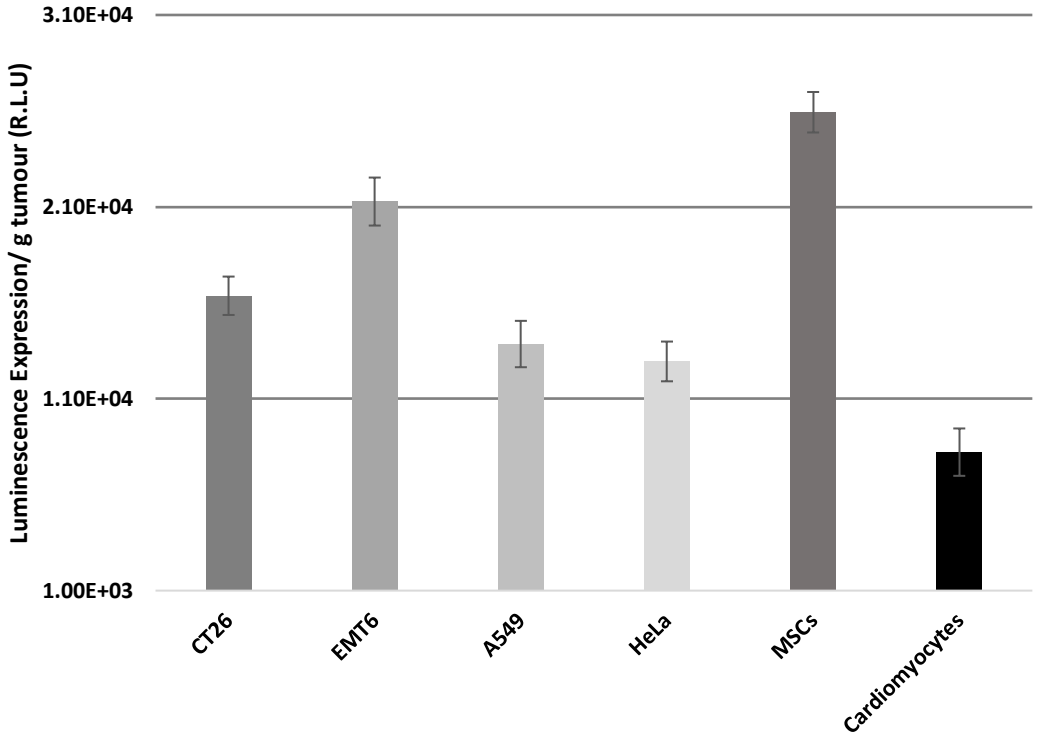

Figure 4.3.7.2 - Maximal luciferase expression achieved for each cell line CT26 has an average of 16.4 x103, with EMT6 cells having an average of 21.3 x103. The A549 and HeLa cell lines had lower expression levels at 13.8 x103 and12.9 x103, respectfully. The MSCs had the highest overall expression at 25.9 x 103 RLU and the cardiomyocytes at 8.2 x103 RLU.

4.4 Discussion

The work presented in this Chapter was designed to further explore the level and cell-specificity of ultrasound-mediated delivery of mRNA. The results from Chapter 2 showed that the parameters used previously required adjustment to enable optimal uptake and delivery. The work in Chapter 3 examined how a change in concentration of cavitation nuclei and the development of an enhanced *in vitro* setup could enable these adjustments. In this Chapter, the change in concentration of cavitation nuclei was implemented, and the maximum time point of expression was examined to provide insights for potential *in vivo* use. Furthermore, as all data to this point had been collected using a single cell line, investigation of a range of different cell

types allowed the impact of the species and organ origin and the transformational status of the cells on delivery efficiency to be studied.

The data for the CT26 cell line was in-line with expectations arising from previous *in vitro* and *in vivo* studies in Chapter 2 and 3. At parameters 2.1 MPa plus STPs, mRNA expression was over 3-fold lower than the level seen at 1.6 MPa with STPs. Indeed, the 2.1MPa group exhibited the lowest expression out of all the ultrasound and STPs groups, and as such, the factors driving the low levels of delivery and expression demonstrated in Chapter 2 become more explicit. The level of destroyed cells, figure 4.3.1.1, paints an even clearer picture of the relationship between the ultrasound/cavitation and the damage caused. Of course, it is essential to note that these cavitation levels occurred in a fixed region within an eppendorf and not with the focal region of the ultrasound being moved around as it is during the exposure of tumours in Chapter 2. It still follows with the data from Chapter 2 that such high levels of pressure and, therefore, cavitation (figure 4.3.1.2) are not conducive to the maintenance of cell viability and, therefore, cellular uptake and expression of mRNA. The value of cavitation monitoring in identifying the point of excessive damage/optimal delivery was also emphasised by these data.

A wide range of other cell types were chosen to validate the universality of the effects reported in CT26 cells. It was important to investigate whether species, organ origin and transformational status had an impact as such factors are important considerations in the further potential clinical and commercial translation of the technology. For example, assuming parameters developed in cancer cell lines for targeted cell kill are automatically transferable to cell engineering approaches using MSCs could limit future success.

The results from testing using these cell types showed an interesting and shared pattern. Specifically, there appears to be a threshold where the ultrasound pressure applied and the cavitation which results is sufficient to ensure uptake and expression of the mRNA, but not at

the expense of cell viability. Typically, there is an increase in luciferase expression, figure 4.3.1.1, in the presence of STPs when the pressure is decreased from 2.1 to 1.85 MPa to 1.6 MPa. After this peak in expression is reached, there is a gradual decline of expression in the lower amplitude pressure groups. This lowering of expression between pressure 1.6 and 0.7 MPa would indicate that it is not simply pressure but cavitation dose that is vital to achieving uptake. Notably, for all cell types, the cell death for these 1.6 MPa – 0.7 MPa groups was much lower (a third of that at 2.1 MPa plus STPs), and the expression levels more than 2-fold higher for 1.6 and 1.5 times higher for 1.35 MPa. The existence of a sweet-spot of cavitation which allows RNA entry without excessive cell death is perhaps not surprising when the likely mechanism of RNA delivery (through cavitation-generated pores in the cell membrane) is also a mechanism of cell death. The 0.7 MPa plus STPs group exhibited very low cavitation levels (~15 au) but demonstrated similar levels of luciferase expression to that of the 2.1MPa group. It is intriguing that despite such low cavitation levels, the level of luciferase expression was 10-fold greater than the level of expression achieved with 0.7MPa but without STPs. This is especially notable as the levels of immediate cell death were similarly low for 0.7MPa with and without STPs, but 0.7MPa with STPs showed approximately 3-fold greater trypan blue staining at 15 min, indicative of membrane disruption. This data indicates that even very low levels of detected cavitation can produce meaningful delivery and perhaps also shows that the sensitivity of the passive cavitation detection and PAM is still suboptimal in terms of detecting the type or level of cavitation that is 'useful'.

Overall, for all pressures and cell lines, there are familiar patterns in how the expression builds to its max, at 10 or 12 hours, and then begins to decrease. The decrease follows a step down of between 10-20% after the maximum for each subsequent time point.

Crucially the controls with no ultrasound exhibited no expression when measured across any time points in any cell line, nor did the control of no ultrasound but with STPs. This clearly

establishes the presence of ultrasound and cavitation as a necessary component in order to achieve delivery. Variation of the exposure pressure served to probe the level of ultrasound that was required.

For the 2.1 MPa group, levels of cavitation, cell death and luciferase expression differed little from those with 2.1 MPa plus STPs. This suggests 2.1MPa is above the cavitation threshold for the non-degassed media the cells were suspended in and that the addition of STPs nuclei was therefore unnecessary. The addition of STPs did appear to have a positive effect in terms of expression and a negative one in terms of cell death, with higher levels of death than at 1.6 MPa, STPs and ultrasound.

Overall, the CT26 cell line results gave some excellent extra insight into the results in Chapter 2 and provided the groundwork for the testing of the additional cell lines mentioned above. These results, in addition to the work in Chapter 3, gives insight and potential parameters for exploring the work reported in Chapter 2 further but moving forward with the parameters explored in this Chapter 4.

The need to compare the CT26 cell line to a cell line that could also be used in an *in vivo* model that required minimal changes to the experimental setup and provided the motivation to study the EMT6 cell line. This murine mammary carcinoma cell line was chosen because it could be implanted into the same mice as the CT26 cell line, and it exhibited similar growth times both *in vitro* and *in vivo*.

The results for the EMT6, when compared with the CT26, show interesting insights. Unsurprisingly the EMT6s exhibited a similar response to the STP cavitation groups as the CT26. At highest pressures, in the 2.1 MPa and STP group, most cells (72%) were destroyed and could no longer be counted, and post-treatment, those that remained exhibited significant ($p<0.5$) levels of cell death compared to the no ultrasound controls. This could indicate that the

EMT6 cells are more sensitive to ultrasound and cavitation than CT26 cells, which initially may seem like a limitation but can be viewed more positively if the aim is to achieve sonopermeabilisation. The EMT6 cells exhibit similar but higher levels of cell death in the cells that remained intact (as defined by trypan blue staining at 15 min), but this did not translate to a decrease in mRNA expression overall. Hence it would appear that similar levels of expression are achievable from lower number of viable cells. Specifically, the 2.1 and 1.85 MPa with STPs groups exhibited higher expression levels for EMT6 cells than the equivalent groups for CT26, even though there was a 4-6% higher death rate for the EMT6 cells. This may indicate that the EMT6 are more responsive to the uptake or are easier to sonopermeabilise. The familiar pattern of 1.6 MPa with STPs as being the most effective was observed again. 1.6 MPa with STPs for EMT6 cells demonstrated a 30% increase in the maximum expression achieved versus the equivalent for CT26, even with a 6% decrease in viability for the EMT6 cells. Cells were plated to a live count (i.e., trypan blue positive cells were excluded from calculations), meaning that the cells that survived the EMT6 cells' treatment must take in more mRNA than the equivalent cells for CT26 or process it more effectively. Similar time vs luciferase expression profiles were evidenced when examining the other pressures. The mRNA only controls, with and without STPs, exhibited no expression.

When comparing CT26 and EMT6, it is evident that the EMT6 samples appear more amenable to uptake and expression of the luciferase mRNA even when the effects of the ultrasound are more damaging. This cell line, EMT6, is used in Chapter 5 for an additional *in vivo* study where the ultrasound parameters are explored further.

To increase the clinical relevance of these studies and test if findings map across species, two human cancer cell lines were also examined. A549s, a human lung carcinoma cell line, and HeLa's, a human ovarian cancer cell line, were used. These cells were treated in the same manner as the CT26 and EMT6 cells.

The results for the A549 and HeLa cells demonstrated significantly ($p<0.05$) lower levels of expression in comparison to the EMT6 and CT26 cells, given that at the maximum, there is a 58-61% difference in luciferase expression between A549s and HeLas and EMT6 cells Figure 4.3.7.2. Both the A549s and HeLa cells exhibited similar levels of death to EMT6 cells by cell counting using automated cell counting and by trypan blue staining, so the lower levels of expression may be due to differences in the rates and levels of global gene expression, rather than differences in sensitivity to cavitation mediated RNA delivery.

The results for the A549s show that the cells exhibit relatively lower expression across all pressures tested but that they may be less sensitive to the pressure change between 1.85 and 1.35 MPa, than the CT26s and EMT6s. The most interesting element of the results is the shift in the time of maximum expression from 10 hours with CT26 and EMT6 to 12 hours post-treatment with A549. This shift was also seen in the results for the HeLa cells. All exposure pressures for both A549 and HeLa exhibit the maximum expression at the 12-hour time point. And both lines exhibited the familiar increase of expression between 6 and 12 hours, followed by a ~ 10-20% drop off over the next 2 hours.

As well as examining human cancer cell lines, human MSCs and rat cardiomyocytes were used. The application of gene therapy is not and should not be limited to cancer. Gene therapy has great clinical and commercial potential. MSCs were explored as an avenue for large-scale application in tissue engineering and cardiomyocytes as a non-cancerous clinical model for cardiac gene therapy. Indeed, efficient and controllable modification of MSCs may allow cell lineage to be directed in a range of useful directions. This can be achieved by the delivery of key transcription factors at the level of protein, RNA or DNA. Protein is expensive to manufacture and hard to deliver, but RNA and DNA are attractive alternatives, with RNA offering the potential advantage that expression of the encoded protein is unlikely to outlast the cell transition which the encoded protein instigates. However, current RNA and DNA delivery

to stem cells is typically attempted using 3 methods, electroporation, lipid mediated delivery or using reagents to disrupt the cell membrane. Each of these methods can suffer from low transfection rates and toxicity to cells.

The MSCs exhibited similar behaviour post-treatment across all the pressures tested, apart from the 2.1 MPa with STPs group, where the number of cells remaining post-treatment was 6-13% lower than that of the CT26, EMT6, A549s and HeLa cell lines. Furthermore, of the remaining cells, a higher proportion stained positively for damage by trypan blue, with 38% compared with a max of 34% for the next highest group, EMT6.

Despite these issues of raised cell death, it was notable that across all the pressures tested, the levels of luciferase expression exhibited by the MSCs was higher when compared with the other cell types. Specifically, the MSCs showed a 2-fold ($p<0.05$) increase in maximal expression compared with the HeLa cell line and a 20% increase ($p<0.05$) compared with EMT6 cells. The exposure pressure vs luciferase expression pattern did not differ from the patterns seen with the other cell types, i.e., 1.6MPa had the maximum expression, and the maximum time of expression was at 12 hours which is in accordance with the other human cell lines used in this Chapter.

The ability to deliver mRNA into MSCs on this time scale without using other expensive and labour-intensive RNA condensing reagents has large commercial potential. An example of this would be treating cells and making them more likely to seed to scaffolds for therapeutic or tissue culturing purposes. However, no direct comparison of cavitation to agents such as lipofectamine have been made in these studies due to the difference in exposure and plating conditions and times (307,308).

To fully characterise the effect of ultrasound and cavitation, comparison to other transfection methods for these cell lines is needed. For example, commonly, when transfection of MSCs is

performed, non-viral transfection is achieved using electroporation (323) or microinjection of cells ex vivo. Electroporation is commonly used by researchers for study of a wide range of cell lines, and is one of the preferred *in vitro* transfection techniques. With MSCs, it has been seen that up to 68% of the live cells can be transfected, but the viability has been reported as low as 54% (324). This does not compare favourably to microinjection, which has a higher reported transfection rate of between 65-75% and higher viability of 75% (325,326). However, microinjection can be limited by its requirement for a high level of training and skill and its low throughput in terms of cell numbers. The advantage of the cavitation approach used here in terms of improved viability is clear with control and refinement of pressure amplitude, allowing up to 75% of cells to remain viable at pressures of 1MPa and below. It is less clear from these studies what % of cells are successfully transfected as the luciferase output used in these studies only provides population-level insight, not an assessment of expression at an individual cell level. It is evident that transfection levels are increased several logs above controls and in studies using propidium iodide that a substantial proportion of cells can be permeabilised and theoretically amenable to mRNA entry. To explore this question further and produce directly comparable data, a green fluorescent protein (GFP) mRNA construct would have been used in addition to luciferase mRNA used, if time and resources permitted. It is noteworthy that compared to microinjection, ultrasound offers the alternative of a high cell throughput, as well as an easy to use and simple, and potentially commercial product and setup. Notably, regardless of the cell type being tested, a strong, predictable, linear relationship (R^2 values between 0.83 and 0.97) between pressure of exposure and level of cavitation detected was produced. Such non-invasive, real-time feedback adds valuable information and control which is missing from alternative approaches, enhancing commercialisation potential further. With additional testing and refinement, such a setup may prove to provide a transfection

efficiency that matches or exceeds the alternative methods. This is discussed further in Chapter 6.

The cardiomyocytes had the least favourable response in terms of the damage and expression resulting from ultrasound exposure. The cells immediately appeared to have a much more disturbed morphology when examined using microscopy, and this was reflected in the low numbers that remained intact post-treatment. Indeed, as shown in figure 4.6.2, only 15% remained whole after being exposed at 2.1 MPa with STPs parameters, and of those, only 45% appeared to be viable cells when stained with trypan blue. In this regard, it is unsurprising that the expression levels were so much lower than those of the other cell lines used. While this result may make it easy to become disheartened, the results remain positive, as RNA has been successfully moved into these hard to transfect cells without the requirement for additional transfection chemicals or media reagents. In terms of transfection efficiency, the rat cardiomyocytes have previously been studied and compared using a GFP encoding DNA lipofectamine (8.1% of cells transfected), electroporation (with 7.5% transfected) and the DNA virus adenovirus (88.1% transfected) (323). Whilst the levels of transfection are over 10-fold higher using adenovirus vs lipofectamine, there is an associated cost of production for adenovirus as well as increased safety implications and concerns over the impact of super-physiological levels of transgene protein expression and of immune responses generated against adenovirus infected cells. For lipofectamine, there are concerns over the cost of the reagents, the labour involved in sample preparation, the volume restrictions associated with its use and the time required for successful peak expression, which appears to be double that needed with cavitation. Such delays may be a consequence of the lack of a mechanism for nuclear entry where DNA delivery is concerned and may mean an extra plating and rescue steps are needed. Ultrasound mediated cavitation may therefore present as a real alternative. The reason why cavitation may allow more rapid expression from delivered mRNA than

chemical transfection reagents currently defies explanation, but may relate to the absence of a need for an 'un-packaging' of the mRNA cargo from the chemicals once within cells.

The ultrasound parameters studied here should be explored further in future work, focusing on refining the ultrasound parameters to fit the requirements of these niche cells. Direct comparison to alternative technologies would be useful in determining the translational potential of this approach and helping define its toxicity, efficacy and usability advantages.

4.5 Conclusion

The work in this Chapter emphasises the importance of understanding the time profile of expression and how the parameters used, and the cell types tested must be considered when planning for and executing the experiment. The uptake and expression of mRNA is typically mediated by chemical reagents and takes some time to occur. Still, ultrasound-mediated cavitation shows a particular strength in achieving the same goal in a shorter time scale. While none of the work here will translate directly to clinical *in vivo* applications, it does present an avenue for *in vitro* transfection of everything from cancer cells to stem cells and even cardiac cells without directly changing the morphology or behaviour of the cells. This work and the system described and used, therefore, represents a potentially attractive platform for the development of *in vitro* transfection devices for cell transfection and tissue engineering applications. Direct comparison of this cavitation system to conventional agents such as lipofectamine would be a useful future direction in gauging the advantages offered.

The work in this Chapter is used as the basis for Chapter 5 and could well be used as the basis of future work for developing bespoke transfection setups for *in vitro* work, emphasising the importance of a tailored approach to cell type. Tailoring which is made easier by the real-time and non-invasive feedback which cavitation monitoring provides.

Chapter 5 – Ultrasound mediated delivery of mRNA to CT26 and EMT6 tumours

5.1 Introduction

The body of work presented in previous Chapters comes together to enable the goal of investigating whether an overall improvement of expression of mRNA encoded firefly luciferase can be achieved *in vivo*. The work in Chapter 2 demonstrated that a new *in vivo* protocol had to be established in order to improve delivery. The work in Chapter 3 established that even with improved ultrasound parameters, additional parameters needed to be considered. These included when mRNA expression was likely at its peak and when best to conclude studies to ensure an accurate representation of the experimental outcome. Therefore, the work in Chapter 3 helped establish the time points for measurements in this Chapter and an effective protocol for *in vitro* transfection of cells. The work in Chapter 4 helped ensure a good understanding of the cell type specificity of ultrasound exposure parameters and mRNA expression profile was attained. The *in vivo* experiments of 'Chapter 5' is another step in finding a robust working protocol for *in vivo* transfection and delivery using ultrasound-mediated cavitation. As such, the studies face many of the same challenges experienced and discussed in Chapters 1, 2 and 3.

For this Chapter, CT26 cell line was used, as previously, so a direct comparison to previous studies could be made. The EMT6 cell line, which was studied in Chapter 4, was also examined in this Chapter. EMT6 cells are a murine cell line and could be used in balb-c mice, just as the CT26 cell lines. This helped ensure that there would be no confounding differences in mRNA delivery or expression due to the use of a different host mouse model.

5.2 Methods

5.2.1 Cell lines and cell culture

Murine colorectal carcinoma CT26.WT cells (ATCC, CRL-2638; American Type Culture Collection, Rockville, MD, USA) were grown to approximately 90% confluence with a minimum of 95% viability using Roswell Park Memorial Institute 1640 medium (RPMI 1640; R8758, Sigma-Aldrich Company Ltd, Dorset, UK) supplemented with 10% fetal bovine serum (FBS; F7524, Sigma-Aldrich, Dorset, UK). Cells were grown to the confluence at 37 °C in a humidified atmosphere of 5% carbon dioxide. Cell culture, rescue and counting were as described in Chapter 2, section 2.2

Murine mammary carcinoma, EMT6 cells (ATCC, CRL-2755; American Type Culture Collection, Rockville, MD, USA) were grown to approximately 90% confluence with a minimum of 95% viability, using Waymouth MB 752/1 media (W1625, Sigma-Aldrich Company Ltd, Dorset, UK) supplemented with 10% fetal bovine serum (FBS; F7524, Sigma-Aldrich, Dorset, UK). The EMT6 cells were harvested in the same manner as the CT26 cells, with RPMI 1640 substituted with Waymouth's MB media, FBS-free. Cells were prepared for implant in FBS-free Waymouth MB media, and a stock solution formed at a concentration of 10E6 cell/mL for implantation.

5.2.2 Tumour inoculation and animal welfare

Tumour implantation and animal welfare tracking was performed in accordance with Home Office regulations under a Home Office approved project licence and personal licence and as described in chapter 2, section 2.2.

5.2.3 mRNA

Non-complexed, i.e. 'naked', mRNA was purchased from Trilink biotechnologies (Product code: L-7202), encoding the firefly luciferase reporter protein. For each tumour, 5 μg of mRNA was used. The luciferase reporter gene expression was measured using IVIS analysis pre-cull

and the luciferase assay (E1500; Promega, Southampton, UK) following cull and tumour excision and homogenisation. In both cases, the standard processing and measurement protocols were followed. IVIS measurement was performed as described in section 5.2.6. For *in vitro* analysis of homogenised samples, the process described in section 5.2.7 was followed.

5.2.4 SonoTran Particles

SonoTran particles (STPs, OxSonics Ltd, UK) were prepared from a stock concentration of 25 mg/mL and diluted to 21.4 mg/mL using 40% glucose to create a new standard stock solution of 21.4 µg/µL in 5% glucose before addition to sample. This stock solution was further diluted by 1:10 in 5% glucose.

5.2.5 Ultrasound set-up

Before treatment, each mouse was welfare assessed, ensuring the mice were healthy regarding weight and monitoring for signs of pain or distress, and tumours were measured. Each mouse was placed under anaesthetic and prepared for treatment as described in chapter 2, section 2.2. The mice were then lowered into a water tank, ensuring the head and face mask remained above the water line and then treated.

Before treatment, a 29-gauge insulin syringe was connected to a 29-gauge needle tip via a 4 cm length of tubing. The RNA (5 µL with 5 µg) was loaded, and the needle tip was inserted into the tumour. After the RNA was injected, 5 µL of PBS was used for flushing the naked mRNA through the cannula. Subsequently, 5 µL of cavitation nuclei (0.1 µg/µL STPs) were flushed through to be followed finally by 10 µL of PBS to ensure cavitation nuclei were in the tumour.

5.2.6 Treatment groups

Post tumour growth and assessment mice were allocated to specific treatment groups. There were two control groups where no ultrasound was used, control at 10 hours and control at 24

hours, for each cell line type (CT26 and EMT6), and 4 ultrasound treatment groups at 1.6, 1.35, 1.0 and 0.7 MPa. All ultrasound exposures used the same parameters described in Chapter 4. For the experiments conducted in this Chapter, there was an N of 4 for each group for both cell lines.

5.2.7 *In vivo* imaging

Each mouse was imaged at two-time points, 8 and 10 hours - to monitor the luciferase transgene expression within the tumours. These time points were chosen based on levels of expression in previous pilot studies discussed in Chapter 3, the results of Chapter 4 and project licence restrictions. The mice were anaesthetised, as described previously, and given an intraperitoneal (IP) injection of Pierce™ D-luciferin Monopotassium Salt (88294, Thermo Fisher Scientific) made up to a concentration of 15.8 mg/mL in PBS and delivered at a volume of 100 µL. The mice were then imaged using a Perkin Elmer Lumina LT series III 10 minutes post the IP injection to allow for adequate tumour uptake of d-luciferin. The mice were recovered within fifteen minutes of the start of the procedure. Mice were monitored for recovery for 30 minutes after the 8-hour imaging session and culled immediately following the 10-hour session. The mice were culled at the end of the 10 hours IVIS imaging session, and tumours were excised. The excised tumours were photographed and frozen in a -80˚C freezer for additional analysis. The IVIS images were later analysed using Perkin Elmer Living images® software, where regions of interest and radiance were analysed for luminescence levels.

5.2.8 Quantification - Luciferase Assay

Tumour samples were measured using the luciferase assay protocol described in Chapter 3, section 3.2.

5.2.9 Statistical Analysis

All statistical analysis was carried out using GraphPad Prism version 8.2

5.3 Results

5.3.1 CT26.WT *in vivo* results

The *in vitro* data obtained using CT26 cells (Chapter 4) showed that high cavitation-mediated RNA delivery levels could be achieved. The question then arose whether such delivery could also be achieved in an intratumoural injection setting. This setting is not favoured in the vast majority of indications but is a viable option for certain easily accessible tumours, for example, the treatment of melanoma using Imlygic. It is also worth noting that the abscopal effect, i.e. the possibility that effective local treatment of a primary tumour may lead to systemic responses against disseminated tumour deposits, using biologic therapeutics is increasingly being seen as a potential means to avoid the need for intravenous delivery.

Mice were implanted with CT26 cells described above in the Methods section 5.2.2. A total of 24 tumours were used for this work. The tumours were randomly allocated to groups, with an N of 4 for each group. Based on the findings of previous chapters, a pressure range (0.7 MPa to 1.6 MPa) was chosen to provide the best chance of achieving optimal delivery with minimal toxicity. After exposure, as described in the section, the mice were imaged using IVIS analysis. The resulting values of the IVIS images can be seen in Figure 5.3.1.1. It can be observed from these images that tumours exposed to 1.6 MPa and STPs or 1.35 MPa, and STPs show a lower signal than those exposed to 1.0 MPa and STPs, 0.7 MPa and STPs and even compared to control tumours which were injected with mRNA and STPs. To corroborate that the signal declines over time, a control group with mRNA and STPs without ultrasound exposure was also included, imaged, and culled at 24 hours. It can be seen in Figure 5.3.1.1 that this control group does decline between 10 and 24 hours. This is in accordance with the work presented in Chapters 2 and 3.

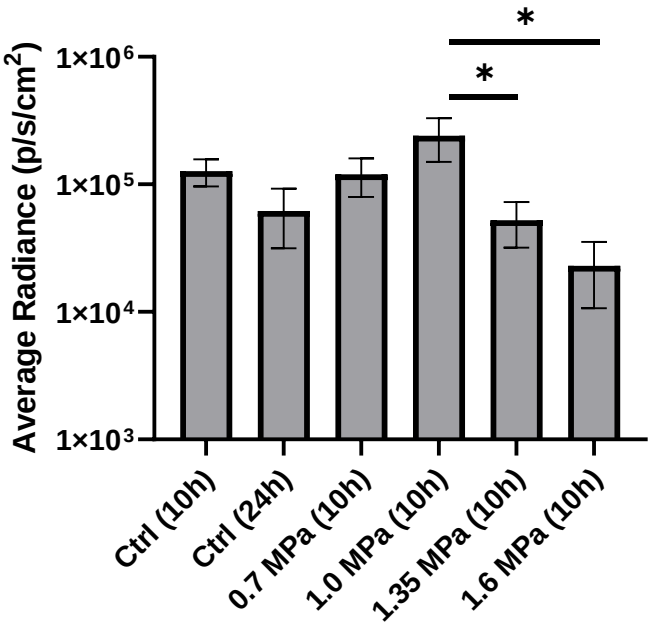

Figure 5.3.1.1 – IVIS luminescence data for CT26 mouse groups. Shown are the average radiance in photons per second per centimetre squared for each tumour's region of interest. N of 4 for each group, with error bars as the standard deviation for the group. Stats by ANOVA, $p<0.05$

Figure 5.3.1.1 presents the group average radiance based on treatment parameters. For all treated mice, a luciferase signal was detected above the background. It can be seen from Figure 5.3.2 that at 10 hours post-treatment, tumours exposed to 1.35 MPa and STPs, gave a 2.2-fold increase in luciferase expression levels when compared to that of tumours exposed to1.6 MPa and STPs), $p<0.05$. Furthermore, tumours exposed to 1.0 MPa and STPs), provided 4.6 times higher signal than 1.35MPa and STPs, and 10.4-times higher expression levels compared to 1.6 MPa and STPs (2.4E5 photons/sec/cm^2 +/- 9.0E4 vs 5.2E4 photons/sec/cm^2 +/-2.0E4 vs 2.3E4 photons/sec/cm^2 +/-1.2E4). When 0.7 MPa and STPs were used, a 2-fold decrease in expression was observed compared with tumours exposed to 1 MPa and STPs. The control group (no US) exhibited over 2 times lower expression levels than that of tumours exposed to 1MPa plus STPs (2.4E5 vs 1.1E5 photons/sec/cm^2, $p<0.05$). Finally, the second arm of the control group measured at a later time point (24 hours) had a 2-fold decrease in luciferase expression compared to the control group tumours measured 14 hours earlier. Areas of expression were limited to the tumour volume for each mouse.

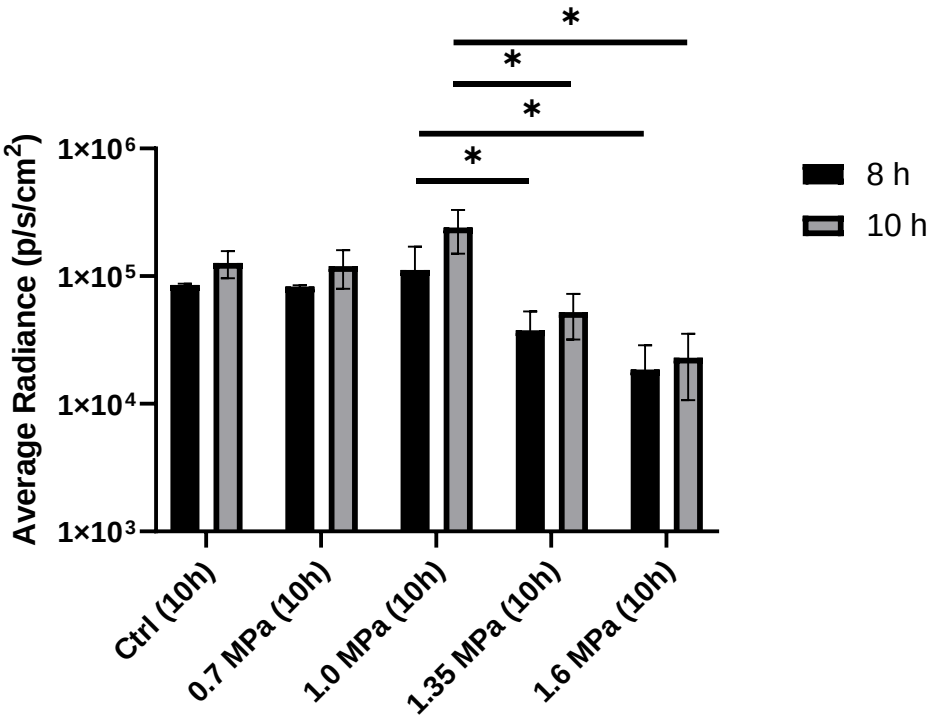

Figure 5.3.1.2: IVIS luminescence data for 6 mouse groups at 8 and 10 hours. Shown are the average radiance in photons per second per centimetre squared for each tumour's region of interest. N of 4 for each group, with error bars as standard deviation for the group

Figure 5.3.1.2 shows the change in expression between 8 and 10 hours. The results here have 10 hours as the final time point, which may raise concerns about missing further increases after 10 hours. Chapter 3 shows that *in vivo,* the end time point of 24 hours produces lower expression levels than seen at 10 hours, as certified by the 24-hour control in this study, also having a lowered expression at 24-hours. As shown in Figure 5.3.1.2, a general pattern can be seen: the expression levels at 8 hours are lower than at 10 hours. At 1.6 MPa, a 23.4% increase between 8 and 10 hours was seen. At 1.35 MPa, a 38.3% increase was observed over the same period. At 1 MPa, the most marked increase (114%) was seen, with the 0.7MPa group demonstrating a 42% increase over these 2 hours whilst the control group showed a change of 48.7%. This, in addition to data in previous chapters, gives confidence that the choice of 10 hours is a good one to represent the point of maximal expression.

The results of the *in vitro* analysis of tumour lysates to give luminescence units/gram of tumour further supported the results from the IVIS imaging (see Figure 5.3.1.4). When 1.6 MPa plus

STPs was used, 13-fold lower expression levels were measured than in tumours treated with 1.35 MPa plus STPs. After 1.0 MPa plus STPs, an 11.7-fold increase in the expression was observed compared to the 1.35 MPa tumours (1.7E7 Luc units/g vs 1.46E6 Luc units/g, $p<0.05$). Notably, the application of ultrasound at 1.0MPa with STPs gave a 2.6-fold increase compared to tumours injected without ultrasound (1.7E7 vs 6.43E6, $p<0.01$). The fact that the expression level decreased between 10 hours and 24 hours by 3.5-fold in the control group provides further evidence that the 10-hour time point represents the peak of expression.

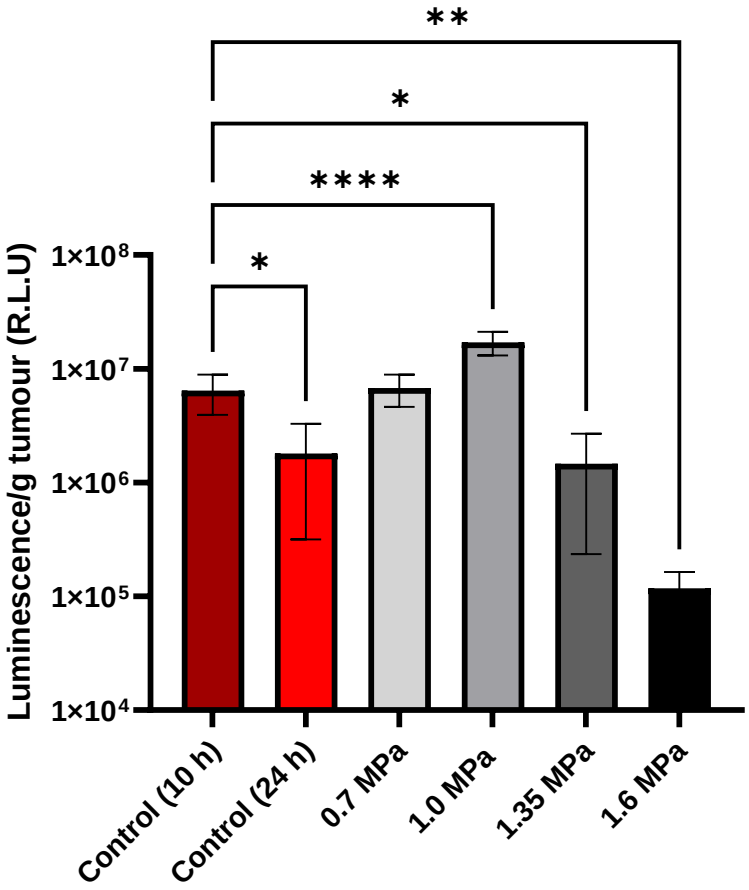

Figure 5.3.1.3: Luciferase expression of excised CT26 tumours using luciferase assay. Samples were measured in triplicate and averaged. N of 4 for each group.

It can be seen from Figure 5.3.1.4 that there was a correlation between pressure and cavitation dose. As can be seen in Figure 5.3.1.3, there is a correlation between pressure and luciferase expression, being that as the pressure decreases from 1.6 MPa to 1.0 MPa, there is an increase

in expression. However, at 0.7 MPa, that relationship breaks down. To examine this further, Figure 5.3.1.4 examines the relationship between chosen pressure and the delivered cavitation.

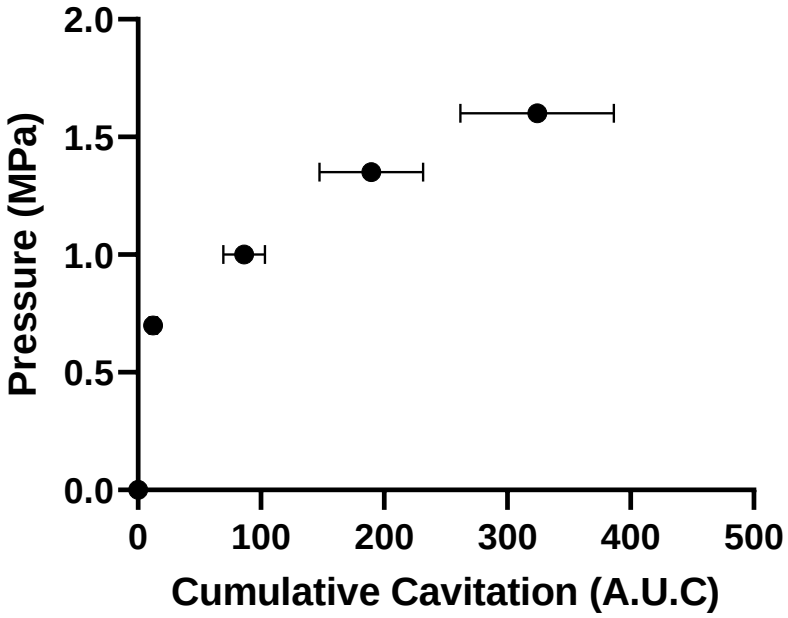

Figure 5.3.1.4: Cumulative cavitation detected, as a function of the area under the curve from generated PAM plots, plotted against pressure amplitude of exposure in MPa. As pressure increases, cavitation can be seen to increase. X error bars represent the standard deviation for each pressure group. N of 4 for each plot.

As the pressure increases from 0.7 MPa to 1.6 MPa, the cavitation detected increases, forming the basis for an inverse relationship between cavitation and luciferase expression. Using the data in previous Chapters and here in Figures 5.3.1.3, 5.3.1.4 and below in 5.3.1.5, it may be possible to identify a treatment window where the pressure and cavitation dose can be chosen to improve luciferase expression further.

Figure 5.3.1.5 shows the mean cumulative cavitation level (for capture and processing of cavitation data, see section 5.2.5) for each group plotted against the mean expression based on the luciferase assay in Figure 5.3.4. This analysis indicates a threshold up to 1MPa / 90 PAM units where an increase in the level of cavitation improves the expression (most likely by improving the delivery). After that point, as the cavitation dosage increases, there is a strong trend towards a decrease in expression levels, as seen at 1.3MPa and 1.6MPa.

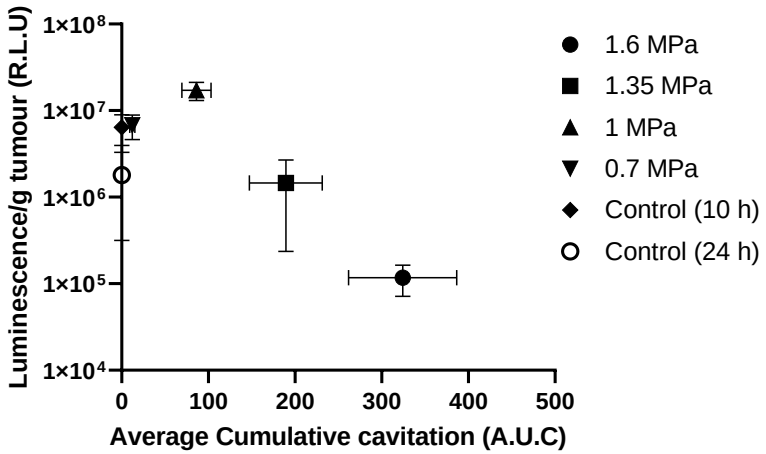

Figure 5.3.1.5: Measured luminescence per gram of tumour homogenate, plotted against the average cumulative cavitation for each group. X error bars are the standard deviation for each group's cavitation measurements, and Y error bars are the standard deviation for the measured luciferase expression. N of 4 for each group.

This analysis may argue for yet further refinement of pressure and cavitation levels in the range of 0.8-1.1 MPa (50-120 PAM units).

5.3.2 EMT6 *in vivo* results

Gene delivery technologies need to provide well-understood activity across a range of potential target cell types. In an ideal situation, such technologies will prove to be 'platform' approaches which require no alteration when the target cell type changes or, more realistically, provide a means of regulating stimulus during treatment in response to feedback. Hence, experiments were repeated in the EMT6 model to test how transposable the optimal exposure parameters identified in CT26 cells are.

Mice were implanted with EMT6 cells described above in the Methods section (5.2.2). A total of 24 tumours were used for this work. The tumours were randomly allocated to treatment groups, with an N of 4 for each group. 10 hours after exposure, the mice were imaged using IVIS analysis, as described in section 5.2.6. A selection of the IVIS images can be seen below in Figure 5.3.2.1. It can be seen from the images that a similar pattern to that of the CT26 IVIS images, Figure 5.2.2.1, is observed. At 1.6 MPa plus STPs and 1.35 MPa plus STPs, the

expression is lower than that achieved using 1.0 MPa plus STPs (5.3E4 photons/sec/cm^2 v 1.12E5 photons/sec/cm^2 v 6.4E5 photons/sec/cm^2). Using 0.7 MPa plus STPs gave similar expression levels to the control group, to which no ultrasound was applied (1.9E5 photons/sec/cm^2 vs 1.7E5 photons/sec/cm^2). As with CT26 tumours, no ultrasound control group showed lower expression at 24 hours than at 10 hours. The results obtained with the EMT6 cells were very similar to the CT26 data. However, the total expression level achieved with EMT6 cells appeared to be 2-3 fold higher than that in CT26 cells, e.g. 6.4E5 photons/sec/cm^2 vs 2.4E5 photons/sec/cm^2 at 1MPa plus STPs.

Figure 5.3.2.2 displays the group average radiance based on treatment parameters. It can be seen from Figure 5.3.2.2 that at 1.35 MPa plus STPs, a 2-fold increase in expression levels is achieved when compared to 1.6 MPa plus STPs. Furthermore, at 1.0 MPa plus STPs, a 5.7-fold higher signal at 1.35 MPa and 12-fold higher expression levels than 1.6MPa is evident. By 0.7 MPa plus STPs, a 3.4-fold decrease in expression compared to 1 MPa plus STPs is observed. The no ultrasound control group exhibits a 3.8-fold lower expression level than 1 MPa (1.7E5 photons/sec/cm^2 vs 6.4E5 photons/sec/cm^2). Therefore, cavitation's benefit appears to be greater in this cell line.

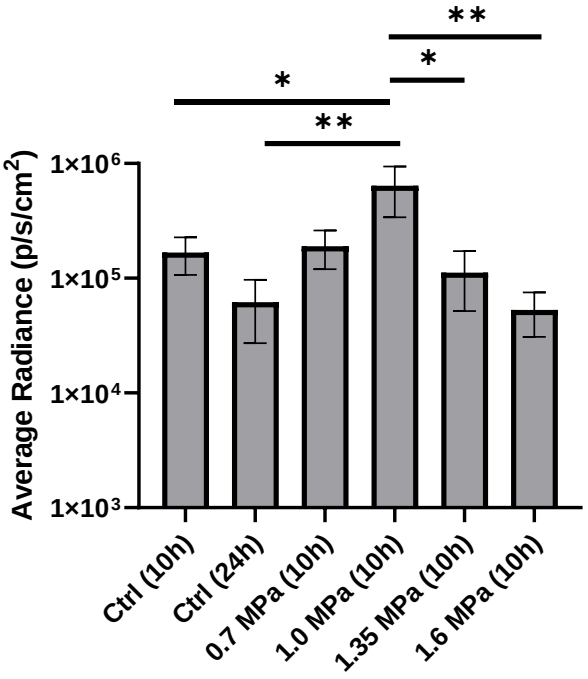

Figure 5.3.2.1 IVIS luminescence data for EMT6 mouse groups. Shown are the average radiance in photons per second per centimetre squared for each tumour's region of interest. N of 4 for each group, with error bars as standard deviation for the group

The results here only include the end time point of 10 hours. This time point most likely represents the peak of luciferase expression as in Chapter 3 by 24 hours post-exposure, lower expression levels are seen, as further verified by the 24-hour control in this study also has a lowered expression at 24-hours. Figure 5.3.2.2 shows the change in expression between 8 and 10 hours, where a general pattern can be seen: the expression levels at 8 hours are lower than that of 10 hours. Tumours exposed to1.6 MPa plus STPs show a 12.8% increase between 8 and 10 hours. Tumours exposed to 1.35 MPa plus STPs, show a 21.2% increase over the same period. Tumours exposed to 1.0 MPa plus STPs show an increase of 45.5%, whilst 0.7 MPa plus STPs demonstrates a 17.6% increase over the same time, and the control group shows a change of 15.9%.

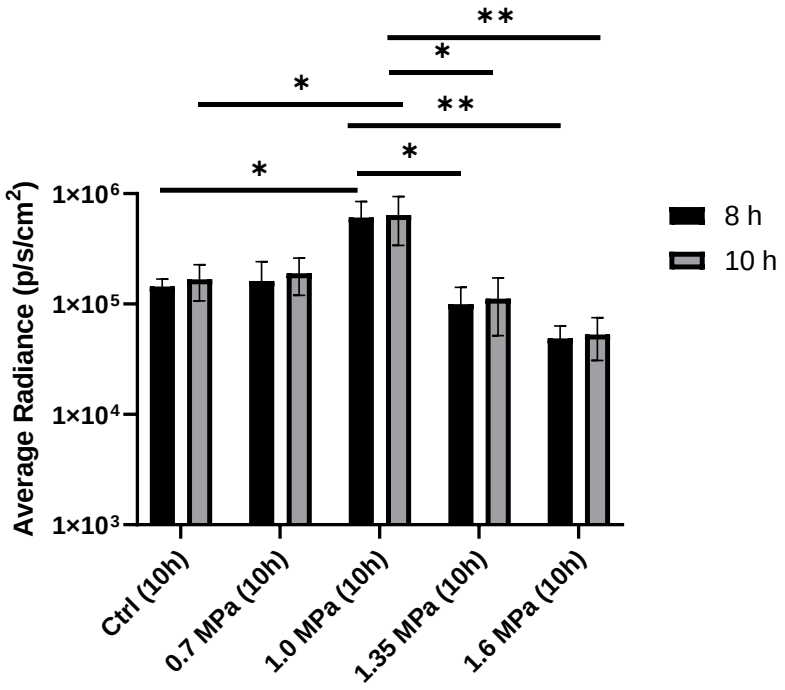

Figure 5.3.2.2 IVIS luminescence data for EMT6 mouse groups at 8 and 10 hours. Shown are the average radiance in photons per second per centimetre squared for each tumour's region of interest. N of 4 for each group, with error bars as standard deviation for the group

Figure 5.3.2.3 shows the luminescence analysis in the tumours after their excision, homogenisation and *in vitro* analysis. Again, the relationship between expression and pressure applied follows the IVIS data in Figure 5.3.2.2. 1.35 MPa plus STPs shows a 10-fold increase in expression compared with 1.6 MPa plus STPs. As with the CT26, 1.0 MPa plus STPs, gave the highest expression, with a 9.8-fold increase compared to 1.6 MPa plus STPs, and a 4.6-fold increase compared to group 1.35 MPa plus STPs. When data for 1.0 MPa plus STPs were compared with the controls, at 10-hours, a 5.5-fold greater level of expression was seen.

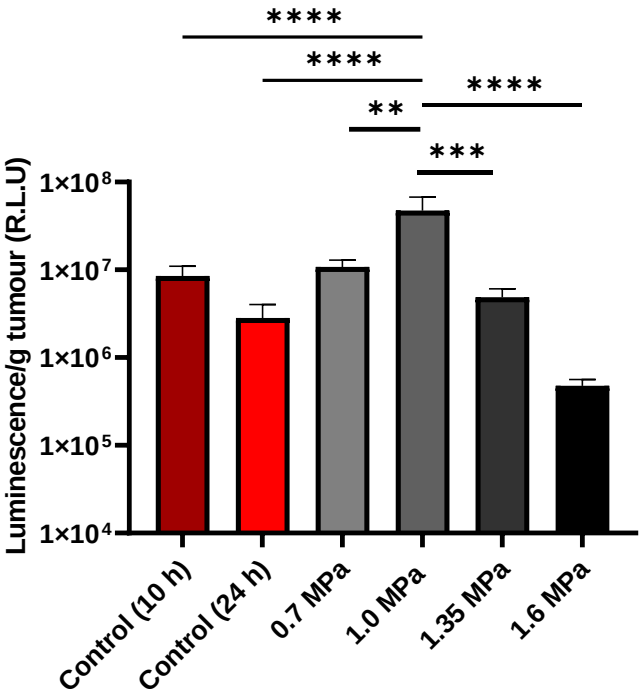

Figure 5.3.2.3 Luciferase expression of excised EMT6 tumours using luciferase assay. Samples were measured in triplicate and averaged. N of 4 for each group. Error bars represent standard deviation, $p<0.001$ as calculated using ANOVA analysis (see methods)

As with the CT26 data, confirming the relationship between pressure and cavitation is essential. Figure 5.3.2.4 below shows that as the mice in each pressure group received higher pressure levels, the cumulative cavitation also increased in a linear, predictable fashion ($R^2 = 0.92$). The variability in that cavitation can be seen on the horizontal error bars representing the standard deviation for each group.

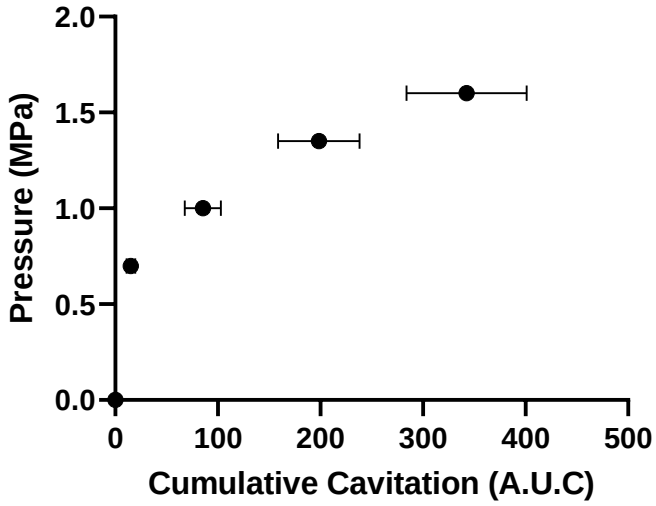

Figure 5.3.2.4 Cumulative cavitation, as a function of the area under the curve from generated PAM plots, plotted against pressure. As pressure increases, cavitation can be seen to increase. X error bars represent the standard deviation for each pressure group. N of 4 for each plot.

Figure 5.2.3.4 shows the average cavitation for each group plotted against the expression based on the luciferase assay in Figure 5.2.3. A pattern in accordance with the CT26 cells in Figure 5.2.3.4 is evident. Specifically, as the cavitation levels increase, the expression increases to a threshold of 1MPa. After 1MPa, as the cavitation dosage increases, there is a strong trend towards a decrease in expression levels for the 1.6 MPa plus STPs and the 1.35 MPa plus STPs treated tumours. Notably, intra-group variation in cavitation and expression can be seen in Figure 5.3.2.5 also, with the same pressure giving slightly different total cavitation levels.

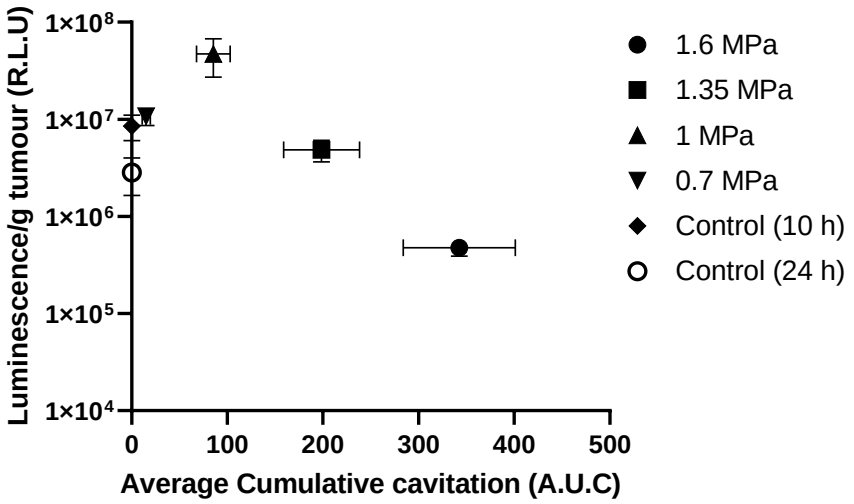

Figure 5.3.2.5 Measured luminescence per gram of EMT6 tumour homogenate, plotted against the average cumulative cavitation for each group. X error bars are the standard deviation for each group's cavitation measurements, and Y error bars are the standard deviation for the measured luciferase expression. N of 4 for each group.

The response of both CT26 and EMT6 tumours are compared using the luciferase assay in Figure 5.3.2.6. For this Figure, the control group is the 10-hour no ultrasound control group for both CT26 and EMT6 tumours. For the 1.6 MPa plus STPs group, there is a significant difference ($p<0.05$) between the response of the CT26, which express 4-fold less luciferase than the equivalent EMT6 group. A comparison of the 1.35 MPa plus STPs groups shows a similar result with a 3.3-fold decrease with CT26 compared to EMT6 tumours. For the 1.0 MPa plus STPs groups, EMT6 tumours had a 4-fold increase in expression levels vs CT26 ($p<0.001$), whilst the 0.7 MPa plus STPs group had a non-significant 1.6-fold increase, and the controls between both groups had a 1.3-fold difference, with the EMT6 controls expressing more luciferase. Hence a greater differential is seen between CT26 and EMT6 tumours at higher cavitation levels compared to 0.7 MPa plus STPs tumours and control tumours. This suggests EMT6 cells are specifically more sensitive/amenable to cavitation-mediated delivery rather than simply benefitting from higher global mRNA processing and translation levels.

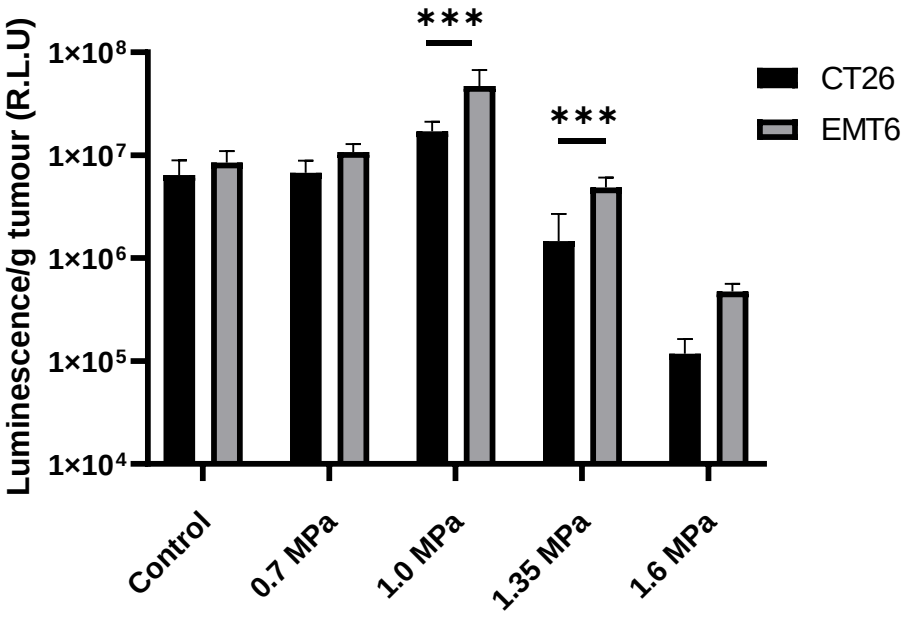

Figure 5.3.2.6 Luciferase expression for each treatment group for CT26 (black bars) and EMT6 (grey bars). Luciferase expression is plotted as R.L.U per gram of tumour. Error bars are the standard deviation for each group, with an N of 4. Error bars represent standard deviation, $p<0.005$ as calculated using ANOVA analysis (see methods)

5.4 Discussion

The work presented in this Chapter brings together the lessons learned from Chapter 2, the *in vitro* and *in vivo* optimisation work of Chapter 3, the *in vitro* experiments using CT26 and EMT6 cells of Chapter 4, and helps elaborate on key timings from all the Chapters.

The first key distinctions between the work in Chapter 5 and Chapter 2 are the changes made in the concentration of STPs, the change in pressure regimes and the change to the end time point of the experiment. CT26 tumours were used again, along with EMT6 tumours, to examine how the change in cancer cell line type may play a role in mRNA's different uptake and expression, as Chapter 4 indicated.

For the CT26 cells, a regime change was required, and these parameters were chosen through the work in Chapters 3 and 4. Reducing pressure and STP concentration and adjusting the end time points produced a compelling case for the relationship between cavitation and RNA delivery. Notably, the optimisations made mean that for the first time in this body of work, a

substantial and significant *in vivo* difference could be detected between control groups without cavitation and a treatment group with a defined level of cavitation.

Figure 5.3.1.1 shows the IVIS results for each group at the end time point of the experiment, and there is an evident decrease in reporter gene expression using the higher pressure of 1.6 MPa plus STPs, compared to 1.35 MPa plus STPs. This decrease is likely due to a higher level of damaging effects of cavitation at 1.6 MPa. This is in accordance with Chapters 2 and 3, where damaging cavitation levels were shown to reduce reporter gene expression. However, the threshold for such detrimental damage appears to be lower (1.35 MPa) *in vivo* than *in vitro*. The highest overall expression levels were obtained at 1 MPa. Notably, the levels obtained outperformed the control groups without ultrasound. These data demonstrate that a sweet spot of pressure/cavitation can be identified, enhancing delivery without an inhibitory level of cell toxicity. The cavitation levels recorded for 1MPa exposure, shown in Figure 6, are three times lower than those achieved following exposure to 1.6MPa, whilst the expression levels were increased 2.6-fold at 1MPa vs 1.6MPa, Figure 5.3.1.3.

When examining the cavitation recorded, it is essential to note that the recorded cavitation events at 1 MPa would be regarded as being low compared to studies in Chapter 2 and that of the 1.6 and 1.35 MPa groups and in publications by Grundy (245), Kwan (186,187) and Myers(187,252). However, this can be rationalised when the cavitation threshold for the STPs is considered. Indeed, Kwan et al. demonstrated that the STPs can nucleate cavitation between 1.0-1.2 MPa (187). Furthermore, the cavitation levels used in the above-cited papers were in a systemic delivery context rather than an intratumoural (IT) context. Given that the concentration of IT injected STPs could be as much as 50 times higher, it is unsurprising to see an effect at what would be deemed a low amplitude pressure for systemic delivery. The greater sensitivity of cells to cavitation-induced damage *in vivo* compared to the *in vitro* set-up in Chapter 3 can be explained by the dense cellular nature of the tumour microenvironment, the

proximity of the cells to cavitation events and the change in interstitial fluid pressure of injecting 25 microlitres directly into the tumour. The difference between *in vitro* cell density and *in vivo* cell density can be over a 1000-fold. Using 1 x10^6 cells/mL for the *in vitro* work conducted in Chapters 2, 3 and 4, is much lower than the estimated cell density in tissue of approximately 1 x10^9 cells. Therefore in the tumour environment the cells are more likely to be closer to ongoing cavitation events.

Furthermore, the underlying viability of cells within a tumour is known to be considerably worse than in the idealised conditions of suspension and monolayer tissue culture growth. Indeed, Katti et al. (327) found that up to 30% of cells from untreated CT26 control tumours were dead when analysed by flow cytometry. Finally, it is also important to note that the cavitation detection equipment and processing script developed were designed for more violent cavitation events following intravenous delivery of STPs. Hence there may be a considerable level of undetected cavitation taking place.

From work in Chapter 4, the end time point of 10 hours was chosen as the best time to cull and remove the tumours for assay. The assay results, Figure 5.3.1.3, show the same trend as the IVIS results, as in, 1.0 MPa with STPs, has higher average luminescence than all the other ultrasound and STP mediated cavitation groups (1.6 MPa, 1.35 MPa and 0.7 MPa). The 0.7 MPa plus STPs group has approximately the same levels of expression as the no ultrasound control group, which would indicate that any effect from the ultrasound and cavitation is achieved above this pressure at these ultrasound parameters of 50,000 cycles, 0.5 MHz, 0.5 Hz PRF and 300s exposure. The no ultrasound control group measured 24 hours post-treatment showed decreased luciferase levels compared to 10 hours. Similarly, in all cases, measurements taken at 8 hours were lower than the levels achieved by 10 hours. These data points show that the 10-hour time point represents the optimal time to end the experiment.

The results of the 0.7 MPa plus STP group, which are very similar to the no ultrasound control group, is unsurprising when looking at the cavitation data in Figure 5.3.1.5. Very few cavitation events were detected at 0.7MPa, effectively nullifying any potential benefit from the cavitation. Moreover, this is reflected in both the IVIS results and the luciferase assay results of Figures 5.3.1.2 and 5.3.1.4.

EMT6 cells were more responsive to the ultrasound parameters used in levels of expression. When compared directly with the CT26 results, Figure 5.3.2.6 shows significant differences between 1.6, 1.35 and 1.0 MPa with STPs. The higher expression levels in these groups follow the *in vitro* experiments discussed in Chapter 4. The reason for the apparent improved response to the ultrasound and cavitation regimes is unknown. However, while the CT26 and EMT6 cells have a difference in response to the ultrasound and cavitation groups, their control groups show no significant difference when compared with each other. This would indicate that the change in expression levels is not solely down to a change in the intrinsic mRNA processing and translation rates of the cell lines and is more likely related to the specific cavitation response of the cell lines.

Breaking down the response of each group for the EMT6 tumours, Figure 5.3.2.2 shows the IVIS values for each. Imaging at the end of the experiment shows a 2-fold difference between the 1.6 plus STPs and 1.35 MPa plus STPs and a 5-fold difference between the 1.35 plus STPs and 1.0 MPa plus STPs groups. This improvement is likely due to some of the issues discussed in Chapter 2. Even at a lower concentration of STPs and lower pressures than in Chapter 2 (2.1 and 1.6 MPa), there is damage within the tumour environment. This is likely due to the nature of intratumoral injection and the poorer underlying viability of the cells within the tumour. When Figure 5.3.2.4 is examined, the luciferase signal, much like shown in the work of Chapter 4, increases between 8 and 10 hours. That change in signal is more intense for the 1.0 MPa plus STPs group, with a 40% change in signal over a 2-hour window. This is likely due to more

mRNA being present and translated by the cells, i.e. enhanced delivery into cells. All the other groups showed a consistent change of 12-16% in the same window of 8 to 10 hours after treatment.

The luciferase assay results, Figure 5.3.2.3, show a significant difference in the expression ($p<0.05$) across the 1.6 -1.0 MPa groups, in accordance with the IVIS, results in Figures 5.3.2.2 and 5.2.3.3. With a nearly 10-fold difference between 1.35 and 1.0 MPa groups and a 100-fold difference between the 1.6 and 1.0 MPa groups, the lower pressure regime works well regarding expression levels. Moreover, it leads to an additional parameter to be explored further as a potential treatment regime with the STPs. With a 5.5-fold difference between the 1.0 MPa and the control group, it can also be shown that the treatment regime has a significant ($p<0.05$) effect on expression mRNA, in contrast to the other treatment groups.

The cavitation versus expression profile for the EMT6 tumours, Figure 5.3.2.5, show a similar pattern to that of the CT26 tumours, Figure 5.3.2.4, whereby as the cavitation is increased above a threshold of 100 cumulative cavitation units (AU), it begins to have a detrimental effect on expression levels. The 1.0 MPa group's cavitation levels for EMT6 tumours are like those achieved in the CT26 tumours. This would indicate that the STPs behave much the same way within both tumour environments, but the expression levels are ten times higher for EMT6 tumours. Again, this would suggest that rather than delivery mechanism playing a role in the high expression levels, the cells and their uptake process and sensitivity to the ultrasound parameters may also play a fundamental role. It is vital to note is that the luciferase levels in the no ultrasound control EMT6 tumours show no significant difference to the no ultrasound control CT26 tumours (8.5E6 R.L.U/g vs 6.8E6 R.L.U/g, $p>0.9$).

These data represent a new and potentially important contribution to the field. Indeed, although previous studies (240) have demonstrated the delivery of RNA constructs into *in vitro*

phantoms and managed to define optimal pressure/cavitation/toxicity/delivery balances for such phantoms, these are the first studies to report on intratumoural treatment and identify optimal cavitation levels. Reassuringly, the apparent benefit of using the specific set of ultrasound parameters identified with STPs was shown to be substantial (2-fold) and significant ($p<0.01$) for both EMT6 and CT26 tumours.

Whilst intratumoural administration is generally not commonly used for many types of therapy, the currently poor PK and BD of nucleotide cancer medicines means their great potential can only be realised by using such a delivery method. From a clinical perspective, IT delivery is unlikely to be a widely adopted methodology moving forward. For example, suppose a needle can reach the sight. In that case, the likelihood is that a surgeon's scalpel could too, and considering surgical resection is one of the most common and successful treatments for tumours, the applicability of IT injection is often restricted to a few treatment approaches in a small number of indications such as melanoma and prostate cancer. However, gene delivery is not restricted to cancer indications, and many diseases and target tissues could benefit from gene delivery where the problem cannot be resolved by cutting. One example of this is seen in Chapter 4 with cardiomyocytes.

The use of naked RNA is uncommon *in vivo* application due to the many issues highlighted in previous Chapters, such as the degradation and lack of systemic circulation time. However, encapsulated RNA as a potential cancer therapeutic is currently being explored in human clinical trials, with 50 mRNA-based cancer trials ongoing (clincicaltrials.gov as of January 2022) (328). When comparing the *in vivo* results reported here, it is important to remember that the RNA is not encapsulated, which would be one method to overcome some of the shortcomings of this study. By moving to an LNP carrier, more effective IT delivery may be achieved, indeed the recent successful deployment of RNA/LNP-based vaccines suggests good effective local delivery. How cavitation impacts and improves LNP/RNA delivery may depend

on how the MOA of LNP entry into the cell aligns with the process of ultrasound-mediated pore formation and propulsion through such pores, but these questions undoubtedly warrant further investigation.

Systemic delivery may remain a challenge even with LNP, as the only nucleotide/LNP formulation currently FDA approved for IV injection shows rapid destabilisation and clearance to the liver (which fortunately happens to be its target) (329). While this is much more common in literature, ultrasound's success rate is variable.

The expression time points in this experiment were chosen based on the pilot studies conducted in Chapter 3, where the maximum time of expression was seen to be on the order of 10 hours. This is much sooner than typically seen with non-viral and viral vectors, for example, the time frame for transgene expression of green fluorescent protein (GFP) using viral vectors as a transfection agent can be on the order of 48-72 hours (330) to reach the maximum.

As firefly luciferase encoding mRNA leads to luciferase enzyme production and then the output of photon generation (once the substrate has been added), it is less prone to confounding background signals often seen with fluorescent proteins, such as GFP. When exciting and measuring fluorescence emission, great care must be taken to eliminate the native signal in the same bandwidth coming from tissue. It is worth noting, however, that GFP does allow the level of expression to be measured per cell, so to extend the work in this thesis and compare this ultrasound-mediated technology to electroporation and chemical transfection, reference to both luciferase and GFP data would be of use.

5.5 Conclusion

For the first time in this body of work, a statistically significant improvement of cavitation-treated tumours compared with control tumours was evidenced. This validates the value in the process of the careful *in vitro* and *in vivo* refinement and improvement of the ultrasound

parameters used. It is still likely that further improvements can be achieved with parameter optimisation (for example, in the range between 0.7 and 1.1 MPa). The expression profiles from this study fit within the broad and varying range of expression profiles reported in the literature.

The overall outcome of these experiments is an exciting one. The method, ultrasound set-up, and parameters have been shown to work and can substantially and significantly improve the expression of mRNA encoded luciferase within the treated tumours.

Chapter 6 – Summary and future work

6.1 Summary

Ultrasound mediated delivery of RNA offers an exciting alternative to current transfection techniques, both in vitro and in vivo. The application of ultrasound for gene delivery is appealing for in vivo delivery due to the ability to target specific tissue, and regions of tissue, in a safe and non-invasive way using a widely clinically accepted technology. The use of ultrasound for in vitro gene delivery offers an opportunity to transfect a wide range of cell types and immediately use the cells for another application without the need for further plating and rescue. . This is a consequence of the fact that the ultrasound can be applied to cells in suspension. In contrast, traditional chemical transfection methods rely on exposure of cells in monolayer culture and typically a further 24 hours of plating before 'harvesting' the cells for use (307,308).

Furthermore, the strong correlation between the level of cavitation instigated and the delivery achieved and the fact that such cavitation can be monitored in real-time in a non-invasive way, means feedback on the success of the procedure is provided. This functionality is not a feature of other gene delivery technologies.

The aim of this body of work changed based on the results obtained early in Chapter 2. Delivery of lipid nanoparticles (LNPs)) and STPs by intratumoural (IT) injection followed by exposure of the tumour to ultrasound exposure had different results than expected. Specifically, the lower expression seen within controls. The results indicated that the presence of ultrasound and STPs hindered the uptake and expression of LNPs at the pressures and exposure parameters used. Hence, further in vitro investigation was warranted before moving forward with further in vivo attempts. This investigation led to the additional work in Chapters 2, 3 and 4, where it was shown that refinement of the ultrasound parameters and delivery protocol was required.

Chapter 2 demonstrates the importance of use of optimised parameters and cavitation dose. Indeed, it can be seen in Chapter 2 that, for IT delivery of naked RNA, the use of 21.4 mg/mL STPs at pressures of 1.6 or 2.1 MPa can have a detrimental effect on the tumour. The levels of cavitation instigated for samples at both these pressures lead to high tumour cell death (up to 74% in the case of 2.1MPa). While this ultimately may be the goal of some treatments, it is not conducive to gene delivery, as the cells need to be alive to translate the RNA into therapeutic protein. Another interesting outcome was that even when STP was used at a 1:10 dilution if 2.1MPa was applied, a high cell death percentage (71%) was still observed. This confirms that both pressure, and concentration of cavitation nuclei need to be carefully considered when delivering intratumourally. It also indicates that at 2.1 MPa there is likely endogenous cavitation, in which case the only way to control this is by lowering the pressure

Chapter 3 further explored the parameters used in the in vivo studies discussed in Chapter 2 and in so doing established a simple protocol to follow to achieve robust transfection of CT26 cells in vitro. Chapter 3 therefore represents a potentially important contribution to the field of transfection technologies, as the relatively simple and chemical-free process developed has several advantages over current commonly used techniques such as transfection reagents and electroporation (135,268,307,331,332). However, it became evident from the experiments presented in Chapters 2 and 3, that a further refinement of the ultrasound pressures used, and validation of the approach in a range of cell types, was required.

Chapter 4 explored the relationship between cavitation and transfection for six different cell lines, from three different species and five different organ systems. The goal of this Chapter was to investigate how the effect of cavitation may impact differently on the viability, and expression of RNA in these different cell lines. Although pressures of 2.1 MPa and 1.85 MPa lead to universally high levels of cell death (ranging 70-85 %) in all cell lines, marked differences were apparent at pressures of 1.6 and 1.35 MPa. For example, at 1.6 MPa the EMT6

cell line showed death percentage of ~45%, with 26% of the cells remaining permeabilised, whereas rat cardiomyocyte cell line showed 64 % cell death but with 42% of the remaining permeabilised.

The reasons for these cell line specific sensitivities could relate to many facets including differences in membrane permeability (255,333,334), levels of functionality in damage repair pathways (335), and differences in the cell's global metabolic and translation activity (336). Much further investigation is needed to unpick the various contributions of such factors, and this discussed in the future work section of this Chapter. It is clear, that although these studies set clear upper toxicity boundaries for pressure and STP concentration which are shared by all cells (i.e., 2.1MPs, 1:10 STP), any further development and commercialisation of the approach would require defined cell type specific delivery 'settings' to be identified and stipulated. One of the cell lines that show the most promise for further investigation are mesenchymal stem cells (MSCs). MSCs have long been explored for a wide range of applications including in therapeutic regenerative medicine in the areas of neurological disorders, cardiac ischemia, diabetes, and bone and cartilage diseases (337). The ability MSCs demonstrate of movement to damaged tissue, the regenerative properties and the differentiation potential that the cells demonstrate offer an avenue of hope for attempting to tackle some of the most prevalent diseases in society. But there are applications where the cell may need to be transfected to display a specific protein but only temporarily, where long term expression would hinder rather than aid in either therapeutic or tissue engineering applications. MSCs have been shown to be difficult to transfect (338). Ultrasound and cavitation provides a new exciting avenue to achieve transfection without chemical modification of the cells, that can be achieved in high volume/concentration of cells, with a limited window where the cells are directly affected by the mechanism and within 12 hours expression can be seen (with FLuc mRNA).

These detailed in vitro studies also helped establish the parameter space of pressure and STP concentration which would be more likely to produce successful damage free delivery in in vivo experiments. A notable change from Chapter 2 was the realisation that, the in vivo IT setting may require a “gentle” cavitation approach in contrast to the pressures and cavitation levels reported for systemic delivery of viruses and antibodies using STPs (242,245).

The role and importance of how the cells are prepared for ultrasound exposure, and the media they are stored in for the duration of exposure with mRNA is critical to a positive outcome. Notably, the exclusion of RNAse by removal of fetal calf serum is vital but its inclusion and exclusion can be used to map the time course of ultrasound mediated delivery. Specifically, it was found that delivery only takes place in the absence of FBS and during the ‘on’ time of the ultrasound and cavitation. The majority of ultrasound and cavitation delivery has been studied using microbubbles, or more recently, nanobubbles and the work presented here agrees with the hypothesis of cavitation causing membrane permeabilisation either through sonoporation or inducing uptake pathways. For this body of work however, it is unlikely that there is a change in uptake pathways or increased endocytosis (in vitro). The results of adding mRNA post ‘ideal’ mRNA exposure conditions (i.e., no FBS present) showed no uptake of mRNA in those cells. This could be due to factors such as the cells being in suspension for example and therefore by the time adhered any mRNA has become non-functional.

The work presented in Chapter 4 shows that for both the CT26 cell line and the EMT6 cell line there are correlations between the pressure applied, the cavitation instigated and the cell viability and reporter gene expression level that results. Such relationships which link delivery to measured cavitation have great potential clinical utility as there are few inexpensive technologies which provide the clinician with real-time feedback on the success of delivery during treatment. One such area for improvement is a universal measurement of such cavitation which would benefit in translation across fields such as medicine and areas of scientific

measurement. This however proves difficult as equipment, software and ultrasound set ups can all effect the data recorded and ultimately the number generated.

As successful transfection requires cells to survive the process in order to express reporter protein it is as expected that cell viability pre and post treatment are critically important. Notably, with optimised parameters viability could be maintained to a level of 80%. Comparison to existing studies in the literature are difficult as cell-line, RNA dose and reporter gene output cannot be easily matched.

Chapter 5 used a similar experimental method of exploring pressure, cavitation, expression and timing of expression to fully define the time-expression profile following ultrasound mediated delivery of the RNA. The results show that the expression increases from 8-12 hours post treatment and begins to decrease thereafter. This was consistent between the two cell lines used, CT26 and EMT6. EMT6 cells were chosen because they could be used in the same mice as used in Chapter 2 and therefore results would be comparable. The decision to end the experiment at 12 hours was made, as control tumours (i.e., injected with RNA without ultrasound) showed a similar pattern of expression, so no bias was found. The results of Chapter 5 show a similar pattern for the CT26 tumours of Chapter 2. Higher pressures, and high doses of cavitation are not conducive to uptake and expression, but as the pressure and therefore cavitation decreased there was an improvement, until the 1.0 MPa group which showed a marked improvement on the control tumours for the first time. The result was consistent between both CT26 and EMT6 tumours and represented a 5.5-fold increase in the US group compared to the non-US group in terms of peak expression. Notably, the cavitation levels for these groups are very low doses, again contrasting markedly with studies following intravenous delivery (243,245). This would indicate a greater sensitivity to cavitation mediated damage following IT delivery than IV delivery and suggests that further refinement of how the cavitation is recorded and processed in the IT setting is required, and discussed further below.

The studies in Chapter 5 therefore established a new ultrasound protocol for vivo IT delivery to add to the in vitro protocol developed in Chapters 3 and 4. The clinical translatability of this process will depend on how the levels of expression match those achieved with alternative technologies. This is hard to assess but there are currently IT gene delivery and nucleotide therapeutics approaches being tested and even used in the melanoma setting (339). The latter of which even performs such injections under ultrasound guidance and so it is not hard to imagine how the technology and parameters described in Chapter 5 may be adapted to this clinical context providing superiority of delivery can be shown. A further advantage of this approach is the feedback provided by cavitation monitoring, and demonstrating that cavitation dose delivered can correlate with expected expression. This would be able to guide clinicals and allow for therapeutic monitoring of disease and progression.

The transfection of cells in suspension using cavitation showed interesting results. The change in time of expression depending on cell line, the effect of the cavitation on each cell line and the ability for the cells to recover and behave as prior to treatment, shows promise for translation of this method from the ultrasound water tank to the bench. The cellular response was dependent on the ultrasound parameters used and the amount of cavitation experienced, which of course can be monitored to provide feedback to the user.

The body of work discussed within this thesis is broad. Both in vivo and in vitro techniques are examined and optimised for the uptake and expression of luciferase mRNA. Over the course of this thesis, the story of a non-working protocol has been refined into a protocol that can be used to transfect cells both in vivo and in vitro.

The in vitro transfection of cells covered 6 cell lines, differing types, cancerous and non-cancerous, and both human and rodent cell lines. The exploration of using these cells led to discovery of how ultrasound mediated delivery, may use the same mechanism in different cell

lines but can give a different level and time of peak expression depending on cell type. The development of a protocol that incorporates the already familiar steps of cell harvesting and the ability to transfect cells over a short period of time (5 minutes) offers the exciting possibility to develop a bench-top device for transfection in research labs. The amenability of such a device to transfection of cells in solution to allow their immediate use or further manipulation is another attractive asset as may be the shortening of the peak of transgene expression from 24 hours with agents such as lipofectamine to 12 hours using cavitation.

The in vivo data is interesting for many reasons, the strength of the expression for control tumours, and the difficulty in matching cavitation between samples. The goal of a positive use for ultrasound was an arduous task, spanning many hours of in vitro work to further refine the ultrasound parameters. During this process the ability to use the ultrasound parameters chosen for in vitro transfection was further explored. An in vivo protocol that allows for, rather than hinders, expression was established. The importance of developing such a protocol can be seen in the potential for its clinical use. A system that allows a non-invasive method of gene delivery in a targeted region could have a fundamental role to play in future treatments of disease.

6.2 Future work

There is a need to explore additional ultrasound parameters for use in vivo. While the 1.0 MPa plus STPs group outperformed controls for both CT26 and EMT6s, there is a need for additional investigation around both the ultrasound parameters employed and how the cavitation is recorded and the processing of the acoustic signal. Additional information in this regard will allow for further refinement of the protocol and aid in delivery.

Additional in vitro work is required also. However, this work could be tailored to refining the in vitro transfection of cells that can be used in vitro for other uses – such as tissue engineering and stem cell modification, or for cell manipulation ex vivo to allow re-infusion (for example in CAR T cell therapy). There is much room to grow in this area, with a fuller investigation into different cavitation nuclei and focusing on optimisation of parameters for both nuclei and cell type, the development of a bench top ultrasound mediated transfection device has much potential. The development of such a device would allow cells to be taken directly from a cell split and be transfected using a simple 5 minute process without the need to formulate the nucleotide. Transfected cells in suspension could then be used directly without need for further plating or culturing. Testing with a wider range of nucleotide therapeutics, including plasmid DNA, will also be of interest as data is gathering that cavitation can be used as a means of permeabilising the nuclear membrane as well as the cytoplasmic membrane, a challenge electroporation devices struggle to meet without causing substantial cell death.

Additional parameter testing with other cavitation nuclei is critical. With this investigation a change to ultrasound parameters and a more effective transfection method may be developed.

While the in vivo results show promise, taking the steps of investigating the use of different cavitation nuclei at different ultrasound parameters may offer a more effective route for in vivo translation. Of course, the use of STPs and LNPs should be explored further as a method for clinically relevant in vivo delivery and offers an exciting route for targeted treatments.

References

1. De Haan P, Van Diemen FR, Toscano MG. Viral gene delivery vectors: the next generation medicines for immune-related diseases. Hum Vaccines Immunother [Internet]. 2021;17(1):14–21. Available from: https://doi.org/10.1080/21645515.2020.1757989

2. Ibraheem D, Elaissari A, Fessi H. Gene therapy and DNA delivery systems. Vol. 459, International Journal of Pharmaceutics. Elsevier; 2014. p. 70–83.

3. Kopechek JA, Carson AR, McTiernan CF, Chen X, Klein EC, Villanueva FS. Cardiac Gene Expression Knockdown Using Small Inhibitory RNA-Loaded Microbubbles and Ultrasound. PLoS One. 2016;11(7):e0159751.

4. Davis PB, Cooper MJ. Vectors for airway gene delivery. Vol. 9, AAPS Journal. 2007. p. 2–5.

5. NHS. Chemotherapy; What happens. 2017.

6. Laudicella M, Walsh B, Burns E, Smith PC. Cost of care for cancer patients in England: Evidence from population-based patient-level data. Br J Cancer [Internet]. 2016;114(11):1286–92. Available from: http://dx.doi.org/10.1038/bjc.2016.77

7. Ramadori G, Cameron S. Effects of systemic chemotherapy on the liver. Ann Hepatol. 2010 Apr 1;9(2):133–43.

8. Schirrmacher V. From chemotherapy to biological therapy: A review of novel concepts to reduce the side effects of systemic cancer treatment (Review). Int J Oncol [Internet]. 2019 Feb 1 [cited 2021 Dec 16];54(2):407–19. Available from: http://www.spandidos-publications.com/10.3892/ijo.2018.4661/abstract

9. Blanco E, Shen H, Ferrari M. Principles of nanoparticles design for overcoming biologica barriers for drug delivery. Nat Biotechnol. 2015;33(9):941–51.

10. Witten J, Ribbeck K. The particle in the spider's web: Transport through biological hydrogels. Nanoscale. 2017;9(24):8080–95.

11. Bobkova S, Gavrilov L, Khokhlova V, Shaw A, Hand J. Focusing of high-intensity ultrasound through the rib cage using a therapeutic random phased array. Ultrasound Med Biol [Internet]. 2010 [cited 2021 Dec 16];36(6):888–906. Available from: https://pubmed.ncbi.nlm.nih.gov/20510186/

12. Kulkarni JA, Cullis PR, Van Der Meel R. Lipid Nanoparticles Enabling Gene Therapies: From Concepts to Clinical Utility. Nucleic Acid Ther. 2018;28(3):146–57.

13. Minchin S, Lodge J. Understanding biochemistry: structure and function of nucleic acids. Essays Biochem [Internet]. 2019 [cited 2021 Dec 16];63(4):433. Available from: /pmc/articles/PMC6822018/

14. Breaker RR, Joyce GF. The Expanding View of RNA and DNA Function. Chem Biol [Internet]. 2014 Sep 18 [cited 2021 Dec 16];21(9):1059. Available from: /pmc/articles/PMC4171699/

15. Khakshoor O, Kool ET. Chemistry of nucleic acids: impacts in multiple fields. Chem Commun (Camb) [Internet]. 2011 [cited 2021 Dec 16];47(25):7018. Available from: /pmc/articles/PMC4445425/

16. Brosius J, Raabe CA. What is an RNA? A top layer for RNA classification. RNA Biol [Internet]. 2016 Feb 1 [cited 2021 Dec 16];13(2):140. Available from: /pmc/articles/PMC4829331/

17. Bottaro S, Di Palma F, Bussi G. The role of nucleobase interactions in RNA structure and dynamics. Nucleic Acids Res [Internet]. 2014 Dec 1 [cited 2021 Dec 16];42(21):13306–14. Available from: https://academic.oup.com/nar/article/42/21/13306/2903225

18. Translation: DNA to mRNA to Protein | Learn Science at Scitable [Internet]. [cited 2021 Dec 16]. Available from: https://www.nature.com/scitable/topicpage/translation-dna-to-mrna-to-protein-393/

19. Alberts B, Johnson A, Lewis J, Raff M, Roberts K, Walter P. From DNA to RNA. 2002 [cited 2021 Dec 16]; Available from: https://www.ncbi.nlm.nih.gov/books/NBK26887/

20. Koellner CM, Mensink KA, Highsmith WE. Basic concepts in human molecular genetics. Mol Pathol Mol Basis Hum Dis. 2018;99–120.

21. Numan M. Basic Genetics and Epigenetics. Neurobiol Soc Behav. 2015;43–62.

22. Houseley J, Tollervey D. The Many Pathways of RNA Degradation. Vol. 136, Cell. 2009. p. 763–76.

23. Chen CYA, Ezzeddine N, Shyu A Bin. Chapter 17 Messenger RNA Half-Life Measurements in Mammalian Cells. Methods Enzymol. 2008;448(08):335–57.

24. Huang Q, Zeng J, Yan J. COVID-19 mRNA vaccines. J Genet Genomics [Internet]. 2021 Feb 20 [cited 2021 Dec 16];48(2):107. Available from: /pmc/articles/PMC7959685/

25. Liu H, Luo M, Wen JK. mRNA stability in the nucleus. Journal of Zhejiang University: Science B. 2014.

26. Fadnes B, Rekdal Ø, Uhlin-Hansen L. The anticancer activity of lytic peptides is inhibited by heparan sulfate on the surface of the tumor cells. BMC Cancer. 2009;9:1–13.

27. Wadhwa A, Aljabbari A, Lokras A, Foged C, Thakur A. Opportunities and challenges in the delivery of mrna-based vaccines [Internet]. Vol. 12, Pharmaceutics. MDPI AG; 2020 [cited 2020 Apr 3]. Available from: http://www.ncbi.nlm.nih.gov/pubmed/32013049

28. Shyu A Bin, Wilkinson MF, Van Hoof A. Messenger RNA regulation: To translate or to degrade. EMBO Journal. 2008.

29. del Pozo-Rodríguez A, Rodríguez-Gascón A, Rodríguez-Castejón J, Vicente-Pascual M, Gómez-Aguado I, Battaglia LS, et al. Gene Therapy. In: Advances in Biochemical Engineering/Biotechnology. 2020.

30. Wang D, McAteer SP, Wawszczyk AB, Russell CD, Tahoun A, Elmi A, et al. An RNA-dependent mechanism for transient expression of bacterial translocation filaments. Nucleic Acids Res [Internet]. 2018 [cited 2021 Dec 16];46(7):3366. Available from: /pmc/articles/PMC5909449/

31. Bai H, Lester GMS, Petishnok LC, Dean DA. Cytoplasmic transport and nuclear import of plasmid DNA. Biosci Rep [Internet]. 2017 Dec 22 [cited 2021 Dec 16];37(6). Available from: /pmc/articles/PMC5705778/

32. Norrisa V. Does the Semiconservative Nature of DNA Replication Facilitate Coherent Phenotypic Diversity? J Bacteriol [Internet]. 2019 [cited 2021 Dec 16];201(12). Available from: /pmc/articles/PMC6531617/

33. Chen B-S, Li C-W. Big mechanisms in systems biology : big data mining, network modeling, and genome-wide data identification.

34. Vaisman A, Woodgate R. Translesion DNA polymerases in eukaryotes: what makes them tick? Crit Rev Biochem Mol Biol [Internet]. 2017 May 4 [cited 2021 Dec 16];52(3):274. Available from: /pmc/articles/PMC5573590/

35. Chen T, Hongdilokkul N, Liu Z, Thirunavukarasu D, Romesberg FE. The Expanding World of DNA and RNA. Curr Opin Chem Biol [Internet]. 2016 Oct 1 [cited 2021 Dec 16];34:80. Available from: /pmc/articles/PMC5107331/

36. Travers A, Muskhelishvili G. DNA structure and function. FEBS J [Internet]. 2015 Jun 1 [cited 2021 Dec 16];282(12):2279–95. Available from: https://onlinelibrary.wiley.com/doi/full/10.1111/febs.13307

37. Bulaklak K, Gersbach CA. The once and future gene therapy. Nat Commun 2020 111 [Internet]. 2020 Nov 16 [cited 2021 Dec 16];11(1):1–4. Available from: https://www.nature.com/articles/s41467-020-19505-2

38. Kamimura K, Suda T, Zhang G, Liu D. Advances in Gene Delivery Systems. Pharmaceut Med. 2011 Oct;25(5):293–306.

39. Hill AB, Chen M, Chen CK, Pfeifer BA, Jones CH. Overcoming gene delivery hurdles: physiological considerations for nonviral vectors. Trends Biotechnol [Internet]. 2016 [cited 2021 Dec 16];34(2):91. Available from: /pmc/articles/PMC5800990/

40. Lino CA, Harper JC, Carney JP, Timlin JA. Delivering CRISPR: a review of the challenges and approaches. Drug Deliv [Internet]. 2018 [cited 2021 Dec 16];25(1):1234. Available from:

/pmc/articles/PMC6058482/

41. Morrison M, de Saille S. CRISPR in context: towards a socially responsible debate on embryo editing. Palgrave Commun 2019 51 [Internet]. 2019 Sep 24 [cited 2021 Dec 16];5(1):1–9. Available from: https://www.nature.com/articles/s41599-019-0319-5

42. Zhang Y, Satterlee A, Huang L. In vivo gene delivery by nonviral vectors: Overcoming hurdles. Mol Ther [Internet]. 2012;20(7):1298–304. Available from: http://dx.doi.org/10.1038/mt.2012.79/nature06264

43. Bulcha JT, Wang Y, Ma H, Tai PWL, Gao G. Viral vector platforms within the gene therapy landscape. Signal Transduct Target Ther 2021 61 [Internet]. 2021 Feb 8 [cited 2021 Dec 16];6(1):1–24. Available from: https://www.nature.com/articles/s41392-021-00487-6

44. White JM, Delos SE, Brecher M, Schornberg K. Structures and Mechanisms of Viral Membrane Fusion Proteins: Multiple Variations on a Common Theme. Crit Rev Biochem Mol Biol [Internet]. 2008 [cited 2021 Dec 16];43(3):189. Available from: /pmc/articles/PMC2649671/

45. Ura T, Okuda K, Shimada M. Developments in Viral Vector-Based Vaccines. Vaccines [Internet]. 2014 Jul 29 [cited 2021 Dec 16];2(3):624. Available from: /pmc/articles/PMC4494222/

46. Mingozzi F, High KA. Immune responses to AAV vectors: overcoming barriers to successful gene therapy. Blood [Internet]. 2013 Jul 4 [cited 2021 Dec 16];122(1):23. Available from: /pmc/articles/PMC3701904/

47. Daya S, Berns KI. Gene therapy using adeno-associated virus vectors. Clinical Microbiology Reviews. 2008.

48. Li H, Yang Y, Hong W, Huang M, Wu M, Zhao X. Applications of genome editing technology in the targeted therapy of human diseases: mechanisms, advances and prospects. Signal Transduct Target Ther 2020 51 [Internet]. 2020 Jan 3 [cited 2021 Dec 16];5(1):1–23. Available from: https://www.nature.com/articles/s41392-019-0089-y

49. Slade N. Viral Vectors in Gene Therapy. Diseases [Internet]. 2018 [cited 2021 Dec 16];6(2):139–43. Available from: /pmc/articles/PMC6023384/

50. Mali S. Delivery systems for gene therapy. Indian Journal of Human Genetics. 2013.

51. Gardlík R, Pálffy R, Hodosy J, Lukács J, Turňa J, Celec P. Vectors and delivery systems in gene therapy. Vol. 11, Medical Science Monitor. International Scientific Information, Inc.; 2005. p. RA110–21.

52. Zhang XX, McIntosh TJ, Grinstaff MW. Functional lipids and lipoplexes for improved gene delivery. Biochimie [Internet]. 2012 Jan [cited 2021 Dec 16];94(1):42. Available from: /pmc/articles/PMC3771368/

53. Liu C, Zhang L, Zhu W, Guo R, Sun H, Chen X, et al. Barriers and Strategies of Cationic Liposomes for Cancer Gene Therapy. Mol Ther - Methods Clin Dev [Internet]. 2020 Sep 11 [cited 2021 Dec 16];18:751–64. Available from: http://www.cell.com/article/S2329050120301649/fulltext

54. Hou X, Zaks T, Langer R, Dong Y. Lipid nanoparticles for mRNA delivery. Nat Rev Mater 2021 612 [Internet]. 2021 Aug 10 [cited 2021 Dec 16];6(12):1078–94. Available from: https://www.nature.com/articles/s41578-021-00358-0

55. Balazs DA, Godbey W. Liposomes for Use in Gene Delivery. J Drug Deliv [Internet]. 2011 Dec 15 [cited 2021 Dec 16];2011:1–12. Available from: /pmc/articles/PMC3066571/

56. Akbarzadeh A, Rezaei-Sadabady R, Davaran S, Joo SW, Zarghami N, Hanifehpour Y, et al. Liposome: classification, preparation, and applications. Nanoscale Res Lett [Internet]. 2013 [cited 2021 Dec 16];8(1):102. Available from: /pmc/articles/PMC3599573/

57. Farago O, Grønbech-Jensen N. Simulation of Self-Assembly of Cationic Lipids and DNA into Structured Complexes. J Am Chem Soc [Internet]. 2009 Mar 4 [cited 2021 Dec 16];131(8):2875–81. Available from: https://pubs.acs.org/doi/abs/10.1021/ja807278p

58. Bozzuto G, Molinari A. Liposomes as nanomedical devices. Int J Nanomedicine [Internet]. 2015 Feb 2

[cited 2021 Dec 16];10:975. Available from: /pmc/articles/PMC4324542/

59. Behzadi S, Serpooshan V, Tao W, Hamaly MA, Alkawareek MY, Dreaden EC, et al. Cellular Uptake of Nanoparticles: Journey Inside the Cell. Chem Soc Rev [Internet]. 2017 Jul 21 [cited 2021 Dec 16];46(14):4218. Available from: /pmc/articles/PMC5593313/

60. Saffari M, Moghimi HR, Dass CR. Barriers to Liposomal Gene Delivery: from Application Site to the Target. Iran J Pharm Res IJPR [Internet]. 2016 Dec 1 [cited 2021 Dec 16];15(Suppl):3. Available from: /pmc/articles/PMC5242347/

61. Banik M, Basu T. Calcium phosphate nanoparticles: a study of their synthesis, characterization and mode of interaction with salmon testis DNA. Dalton Trans. 2014;

62. Sokolova V V., Radtke I, Heumann R, Epple M. Effective transfection of cells with multi-shell calcium phosphate-DNA nanoparticles. Biomaterials. 2006;

63. Welzel T, Radtke I, Meyer-Zaika W, Heumann R, Epple M. Transfection of cells with custom-made calcium phosphate nanoparticles coated with DNA. J Mater Chem [Internet]. 2004 Jul 14 [cited 2021 Dec 16];14(14):2213–7. Available from: https://pubs.rsc.org/en/content/articlehtml/2004/jm/b401644k

64. Khalifehzadeh R, Arami H. Biodegradable Calcium Phosphate Nanoparticles for Cancer Therapy. Adv Colloid Interface Sci [Internet]. 2020 May 1 [cited 2021 Dec 16];279:102157. Available from: /pmc/articles/PMC7261203/

65. Jordan M, Schallhorn A, Wurm FM. Transfecting mammalian cells: optimization of critical parameters affecting calcium-phosphate precipitate formation. Nucleic Acids Res [Internet]. 1996 [cited 2021 Dec 16];24(4):596–601. Available from: https://pubmed.ncbi.nlm.nih.gov/8604299/

66. Ziello JE, Huang Y, Jovin IS. Cellular endocytosis and gene delivery. Mol Med. 2010;16(5–6):222–9.

67. Sousa De Almeida M, Susnik E, Drasler B, Taladriz-Blanco P, Petri-Fink A, Rothen-Rutishauser B. Understanding nanoparticle endocytosis to improve targeting strategies in nanomedicine. Chem Soc Rev [Internet]. 2021 May 11 [cited 2021 Dec 16];50(9):5397–434. Available from: https://pubs.rsc.org/en/content/articlehtml/2021/cs/d0cs01127d

68. Guo L, Wang L, Yang R, Feng R, Li Z, Zhou X, et al. Optimizing conditions for calcium phosphate mediated transient transfection. Saudi J Biol Sci [Internet]. 2017 Mar 1 [cited 2021 Dec 16];24(3):622. Available from: /pmc/articles/PMC5372392/

69. Scioli Montoto S, Muraca G, Ruiz ME. Solid Lipid Nanoparticles for Drug Delivery: Pharmacological and Biopharmaceutical Aspects. Front Mol Biosci. 2020 Oct 30;7:319.

70. Granot Y, Peer D. Delivering the right message: Challenges and opportunities in lipid nanoparticles-mediated modified mRNA therapeutics—An innate immune system standpoint. Semin Immunol [Internet]. 2017;34(July):68–77. Available from: https://doi.org/10.1016/j.smim.2017.08.015

71. Cheng X, Lee RJ. The role of helper lipids in lipid nanoparticles (LNPs) designed for oligonucleotide delivery. Adv Drug Deliv Rev [Internet]. 2016;99:129–37. Available from: http://dx.doi.org/10.1016/j.addr.2016.01.022

72. Harush-Frenkel O, Rozentur E, Benita S, Altschuler Y. Surface charge of nanoparticles determines their endocytic and transcytotic pathway in polarized MDCK cells. Biomacromolecules. 2008;9(2):435–43.

73. Carboni V, Maaliki C, Alyami M, Alsaiari S, Khashab N. Synthetic Vehicles for Encapsulation and Delivery of CRISPR/Cas9 Gene Editing Machinery. Adv Ther. 2019 Apr;2(4):1800085.

74. Joehanes R, Johnson AD, Barb JJ, Raghavachari N, Liu P, Woodhouse KA, et al. Gene expression analysis of whole blood, peripheral blood mononuclear cells, and lymphoblastoid cell lines from the Framingham Heart Study. Physiol Genomics [Internet]. 2012 Jan [cited 2021 Dec 16];44(1):59–75. Available from: https://journals.physiology.org/doi/abs/10.1152/physiolgenomics.00130.2011

75. Kauffman KJ, Dorkin JR, Yang JH, Heartlein MW, Derosa F, Mir FF, et al. Optimization of Lipid Nanoparticle Formulations for mRNA Delivery in Vivo with Fractional Factorial and Definitive Screening Designs. Nano Lett. 2015;

76. Jokerst J V., Lobovkina T, Zare RN, Gambhir SS. Nanoparticle PEGylation for imaging and therapy.

Nanomedicine. 2011.

77. Hadinoto K, Sundaresan A, Cheow WS. Lipid-polymer hybrid nanoparticles as a new generation therapeutic delivery platform: A review. Eur J Pharm Biopharm [Internet]. 2013;85(3 PART A):427–43. Available from: http://dx.doi.org/10.1016/j.ejpb.2013.07.002

78. Suk JS, Xu Q, Kim N, Hanes J, Ensign LM, Sciences H, et al. PEGylation as a strategy for improving nanoparticle-based drug and gene delivery. 2017;99:28–51.

79. Gulati NM, Stewart PL, Steinmetz NF. Bio inspired shielding strategies for nanoparticle drug delivery applications. Mol Pharm [Internet]. 2018 Aug 6 [cited 2021 Dec 16];15(8):2900. Available from: /pmc/articles/PMC6223124/

80. Ta HT, Truong NP, Whittaker AK, Davis TP, Peter K. The effects of particle size, shape, density and flow characteristics on particle margination to vascular walls in cardiovascular diseases. Expert Opin Drug Deliv [Internet]. 2018 Jan 2 [cited 2021 Dec 16];15(1):33–45. Available from: https://pubmed.ncbi.nlm.nih.gov/28388248/

81. Schlicher RK, Radhakrishna H, Tolentino TP, Apkarian RP, Zarnitsyn V, Prausnitz MR. Mechanism of intracellular delivery by acoustic cavitation. Ultrasound Med Biol. 2006;32(6):915–24.

82. Kou L, Sun J, Zhai Y, He Z. The endocytosis and intracellular fate of nanomedicines: Implication for rational design. Asian J Pharm Sci [Internet]. 2013;8(1):1–10. Available from: http://dx.doi.org/10.1016/j.ajps.2013.07.001

83. Brock DJ, Kondow-Mcconaghy HM, Hager EC, Pellois JP. Endosomal escape and cytosolic penetration of macromolecules mediated by synthetic delivery agents. Bioconjug Chem [Internet]. 2019 Feb 20 [cited 2021 Dec 16];30(2):293. Available from: /pmc/articles/PMC6561124/

84. Hanahan D, Weinberg RA. Hallmarks of cancer: The next generation. Cell [Internet]. 2011;144(5):646–74. Available from: http://dx.doi.org/10.1016/j.cell.2011.02.013

85. Nagy JA, Chang SH, Dvorak AM, Dvorak HF. Why are tumour blood vessels abnormal and why is it important to know? Vol. 100, British Journal of Cancer. 2009. p. 865–9.

86. Chauhan VP, Stylianopoulos T, Boucher Y, Jain RK. Delivery of Molecular and Nanoscale Medicine to Tumors: Transport Barriers and Strategies. Annu Rev Chem Biomol Eng. 2011;2(1):281–98.

87. Rockwell S, Dobrucki IT, Kim EY, Marrison ST, Vu VT. Hypoxia and radiation therapy: past history, ongoing research, and future promise. Curr Mol Med. 2009;9(4):442–58.

88. Muz B, de la Puente P, Azab F, Azab AK. The role of hypoxia in cancer progression, angiogenesis, metastasis, and resistance to therapy. Hypoxia. 2015;83.

89. Arvanitis CD, Bazan-Peregrino M, Rifai B, Seymour LW, Coussios CC. Cavitation-Enhanced Extravasation for Drug Delivery. Ultrasound Med Biol. 2011;37(11):1838–52.

90. Jain RK, Forbes NS. Can engineered bacteria help control cancer? Proc Natl Acad Sci U S A. 2001;98(26):14748–50.

91. Zhou Y. Understanding the cancer/tumor biology from 2D to 3D. Vol. 8, Journal of Thoracic Disease. AME Publishing Company; 2016. p. E1484–6.

92. Padera TP, Meijer EFJ, Munn LL. The Lymphatic System in Disease Processes and Cancer Progression. Annu Rev Biomed Eng. 2016;18(1):125–58.

93. Padera TP, Stoll BR, Tooredman JB, Capen D, Di Tomaso E, Jain RK. Cancer cells compress intratumour vessels. Nature. 2004;427(6976):695.

94. Nathanson SD, Nelson L. Interstitial fluid pressure in breast cancer, benign breast conditions, and breast parenchyma. Ann Surg Oncol. 1994;1(4):333–8.

95. Fukumura D, Jain RK. Tumor microenvironment abnormalities: Causes, consequences, and strategies to normalize. J Cell Biochem. 2007;101(4):937–49.

96. Smith JH, Humphrey JAC. Interstitial transport and transvascular fluid exchange during infusion into

brain and tumor tissue. Microvasc Res. 2007;73(1):58–73.

97. Frantz C, Stewart KM, Weaver VM. The extracellular matrix at a glance. J Cell Sci. 2010;123(24):4195–200.

98. Oskarsson T. Extracellular matrix components in breast cancer progression and metastasis. Breast [Internet]. 2013;22(S2):S66–72. Available from: http://dx.doi.org/10.1016/j.breast.2013.07.012

99. Yue B. Biology of the extracellular matrix: An overview. J Glaucoma. 2014;23(8):S20–3.

100. Lieleg O, Baumgärtel RM, Bausch AR. Selective filtering of particles by the extracellular matrix: An electrostatic bandpass. Biophys J. 2009;97(6):1569–77.

101. Kihara T, Ito J, Miyake J. Measurement of biomolecular diffusion in extracellular matrix condensed by fibroblasts using fluorescence correlation spectroscopy. PLoS One. 2013;8(11).

102. Mouw JK, Ou G, Weaver VM, Regeneration T, Francisco S, Francisco S, et al. Extracellular matrix assembly: a multiscale deconstruction. 2015;15(12):771–85.

103. Gustafson HH, Holt-Casper D, Grainger DW, Ghandehari H, Grainger D. Nanoparticle Uptake: The Phagocyte Problem. Nano Today. 2015;10(4):487–510.

104. Longmire M, Choyke PL, Kobayashi H. Clearance properties of nano-sized particles and molecules as imagin agents: consideration and caveats. Nanomedicine (Lond). 2008;3(5):703–17.

105. Zhang B, Hu Y, Pang Z. Modulating the tumor microenvironment to enhance tumor nanomedicine delivery. Front Pharmacol. 2017 Dec 22;8(DEC):952.

106. Jain RK. Normalizing tumor microenvironment to treat cancer: Bench to bedside to biomarkers. J Clin Oncol. 2013;31(17):2205–18.

107. Liu LJ, Schlesinger M. Interstitial hydraulic conductivity and interstitial fluid pressure for avascular or poorly vascularized tumors. J Theor Biol [Internet]. 2015;380:1–8. Available from: http://dx.doi.org/10.1016/j.jtbi.2015.05.012

108. Alberts B, Johnson A, Lewis J. The Extracellular Matrix of Animals. Mol Biol Cell. 2002;i:1–25.

109. Xiwei Zheng, Cong Bi, Marissa Brooks and DSH. Proteoglycan form and function: A comprehensive nomenclature of proteoglycans. Anal Chem. 2015;25(4):368–79.

110. Mason A. Neoproteoglycans in tissue engineering. 2009;19(10):389–99.

111. Rakesh K. Jain and Triantafyllos Stylianopoulos. Delivering nanomedicine to solid tumors. Nat Rev Clin Oncol. 2010;653–664.

112. Stylianopoulos T, Poh MZ, Insin N, Bawendi MG, Fukumura D, Munn LL, et al. Diffusion of particles in the extracellular matrix: The effect of repulsive electrostatic interactions. Biophys J [Internet]. 2010;99(5):1342–9. Available from: http://dx.doi.org/10.1016/j.bpj.2010.06.016

113. Xiwei Zheng, Cong Bi, Marissa Brooks and DSH. Delivery of cancer therapeutics to extracellular and intracellular targets: Determinants, barriers, challenges and opportunities. Anal Chem. 2015;25(4):368–79.

114. Manuscript A, Structures T. Biocompatible and bioactive surface modifications for prolonged in vivo efficacy. 2009;6(3):247–53.

115. Deshpande PP, Biswas S, Torchilin VP. Current trends in the use of liposomes for tumor targeting. Nanomedicine (Lond). 2013;8(9):1–32.

116. Mo S, Carlisle R, Laga R, Myers R, Graham S, Cawood R, et al. Increasing the density of nanomedicines improves their ultrasound-mediated delivery to tumours. J Control Release [Internet]. 2015;210:10–8. Available from: http://dx.doi.org/10.1016/j.jconrel.2015.05.265

117. Lea-Banks H, Teo B, Stride E, Coussios CC. The effect of particle density on ultrasound-mediated transport of nanoparticles. Phys Med Biol. 2016;61(22):7906–18.

118. Baxter LT, Jain RK. Transport of fluid and macromolecules in tumors. I. Role of interstitial pressure

and convection. Microvasc Res. 1989;37(1):77–104.

119. Liu LJ, Brown SL, Ewing JR, Schlesinger M. Phenomenological model of interstitial fluid pressure in a solid tumor. Phys Rev E - Stat Nonlinear, Soft Matter Phys. 2011;84(2):1–9.

120. Heldin CH, Rubin K, Pietras K, Östman A. High interstitial fluid pressure - An obstacle in cancer therapy. Nat Rev Cancer. 2004;4(10):806–13.

121. Hashizume H, Baluk P, Morikawa S, McLean JW, Thurston G, Roberge S, et al. Openings between defective endothelial cells explain tumor vessel leakiness. Am J Pathol. 2000;156(4):1363–80.

122. Bergers G. The role of pericytes in blood-vessel formation and maintenance. Neuro Oncol. 2005;7(4):452–64.

123. Stylianopoulos T, Jain RK. Combining two strategies to improve perfusion and drug delivery in solid tumors. Proc Natl Acad Sci. 2013;110(46):18632–7.

124. Wiig H, Tveit E, Hultborn R, Reed RK, Weiss L. Interstitial fluid pressure in DMBA-induced rat mammary tumours. Scand J Clin Lab Invest. 1982;42(November):159–64.

125. Mason A. Prospective of Colon Cancer Treatments and Scope for Combinatorial Approach to Enhanced Cancer Cell Apoptosis. 2009;19(3):389–99.

126. Sartorelli AC. Antineoplastic and Immunosuppressive Agents, Part 1. 2013. 175 p.

127. Forster JC, Harriss-Phillips WM, Douglass MJ, Bezak E. A review of the development of tumor vasculature and its effects on the tumor microenvironment. Hypoxia (Auckland, NZ). 2017;5:21–32.

128. Kato Y, Ozawa S, Miyamoto C, Maehata Y, Suzuki A, Maeda T, et al. Acidic extracellular microenvironment and cancer. Cancer Cell Int. 2013;13(1):1–8.

129. Brizel DM, Schroeder T, Scher RL, Walenta S, Clough RW, Dewhirst MW, et al. Elevated tumor lactate concentrations predict for an increased risk of metastases in head-and-neck cancer. Int J Radiat Oncol Biol Phys. 2001;51(2):349–53.

130. McFate T, Mohyeldin A, Lu H, Thakar J, Henriques J, Halim ND, et al. Pyruvate dehydrogenase complex activity controls metabolic and malignant phenotype in cancer cells complex activity controls metabolic and malignant phenotype in cancer cells. J Biol Chem. 2008;283(33):22700–8.

131. Fischer K, Hoffmann P, Voelkl S, Meidenbauer N, Ammer J, Edinger M, et al. Inhibitory effect of tumor cell-derived lactic acid on human T cells. Blood. 2007;109(9):3812–9.

132. Sattler UGA, Meyer SS, Quennet V, Hoerner C, Knoerzer H, Fabian C, et al. Glycolytic metabolism and tumour response to fractionated irradiation. Radiother Oncol. 2010;94(1):102–9.

133. Liu J, Huang Y, Kumar A, Tan A, Jin S, Mozhi A, et al. PH-Sensitive nano-systems for drug delivery in cancer therapy. Biotechnol Adv. 2014;32(4):693–710.

134. Torchilin LZ and VP. Stimulus-responsive nanopreparations for tumor targeting. NIH Public Access Author Manuscr. 2014;5(1):1–20.

135. Gehl J. Electroporation: Theory and methods, perspectives for drug delivery, gene therapy and research. Acta Physiologica Scandinavica. 2003.

136. Heller LC, Ugen K, Heller R. Electroporation for targeted gene transfer. Expert Opin Drug Deliv. 2005;

137. Stewart MP, Langer R, Jensen KF. Intracellular Delivery by Membrane Disruption: Mechanisms,Strategies, and Concepts. Chem Rev [Internet]. 2018 Aug 22 [cited 2021 Dec 16];118(16):7409. Available from: /pmc/articles/PMC6763210/

138. Sokołowska E, Błachnio-Zabielska AU. A Critical Review of Electroporation as A Plasmid Delivery System in Mouse Skeletal Muscle. Int J Mol Sci [Internet]. 2019 Jun 1 [cited 2021 Dec 16];20(11). Available from: /pmc/articles/PMC6600476/

139. Ajiki T, Murakami T, Kobayashi Y, Hakamata Y, Wang J, Inoue S, et al. Long-lasting gene expression by particle-mediated intramuscular transfection modified with bupivacaine: Combinatorial gene therapy with IL-12 and IL-18 cDNA against rat sarcoma at a distant site. Cancer Gene Ther. 2003;

140. O'Brien JA, Lummis SCR. Nano-biolistics: a method of biolistic transfection of cells and tissues using a gene gun with novel nanometer-sized projectiles. BMC Biotechnol [Internet]. 2011 Jun 10 [cited 2021 Dec 16];11:66. Available from: /pmc/articles/PMC3144454/

141. Villemejane J, Mir LM. Physical methods of nucleic acid transfer: general concepts and applications. Br J Pharmacol [Internet]. 2009 May [cited 2021 Dec 16];157(2):207. Available from: /pmc/articles/PMC2697808/

142. Koike H, Tomita N, Azuma H, Taniyama Y, Yamasaki K, Kunugiza Y, et al. An efficient gene transfer method mediated by ultrasound and microbubbles into the kidney. Wiley Online Libr [Internet]. 2005 Jan [cited 2021 Dec 16];7(1):108–16. Available from: https://onlinelibrary.wiley.com/doi/abs/10.1002/jgm.632?casa_token=pPgo4WIN2dkAAAAA:nvRYDZKG2XrzEl8ET_whsfi26gItSgb4eU-W66C08uucBJfdGsiRuHFYnbZoasFCJxRemt5IO6bP117EVQ

143. Lawrie A, Brisken A, Francis S, therapy DC-G, 2000 undefined. Microbubble-enhanced ultrasound for vascular gene delivery. nature.com [Internet]. [cited 2021 Dec 16]; Available from: https://www.nature.com/articles/3301339

144. Taniyama Y, Tachibana K, Hiraoka K, therapy MA-G, 2002 undefined. Development of safe and efficient novel nonviral gene transfer using ultrasound: enhancement of transfection efficiency of naked plasmid DNA in skeletal. nature.com [Internet]. [cited 2021 Dec 16]; Available from: https://www.nature.com/articles/3301678

145. Lu Q, Liang H, Partridge T, therapy MB-G, 2003 undefined. Microbubble ultrasound improves the efficiency of gene transduction in skeletal muscle in vivo with reduced tissue damage. nature.com [Internet]. [cited 2021 Dec 16]; Available from: https://www.nature.com/articles/3301913

146. Manome Y, Nakamura M, Ohno T, Furuhata H. Ultrasound facilitates transduction of naked plasmid DNA into colon carcinoma cells in vitro and in vivo. Hum Gene Ther. 2000 Jul 20;11(11):1521–8.

147. Mitragotri S. Healing sound: the use of ultrasound in drug delivery and other therapeutic applications. Nat Rev Drug Discov 2005 43 [Internet]. 2005 Mar [cited 2021 Dec 16];4(3):255–60. Available from: https://www.nature.com/articles/nrd1662

148. Helfield B, Chen X, Watkins SC, Villanueva FS. Biophysical insight into mechanisms of sonoporation. Proc Natl Acad Sci U S A. 2016;113(36):9983–8.

149. Nejad SM, Hosseini H, Akiyama H, Tachibana K. Reparable cell sonoporation in suspension: Theranostic potential of microbubble. Theranostics. 2016;6(4):446–55.

150. Bonamassa B, Hai L, Liu D. Hydrodynamic Gene Delivery and Its Applications in Pharmaceutical Research. Pharm Res [Internet]. 2011 Apr [cited 2021 Dec 17];28(4):694. Available from: /pmc/articles/PMC3064722/

151. Suda T, Liu D. Hydrodynamic Gene Delivery: Its Principles and Applications. Mol Ther. 2007 Dec 1;15(12):2063–9.

152. Hur J, Chung AJ. Microfluidic and Nanofluidic Intracellular Delivery. Adv Sci [Internet]. 2021 Aug 1 [cited 2021 Dec 17];8(15). Available from: /pmc/articles/PMC8336510/

153. Statistics on Obesity, Physical Activity and Diet, England, 2020 - NHS Digital [Internet]. [cited 2021 Dec 17]. Available from: https://digital.nhs.uk/data-and-information/publications/statistical/statistics-on-obesity-physical-activity-and-diet/england-2020

154. Klibanov AL, Hossack JA. Ultrasound in Radiology: from Anatomic, Functional, Molecular Imaging to Drug Delivery and Image-Guided Therapy. Invest Radiol [Internet]. 2015 Sep 20 [cited 2021 Dec 17];50(9):657. Available from: /pmc/articles/PMC4580624/

155. Izadifar Z, Izadifar Z, Chapman D, Babyn P. An Introduction to High Intensity Focused Ultrasound: Systematic Review on Principles, Devices, and Clinical Applications. J Clin Med [Internet]. 2020 Feb 1 [cited 2021 Dec 17];9(2). Available from: /pmc/articles/PMC7073974/

156. Purves D, Augustine GJ, Fitzpatrick D, Katz LC, LaMantia A-S, McNamara JO, et al. The Audible Spectrum. 2001 [cited 2021 Dec 17]; Available from: https://www.ncbi.nlm.nih.gov/books/NBK10924/

157. Hasegawa K, Namekawa K, Takayanagi S, Akiyama I. Preliminary Investigation of Magnetic Resonance Imaging Guided Beamforming in Flexible Type Ultrasonic Array Transducers. Front Phys. 2021 Mar 18;9:115.

158. Laugier P, Haïat G. Introduction to the Physics of Ultrasound. Bone Quant Ultrasound [Internet]. 2011 [cited 2021 Dec 17];29–45. Available from: https://link.springer.com/chapter/10.1007/978-94-007-0017-8_2

159. Sigrist RMS, Liau J, Kaffas A El, Chammas MC, Willmann JK. Ultrasound elastography: Review of techniques and clinical applications. Theranostics. 2017;7(5):1303–29.

160. Aldrich JE. Basic physics of ultrasound imaging. Crit Care Med [Internet]. 2007 May [cited 2021 Dec 17];35(5 SUPPL.). Available from: https://journals.lww.com/ccmjournal/Fulltext/2007/05001/Basic_physics_of_ultrasound_imaging.3.aspx

161. Martin DJ, Wells ITP, Goodwin CR. Physics of ultrasound. Anaesth Intensive Care Med. 2015 Mar 1;16(3):132–5.

162. Humphrey VF. Ultrasound and matter—Physical interactions. Prog Biophys Mol Biol. 2007 Jan 1;93(1–3):195–211.

163. Coussios CC, Farny CH, ter Haar G, Roy RA. Role of acoustic cavitation in the delivery and monitoring of cancer treatment by high-intensity focused ultrasound (HIFU). https://doi.org/101080/02656730701194131 [Internet]. 2009 [cited 2021 Dec 17];23(2):105–20. Available from: https://www.tandfonline.com/doi/abs/10.1080/02656730701194131

164. Borkent BM, Gekle S, Prosperetti A, Lohse D. Nucleation threshold and deactivation mechanisms of nanoscopic cavitation nuclei. Phys Fluids [Internet]. 2009 Oct 19 [cited 2021 Dec 17];21(10):102003. Available from: https://aip.scitation.org/doi/abs/10.1063/1.3249602

165. Barney CW, Dougan CE, McLeod KR, Kazemi-Moridani A, Zheng Y, Ye Z, et al. Cavitation in soft matter. Proc Natl Acad Sci [Internet]. 2020 Apr 28 [cited 2021 Dec 17];117(17):9157–65. Available from: https://www.pnas.org/content/117/17/9157

166. Bader KB, Vlaisavljevich E, Maxwell AD. For Whom the Bubble Grows: Physical Principles of Bubble Nucleation and Dynamics in Histotripsy Ultrasound Therapy. Ultrasound Med Biol [Internet]. 2019 May 1 [cited 2021 Dec 17];45(5):1056–80. Available from: https://pubmed.ncbi.nlm.nih.gov/30922619/

167. Alavi Tamaddoni H, Duryea AP, Vlaisavljevich E, Xu Z, Hall TL. Acoustic Methods for Increasing the Cavitation Initiation Pressure Threshold. IEEE Trans Ultrason Ferroelectr Freq Control [Internet]. 2018 Nov 1 [cited 2021 Dec 17];65(11):2012. Available from: /pmc/articles/PMC6486826/

168. Qin D, Zou Q, Lei S, Wang W, Li Z. Cavitation Dynamics and Inertial Cavitation Threshold of Lipid Coated Microbubbles in Viscoelastic Media with Bubble–Bubble Interactions. Micromachines 2021, Vol 12, Page 1125 [Internet]. 2021 Sep 18 [cited 2021 Dec 17];12(9):1125. Available from: https://www.mdpi.com/2072-666X/12/9/1125/htm

169. Wu J, Nyborg WL. Ultrasound, cavitation bubbles and their interaction with cells. Advanced Drug Delivery Reviews. 2008.

170. Rooney JA. Hemolysis near an ultrasonically pulsating gas bubble. Science (80-). 1970;

171. Lin Y, Lin L, Cheng M, Jin L, Du L, Han T, et al. Effect of acoustic parameters on the cavitation behavior of SonoVue microbubbles induced by pulsed ultrasound. Ultrason Sonochem [Internet]. 2017;35:176–84. Available from: http://dx.doi.org/10.1016/j.ultsonch.2016.09.016

172. Takahashi M, Chiba K, Li P. Free-Radical Generation from Collapsing Microbubbles in the Absence of a Dynamic Stimulus. J Phys Chem B [Internet]. 2007 Feb 15 [cited 2021 Dec 17];111(6):1343–7. Available from: https://pubs.acs.org/doi/abs/10.1021/jp0669254

173. O'Brien WD. Ultrasound-biophysics mechanisms. Prog Biophys Mol Biol. 2007 Jan;93(1–3):212–55.

174. Carvell KJ, Bigelow TA. Dependence of cavitation bubble size on pressure amplitude at therapeutic levels. AIP Conf Proc. 2009;1113:63–7.

175. Burgess MT, Porter TM. Control of Acoustic Cavitation for Efficient Sonoporation with Phase-Shift

Nanoemulsions. Ultrasound Med Biol. 2019;45(3):846–58.

176. Liu WW, Liu SW, Liou YR, Wu YH, Yang YC, Wang CRC, et al. Nanodroplet-Vaporization-Assisted Sonoporation for Highly Effective Delivery of Photothermal Treatment. Sci Reports 2016 61 [Internet]. 2016 Apr 20 [cited 2021 Dec 17];6(1):1–14. Available from: https://www.nature.com/articles/srep24753

177. Borden MA, Dayton PA, Slagle C, Walmer RW. Ultrasound Contrast Agents. Mol Imaging [Internet]. 2021 Jan 1 [cited 2021 Dec 17];639–53. Available from: https://linkinghub.elsevier.com/retrieve/pii/B9780128163863000387

178. Zhao N, Woodle MC, Mixson AJ. Advances in delivery systems for doxorubicin. J Nanomed Nanotechnol [Internet]. 2018 [cited 2021 Dec 17];9(5). Available from: /pmc/articles/PMC6319900/

179. Kamaly N, Yameen B, Wu J, Farokhzad OC. Degradable Controlled-Release Polymers and Polymeric Nanoparticles: Mechanisms of Controlling Drug Release. Chem Rev [Internet]. 2016 Feb 24 [cited 2021 Dec 17];116(4):2602. Available from: /pmc/articles/PMC5509216/

180. Wang K, Tang Z, Yang CJ, Kim Y, Fang X, Li W, et al. Molecular Engineering of DNA: Molecular Beacons. Angew Chem Int Ed Engl [Internet]. 2009 Jan 19 [cited 2021 Dec 17];48(5):856. Available from: /pmc/articles/PMC2772660/

181. Lee S, Jeon H, Shim S, Im M, Kim J, Kim JH, et al. Preclinical study to improve microbubble-mediated drug delivery in cancer using an ultrasonic probe with an interchangeable acoustic lens. Sci Rep [Internet]. 2021 Dec 1 [cited 2021 Dec 17];11(1):12654. Available from: /pmc/articles/PMC8209130/

182. Nakamura Y, Mochida A, Choyke PL, Kobayashi H. Nano-drug delivery: Is the enhanced permeability and retention (EPR) effect sufficient for curing cancer? Bioconjug Chem [Internet]. 2016 Oct 19 [cited 2021 Dec 17];27(10):2225. Available from: /pmc/articles/PMC7397928/

183. Chen H, Hwang JH. Ultrasound-targeted microbubble destruction for chemotherapeutic drug delivery to solid tumors. J Ther Ultrasound [Internet]. 2013 Jul 1 [cited 2021 Dec 17];1(1):10. Available from: /pmc/articles/PMC4265893/

184. Wischhusen J, Padilla F. Ultrasound-Targeted Microbubble Destruction (UTMD) for Localized Drug Delivery into Tumor Tissue. IRBM. 2019 Feb 1;40(1):10–5.

185. Important Safety Information on SonoVue® (8 microlitres/ml powder and solvent for dispersion for injection) Use in Critically ill Patients | Bracco Imaging [Internet]. [cited 2021 Dec 17]. Available from: https://imaging.bracco.com/se-sv/produkter-och-l-sningar/kontrastf-rst-rkt-ultraljud/sonovue/important-safety-information-sonovue-8

186. Kwan JJ, Myers R, Coviello CM, Graham SM, Shah AR, Stride E, et al. Ultrasound-Propelled Nanocups for Drug Delivery. Small. 2015;11(39):5305–14.

187. Kwan JJ, Graham S, Myers R, Carlisle R, Stride E, Coussios CC. Ultrasound-induced inertial cavitation from gas-stabilizing nanoparticles. Phys Rev E - Stat Nonlinear, Soft Matter Phys [Internet]. 2015 Aug 19 [cited 2021 Dec 17];92(2):023019. Available from: https://journals.aps.org/pre/abstract/10.1103/PhysRevE.92.023019

188. Evaluating the circulation time of different formulations of microbubbles, continuation | Mattilsynet [Internet]. [cited 2021 Dec 17]. Available from: https://www.mattilsynet.no/dyr_og_dyrehold/dyrevelferd/forsoksdyr/forsoksdyrsoknader/evaluating_the_circulation_time_of_different_formulations_of_microbubbles_continuation.24529

189. Bazan-Peregrino M, Rifai B, Carlisle RC, Choi J, Arvanitis CD, Seymour LW, et al. Cavitation-enhanced delivery of a replicating oncolytic adenovirus to tumors using focused ultrasound. J Control Release. 2013;169(1–2):40–7.

190. Hwang JH, Tu J, Brayman AA, Matula TJ, Crum LA. Correlation between inertial cavitation dose and endothelial cell damage in vivo. Ultrasound Med Biol [Internet]. 2006 Oct [cited 2022 Jan 16];32(10):1611–9. Available from: https://pubmed.ncbi.nlm.nih.gov/17045882/

191. Paris JL, Mannaris C, Cabañas MV, Carlisle R, Manzano M, Vallet-Regí M, et al. Ultrasound-mediated cavitation-enhanced extravasation of mesoporous silica nanoparticles for controlled-release drug delivery. Chem Eng J [Internet]. 2018;340(December 2017):2–8. Available from:

https://doi.org/10.1016/j.cej.2017.12.051

192. Lee S, Han H, Koo H, Na JH, Yoon HY, Lee KE, et al. Extracellular matrix remodeling in vivo for enhancing tumor-targeting efficiency of nanoparticle drug carriers using the pulsed high intensity focused ultrasound. J Control Release [Internet]. 2017;263:68–78. Available from: http://dx.doi.org/10.1016/j.jconrel.2017.02.035

193. McEwan C, Owen J, Stride E, Fowley C, Nesbitt H, Cochrane D, et al. Oxygen carrying microbubbles for enhanced sonodynamic therapy of hypoxic tumours. J Control Release [Internet]. 2015;203:51–6. Available from: http://dx.doi.org/10.1016/j.jconrel.2015.02.004

194. Li T, Liu G, Li J, Wang X, Liu Q, Liu Z, et al. Mechanisms of Prostate Permeability Triggered by Microbubble-Mediated Acoustic Cavitation. Cell Biochem Biophys. 2012;64(2):147–53.

195. Lentacker I, De Cock I, Deckers R, De Smedt SC, Moonen CTW. Understanding ultrasound induced sonoporation: Definitions and underlying mechanisms. Adv Drug Deliv Rev. 2014 Jun 15;72:49–64.

196. Valiunas V, Wang HZ, Li L, Gordon C, Valiuniene L, Cohen IS, et al. A comparison of two cellular delivery mechanisms for small interfering RNA. Physiol Rep [Internet]. 2015 Feb 1 [cited 2022 Jan 11];3(2):e12286. Available from: https://onlinelibrary.wiley.com/doi/full/10.14814/phy2.12286

197. Ashokkumar M. The characterization of acoustic cavitation bubbles – An overview. Ultrason Sonochem. 2011 Jul 1;18(4):864–72.

198. Gullino PM. Diffusion and Convection in Normal and Neoplastic Tissues. Cancer Res. 1974;34(10):2814–22.

199. Islam N, Miklavcic SJ, Bradshaw-Hajek BH, White LR. Convective and diffusive effects on particle transport in asymmetric periodic capillaries. PLoS One [Internet]. 2017 Aug 1 [cited 2021 Dec 17];12(8). Available from: /pmc/articles/PMC5571904/

200. Manasseh R. Acoustic Bubbles, Acoustic Streaming, and Cavitation Microstreaming. Handb Ultrason Sonochemistry [Internet]. 2016 Jan 1 [cited 2021 Dec 17];33–68. Available from: https://link.springer.com/referenceworkentry/10.1007/978-981-287-278-4_5

201. Pitt WG, Husseini GA, Staples BJ. Ultrasonic drug delivery--a general review. Expert Opin Drug Deliv. 2004;1(1):37–56.

202. Krasovitski B, Kimmel E. Shear stress induced by a gas bubble pulsating in an ultrasonic field near a wall. IEEE Trans Ultrason Ferroelectr Freq Control. 2004 Aug;51(8):973–9.

203. Bader KB, Vlaisavljevich E, Maxwell AD. For whom the bubble grows: Physical principles of bubble nucleation and dynamics in histotripsy ultrasound therapy. Ultrasound Med Biol [Internet]. 2019 May 1 [cited 2021 Dec 17];45(5):1056. Available from: /pmc/articles/PMC6524960/

204. Woodbury DJ, Richardson ES, Grigg AW, Welling RD, Knudson BH. Reducing liposome size with ultrasound: bimodal size distributions. J Liposome Res [Internet]. 2006 Feb [cited 2021 Dec 17];16(1):57–80. Available from: https://pubmed.ncbi.nlm.nih.gov/16556550/

205. Sundaram J, Mellein BR, Mitragotri S. An experimental and theoretical analysis of ultrasound-induced permeabilization of cell membranes. Biophys J. 2003;

206. Guzmán HR, McNamara AJ, Nguyen DX, Prausnitz MR. Bioeffects caused by changes in acoustic cavitation bubble density and cell concentration: A unified explanation based on cell-to-bubble ratio and blast radius. Ultrasound Med Biol. 2003;

207. Fan Z, Kumon RE, Deng CX. Mechanisms of microbubble-facilitated sonoporation for drug and gene delivery. Ther Deliv [Internet]. 2014 [cited 2021 Dec 17];5(4):467. Available from: /pmc/articles/PMC4116608/

208. Fulda S, Gorman AM, Hori O, Samali A. Cellular stress responses: Cell survival and cell death. Int J Cell Biol. 2010;

209. Dammes N, Peer D. Monoclonal antibody-based molecular imaging strategies and theranostic opportunities. Theranostics [Internet]. 2020 [cited 2021 Dec 17];10(2):938. Available from: /pmc/articles/PMC6929980/

210. van der Meel R, Sulheim E, Shi Y, Kiessling F, Mulder WJM, Lammers T. Smart cancer nanomedicine. Nat Nanotechnol 2019 1411 [Internet]. 2019 Nov 6 [cited 2021 Dec 17];14(11):1007–17. Available from: https://www.nature.com/articles/s41565-019-0567-y

211. Miller DL. Overview of experimental studies of biological effects of medical ultrasound caused by gas body activation and inertial cavitation. Prog Biophys Mol Biol. 2007;93(1–3):314–30.

212. Miller DL, Smith NB, Bailey MR, Czarnota GJ, Hynynen K, Makin IRS. Overview of Therapeutic Ultrasound Applications and Safety Considerations. J Ultrasound Med [Internet]. 2012 Apr 1 [cited 2021 Dec 17];31(4):623. Available from: /pmc/articles/PMC3810427/

213. Haen SP, Pereira PL, Salih HR, Rammensee HG, Gouttefangeas C. More Than Just Tumor Destruction: Immunomodulation by Thermal Ablation of Cancer. Clin Dev Immunol [Internet]. 2011 [cited 2021 Dec 17];2011. Available from: /pmc/articles/PMC3254009/

214. Mechanisms of Action - Focused Ultrasound Foundation [Internet]. [cited 2021 Dec 17]. Available from: https://www.fusfoundation.org/the-technology/mechanisms-of-action

215. Kennedy JE. High-intensity focused ultrasound in the treatment of solid tumours. Nat Rev Cancer [Internet]. 2005 Apr [cited 2022 Jun 9];5(4):321–7. Available from: https://pubmed.ncbi.nlm.nih.gov/15776004/

216. Crake C, Owen J, Smart S, Coviello C, Coussios CC, Carlisle R, et al. Enhancement and Passive Acoustic Mapping of Cavitation from Fluorescently Tagged Magnetic Resonance-Visible Magnetic Microbubbles In Vivo. Ultrasound Med Biol. 2016 Dec 1;42(12):3022–36.

217. Wang Y, Miao L, Satterlee A, Huang L. Delivery of oligonucleotides with lipid nanoparticles. Adv Drug Deliv Rev [Internet]. 2015;87:68–80. Available from: http://dx.doi.org/10.1016/j.addr.2015.02.007

218. Nimesh S, Halappanavar S, Kaushik NK, Kumar P. Advances in gene delivery systems. Biomed Res Int. 2015;2015(i):2–4.

219. Van Lint S, Heirman C, Thielemans K, Breckpot K. From a chemical blueprint for protein production to an off-the-shelf therapeutic. Hum Vaccines Immunother. 2013;9(2):265–74.

220. Su X, Fricke J, Kavanagh DG, Irvine DJ. In vitro and in vivo mRNA delivery using lipid-enveloped pH-responsive polymer nanoparticles. Mol Pharm. 2011;8(3):774–87.

221. Oberli MA, Reichmuth AM, Dorkin JR, Mitchell MJ, Fenton OS, Jaklenec A, et al. Lipid Nanoparticle Assisted mRNA Delivery for Potent Cancer Immunotherapy. Nano Lett. 2017;17(3):1326–35.

222. Lutz J, Lazzaro S, Habbeddine M, Schmidt KE, Baumhof P, Mui BL, et al. Unmodified mRNA in LNPs constitutes a competitive technology for prophylactic vaccines. npj Vaccines [Internet]. 2017;2(1):1–9. Available from: http://dx.doi.org/10.1038/s41541-017-0032-6

223. Stewart M. Nuclear export of mRNA. Trends in Biochemical Sciences. 2010.

224. Bahl K, Senn JJ, Yuzhakov O, Bulychev A, Brito LA, Hassett KJ, et al. Preclinical and Clinical Demonstration of Immunogenicity by mRNA Vaccines against H10N8 and H7N9 Influenza Viruses. Mol Ther. 2017;

225. Lee CS, Bishop ES, Zhang R, Yu X, Farina EM, Yan S, et al. Adenovirus-mediated gene delivery: Potential applications for gene and cell-based therapies in the new era of personalized medicine. Genes and Diseases. 2017.

226. Allen TM, Cullis PR. Liposomal drug delivery systems: From concept to clinical applications. Advanced Drug Delivery Reviews. 2013.

227. Lieleg O, Vladescu I, Ribbeck K. Characterization of particle translocation through mucin hydrogels. Biophys J [Internet]. 2010;98(9):1782–9. Available from: http://dx.doi.org/10.1016/j.bpj.2010.01.012

228. Swartz MA, Fleury ME. Interstitial Flow and Its Effects in Soft Tissues. Annu Rev Biomed Eng. 2007;9(1):229–56.

229. Hoy SM. Patisiran: First Global Approval. Drugs [Internet]. 2018 Oct 1 [cited 2021 Dec

17];78(15):1625–31. Available from: https://pubmed.ncbi.nlm.nih.gov/30251172/

230. Chen B, Dai W, He B, Zhang H, Wang X, Wang Y, et al. Current multistage drug delivery systems based on the tumor microenvironment. Vol. 7, Theranostics. Ivyspring International Publisher; 2017. p. 538–58.

231. Maeda H, Tsukigawa K, Fang J. A Retrospective 30 Years After Discovery of the Enhanced Permeability and Retention Effect of Solid Tumors: Next-Generation Chemotherapeutics and Photodynamic Therapy—Problems, Solutions, and Prospects. Microcirculation. 2016;23(3):173–82.

232. Steeg PS. Targeting metastasis. Nature Reviews Cancer. 2016.

233. Li R, He Y, Zhang S, Qin J, Wang J. Cell membrane-based nanoparticles: a new biomimetic platform for tumor diagnosis and treatment. Acta Pharm Sin B [Internet]. 2018;8(1):14–22. Available from: http://dx.doi.org/10.1016/j.apsb.2017.11.009

234. Gong J, Chehrazi-Raffle A, Reddi S, Salgia R. Development of PD-1 and PD-L1 inhibitors as a form of cancer immunotherapy: A comprehensive review of registration trials and future considerations. Vol. 6, Journal for ImmunoTherapy of Cancer. BioMed Central Ltd.; 2018.

235. Graham SM, Carlisle R, Choi JJ, Stevenson M, Shah AR, Myers RS, et al. Inertial cavitation to non-invasively trigger and monitor intratumoral release of drug from intravenously delivered liposomes. J Control Release. 2014;

236. Clinical Trials [Internet]. 2020 [cited 2020 Apr 1]. Available from: https://clinicaltrials.gov

237. Kose N, Fox JM, Sapparapu G, Bombardi R, Tennekoon RN, Dharshan De Silva A, et al. A lipid-encapsulated mRNA encoding a potently neutralizing human monoclonal antibody protects against chikungunya infection. Sci Immunol. 2019;

238. Midoux P, Pichon C. Lipid-based mRNA vaccine delivery systems. Expert Rev Vaccines. 2014;14(2):221–34.

239. Shim MS, Kwon YJ. Efficient and targeted delivery of siRNA in vivo. FEBS Journal. 2010.

240. Nwokeoha S. Lithotripter Shock Wave induced RNA-based Gene Therapy. 2017;

241. Lyon PC, Griffiths LF, Lee J, Chung D, Carlisle R, Wu F, et al. Clinical trial protocol for TARDOX: A phase I study to investigate the feasibility of targeted release of lyso-thermosensitive liposomal doxorubicin (ThermoDox®) using focused ultrasound in patients with liver tumours. J Ther Ultrasound [Internet]. 2017 Nov 2 [cited 2021 Dec 17];5(1):1–8. Available from: https://jtultrasound.biomedcentral.com/articles/10.1186/s40349-017-0104-0

242. Grundy M, Bau L, Hill C, Paverd C, Mannaris C, Kwan J, et al. Improved therapeutic antibody delivery to xenograft tumors using cavitation nucleated by gas-entrapping nanoparticles. Nanomedicine. 2021 Jan 1;16(1):37–50.

243. Hill C, Carlisle R. Achieving systemic delivery of oncolytic viruses. https://doi.org/101080/1742524720191617269 [Internet]. 2019 Jun 3 [cited 2021 Dec 17];16(6):607–20. Available from: https://www.tandfonline.com/doi/abs/10.1080/17425247.2019.1617269

244. Smith C, Mannaris C, Katti P, Paverd C, Coviello C, Carlisle R, et al. Applications, mechanisms and real-time monitoring of enhanced drug transport by sustained inertial cavitation. J Acoust Soc Am. 2019 Oct;146(4):2991–2991.

245. Grundy M, Bau L, Hill C, Paverd C, Mannaris C, Kwan J, et al. Improved therapeutic antibody delivery to xenograft tumors using cavitation nucleated by gas-entrapping nanoparticles. Nanomedicine [Internet]. 2021 Jan 1 [cited 2021 Dec 17];16(1):37–50. Available from: https://www.futuremedicine.com/doi/abs/10.2217/nnm-2020-0263

246. Dewhirst MW, Secomb TW. Transport of drugs from blood vessels to tumour tissue. Nat Rev Cancer [Internet]. 2017;17(12):738–50. Available from: http://dx.doi.org/10.1038/nrc.2017.93

247. Harkness JE, Wagner JE. The biology and medicine of rabbits and rodents. 1989 [cited 2022 Jan 16];230. Available from: https://books.google.com/books/about/The_Biology_and_Medicine_of_Rabbits_and.html?id=ky1tAAA

248. Reichmuth AM, Oberli MA, Jeklenec A, Langer R, Blankschtein D. mRNA vaccine delivery using lipid nanoparticles. Ther Deliv. 2016;

249. Zhang J, Shrivastava S, Cleveland RO, Rabbitts TH. Lipid-mRNA Nanoparticle Designed to Enhance Intracellular Delivery Mediated by Shock Waves. ACS Appl Mater Interfaces. 2019;11(11):10481–91.

250. Liu Y, Beyer A, Aebersold R. On the Dependency of Cellular Protein Levels on mRNA Abundance. Cell. 2016.

251. Wu SK, Chu PC, Chai WY, Kang ST, Tsai CH, Fan CH, et al. Characterization of different microbubbles in assisting focused ultrasound-induced blood-brain barrier opening. Sci Rep. 2017;7.

252. Myers R, Grundy M, Rowe C, Coviello CM, Bau L, Erbs P, et al. Ultrasound-mediated cavitation does not decrease the activity of small molecule, antibody or viral-based medicines. Int J Nanomedicine. 2018;

253. Wu X, Giridhar Babu A, Kim BL, Kim JO, Shin JH, Kim DP. Ultrasound-mediated intracellular delivery of fluorescent dyes and DNA into microalgal cells. Algal Res [Internet]. 2016;15:210–6. Available from: http://dx.doi.org/10.1016/j.algal.2016.02.017

254. Ibsen S, Schutt CE, Esener S. Microbubble-mediated ultrasound therapy: A review of its potential in cancer treatment. Vol. 7, Drug Design, Development and Therapy. Dove Press; 2013. p. 375–88.

255. Fan P, Yang D, Wu J, Yang Y, Guo X, Tu J, et al. Cell-cycle-dependences of membrane permeability and viability observed for HeLa cells undergoing multi-bubble-cell interactions. Ultrason Sonochem [Internet]. 2019;53(January):178–86. Available from: https://doi.org/10.1016/j.ultsonch.2019.01.005

256. Cao J, Hu C, Zhou H, Qiu F, Chen J, Zhang J, et al. Microbubble-Mediated Cavitation Promotes Apoptosis and Suppresses Invasion in AsPC-1 Cells. Ultrasound Med Biol. 2021 Feb 1;47(2):323–33.

257. Itah Z, Oral O, Perk OY, Sesen M, Demir E, Erbil S, et al. Hydrodynamic cavitation kills prostate cells and ablates benign prostatic hyperplasia tissue. Exp Biol Med. 2013 Nov;238(11):1242–50.

258. Smith C. Doppler Passive Acoustic Mapping in Ultrasound Therapy. :1–31.

259. Schlicher RK, Hutcheson JD, Radhakrishna H, Apkarian RP, Prausnitz MR. Changes in Cell Morphology Due to Plasma Membrane Wounding by Acoustic Cavitation. Ultrasound Med Biol. 2010;36(4):677–92.

260. Yin Y, Jiang X, Sun L, Li H, Su C, Zhang Y, et al. Continuous inertial cavitation evokes massive ROS for reinforcing sonodynamic therapy and immunogenic cell death against breast carcinoma. Nano Today. 2021 Feb 1;36:101009.

261. Sharpe M, Mount N. Genetically modified T cells in cancer therapy: opportunities and challenges. Dis Model Mech. 2015 Apr 1;8(4):337–50.

262. Chen SG, Ugwu F, Li WC, Caplice NM, Petcu E, Yip SP, et al. Vascular Tissue Engineering: Advanced Techniques and Gene Editing in Stem Cells for Graft Generation. Tissue Eng Part B Rev [Internet]. 2021 Feb 1 [cited 2022 Jan 11];27(1):14–28. Available from: https://pubmed.ncbi.nlm.nih.gov/32503391/

263. Hong M, Clubb JD, Chen YY. Engineering CAR-T Cells for Next-Generation Cancer Therapy. Cancer Cell. 2020 Oct 12;38(4):473–88.

264. Devetzi M, Goulielmaki M, Khoury N, Spandidos DA, Sotiropoulou G, Christodoulou I, et al. Genetically-modified stem cells in treatment of human diseases: Tissue kallikrein (KLK1)-based targeted therapy (Review). Int J Mol Med [Internet]. 2018 Mar 1 [cited 2022 Jan 11];41(3):1177–86. Available from: http://www.spandidos-publications.com/10.3892/ijmm.2018.3361/abstract

265. Pardi N, Tuyishime S, Muramatsu H, Kariko K, Mui BL, Tam YK, et al. Expression kinetics of nucleoside-modified mRNA delivered in lipid nanoparticles to mice by various routes. J Control Release. 2015;

266. Prel A, Caval V, Gayon R, Ravassard P, Duthoit C, Payen E, et al. Highly efficient in vitro and in vivo

delivery of functional RNAs using new versatile MS2-chimeric retrovirus-like particles. Mol Ther - Methods Clin Dev [Internet]. 2015 Apr 29 [cited 2022 Jan 11];2:15039. Available from: http://www.cell.com/article/S2329050116300511/fulltext

267. Pinel K, Lacoste J, Plane G, Ventura M, Couillaud F. Long-term in vivo imaging of translated RNAs for gene therapy. Gene Ther 2014 214 [Internet]. 2014 Jan 16 [cited 2022 Jan 11];21(4):434–9. Available from: https://www.nature.com/articles/gt201389

268. Gonzalez G, Pfannes L, Brazas R, Striker R. Selection of an optimal RNA transfection reagent and comparison to electroporation for the delivery of viral RNA. J Virol Methods. 2007 Oct 1;145(1):14–21.

269. Lundberg P, El-Andaloussi S, Sütlü T, Johansson H, Langel Ü. Delivery of short interfering RNA using endosomolytic cell-penetrating peptides. FASEB J [Internet]. 2007 Sep 1 [cited 2022 Jan 15];21(11):2664–71. Available from: https://onlinelibrary.wiley.com/doi/full/10.1096/fj.06-6502com

270. Reslan L, Mestas JL, Herveau S, Béra JC, Dumontet C. Transfection of cells in suspension by ultrasound cavitation. J Control Release [Internet]. 2010 [cited 2022 Jan 15];142(2):251–8. Available from: https://pubmed.ncbi.nlm.nih.gov/19896995/

271. Karki A, Giddings E, Carreras A, Champagne D, Fortner K, Rincon M, et al. Sonoporation as an Approach for siRNA delivery into T cells. Ultrasound Med Biol [Internet]. 2019 Dec 1 [cited 2022 Jan 15];45(12):3222–31. Available from: https://pubmed.ncbi.nlm.nih.gov/31540758/

272. Fedorov Y, King A, Anderson E, Karpilow J, Ilsey D, Marshall W, et al. Different delivery methods—different expression profiles. Nat Methods 2005 24 [Internet]. 2005 Apr [cited 2022 Jan 15];2(4):241–241. Available from: https://www.nature.com/articles/nmeth0405-241

273. Sun W, Xing C, Zhao L, Zhao P, Yang G, Yuan L. Ultrasound Assisted Exosomal Delivery of Tissue Responsive mRNA for Enhanced Efficacy and Minimized Off-Target Effects. Mol Ther - Nucleic Acids. 2020 Jun 5;20:558–67.

274. Yoon S, Wang P, Peng Q, Wang Y, Shung KK. Acoustic-transfection for genomic manipulation of single-cells using high frequency ultrasound. Sci Reports 2017 71 [Internet]. 2017 Jul 13 [cited 2022 Jan 15];7(1):1–11. Available from: https://www.nature.com/articles/s41598-017-05722-1

275. Kopechek JA, McTiernan CF, Chen X, Zhu J, Mburu M, Feroze R, et al. Ultrasound and microbubble-targeted delivery of a microRNA inhibitor to the heart suppresses cardiac hypertrophy and preserves cardiac function. Theranostics. 2019;9(23):7088–98.

276. Rychak JJ, Klibanov AL. Nucleic acid delivery with microbubbles and ultrasound. Adv Drug Deliv Rev [Internet]. 2014 Jun 15 [cited 2022 Jan 15];72:82. Available from: /pmc/articles/PMC4204336/

277. Hu Y, Wan JMF, Yu ACH. Membrane Perforation and Recovery Dynamics in Microbubble-Mediated Sonoporation. Ultrasound Med Biol. 2013;39(12):2393–405.

278. Suzuki R, Namai E, Oda Y, Nishiie N, Otake S, Koshima R, et al. Cancer gene therapy by IL-12 gene delivery using liposomal bubbles and tumoral ultrasound exposure. J Control Release. 2010;142(2):245–50.

279. De Cock I, Zagato E, Braeckmans K, Luan Y, de Jong N, De Smedt SC, et al. Ultrasound and microbubble mediated drug delivery: Acoustic pressure as determinant for uptake via membrane pores or endocytosis. J Control Release. 2015 Jan 10;197:20–8.

280. Pan H, Zhou Y, Izadnegahdar O, Cui J, Deng CX. Study of sonoporation dynamics affected by ultrasound duty cycle. Ultrasound Med Biol. 2005 Jun 1;31(6):849–56.

281. Meijering BDM, Juffermans LJM, Van Wamel A, Henning RH, Zuhorn IS, Emmer M, et al. Ultrasound and microbubble-targeted delivery of macromolecules is regulated by induction of endocytosis and pore formation. Circ Res [Internet]. 2009 Mar 13 [cited 2022 Jan 16];104(5):679–87. Available from: https://www.ahajournals.org/doi/abs/10.1161/CIRCRESAHA.108.183806

282. Man VH, Truong PM, Li MS, Wang J, Van-Oanh NT, Derreumaux P, et al. Molecular Mechanism of the Cell Membrane Pore Formation Induced by Bubble Stable Cavitation. J Phys Chem B [Internet]. 2019 Oct 1 [cited 2022 Jan 16];123(1):71–8. Available from: https://pubmed.ncbi.nlm.nih.gov/30540473/

283. Deng CX, Sieling F, Pan H, Cui J. Ultrasound-induced cell membrane porosity. Ultrasound Med Biol [Internet]. 2004 Apr [cited 2022 Jan 16];30(4):519–26. Available from: https://pubmed.ncbi.nlm.nih.gov/15121254/

284. Hu Y, Wan JMF, Yu ACH. Membrane Perforation and Recovery Dynamics in Microbubble-Mediated Sonoporation. Ultrasound Med Biol. 2013 Dec 1;39(12):2393–405.

285. Zeghimi A, Escoffre JM, Bouakaz A. Role of endocytosis in sonoporation-mediated membrane permeabilization and uptake of small molecules: A electron microscopy study. Phys Biol. 2015;12(6).

286. Fan Z, Liu H, Mayer M, Deng CX. Spatiotemporally controlled single cell sonoporation. Proc Natl Acad Sci U S A. 2012;109(41):16486–91.

287. Meairs S, Hennerici M, Mohr JP. Ultrasonography. Stroke. 2011 Jan 1;831–69.

288. Choi JJ, Feshitan JA, Baseri B, Wang S, Tung YS, Borden MA, et al. Microbubble-Size Dependence of Focused Ultrasound-Induced Blood–Brain Barrier Opening in Mice In Vivo. IEEE Trans Biomed Eng [Internet]. 2010 Jan [cited 2022 Jan 16];57(1):145. Available from: /pmc/articles/PMC3968777/

289. Oddo L, Paradossi G, Cerroni B, Ben-Harush C, Ariel E, Di Meco F, et al. In Vivo Biodistribution of Engineered Lipid Microbubbles in Rodents. ACS Omega [Internet]. 2019 Aug 20 [cited 2022 Jan 16];4(8):13371–81. Available from: https://pubs.acs.org/doi/full/10.1021/acsomega.9b01544

290. Khokhlova TD, Haider Y, Hwang JH. Therapeutic potential of ultrasound microbubbles in gastrointestinal oncology: recent advances and future prospects. Therap Adv Gastroenterol [Internet]. 2015 Nov 13 [cited 2022 Jan 16];8(6):384–94. Available from: http://www.ncbi.nlm.nih.gov/pubmed/26557894

291. Xu S, Ye D, Wan L, Shentu Y, Yue Y, Wan M, et al. Correlation Between Brain Tissue Damage and Inertial Cavitation Dose Quantified Using Passive Cavitation Imaging. Ultrasound Med Biol [Internet]. 2019 Oct 1 [cited 2022 Jan 16];45(10):2758–66. Available from: https://pubmed.ncbi.nlm.nih.gov/31378549/

292. Warnez M, Vlaisavljevich E, Xu Z. Damage mechanisms for ultrasound-induced cavitation in tissue ARTICLES YOU MAY BE INTERESTED IN. 2017 [cited 2022 Jan 16];1821:80004. Available from: https://doi.org/10.1063/1.4977634

293. Zhou Y, Shi J, Cui J, Deng CX. Effects of extracellular calcium on cell membrane resealing in sonoporation. J Control Release [Internet]. 2008 Feb 18 [cited 2022 Jan 16];126(1):34. Available from: /pmc/articles/PMC2270413/

294. Wei Z, Batagov AO, Carter DRF, Krichevsky AM. Fetal Bovine Serum RNA Interferes with the Cell Culture derived Extracellular RNA. Sci Reports 2016 61 [Internet]. 2016 Aug 9 [cited 2022 Jan 16];6(1):1–6. Available from: https://www.nature.com/articles/srep31175

295. Hahn J, Wickham SFJ, Shih WM, Perrault SD. Addressing the Instability of DNA Nanostructures in Tissue Culture. ACS Nano [Internet]. 2014 Sep 23 [cited 2022 Jan 16];8(9):8765. Available from: /pmc/articles/PMC4174095/

296. Schlake T, Thess A, Fotin-Mleczek M, Kallen KJ. Developing mRNA-vaccine technologies. RNA Biol [Internet]. 2012 [cited 2022 Jan 16];9(11):1319. Available from: /pmc/articles/PMC3597572/

297. Li B, Luo X, Dong Y. Effects of Chemically Modified Messenger RNA on Protein Expression. Bioconjug Chem [Internet]. 2016 Mar 16 [cited 2022 Jan 16];27(3):849–53. Available from: https://pubmed.ncbi.nlm.nih.gov/26906521/

298. Amero P, Khatua S, Rodriguez-Aguayo C, Lopez-Berestein G. Aptamers: Novel Therapeutics and Potential Role in Neuro-Oncology. Cancers (Basel) [Internet]. 2020 Oct 1 [cited 2022 Jan 16];12(10):1–29. Available from: /pmc/articles/PMC7600320/

299. Tuerk C, Gold L. Systematic evolution of ligands by exponential enrichment: RNA ligands to bacteriophage T4 DNA polymerase. Science [Internet]. 1990 [cited 2022 Jan 16];249(4968):505–10. Available from: https://pubmed.ncbi.nlm.nih.gov/2200121/

300. Schlicher RK, Hutcheson JD, Radhakrishna H, Apkarian RP, Prausnitz MR. Changes in Cell

Morphology Due to Plasma Membrane Wounding by Acoustic Cavitation. Ultrasound Med Biol. 2010;36(4):677–92.

301. Zhou QL, Chen ZY, Wang YX, Yang F, Lin Y, Liao YY. Ultrasound-mediated local drug and gene delivery using nanocarriers. BioMed Research International. 2014.

302. Helfield B, Chen X, Watkins SC, Villanueva FS. Biophysical insight into mechanisms of sonoporation. Proc Natl Acad Sci U S A [Internet]. 2016 Sep 6 [cited 2021 Dec 16];113(36):9983–8. Available from: https://www.pnas.org/content/113/36/9983

303. Caskey CF, Stieger SM, Qin S, Dayton PA, Ferrara KW. Direct observations of ultrasound microbubble contrast agent interaction with the microvessel wall. J Acoust Soc Am. 2007;122(2):1191–200.

304. Laing ST, Kim H, Kopechek JA, Parikh D, Huang S, Klegerman ME, et al. Ultrasound-mediated delivery of echogenic immunoliposomes to porcine vascular smooth muscle cells in vivo. J Liposome Res. 2010;20(2):160–7.

305. Haag P, Frauscher F, Gradl J, Seitz A, Schäfer G, Lindner JR, et al. Microbubble-enhanced ultrasound to deliver an antisense oligodeoxynucleotide targeting the human androgen receptor into prostate tumours. J Steroid Biochem Mol Biol. 2006;102(1-5 SPEC. ISS.):103–13.

306. Suzuki R, Namai E, Oda Y, Nishiie N, Otake S, Koshima R, et al. Cancer gene therapy by IL-12 gene delivery using liposomal bubbles and tumoral ultrasound exposure. J Control Release [Internet]. 2010 Mar [cited 2022 Jan 15];142(2):245–50. Available from: https://pubmed.ncbi.nlm.nih.gov/19883708/

307. Technologies L. Lipofectamine ® RNAiMAX Reagent Lipofectamine ® RNAiMAX Transfection Protocol Scaling Up or Down Transfections Limited Product Warranty and Disclaimer Details Package Contents. [cited 2022 Jan 16]; Available from: www.lifetechnologies.com/support.

308. Technologies L. Lipofectamine ® 2000 Reagent Protocol Outline. 2000 [cited 2022 Jan 16]; Available from: www.lifetechnologies.com/support.

309. Propidium Iodide [Internet]. [cited 2022 Jan 16]. Available from: https://www.thermofisher.com/order/catalog/product/P1304MP

310. Brana C, Benham C, Sundstrom L. A method for characterising cell death in vitro by combining propidium iodide staining with immunohistochemistry. Brain Res Protoc. 2002 Oct 1;10(2):109–14.

311. Crowley LC, Scott AP, Marfell BJ, Boughaba JA, Chojnowski G, Waterhouse NJ. Measuring Cell Death by Propidium Iodide Uptake and Flow Cytometry. Cold Spring Harb Protoc [Internet]. 2016 Jul 1 [cited 2022 Jan 16];2016(7):pdb.prot087163. Available from: http://cshprotocols.cshlp.org/content/2016/7/pdb.prot087163.full

312. Kooiman K, Foppen-Harteveld M, Der Steen AFWV, De Jong N. Sonoporation of endothelial cells by vibrating targeted microbubbles. J Control Release [Internet]. 2011;154(1):35–41. Available from: http://dx.doi.org/10.1016/j.jconrel.2011.04.008

313. Wang M, Zhang Y, Cai C, Tu J, Guo X, Zhang D. Sonoporation-induced cell membrane permeabilization and cytoskeleton disassembly at varied acoustic and microbubble-cell parameters. Sci Rep [Internet]. 2018;8(1):1–12. Available from: http://dx.doi.org/10.1038/s41598-018-22056-8

314. Zhao L, Feng Y, Shi A, Zong Y, Wan M. Apoptosis Induced by Microbubble-Assisted Acoustic Cavitation in K562 Cells: The Predominant Role of the Cyclosporin A-Dependent Mitochondrial Permeability Transition Pore. Ultrasound Med Biol. 2015;41(10):2755–64.

315. Aron M, Vince O, Gray M, Mannaris C, Stride E. Investigating the Role of Lipid Transfer in Microbubble-Mediated Drug Delivery. Langmuir. 2019;35(40):13205–15.

316. Andreason GL, Evans GA. Optimization of electroporation for transfection of mammalian cell lines. Anal Biochem. 1989 Aug 1;180(2):269–75.

317. Du X, Wang J, Zhou Q, Zhang L, Wang S, Zhang Z, et al. Advanced physical techniques for gene delivery based on membrane perforation. Drug Deliv [Internet]. 2018 [cited 2022 Jan 15];25(1):1516–25. Available from: https://pubmed.ncbi.nlm.nih.gov/29968512/

318. Manjila SB, Baby JN, Bijin EN, Constantine I, Pramod K, Valsalakumari J. Novel gene delivery

systems. Int J Pharm Investig [Internet]. 2013 [cited 2021 Dec 16];3(1):1. Available from: /pmc/articles/PMC3687232/

319. Hawley-Nelson P, Ciccarone V, Moore ML. Transfection of Cultured Eukaryotic Cells Using Cationic Lipid Reagents. Curr Protoc Mol Biol [Internet]. 2008 Jan 1 [cited 2022 Jan 16];81(1):9.4.1-9.4.17. Available from: https://onlinelibrary.wiley.com/doi/full/10.1002/0471142727.mb0904s81

320. Cell Culture Basics Handbook.

321. Transfecting Mammalian Cells with RNA, Continued. [cited 2022 Jan 16]; Available from: www.lifetechnologies.com/support

322. Wang T, Larcher LM, Ma L, Veedu RN. Systematic Screening of Commonly Used Commercial Transfection Reagents towards Efficient Transfection of Single-Stranded Oligonucleotides. Mol A J Synth Chem Nat Prod Chem [Internet]. 2018 Oct 8 [cited 2022 Jan 16];23(10). Available from: /pmc/articles/PMC6222501/

323. Djurovic S, Iversen N, Jeansson S, Hoover F, Christensen G. Comparison of nonviral transfection and adeno-associated viral transduction on cardiomyocytes. Mol Biotechnol 2004 281 [Internet]. 2004 [cited 2022 Jan 16];28(1):21–31. Available from: https://link.springer.com/article/10.1385/MB:28:1:21

324. Aslan H, Zilberman Y, Arbeli V, Sheyn D, Matan Y, Liebergall M, et al. Nucleofection-based ex vivo nonviral gene delivery to human stem cells as a platform for tissue regeneration. Tissue Eng [Internet]. 2006 Apr [cited 2022 Jan 16];12(4):877–89. Available from: https://pubmed.ncbi.nlm.nih.gov/16674300/

325. Tsulaia T V., Prokopishyn NL, Yao A, Victor Carsrud ND, Clara Carou M, Brown DB, et al. Glass needle-mediated microinjection of macromolecules and transgenes into primary human mesenchymal stem cells. J Biomed Sci [Internet]. 2003 May [cited 2022 Jan 16];10(3):328–36. Available from: https://pubmed.ncbi.nlm.nih.gov/12711860/

326. Han SW, Nakamura C, Kotobuki N, Obataya I, Ohgushi H, Nagamune T, et al. High-efficiency DNA injection into a single human mesenchymal stem cell using a nanoneedle and atomic force microscopy. Nanomedicine [Internet]. 2008 Sep [cited 2022 Jan 16];4(3):215–25. Available from: https://pubmed.ncbi.nlm.nih.gov/18501680/

327. Katti P. Drug-device development: cancer immunotherapy with therapeutic, ultrasound-mediated delivery. 2020;

328. Search of: mRNA | Active, not recruiting Studies | Cancer - List Results - ClinicalTrials.gov [Internet]. [cited 2022 Jan 18]. Available from: https://clinicaltrials.gov/ct2/results?term=mRNA&cond=Cancer&recrs=d&age_v=&gndr=&type=&rslt=&Search=Apply

329. Zhang X, Goel V, Attarwala H, Sweetser MT, Clausen VA, Robbie GJ. Patisiran Pharmacokinetics, Pharmacodynamics, and Exposure-Response Analyses in the Phase 3 APOLLO Trial in Patients With Hereditary Transthyretin-Mediated (hATTR) Amyloidosis. J Clin Pharmacol [Internet]. 2020 Jan 1 [cited 2022 Feb 10];60(1):37–49. Available from: https://pubmed.ncbi.nlm.nih.gov/31322739/

330. Nash KL, Lever AML. Green fluorescent protein: green cells do not always indicate gene expression. Gene Ther 2004 1111 [Internet]. 2004 Mar 25 [cited 2022 Feb 10];11(11):882–3. Available from: https://www.nature.com/articles/3302246

331. Heller R, Jaroszeski M, Atkin a, Moradpour D, Gilbert R, Wands J, et al. In vivo gene electroinjection and expression in rat liver. FEBS Lett. 1996;

332. Mali S. Delivery systems for gene therapy. Vol. 19, Indian Journal of Human Genetics. 2013. p. 3–8.

333. Klein VG, Townsend CE, Testa A, Zengerle M, Maniaci C, Hughes SJ, et al. Understanding and Improving the Membrane Permeability of VH032-Based PROTACs. ACS Med Chem Lett [Internet]. 2020 Sep 10 [cited 2022 Jan 18];11(9):1732–8. Available from: https://pubs.acs.org/doi/full/10.1021/acsmedchemlett.0c00265

334. Yang NJ, Hinner MJ. Getting Across the Cell Membrane: An Overview for Small Molecules, Peptides, and Proteins. Methods Mol Biol [Internet]. 2015 [cited 2022 Jan 18];1266:29. Available from:

/pmc/articles/PMC4891184/

335. Duan X, Zhou Q, Wan JMF, Yu ACH. Sonoporation generates downstream cellular impact after membrane resealing. Sci Reports 2021 111 [Internet]. 2021 Mar 4 [cited 2022 Jan 18];11(1):1–12. Available from: https://www.nature.com/articles/s41598-021-84341-3

336. Balukoff NC, Ho JJD, Theodoridis PR, Wang M, Bokros M, Llanio LM, et al. A translational program that suppresses metabolism to shield the genome. Nat Commun 2020 111 [Internet]. 2020 Nov 13 [cited 2022 Jan 18];11(1):1–15. Available from: https://www.nature.com/articles/s41467-020-19602-2

337. Hmadcha A, Martin-Montalvo A, Gauthier BR, Soria B, Capilla-Gonzalez V. Therapeutic Potential of Mesenchymal Stem Cells for Cancer Therapy. Front Bioeng Biotechnol. 2020 Feb 5;8:43.

338. Hamann A, Nguyen A, Pannier AK. Nucleic acid delivery to mesenchymal stem cells: a review of nonviral methods and applications. J Biol Eng [Internet]. 2019 Jan 18 [cited 2022 Jan 15];13(1). Available from: /pmc/articles/PMC6339289/

339. Menezes ME, Talukdar S, Wechman SL, Das SK, Emdad L, Sarkar D, et al. Prospects of Gene Therapy to Treat Melanoma. Adv Cancer Res. 2018 Jan 1;138:213–37.